

UNDERSTANDING THE ROLE OF THE STREAM-GROUNDWATER INTERFACE IN
DISSOLVED ORGANIC CARBON CYCLING IN A THIRD-ORDER,
LOWLAND RIVER NETWORK

By

Sydney S. Ruhala

A THESIS

Submitted to
Michigan State University
in partial fulfillment of the requirements
for the degree of

Geological Sciences – Master of Science

2017

ABSTRACT

UNDERSTANDING THE ROLE OF THE STREAM-GROUNDWATER INTERFACE IN DISSOLVED ORGANIC CARBON CYCLING IN A THIRD-ORDER, LOWLAND RIVER NETWORK

By

Sydney S. Ruhala

Global carbon models currently underrepresent the contribution of carbon dioxide (CO₂) emissions from stream channels to the atmosphere since streams have traditionally been viewed as passive drainage systems for terrestrial landscapes. However, recent studies have shown that rivers are a significant source of CO₂ (a greenhouse gas) to the atmosphere, indicating that much of the organic carbon entering rivers (predominantly as dissolved organic carbon (DOC)) experiences significant in-stream biogeochemical degradation. The zone beneath and alongside of the stream where stream water-groundwater interactions occur (i.e., the hyporheic zone, HZ) may be an important location within river networks for DOC processing (e.g., degradation, consumption), since it is a hotspot for microbial activity and biogeochemical reactions. This thesis assesses the role of the HZ (e.g., source vs. sink of carbon) in DOC cycling in a third-order, lowland watershed in Michigan, USA and represents one of the first watershed-scale HZ sampling efforts. Our findings indicate that the HZ is a location for DOC processing in stream networks and that the processing signal is observable at the watershed scale. The HZ in this small, groundwater-fed stream network likely acts as a sink, consuming DOC via aerobic, microbial respiration. In addition, our analysis suggests that the HZ may act as a larger sink for DOC in headwater streams than in higher stream orders in this river network.

Copyright by
SYDNEY S. RUHALA
2017

ACKNOWLEDGMENTS

This project was partially funded by a Geological Society of America Graduate Student Research Grant as well as by the NSF Long-term Ecological Research Program (DEB 1027253) at the Kellogg Biological Station and by Michigan State University AgBioResearch. I would like to thank the Department of Earth and Environmental Sciences for their support as well as my co-advisors, Dr. David T. Long and Dr. Jay P. Zarnetske and my committee member, Dr. Stephen K. Hamilton, for their advice and guidance.

TABLE OF CONTENTS

LIST OF TABLES	vii
LIST OF FIGURES	viii
KEY TO ABBREVIATIONS	xii
CHAPTER 1: INTRODUCTION	1
CHAPTER 2: A PRELIMINARY STUDY OF TRENDS IN DISSOLVED ORGANIC CARBON QUANTITY AND QUALITY ACROSS THE STREAM-GROUNDWATER INTERFACE OF A THIRD-ORDER, LOWLAND RIVER NETWORK	6
2.1 Introduction	6
2.2 Background	8
2.2.1 <i>Field Site Description</i>	8
2.2.2 <i>Hydrology</i>	9
2.3 Methods	12
2.3.1 <i>Sample Collection</i>	12
2.3.2 <i>Analytical Methods</i>	15
2.3.3 <i>Optical Indices</i>	16
2.3.4 <i>Vertical Porewater Profiles</i>	17
2.4 Results	18
2.4.1 <i>Results of the Vertical Porewater Profiles</i>	18
2.4.2 <i>DOC Variance and Mixing Zone Model</i>	21
2.5 Discussion	26
2.6 Conclusions	30
CHAPTER 3: DETERMINING HOW DISSOLVED ORGANIC CARBON IS TRANSFORMED AT THE STREAM-GROUNDWATER INTERFACE ACROSS A THIRD- ORDER, LOWLAND RIVER NETWORK	31
3.1 Introduction	31
3.2 Background	35
3.2.1 <i>Field Site Description</i>	35
3.2.2 <i>Hydrology</i>	36
3.3 Methods	38
3.3.1 <i>Sample Collection</i>	38
3.3.2 <i>Analytical Methods</i>	42
3.3.3 <i>Optical Indices</i>	42
3.3.4 <i>Vertical Porewater Profiles</i>	43
3.4 Results	44
3.4.1 <i>Composite Vertical Porewater Profiles</i>	44
3.4.2 <i>Rates of Change in DOC Quantity and Quality with Depth</i>	47
3.4.3 <i>DOC Metabolism</i>	52

LIST OF TABLES

Table 1: Summary of optical DOC indices.....	17
Table 2: Summary of the rate constants for DOC concentration and $SUVA_{254}$	48
Table 3: Summary of the known strengths and limitations of in-situ optical instruments	78
Table A1: Supplemental information for the 2015 sampling sites	97
Table A2: Synoptic sampling data for 2015	115
Table B1: Supplemental information for the 2016 sampling sites	124

LIST OF FIGURES

Figure 1: Conceptual model of the hyporheic zone	5
Figure 2: Topographic map of Augusta Creek watershed	10
Figure 3: 2015 USGS hydrographs for Augusta Creek	11
Figure 4: Map of Augusta Creek sampling sites in 2015.....	14
Figure 5: Sampling scheme.....	15
Figure 6: Example of a vertical porewater profile	17
Figure 7: Vertical porewater profiles of DOC concentration and optical indices	20
Figure 8: Model used to identify mixing zone depths	22
Figure 9: DOC concentration and optical indices within the mixing zone.....	24
Figure 10: 2016 USGS hydrographs for Augusta Creek	37
Figure 11: Map of Augusta Creek sampling sites in 2016.....	40
Figure 12: Subplots of labeled sampling sites across Augusta Creek	41
Figure 13: Composite vertical porewater profiles	46
Figure 14: Using a first-order rate law to determine rate constants.....	47
Figure 15: Changes in rate constants and VHG across the stream network	51
Figure 16: Example of a metabolism plot.....	52
Figure 17: Metabolism plots for Augusta Creek.....	54
Figure 18: Plots of HZ function	60
Figure 19: A simplified Jablonski diagram.....	69
Figure 20: Plots of DOC concentration versus time using a variation of sampling frequencies ...	72
Figure 21: In-situ optical instruments	73
Figure 22: Plot of discharge and FDOM concentration versus time.....	77

Figure 23: Diurnal trends for CDOM and absorbance.....	84
Figure 24: Hysteresis trends.....	87
Figure 25: DOC flux versus discharge.....	89
Figure A1: Map of Augusta Creek watershed with land use	98
Figure A2: Site A Vertical Porewater Profiles	99
Figure A3: Site B Vertical Porewater Profiles.....	100
Figure A4: Site C Vertical Porewater Profiles.....	101
Figure A5: Site D Vertical Porewater Profiles	102
Figure A6: Site F Vertical Porewater Profiles	103
Figure A7: Site G Vertical Porewater Profiles	104
Figure A8: Site H Vertical Porewater Profiles	105
Figure A9: Site I Vertical Porewater Profiles	106
Figure A10: Site J Vertical Porewater Profiles.....	107
Figure A11: Site K Vertical Porewater Profiles	108
Figure A12: Site L Vertical Porewater Profiles	109
Figure A13: Site M Vertical Porewater Profiles.....	110
Figure A14: Site O Vertical Porewater Profiles	111
Figure A15: Site P Vertical Porewater Profiles	112
Figure A16: Site Q Vertical Porewater Profiles	113
Figure A17: Site R Vertical Porewater Profiles.....	114
Figure B1: Site A1 Vertical Porewater Profiles.....	125
Figure B2: Site A2 Vertical Porewater Profiles.....	126
Figure B3: Site A3 Vertical Porewater Profiles.....	127
Figure B4: Site B1 Vertical Porewater Profiles	128

Figure B5: Site B2 Vertical Porewater Profiles	129
Figure B6: Site C1 Vertical Porewater Profiles	130
Figure B7: Site C2 Vertical Porewater Profiles	131
Figure B8: Site C3 Vertical Porewater Profiles	132
Figure B9: Site C4 Vertical Porewater Profiles	133
Figure B10: Site E1 Vertical Porewater Profiles	134
Figure B11: Site E2 Vertical Porewater Profiles	135
Figure B12: Site E3 Vertical Porewater Profiles	136
Figure B13: Site F1 Vertical Porewater Profiles	137
Figure B14: Site F2 Vertical Porewater Profiles	138
Figure B15: Site F3 Vertical Porewater Profiles	139
Figure B16: Site F4 Vertical Porewater Profiles	140
Figure B17: Site G1 Vertical Porewater Profiles.....	141
Figure B18: Site G2 Vertical Porewater Profiles.....	142
Figure B19: Site H1 Vertical Porewater Profiles.....	143
Figure B20: Site H2 Vertical Porewater Profiles.....	144
Figure B21: Site H3 Vertical Porewater Profiles.....	145
Figure B22: Site I1 Vertical Porewater Profiles	146
Figure B23: Site I2 Vertical Porewater Profiles	147
Figure B24: Site J1 Vertical Porewater Profiles	148
Figure B25: Site K1 Vertical Porewater Profiles.....	149
Figure B26: Site K2 Vertical Porewater Profiles.....	150
Figure B27: Site L1 Vertical Porewater Profiles	151

Figure B28: Site L2 Vertical Porewater Profiles	152
Figure B29: Site L3 Vertical Porewater Profiles	153
Figure B30: Site M1 Vertical Porewater Profiles	154
Figure B31: Site M2 Vertical Porewater Profiles	155
Figure B32: Site O1 Vertical Porewater Profiles.....	156
Figure B33: Site O2 Vertical Porewater Profiles.....	157
Figure B34: Site R1 Vertical Porewater Profiles	158
Figure B35: Site R2 Vertical Porewater Profiles	159
Figure B36: Site R3 Vertical Porewater Profiles	160
Figure B37: Site R4 Vertical Porewater Profiles	161
Figure B38: Site S1 Vertical Porewater Profiles	162
Figure B39: Site S2 Vertical Porewater Profiles	163

KEY TO ABBREVIATIONS

C – Carbon

CO₂ – Carbon dioxide

DOM – Dissolved Organic Matter

POC – Particulate Organic Carbon

DOC – Dissolved Organic Carbon

NPOC – Non-Purgeable Organic Carbon

Cl⁻ – Chloride

NO₃⁻ – Nitrate

SO₄²⁻ – Sulfate

CaCO₃ – Calcium carbonate

HCO₃⁻ – Bicarbonate

SW-GW – Stream Water-Groundwater

HZ – Hyporheic Zone

KBS – Kellogg Biological Station

USGS – United States Geological Survey

°C – Degrees Celsius

DO – Dissolved Oxygen

HDPE – High Density Polyethylene

US EPA – United States Environmental Protection Agency

SUVA₂₅₄ – Specific Ultraviolet Absorbance at 254 nm

UV-VIS – Ultraviolet-Visible

λ – Wavelength

SD – Standard Deviation

VHG – Vertical Head Gradient

CDOM – Chromophoric fraction of DOM

FDOM – Fluorescent DOM

QSE – Quinine Sulfate Equivalents

LED – Light Emitting Diode

FI – Fluorescence Index

CHAPTER 1: INTRODUCTION

Understanding the global carbon (C) cycle, including its dominant sources and sinks and associated fluxes, is of critical importance to mitigating future climate change. Previous models have underrepresented the emissions of carbon dioxide (CO₂) from stream channels to the atmosphere since streams have traditionally been viewed as passive drainage systems for terrestrial landscapes (Boulton et al., 1998; Battin et al., 2009; Boano et al., 2014). However, recent studies revealed that streams exhibit strong, net heterotrophy (i.e., community respiration considerably exceeds gross primary production), globally generating 1.8 ± 0.25 Pg CO₂ each year - a rate 6 times greater than lakes and reservoirs combined (Battin et al. 2008; Butman and Raymond, 2011; Raymond et al., 2013). This indicates that rivers* are a significant source of CO₂ (a greenhouse gas) to the atmosphere and that much of the organic C entering rivers is, in fact, undergoing significant in-stream biogeochemical degradation (Battin et al., 2008). Thus, further study of C cycling in rivers is warranted, so that rivers can be more accurately represented in global C models.

Carbon in natural waters can exist in several different forms: 1) as particulate organic carbon (POC) such as woody debris and leaf litter, 2) as dissolved organic carbon (DOC) and 3) as dissolved inorganic carbon including CO₂ and bicarbonate (HCO₃⁻; Cory et al., 2011). Here, we focus on DOC since it is often the major form of organic C in streams and is the most susceptible to respiratory conversion to CO₂ and subsequent emission (e.g., Aiken, 2014). DOC is operationally defined as any organic C that is able to pass through a filter of a specified pore size (e.g., typically 0.7 μm, 0.45 μm or smaller), and can include some colloidal matter as well as dissolved compounds. The composition of DOC is complex, consisting of a mixture of water-

* For the purposes of this thesis, the terms “river(s)” and “stream(s)” are used interchangeably.

soluble, organic molecules with varying chemical structures (e.g., molecular weight and aromaticity), which is largely dependent on its source material. For example, microbially- and algal-derived DOC that is produced within the stream (i.e., autochthonous DOC) tends to have a lower molecular weight and be less aromatic than terrestrially-derived DOC from vascular plant sources (i.e., allochthonous DOC; McKnight et al., 2001; McDonald et al., 2004; Fellman et al., 2010). Some general processes that produce DOC include organic matter leaching and decomposition, chemical degradation, and exudates from primary production (e.g., Thurman, 1985; Cory et al., 2011; Jollymore et al., 2012).

DOC plays several critical roles in stream C cycling (Cory et al., 2011). For instance, DOC produces CO₂ when remineralized, fuels stream metabolism, and regulates additional biogeochemical cycles (e.g., nitrogen transformations, trace metal complexation; Aiken, 2014). As a result, stream DOC dynamics influence C cycling on local to global scales (Battin et al., 2009). Despite its importance, the nature of in-stream DOC processing, including rates, pathways and transformations, remains inadequately quantified (e.g., Sobczak and Findlay, 2002). Thus, the mechanisms of stream DOC processing need to be investigated including, 1) where DOC processing occurs within rivers, 2) the dominant biogeochemical transformation processes, and 3) how those processes affect the fate of DOC transported downstream (e.g., uptake via microbial processes, remineralization). This knowledge will help improve the current understanding of stream C cycling as well as help predict how streams and ultimately the global C cycle will respond to changes in loading of DOC. For example, increases in stream DOC transport have been occurring in parts of North America and northern Europe, for reasons that remain unclear (Monteith et al., 2007; Laudon et al., 2011).

The zone beneath and alongside of the stream where stream water-groundwater (SW-GW) interactions occur (i.e., the hyporheic zone, HZ) may be an important location within river networks for DOC processing. The HZ is a hotspot for microbial activity and biogeochemical reactions. (Figure 1; Storey et al., 1999; Baker et al., 1999; Fischer et al., 2005; Battin et al., 2009; Zarnetske et al., 2011). This increased activity is the result of the mixing of two chemically distinct waters (i.e., SW and GW), which creates a transitional zone in the subsurface sediments, promoting both biological and chemical diversity (e.g., microbial communities, metabolic rates, chemical reactions; Valett et al., 1996; Hedin et al., 1998; Findlay and Sobczak, 2000; Nogaro et al., 2013; Boano et al., 2014). In addition, residence times increase in the HZ due to slow porewater transport, creating a longer exposure time of stream-borne constituents (e.g., C, nutrients) to microbial communities, which facilitates reaction/metabolism (Battin et al., 2008; Harvey et al., 2013; Boano et al., 2014). Due to the combination of high biological diversity, strong chemical gradients, and increased residence times, it is expected that the HZ is a significant processor of stream DOC.

Previous small-scale field (e.g., reach scale) and mesocosm studies have observed decreasing DOC concentrations along hyporheic flowpaths, suggesting that the HZ is effective at processing DOC and may act as an important sink for DOC in stream networks (Findlay et al., 1993; Findlay and Sobczak, 1996; Schindler and Krabbenhoft, 1998; Sobczak and Findlay, 2002; Zarnetske et al., 2011). Although consistent patterns in DOC quantity, in terms of concentrations, have been documented along individual hyporheic flowpaths, few studies have thoroughly characterized changes in DOC quality (i.e., molecular characteristics, composition) within the HZ (Findlay and Sobczak, 1996). DOC quality is a critical variable to include in stream C studies since the quality of DOC impacts its bioavailability and reactivity (i.e., lability), which

ultimately affects downstream ecosystems and water quality (Fellman et al., 2010; Cory et al., 2011). Furthermore, DOC quality can change independently of DOC concentration and only a relatively small fraction of total DOC can drive microbial metabolism (Lutz et al., 2012), thus changes in DOC quantity alone do not fully reflect hyporheic DOC dynamics.

Hence, the overarching objectives of this thesis are to: 1) evaluate DOC quantity and quality within the HZ of a third-order, lowland river network to determine the role (i.e., source vs. sink) of the HZ in stream DOC cycling at the watershed scale (Ch. 2 and 3) and 2) evaluate a series of analytical methods used to quantify stream DOC quality in a rapid and cost-effective way, including new, in-situ DOC sensor technologies (Ch. 4). Specifically, Chapter 2 is a preliminary study that focuses on whether the HZ is an important location for stream DOC processing and if a processing signal is observable at the watershed scale. Chapter 3 focuses on how the HZ processes stream DOC and if the dominant biogeochemical transformation mechanism(s) is consistent throughout the stream network. Lastly, Chapter 4 provides a review of new in-situ optical methods for measuring DOC quality in stream networks, which is a critical variable when studying in-stream C cycling (Ruhala and Zarnetske, 2017).

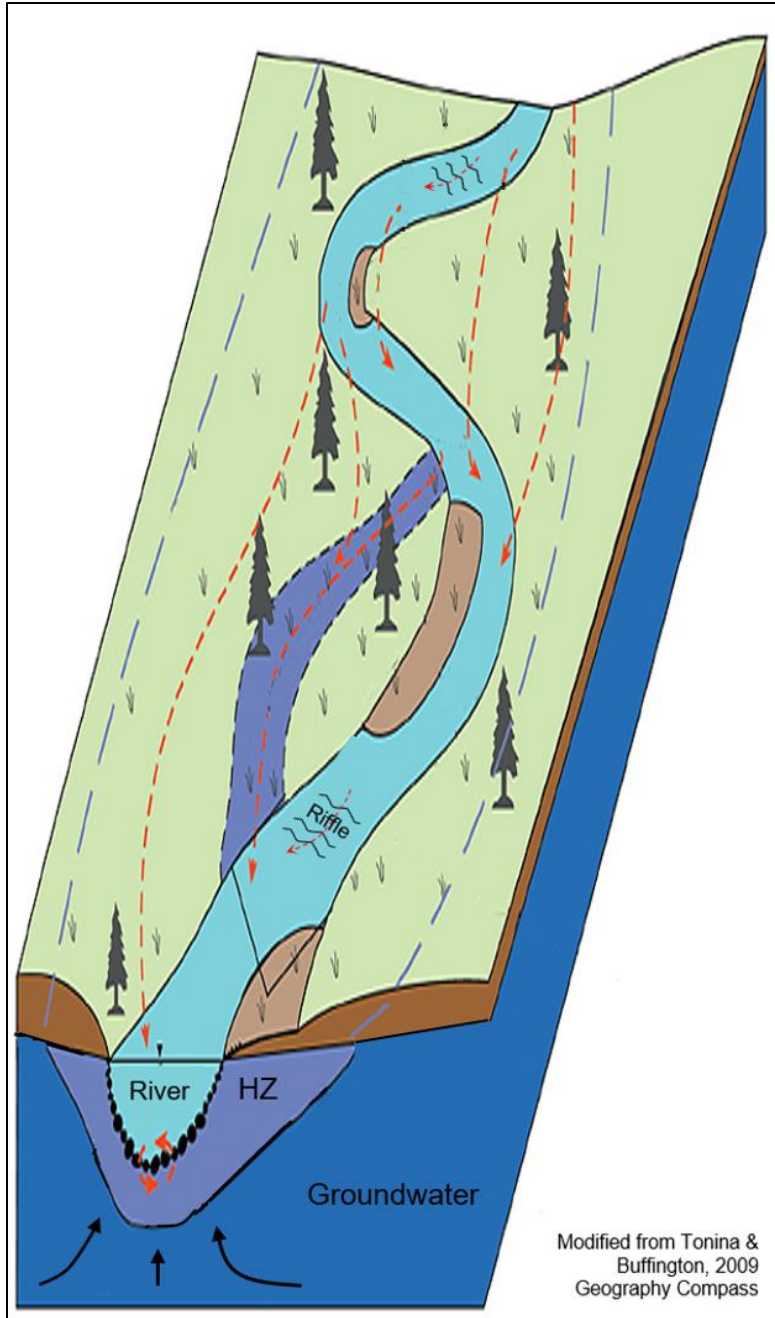


Figure 1: Conceptual model of the hyporheic zone. This diagram depicts the extent of a representative HZ. The red dashed lines (--) indicate hyporheic flow and the black arrows (→) indicate groundwater flow. Image modified from Tonina and Buffington (2009).

CHAPTER 2: A PRELIMINARY STUDY OF TRENDS IN DISSOLVED ORGANIC CARBON QUANTITY AND QUALITY ACROSS THE STREAM-GROUNDWATER INTERFACE OF A THIRD-ORDER, LOWLAND RIVER NETWORK

2.1 Introduction

The zone beneath and alongside of the stream where stream water-groundwater (SW-GW) interactions occur (i.e., the hyporheic zone, HZ) may be an important location within river networks for dissolved organic carbon (DOC) processing (e.g., degradation, consumption) since it is a hotspot for microbial activity and biogeochemical reactions (Storey et al., 1999; Baker et al., 1999; Fischer et al., 2005; Battin et al., 2009; Zarnetske et al., 2011). Previous small-scale field (e.g., reach scale) and mesocosm studies have observed decreasing DOC concentrations along hyporheic flowpaths, suggesting that the HZ is effective at consuming DOC and therefore may be an important sink for DOC in stream networks (Findlay et al., 1993; Findlay and Sobczak, 1996; Schindler and Krabbenhoft, 1998; Sobczak and Findlay, 2002; Zarnetske et al., 2011). However, hyporheic processes are also expected to impact stream DOC cycling on larger scales (e.g., the watershed scale; Boano et al., 2014). Yet, few studies have assessed hyporheic DOC cycling across entire watersheds, and those that have, relied heavily on mathematical models more than empirical field data (e.g., Wondzell, 2011; Boano et al., 2014; Kiel and Cardenas, 2014; Gomez-Velez and Harvey, 2014).

Here, we uniquely couple trends in hyporheic DOC quantity and quality from a watershed-scale field study to assess the role of the HZ in DOC cycling within stream networks. DOC quality is included as a variable since the quality of DOC impacts its bioavailability and reactivity (i.e., lability), which ultimately affects downstream ecosystems and water quality (Fellman et al., 2010; Cory et al., 2011) and may vary independently of DOC concentration

(Lutz et al., 2012). This approach will allow us to identify if the HZ is an important location for DOC processing and how it controls the fate of DOC transported downstream.

The following central research questions are addressed in this study: 1) is the HZ a significant location for processing (e.g., degradation, consumption) of stream DOC? and if so, 2) can a processing signal be observed at larger scales (i.e., across the entire watershed and/or within stream orders). We hypothesize that the HZ is a significant location for processing of stream DOC. If our hypothesis is true, then we predict:

- 1) Decreasing DOC concentrations will be observed along hyporheic flowpaths throughout the watershed, similar to the results found in previous small-scale field and mesocosm studies.
- 2) The high rates of microbial activity in the HZ will alter overall DOC quality in the HZ, as indicated by the presence of less aromatic and lower molecular weight DOC when compared to stream water.
- 3) The variance in DOC quantity and quality will be greatest in the HZ when compared to stream water and groundwater conditions due to the high DOC processing rates in the HZ.

To test our predictions, we use field observations of DOC and hydrologic conditions collected across the third-order, mixed land use watershed of Augusta Creek in southwestern Michigan, USA (42°21'12"N, 85°21'14"W), which is adjacent to the Kellogg Biological Station (KBS), a Michigan State University field research station.

2.2 Background

2.2.1 *Field Site Description*

A synoptic HZ sampling campaign was conducted over an 8-day period in August 2015 across the Augusta Creek watershed, which is located in Barry and Kalamazoo counties in southwestern Michigan and is part of the larger Kalamazoo River watershed (Figure 2). This watershed was selected as the field site because Augusta Creek is a historically important stream for biogeochemical and ecological research (e.g., it was an original River Continuum Concept site; Vannote et al. 1980), has a long-term and active United States Geological Survey (USGS) gaging station (04105700), and is easily accessible through the roadways and university lands. The geology of the watershed has been heavily influenced by glacial activity (i.e., ice advancement and retreat), most recently in the late Pleistocene Epoch (Dunbar, 1962). As a result, the watershed is underlain by deep glacial drift deposits consisting of mixtures of gravel, sand, silt, and clay, varying in thickness from 40 to 120 m across the watershed (FTWRC, 2011).

Augusta Creek is a third-order, lowland watershed draining 98 km² (Figure 2, Strahler, 1957). Most of the tributaries originate in groundwater-fed lakes and low-lying wetlands (Manny and Wetzel, 1973; FTWRC, 2011). The three dominant land cover types are 1) 47% agriculture (crops and pastures), 2) 23% upland forest (mainly deciduous), and 3) 20% wetland/marsh complexes (FTWRC, 2011; Figure A1; Table A1). The mean annual precipitation for the Augusta Creek watershed is 925 mm, while the total precipitation in 2015 was 1,154 mm (FTWRC, 2011; KBS-LTER, Dataset KBS002). Soils are typically sandy to loamy in uplands, with organic (muck) soils in the riparian wetlands, and patches of muck along the stream channel (FTWRC, 2011). Soil infiltration rates throughout the watershed range from 12.7 to 25.4 mm/h (FTWRC, 2011). The mean stream slope is approximately 2.03 m/km (Manny and Wetzel,

1973) and the average grain size diameter (d_{50}) for the upper streambed sediments (i.e., shallower than 20 cm), determined from stream sediment samples collected at 16 sites across the watershed, is 0.90 mm (Table A1). In addition, clay and marl (CaCO_3 -rich) lenses are found throughout the streambed sediments.

In terms of stream chemistry, Augusta Creek is a hard water stream with a total hardness of about 280 mg/L (Mahan and Cummins, 1974; King 1978). Alkalinity typically ranges from 160 to 210 mg/L as CaCO_3 , while pH ranges from 7.5 to 8.7 (Manny and Wetzel, 1973; Mahan and Cummins, 1974; King, 1978). Calcite (CaCO_3) precipitates are often found on stones on the stream bottom. Sampling of Augusta Creek from 1997-2015 has shown that stream DOC concentrations typically range from 2 to 12 mg/L (Hamilton, unpublished data)

2.2.2 Hydrology

Augusta Creek exhibits a discharge flow regime characterized as having minimal within- and among-year variation (Url and Hart 1992, Poff et al., 1997). Based on recent and historical discharge measurements collected at the USGS gaging station (04105700) located on the lower main stem above the Kalamazoo River confluence (Figure 2), Augusta Creek's discharge typically varies between 0.57 to 2.83 m^3/s , with occasional peak flow events. This range in discharge was observed from August 2014 – August 2015 (with ~3 peak flow events) as well as over several years prior (Figure 3A). The synoptic HZ sampling campaign took place from August 10 – August 18, 2015, during which the average discharge was 1.23 m^3/sec , slightly higher than the previous 5-year average of 1.05 m^3/sec for the month of August (USGS, 2016, Station 04105700). During the sampling period, discharge varied some from 0.93 to 1.93 m^3/sec , with two notable precipitation events, one on August 10 and another on August 17. However, discharge remained relatively stable over most of the sampling period (Figure 3B).

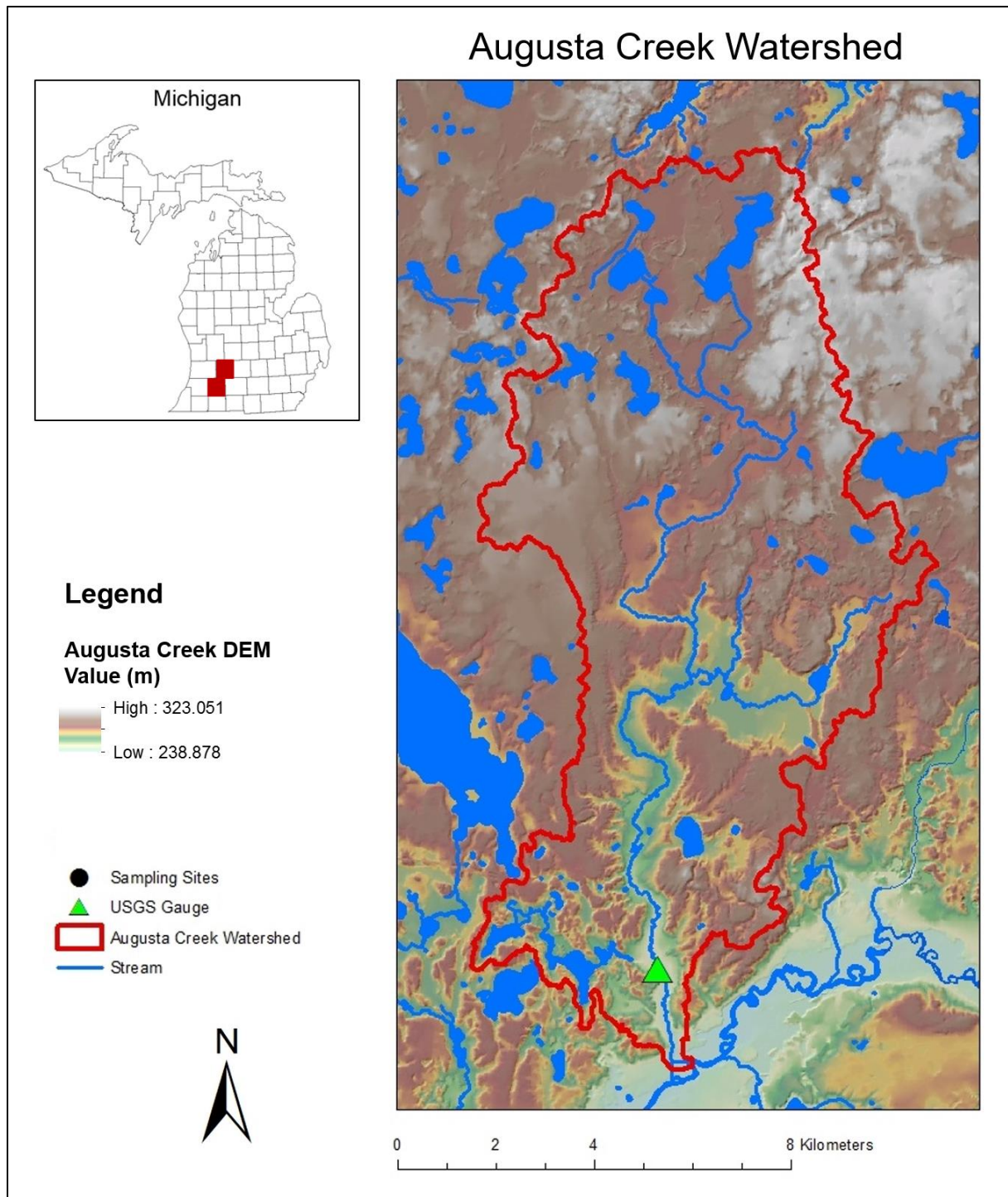


Figure 2: Topographic map of Augusta Creek watershed. Inset shows its location in Barry and Kalamazoo counties, Michigan, USA.

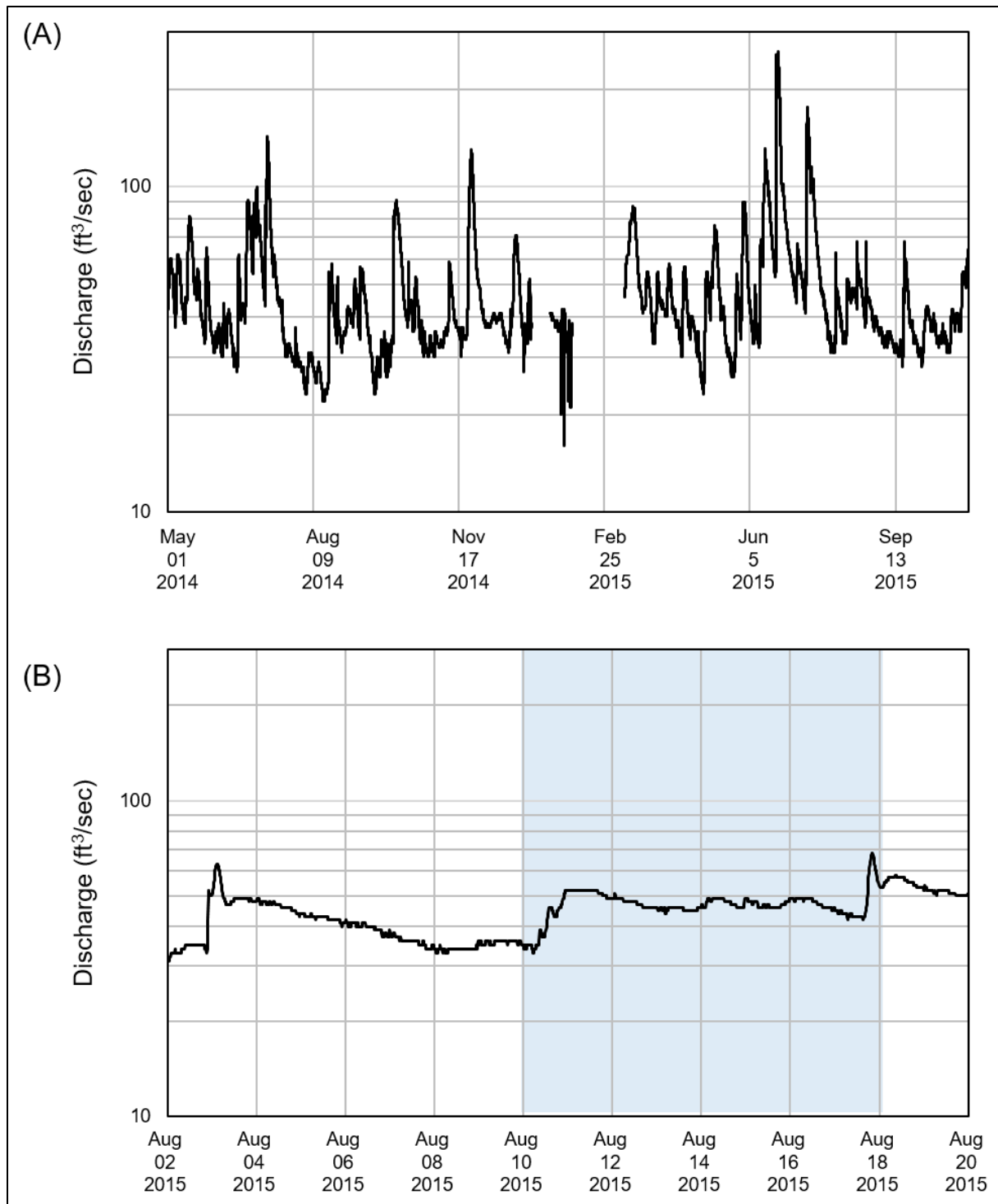


Figure 3: 2015 USGS hydrographs for Augusta Creek. Stream discharge data collected from the Augusta Creek gaging station, #04105700 from A) May 2014 – November 2015 and B) during the synoptic HZ sampling campaign from August 10 – August 18, 2015, highlighted in the blue shaded box. Data from US Geological Survey National Water Information System (nwis.waterdata.usgs.gov, accessed 4 Nov 2016).

2.3 Methods

2.3.1 Sample Collection

Hyporheic Zone porewaters, along with stream water and groundwater, were sampled at 16 sites across the Augusta Creek watershed (Figure 4) varying in land use/cover and stream order (Table A1). Hyporheic porewater samples were collected using a MINIPOINT porewater sampler, which is a custom-built system for temporary installation of nested piezometers (Duff et al., 1998; Figure 5A). The MINIPOINT consists of six 50 cm long by 0.5 cm-diameter piezometers arranged in a 10 cm-diameter circular array (Figure 5A). The piezometers are adjustable allowing for high-resolution, vertical porewater profile sampling that is minimally disruptive to the sediment column as well as the ambient chemical and biological processes occurring in the HZ (Duff et al., 1998). For this study, the 6 piezometers were vertically staggered at sediment depths of 2.5, 5.0, 7.5, 10, 15, and 20 cm. Three MINIPOINT samplers (for triplicate sampling) were deployed at each site as close together as possible (Figure 5B). The placement of MINIPOINTs was largely dependent on finding areas where the sediment type was conducive to the piezometers, which means samples were not collected in cobbly or clayey sediments that preclude installation of the sampler. Porewater samples were extracted using peristaltic pumps (i.e., Cole Palmer Masterflex L/S Peristaltic Pump) set at low flow rates (i.e., 1.5-2.5 mL min⁻¹) to minimize or eliminate the disturbances to the natural groundwater flow field (Harvey and Fuller, 1998). Approximately 60 mL of sample per depth was pumped into a 100-mL BD syringe that was connected with the peristaltic pump and corresponding piezometer using Tygon tubing with a 1.59-mm inner diameter and Masterflex Norprene Food Tubing with a 1.59-mm inner diameter. Samples were simultaneously collected from all 6 HZ depths. This was repeated for each of the three MINIPOINTs deployed at a site. In addition, a single stream water

sample per site, 60 mL in volume, was collected approximately 25-35 cm below the stream free-surface using a 10- mL BD syringe. A single groundwater sample per site, 60 mL in volume, was collected from a drive-point well installed to a depth of 60 cm below the stream-sediment interface. The drive-point well was purged and allowed to equilibrate before the sample was drawn directly into a 100-mL BD syringe. All samples (i.e., stream water, groundwater, and HZ) were filtered in the field using glass microfiber filters (i.e., Whatman GF/F 25 mm-diameter filters, 0.7 μm pore size) into 60-mL acid-washed HDPE amber bottles (to prevent photodegradation) and kept on ice as required by US EPA method 415.3 (Potter and Wimsatt, 2003). The samples were then filtered through cellulose acetate filters (i.e., Sartorius Stedim, 0.2 μm pore size) within 12 hours and stored at 4°C until analyzed (see Section 2.3.2).

Dissolved oxygen (DO) was measured at each site using a fiber-optic oxygen meter (i.e., Pyro Science FireStingO₂ with Robust Oxygen Probes, Pyro Science, Aachen, Germany). DO readings were taken at HZ depths of 2.5, 5.0, 10, and 20 cm from each MINIPOINT as well as for stream water and groundwater in conjunction with sample collection. In addition, temperature was measured once at each HZ depth and in the stream and groundwater samples using the fiber-optic oxygen meter. Lastly, sediment cores of the upper 20 cm of the stream bed were collected and used to determine the grain size distribution for each site, from which D₅₀ values were calculated (Table A1).

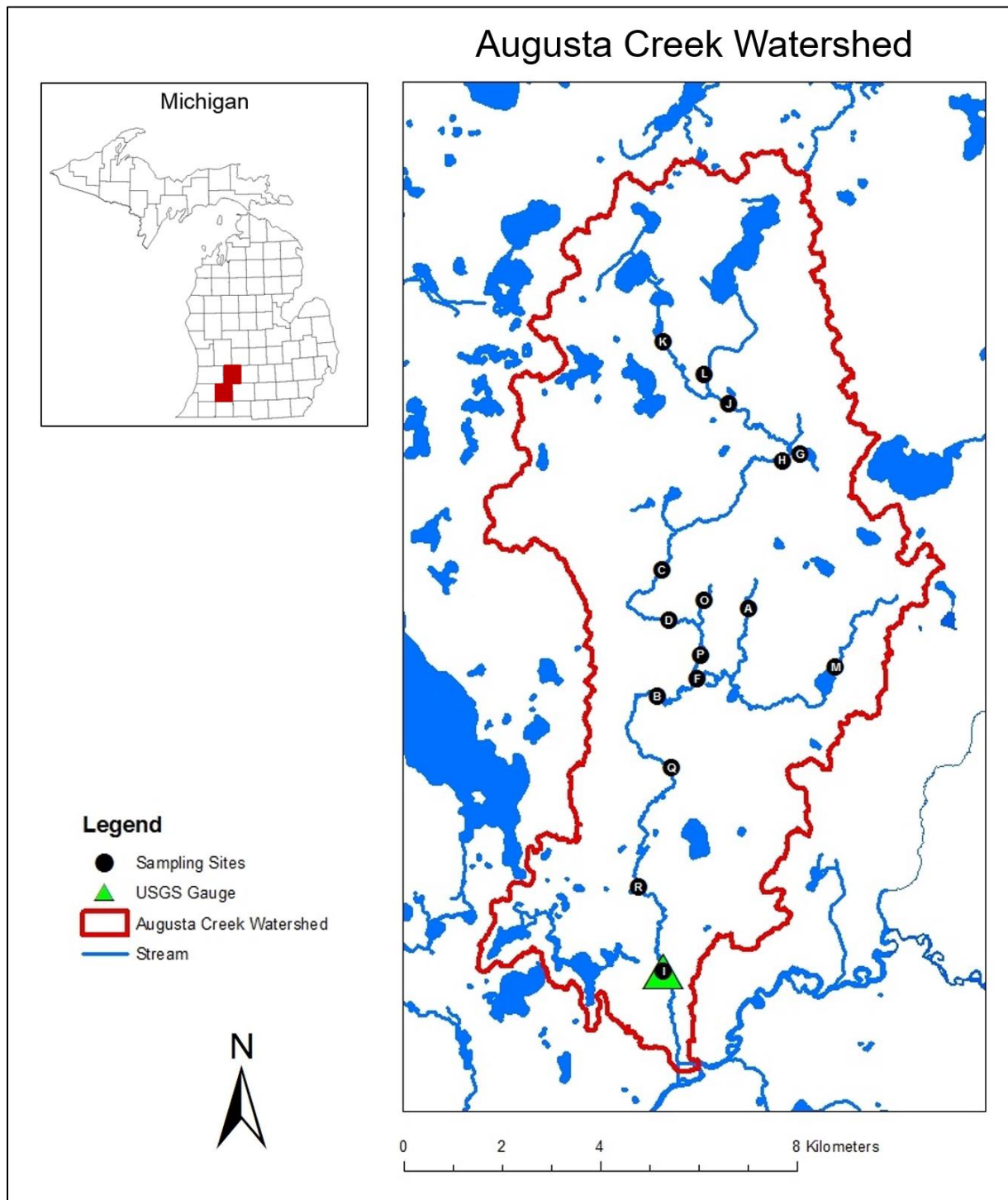


Figure 4: Map of Augusta Creek sampling sites in 2015. A map of the 16 sites sampled during the 2015 synoptic HZ sampling campaign across the third-order, groundwater-fed watershed of Augusta Creek, Michigan, USA.

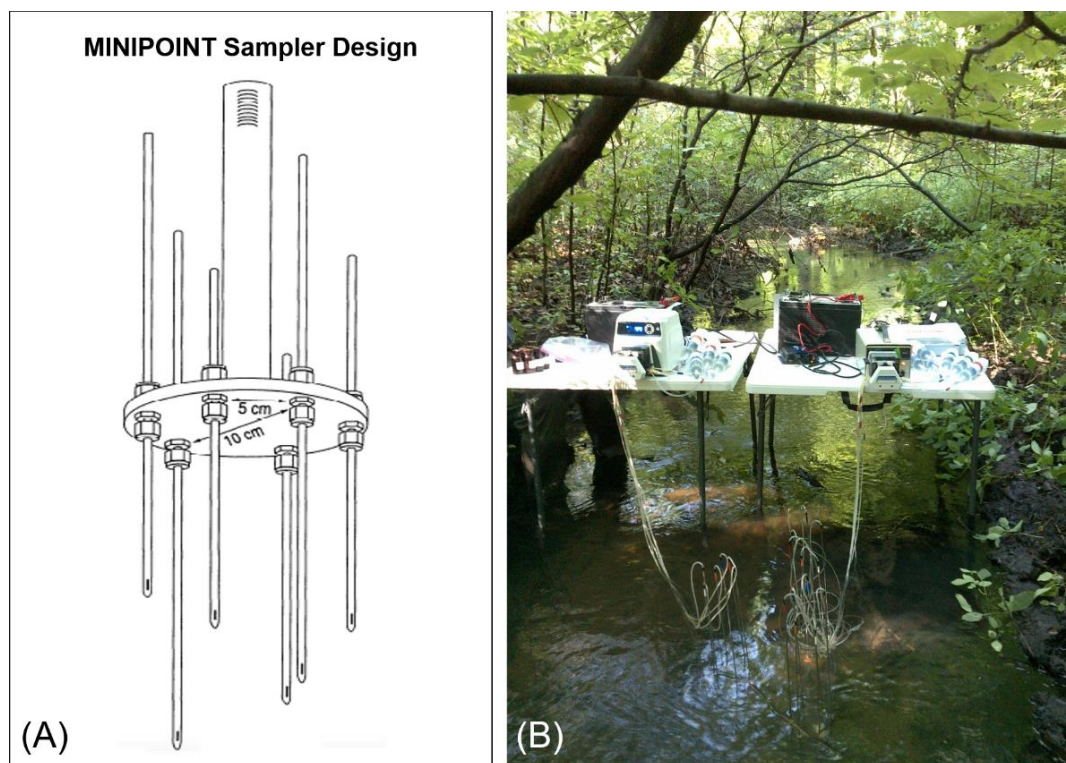


Figure 5: Sampling scheme. A) MINIPOINT sampler design (Duff et al., 1998) used for HZ sampling. B) Field setup used at each of the 16 sites sampled across Augusta Creek.

2.3.2 Analytical Methods

All samples were analyzed in the laboratory within 4 months of collection. DOC concentrations (reported as Non-Purgeable Organic Carbon, NPOC) were analyzed via high-temperature combustion using a Shimadzu TOC-L Analyzer (Shimadzu Scientific Instruments, Kyoto, Japan). In addition, a Dionex ICS-2100 ion chromatograph (Thermo Fisher Scientific, Massachusetts, USA) was used to analyze the samples for NO_3^- , Cl^- , and SO_4^{2-} concentrations. Ion analysis was completed using an AS19 Dionex IonPac column (2 x 250 mm) with a potassium hydroxide (KOH) eluent generator and a 0.25 mL/min flow rate. To infer DOC quality, optically-derived DOC variables were determined from absorbance data using a Shimadzu dual-beam UV 1800 spectrophotometer (Shimadzu Scientific Instruments, Kyoto, Japan). Absorbance readings were taken over the entire UV-VIS range from 220 to 800 nm using

semi-micro, BrandTech cuvettes with a 1-cm path length and EPure water (i.e., 18 ohm, Barnstead EPure system) as the blank. Each cuvette was triplicate rinsed with EPure water between samples. For calculations of the optically-derived variables see Section 2.3.3.

2.3.3 *Optical Indices*

The structural complexity of DOC makes it difficult to study DOC composition, which is a determining factor of DOC quality, via direct molecular techniques (Cory et al., 2011). Instead, several optical properties of DOC determined via ultraviolet-visible (UV-VIS) absorbance spectroscopy can be used to assess the chemical structure and thus the quality of DOC (e.g., Weishaar et al., 2003; Cory et al., 2011; Jollymore et al., 2012; Creed et al. 2015). In this study, specific ultraviolet absorbance at a wavelength (λ) of 254 nm (i.e., $SUVA_{254}$) was used to indicate DOC aromaticity. $SUVA_{254}$ is obtained by measuring the sample's absorbance at $\lambda=254$ nm and dividing by the DOC concentration of the sample (Equation 2.1; units are L/mg C/m).

$$SUVA_{254} = \frac{\text{Absorbance}_{254 \text{ nm}}}{\text{DOC concentration}} \quad (2.1)$$

A $\lambda=254$ nm is used because electron structures associated with aromatic C molecules absorb energy at this wavelength, while other structures do not (Weishaar et al., 2003). Therefore the absorbance reading is directly related to the amount of aromatic C within the total DOC sample. Higher $SUVA_{254}$ values are associated with increased aromaticity (Table 1; Weishaar et al., 2003).

The optical data were also used to calculate a spectral slope ratio (S_R) for each sample. S_R is used as a proxy for molecular weight; S_R increases with decreasing molecular weight (Table 1; Helms et al., 2008). To calculate S_R , absorbance values were measured over 220 to 800 nm and a ratio of the slopes of the 275 – 295 nm ($S_{275-295}$) absorbance spectra and the 350 – 400 nm ($S_{350-400}$) absorbance spectra was calculated (Equation 2.2).

$$S_R = \frac{S_{275 \text{ nm} - 295 \text{ nm}}}{S_{350 \text{ nm} - 400 \text{ nm}}} \quad (2.2)$$

A summary of the optical indices and their relationship to DOC molecular characteristics is provided in Table 1.

Table 1: Summary of optical DOC indices

Optical Indices	Aromaticity	Molecular Weight
SUVA ₂₅₄	Positive Correlation	
Spectral Slope (S _R)		Negative Correlation

2.3.4 Vertical Porewater Profiles

To observe trends in DOC quantity and quality, vertical porewater profiles of the optical properties as well as the sampled chemical species were created for each site using mean and standard deviation of the triplicate hyporheic samples (e.g., DOC concentrations measured from a depth of 2.5 cm in MINIPOINT 1, 2, and 3), which was compared with the stream water and groundwater values (Figure 6).

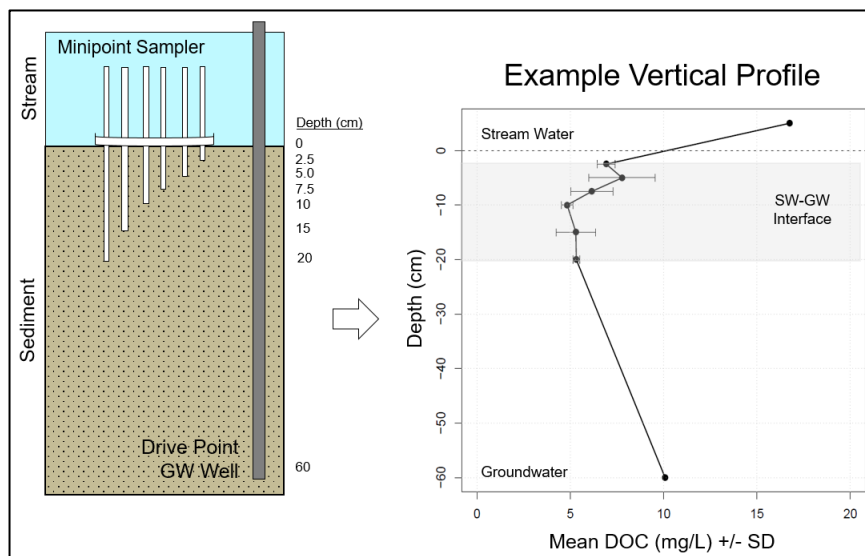


Figure 6: Example of a vertical porewater profile. The sediment interface (i.e., 0 cm) is shown by the dashed line.

2.4 Results

The average DOC concentration in stream water collected from the 16 sampling sites was 9.97 mg/L, which falls within the previously reported range for DOC concentrations in Augusta Creek of 2-12 mg/L (Hamilton, unpublished data). The range of DOC measured in stream water was 6.17 to 16.75 mg/L with a median value of 9.73 mg/L. For groundwater, the average DOC concentration across the watershed was lower than that of stream water at 6.62 mg/L and ranged from 3.06 to 16 mg/L with a median value of 5.76 mg/L.

2.4.1 Results of the Vertical Porewater Profiles

Individual vertical porewater profiles of DOC concentration, DO, SUVA₂₅₄, and S_R for all 16 sites were averaged to create a composite vertical porewater profile, representative of the average DOC conditions in the HZ across Augusta Creek (Figure 7, graphs labeled “All Sites”). Vertical profiles were also grouped by stream order and then averaged, to create vertical profiles representative of average HZ DOC conditions within each stream order.

The vertical profiles show decreasing DOC concentrations with depth through the HZ (i.e., 2.5 – 20 cm), for the watershed-wide mean profile as well as the mean profiles for each stream order (Figure 7A). However, a slight increase in DOC concentration was observed between depths 7.5 and 10 cm in the third-order vertical profile (Figure 7A), which may be due to outliers such as Site F (Figure A6), which exhibited an increase in DOC concentration at intermediate HZ depths. DOC concentrations at the 2.5 cm depth were lower than the DOC concentrations observed in the stream channel for all averaged vertical profiles. In addition, all of the averaged profiles exhibited lower DOC concentration at deeper HZ depths (e.g., 10, 15, and/or 20 cm) than observed in the underlying groundwater.

Dissolved oxygen also exhibited decreasing concentration with HZ depth in the watershed mean profile and in the mean profiles of each stream order (Figure 7B). The stream water across Augusta Creek was oxygenated with DO levels greater than 5 mg/L during the sampling campaign, while the groundwater measurements taken from 60 cm in depth show oxygen depletion to 2 mg/L or less. Groundwater DO was not measured at first-order sites due to interference of clay layers and problems with the fiber-optic oxygen meter. An increase in DO between depths 15 and 20 cm is observed in the third-order vertical profile, and thus also reflected in the watershed averaged vertical profile. Again, this increase may be the result of several outliers (see Appendix A).

Regarding the optical properties, decreasing $SUVA_{254}$ values were observed in the watershed mean profile and in the mean profiles for each stream order (Figure 7C). However, the first-order vertical profile showed an increase in $SUVA_{254}$ at intermediate HZ depths, which may also be the result of outliers, including Site L (Figure A12). Lastly, S_R showed slight increases with HZ depth in the watershed vertical profile, the first-order vertical profile, and third-order vertical profile, while the second-order profile exhibited decreasing S_R values, especially at deeper (i.e., > 10 cm) HZ depths (Figure 7D).

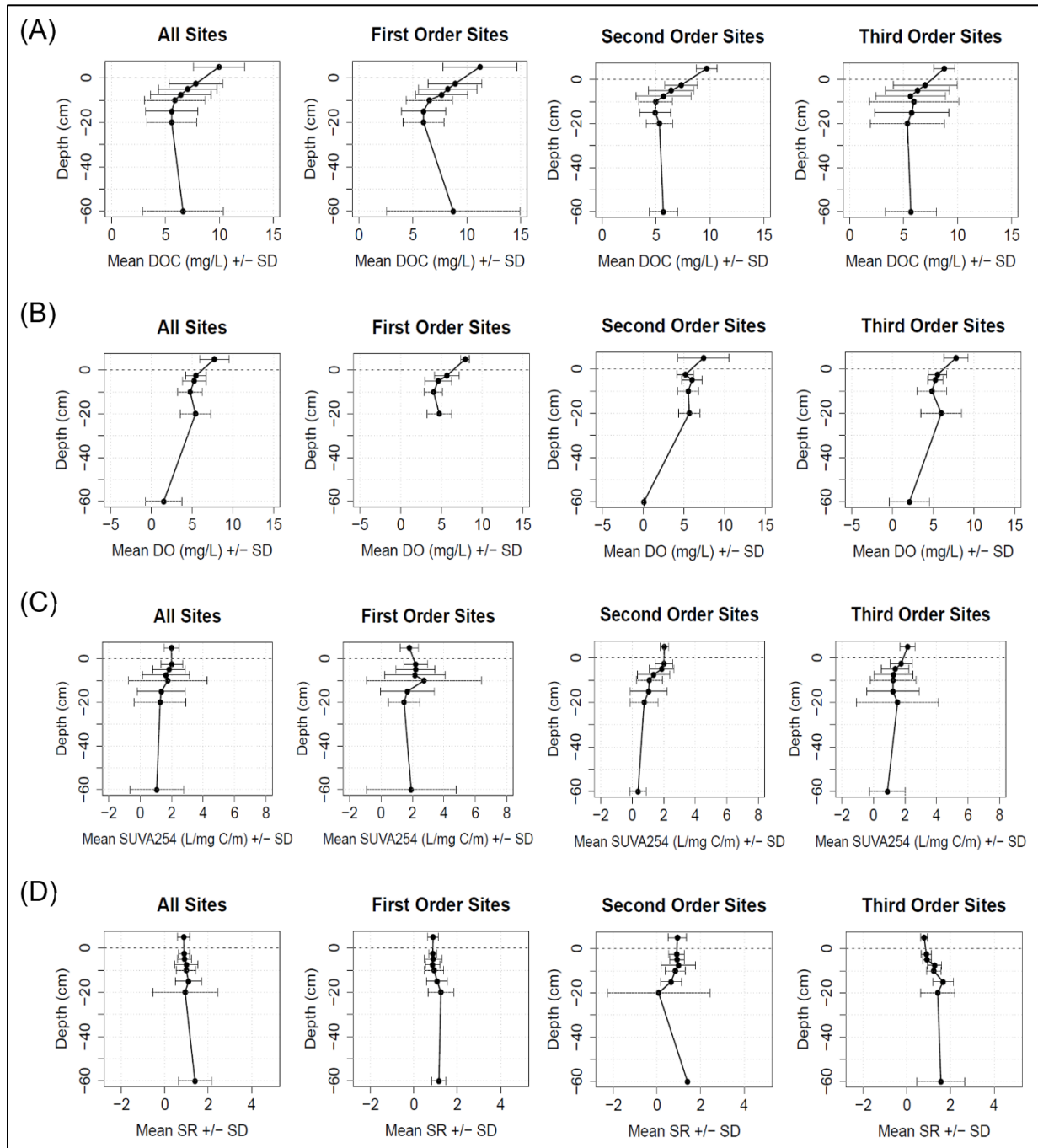


Figure 7: Vertical porewater profiles of DOC concentration and optical indices. Vertical profiles of A) mean DOC, B) mean DO, C) mean SUVA₂₅₄, and D) mean S_R of all 16 sites and by stream order. Each plot includes standard deviation bars; n=16 for “all sites”, n=6 for “1st order sites”, n=5 for “2nd order sites” and n=5 for “3rd order sites.”

2.4.2 DOC Variance and Mixing Zone Model

The averaged vertical profiles showed increased variance (shown as SD) at intermediate HZ depths (i.e., ~7.5 to 15 cm) for DOC concentration and SUVA₂₅₄ (Figure 7A, C). An exception to this is the averaged profile for SUVA₂₅₄ across third-order sites, which showed maximum variance at 20 cm. S_R also exhibited increased variance at deeper HZ depths (i.e., ~20 cm), especially for second-order sites (Figure 7D).

It is important to note that while stream water variance is small (with the exception of DOC concentration for first-order sites), groundwater variance for both DOC quantity and quality indicators was significantly larger than expected (e.g., see first-order sites for DOC concentration; Figure 7A). Considering that many of the sampling sites are likely groundwater upwelling areas (see Section 2.2.1), the trends in DOC conditions observed in Figure 7 may be influenced by the variable chemistry of upwelling groundwater. As a way to verify that the trends we are observing are the result of HZ processes and not due simply to variable contributions of upwelling groundwater, a mixing zone model was created to identify the subsurface depths that showed a mixing signal (Figure 8). This was done since strong groundwater upwelling could condense the mixing zone (i.e., HZ) to depths shallower than 20 cm (e.g., Boano et al., 2014; Creed et al., 2015).

To identify the mixing zone within the overall vertical profile, we used a conservative (i.e., non-reactive) chemical, specifically chloride (Cl⁻), in combination with temperature to observe the depth (i.e., shallower than 60 cm) at which the groundwater signal ended and the profile shifted to resembling a mixing signal of both groundwater and stream water (e.g., Peters and Ratcliffe, 1998). Figure 8 presents the conceptual model used to identify the mixing zone.

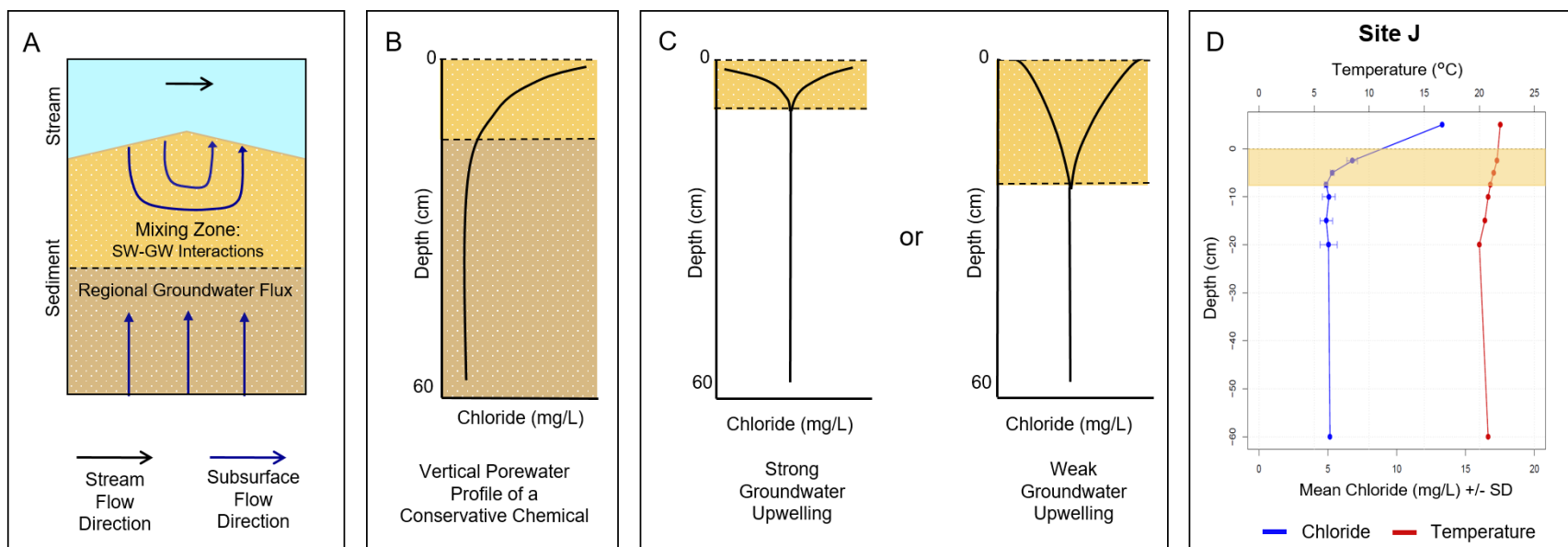


Figure 8: Model used to identify mixing zone depths. A) Conceptual model of the SW-GW interactions in a simple stream bedform and B) the resulting vertical porewater profile of a conservative chemical. C) The vertical profile for a conservative chemical can deviate from the groundwater signal such that the concentration decreases or increases to the streambed surface, based on the concentration of the chemical in the stream water. The depth at which the profile deviates from the groundwater signal is indicative of the groundwater flux (i.e., weak or strong). D) For Site J the Cl^- concentration deviates from that of groundwater at a depth of 7.5 cm. The temperature profile is used in support of the interpretation of the Cl^- profile.

Within a simple stream bedform (e.g., a small ripple), underlying groundwater will upwell towards the stream-sediment interface where it will then meet downwelling stream water at a given depth to create a zone in which SW-GW interactions occur (i.e., the HZ; Figure 8A). If concentrations differ between stream water and groundwater, conservative chemicals like Cl^- can be used to determine the extent of the mixing zone. A vertical porewater profile of Cl^- concentrations will resemble the Cl^- concentration of groundwater at all depths below the mixing zone (Figure 8B). Within the SW-GW mixing zone, the Cl^- concentrations will reflect the relative proportions of stream water and groundwater (e.g., dilution, Figure 8C). Thus, the Cl^- concentrations indicate the extent of the mixing zone (Figure 8B and C). In addition, temperature behaves similarly to conservative chemicals and will resemble groundwater temperature until the mixing zone is reached where temperature will begin to vary. Therefore, temperature profiles were used to support the interpretation of Cl^- profiles.

As an example, Figure 8D shows how the mixing zone was qualitatively determined for Site J, where the Cl^- concentration indicates stream water influence to a depth of 7.5 cm. Therefore the mixing zone for Site J exists between depths of 0 and 7.5 cm. This process was repeated for all 16 sites (Table A1) and new vertical profiles representative of the average mixing zone for the watershed and each stream order were recalculated and are presented in Figure 9.

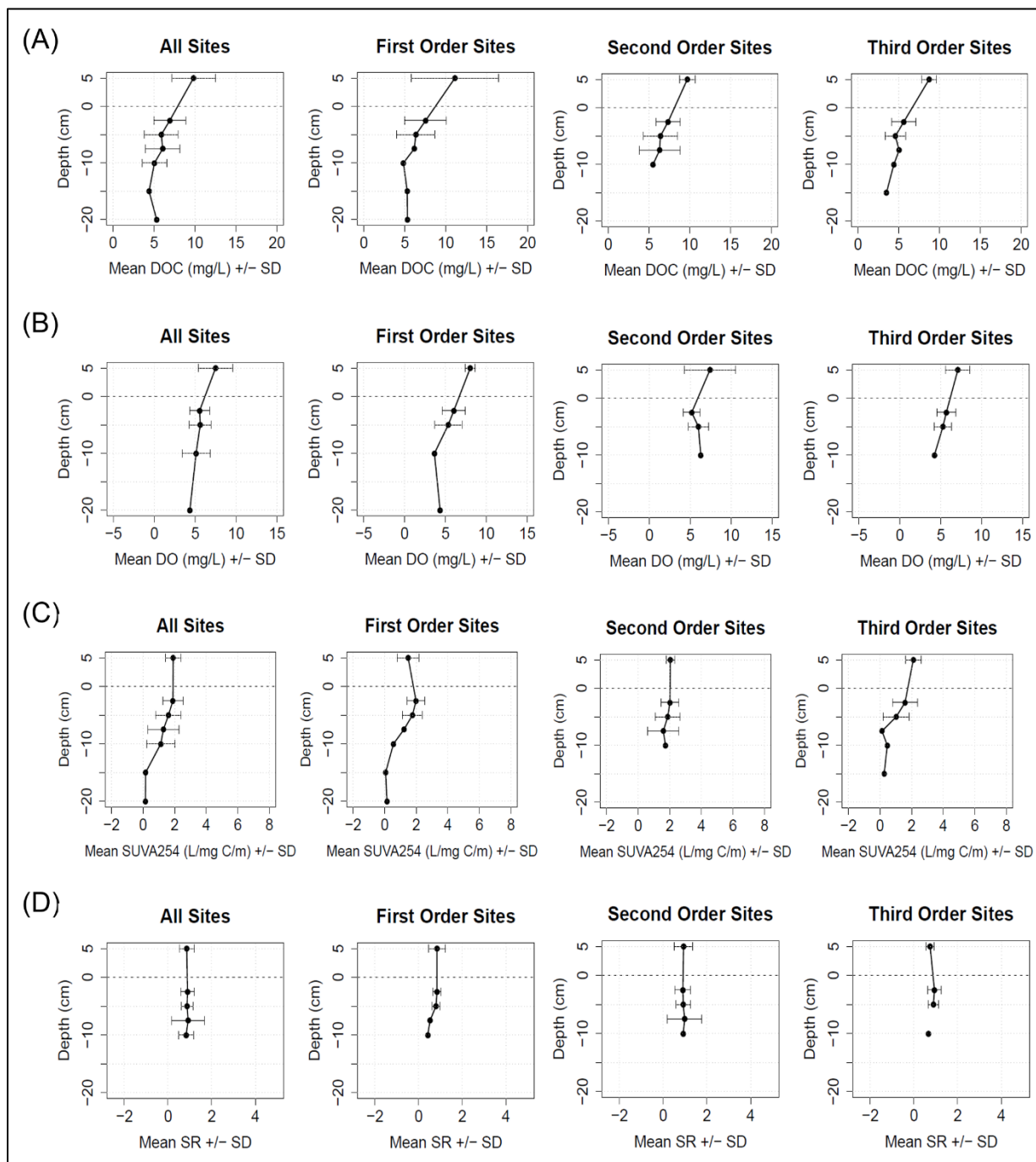


Figure 9: DOC concentration and optical indices within the mixing zone. Vertical profiles of A) mean DOC, B) mean DO, C) mean SUVA₂₅₄, and D) mean S_R including only depths with a mixing zone signal. Standard deviation was calculated for all depths where n > 3.

The vertical profiles of the averaged DOC quantity and quality conditions created using the mixing zone model only extend to a depth of 20 cm or shallower since the groundwater samples taken at 60 cm depth are assumed to be below the mixing zone. In addition, error bars are only included where $n > 3$. Along the mixing zone profile for the watershed and for each stream order, DOC concentration, DO (with the exception of the second-order profile) and $SUVA_{254}$ decreased with depth, while S_R trends remained relatively stable, showing slight decreases at deeper mixing zone depths (i.e., ~10 cm; Figure 9). These trends are consistent with those observed in Figure 7. However, after identifying the mixing zone and using only depths with a mixing zone signal, the vertical profiles for the watershed and each stream order showed smaller changes in variance between stream water and mixing zone depths (i.e., more consistent variance is observed along the profile) for DOC concentration, DO, $SUVA_{254}$ and S_R (Figure 9). Additionally, in some cases, the variance observed in the stream water was larger than the variance seen at mixing zone depths (e.g., Figure 9A, B). Lastly, it was observed that the mixing zone becomes shallower (i.e., does not extend as far into the sediment) as stream order increases, as exhibited by the shortened vertical profiles for all variables across second- and third-order sites (Figure 9).

2.5 Discussion

The averaged vertical profiles (see Section 2.4.1, Figure 7A) as well as most (i.e., 14 out of 16) of the individual site profiles (see Appendix A) showed decreasing DOC concentration with depth through the HZ. This supports the first prediction that DOC concentration will decrease with increasing HZ flowpath length and is in agreement with previous findings from small-scale field and mesocosm studies, suggesting that the HZ acts as a sink for DOC in this stream network (Findlay et al., 1993; Findlay and Sobczak, 1996; Schindler and Krabbenhoft, 1998; Sobczak and Findlay, 2002; Zarnetske et al., 2011). Furthermore, DOC in the HZ decreased to concentrations lower than that of stream water or groundwater, indicating that mixing of the two end members (i.e., SW and GW) alone cannot account for the observed decreases in DOC concentration (e.g., Pinder and Jones, 1969). Thus, physicochemical and/or biological reactions are most likely occurring in the HZ, consuming DOC.

One potential processing mechanism of DOC in the HZ is aerobic, microbial respiration (i.e., consumption of DOC and release of CO₂). Aerobic, microbial respiration will result in decreased DOC concentrations with concomitant consumption of DO (e.g., Findlay and Sobczak, 1996). Likewise, aerobic, microbial respiration will alter DOC quality by preferentially respiring the more labile fraction, resulting in lower molecular weight and less aromatic residual DOC (e.g., McKnight et al., 2001; Fellman et al., 2010; Cory et al., 2011; Mann et al., 2012; Creed et al., 2015; Helton et al., 2015). The DO profiles showed decreasing DO with depth in the HZ, which supports the hypothesis of aerobic, microbial respiration. In addition, SUVA₂₅₄ and hence the aromaticity of DOC decreased with depth in the HZ (with the exception of first-order intermediate depths, Figure 7C). S_R exhibited a slight increase with depth in the HZ, indicating a decrease in the mean molecular weight of DOC (Table 1, Weishaar et al., 2003; Helms et al.,

2008). Both optical properties therefore suggest that the DOC in the HZ changes as a result of microbial processing, thus supporting the second prediction.

When observing the trends in variance for DOC quantity and quality, variance increased in the HZ, supporting the third prediction. However, the groundwater variance was larger than expected (Figure 7) since regional groundwater should be relatively homogenized (i.e., chemically) due to longer flow paths and increased residence times (e.g., Vannote et al., 1980; Boano et al., 2014). The larger variance might result from the groundwater having a more variable chemistry than previously acknowledged or the sampling depth of 60 cm may not fully represent the regional groundwater. In addition, since Augusta Creek is groundwater-fed, upwelling groundwater may limit the extent of the HZ, resulting in a smaller region of SW-GW interactions (e.g., Cardenas and Wilson, 2007; Boano et al., 2009).

Therefore as described in Section 2.4.2, a mixing zone model was used to identify the mixing zone at each site to determine if the observed DOC trends in the averaged vertical profiles were the result of strong groundwater upwelling or HZ processes. For most sampled sites across Augusta Creek, the mixing zone did not extend to 20 cm (Table A1). However, once the vertical profiles were adjusted to account for shallower mixing zones, it was observed that the DOC quantity and quality variables showed trends consistent with the results presented in Figure 7, supporting the hypothesis of DOC processing (likely via aerobic, microbial respiration) in the HZ (Figure 9). However, smaller changes in variance were observed between stream water and hyporheic depths (i.e., more consistent variance was observed along the profile) for DOC concentration, DO, SUVA₂₅₄ and S_R (Figure 9) and in some cases, the variance observed in the stream water was larger than the variance seen within the HZ (e.g., Figure 9A, B).

This observation of decreased variance observed at subsurface depths when using the mixing zone model no longer supports the third prediction. However, this may be the result of not capturing all of the variation within DOC quantity and quality variables due to the decreased sample size. It may also indicate that the biogeochemical transformation mechanisms in the HZ result in a homogenized pool of DOC. Lastly, mixing zone profiles also showed that the extent of the HZ decreased as stream order increased, indicating that the influence of HZ processes on stream C cycling may change across the stream network.

Overall, these findings indicate that the HZ is a location for net removal of DOC in this river network and that the processing signal can be observed at larger scales (i.e., across the entire watershed and within stream orders), as demonstrated from the averaged vertical porewater profiles (Figure 7). In addition, the optical indices used to infer DOC quality suggest that aerobic, microbial respiration may be an important processing mechanism in the HZ.

However, there are several remaining questions:

- 1) What is the dominant transformation mechanism(s) consuming DOC in the HZ?
- 2) Is the dominant transformation mechanism consistent across the river network?
- 3) Is the potential for DOC transformation in the HZ consistent across the river network?
- 4) Does the net removal of DOC occur all year? It could be lesser in cooler seasons, or greater during autumn leaf fall and consequent leaching of labile DOC, or during spring peaks in epilithic algal production.

To more accurately assess the dominant transformation mechanisms (e.g., biotic vs. abiotic processes) and how they vary across the watershed, vertical profiles from individual sites need to be analyzed. In addition, by studying DOC dynamics within the HZ on a site-by-site basis, we can also gain an understanding of not only how the HZ transforms DOC (e.g., the

dominant transformation mechanism(s), source vs. sink), but also if the potential for transformation of DOC in the HZ changes based on location in the watershed. As discussed, the mixing zone vertical profiles from this study (Figure 9) showed that the depth of the HZ decreased as stream order increased. This would suggest that the potential for DOC transformation (e.g., consumption) in the HZ changes across stream order, with the HZ having a higher potential to process DOC in headwater streams than in larger stream orders (e.g., Vannote et al., 1980; Boano et al., 2014; Creed et al., 2015).

Additional chemical (e.g., improved DO measurements) and hydrological data (e.g., vertical head gradient, improved groundwater measurements) need to be collected at each site, and more sites need to be sampled across the watershed to address these remaining questions. Thus, a second synoptic HZ sampling campaign was conducted in August 2016 and the results are presented in Chapter 3.

2.6 Conclusions

Hyporheic Zone trends in DOC quantity and quality observed from the 2015 watershed-scale synoptic sampling campaign across the Augusta Creek watershed support findings from earlier small-scale field and mesocosm studies, indicating that the HZ is a location for processing of DOC and likely acts as a net sink for DOC in this river network. However, in strongly gaining, groundwater-fed, stream networks, the depth of the SW-GW mixing zone (i.e., HZ) may be limited. Thus, it is important to be able to quantify the depth of the HZ when studying processes at the SW-GW interface. Additionally, more detailed chemical (e.g., DO) and hydrological data are needed to accurately identify processes driving DOC transformations in the HZ (e.g., aerobic, microbial respiration) and how the role (e.g., source vs. sink) of the HZ changes across river networks as well as at individual sites. Nonetheless, this study has highlighted a potentially important location for DOC processing in streams and therefore the HZ may need to be accounted for in C budget models.

CHAPTER 3: DETERMINING HOW DISSOLVED ORGANIC CARBON IS TRANSFORMED AT THE STREAM-GROUNDWATER INTERFACE ACROSS A THIRD-ORDER, LOWLAND RIVER NETWORK

3.1 Introduction

To understand the role of the hyporheic zone (HZ) in stream carbon (C) cycling, studies of HZ processes need to be conducted at the watershed scale (e.g., Boano et al., 2014). In Chapter 2, we used synoptic sampling of the HZ across a third-order, lowland watershed to assess if dissolved organic carbon (DOC) processing was occurring within the HZ. The findings indicate that the HZ is a location for DOC processing in this river network and that the processing signal is observable at the watershed scale. Yet, questions remain about how DOC is processed in the HZ at the watershed-scale. For example, in Chapter 2 we were able to show that on average DOC was consumed (i.e., removed from solution) over HZ depths by using “composite” or averaged vertical porewater profiles to study trends in DOC quantity and quality. This, suggests that the HZ may act as a sink for DOC in this stream network (e.g., Sobczak and Findlay, 2002). However, we could not fully identify the dominant biogeochemical transformation mechanisms (e.g., biotic vs. abiotic processes) consuming DOC in the HZ, even though we presented evidence that microbial respiration may be important.

This chapter focuses on identifying the dominant biotic (e.g., aerobic, microbial respiration) or abiotic (e.g., adsorption to sediments) biogeochemical processes driving DOC transformations in the HZ and on assessing how the role of the HZ as a processor of stream DOC varies across a river network (e.g., varying processing mechanisms, varying potential for transformation). This is accomplished at the network scale by utilizing hyporheic trends in DOC quantity and quality, improved dissolved oxygen (DO) measurements and local flow patterns (i.e., upwelling vs. downwelling) on a site-by-site basis. The central research questions are: 1)

how is DOC processed (i.e., consumed) in the HZ? and 2) does the potential for DOC transformation (i.e., the processing potential) in the HZ change based on location (e.g., stream order) in the stream network?

Previous work demonstrated that the HZ is a zone with high biological diversity, strong chemical gradients (e.g., Valett et al., 1996; Hedin et al., 1998; Findlay and Sobczak, 2000; Zarnetske et al., 2011; Nogaro et al., 2013; Boano et al., 2014) and increased residence times (e.g., Battin et al., 2008; Harvey et al., 2013; Boano et al., 2014), all of which promote biotic processes (e.g., microbial metabolism). Additionally, previous work has shown that DOC sorption to sediments (i.e., abiotic processes) also occurs in the HZ (e.g., McDowell, 1985; Fiebig and Lock, 1991; Findlay and Sobczak 1996). While, abiotic sorption of DOC to hyporheic sediment does occur, it is limited by sorption sites and will equilibrate with the DOC concentration of upwelling/downwelling waters (e.g., Day et al., 1994; Kaplan and Newbold, 2000). Thus, for continued sorption of DOC, the previously sorbed DOC must be removed via microbial metabolism in order to regenerate sorption sites (e.g., Kaplan and Newbold, 2000). Therefore, on short time scales, sorption of DOC to hyporheic sediments should not be a significant or consistent sink for DOC in the HZ (e.g., Dahm, 1981; Fiebig, 1995).

Given the assertion that abiotic sorption would have limited influence on DOC concentrations, we hypothesize that biotic processes, rather than abiotic processes, are predominantly transforming DOC in the HZ. Specifically, we hypothesize that aerobic, microbial respiration is the dominant transformation mechanism consuming DOC in the HZ and thus, the HZ acts as a sink for DOC in this river network. If true, then we predict that:

- 1) Decreasing DOC and DO concentrations will be observed with increasing HZ depth throughout the watershed.

- 2) $SUVA_{254}$ will decrease with depth in the HZ, while S_R will increase with depth in the HZ, indicating the presence of less aromatic and lower molecular weight DOC.

In addition, we hypothesize that the potential for DOC transformation in the HZ varies across the watershed, assuming that a framework similar to the River Continuum Concept also applies to the stream water-groundwater (SW-GW) interface (Vannote et al., 1980). If this second hypothesis is true, then we predict that:

- 1) The processing potential of the HZ (i.e., acting as a consumer/sink) of stream DOC will become less significant with increasing stream order, exhibited by lower rates of consumption of DOC and lower rates of change in the DOC quality indicators.
- 2) The processing potential of the HZ will be less significant at sites where upwelling groundwater limits the SW-GW mixing depth, again exhibited by lower rates of consumption of DOC and lower rates of change in DOC quality indicators.

Prediction 1 is based on changes in chemical and physical conditions along the stream channel (e.g., Vannote et al., 1980; Battin et al., 2008). For example, changes in channel slope and streambed morphology tend to limit surface-subsurface exchange in higher stream orders (Battin et al., 2008). In addition, subsurface flowpaths that feed higher stream orders also tend to be more homogenized (i.e., lower chemical variation) due to longer residence times, limiting microbial reactivity (Battin et al., 2008; Harvey et al., 2013; Boano et al., 2014). Furthermore, the stream also becomes less connected to adjacent wetlands and the terrestrial landscape as stream order increases, reducing inputs of complex allochthonous (e.g., terrestrial vascular-plant derived) DOC (Vannote et al., 1980). For prediction 2, upwelling groundwater may limit the extent of the HZ, resulting in a smaller region of SW-GW interactions, limiting HZ processing of DOC (e.g., Cardenas and Wilson, 2007; Boano et al., 2009).

To test these predictions, a second synoptic HZ sampling campaign was conducted in 2016 across Augusta Creek in southwestern Michigan, USA (42°21'12"N, 85°21'14"W). A total of 39 sites were sampled, covering more of the watershed than in the 2015 survey discussed in Chapter 2, and additional chemical and hydrological (e.g., vertical head gradient) measurements were taken to improve our ability to identify changes in DOC quantity and quality and to assess DOC transformation mechanisms.

3.2 Background

3.2.1 Field Site Description

A synoptic HZ sampling campaign was conducted over an 8-day period in August 2016 across the Augusta Creek watershed, which is located in Barry and Kalamazoo counties in southwestern Michigan and is part of the larger Kalamazoo River watershed (see Chapter 2, Figure 2). This watershed was selected as the field site because Augusta Creek is a historically important stream for biogeochemical and ecological research (e.g., it was an original River Continuum Concept site; Vannote et al. 1980), has a long-term and active United States Geological Survey (USGS) gaging station (04105700), and is easily accessible through roadways and university lands. The geology of the watershed has been heavily influenced by glacial activity (i.e., ice advancement and retreat), most recently in the late Pleistocene Epoch (Dunbar, 1962). As a result, the watershed is underlain by deep glacial drift deposits consisting of mixtures of gravel, sand, silt, and clay, varying in thickness from 40 to 120 m across the watershed (FTWRC, 2011).

Augusta Creek is a third-order, lowland watershed draining 98 km² (see Chapter 2, Figure 2; Strahler, 1957). Most of the tributaries originate in groundwater-fed lakes and low-lying wetlands (Manny and Wetzel, 1973; FTWRC, 2011). The three dominant land cover types are 1) 47% agriculture (crops and pastures), 2) 23% upland forest (mainly deciduous), and 3) 20% wetland/marsh complexes (FTWRC, 2011; Figure A1). The mean annual precipitation is 925 mm, while the total precipitation in 2016 was 975 mm (FTWRC, 2011; KBS-LTER, Dataset KBS002). Soils are typically sandy to loamy in uplands, with organic (muck) soils in the riparian wetlands, and patches of muck along the stream channel (FTWRC, 2011). Soil infiltration rates throughout the watershed range from 12.7 to 25.4 mm/h and the mean stream slope is

approximately 2.03 m/km (Manny and Wetzel, 1973; FTWRC, 2011). In addition, clay and marl (CaCO₃-rich) lenses are found throughout the streambed sediments.

In terms of stream chemistry, Augusta Creek is a hard water stream with a total hardness of about 280 mg/L (Mahan and Cummins, 1974; King 1978). Alkalinity typically ranges from 160 to 210 mg/L as CaCO₃, while pH ranges from 7.5 to 8.7 (Manny and Wetzel, 1973; Mahan and Cummins, 1974; King, 1978). Calcite (CaCO₃) precipitates are often found on stones on the stream bottom. Sampling of Augusta Creek from 1997-2015 has shown that stream DOC concentrations typically range from 2 to 12 mg/L (Hamilton, unpublished data)

3.2.2 Hydrology

Augusta Creek exhibits a discharge flow regime characterized as having minimal within- and among-year variation (Url and Hart 1992, Poff et al., 1997). Based on recent and historical discharge measurements collected at the USGS gaging station (04105700) located on the lower main stem above the Kalamazoo River confluence (Figure 11), Augusta Creek discharge typically varies between 0.57 to 2.83 m³/s, with occasional peak flow events. This range in discharge was observed from August 2015 – August 2016 (with the exception of a peak flow event in late August 2016) as well as over several years prior (Figure 10A). The synoptic HZ sampling campaign took place from August 15 – August 22, 2016, during which the average discharge was 1.35 m³/sec, higher than the previous 5-year average of 1.08 m³/sec for the month of August (USGS, 2017, Station 04105700). During the sampling period, discharge varied some from 1.08 to 3.65 m³/sec, with one notable precipitation event on August 15 and another smaller precipitation on August 21 (Figure 10B).

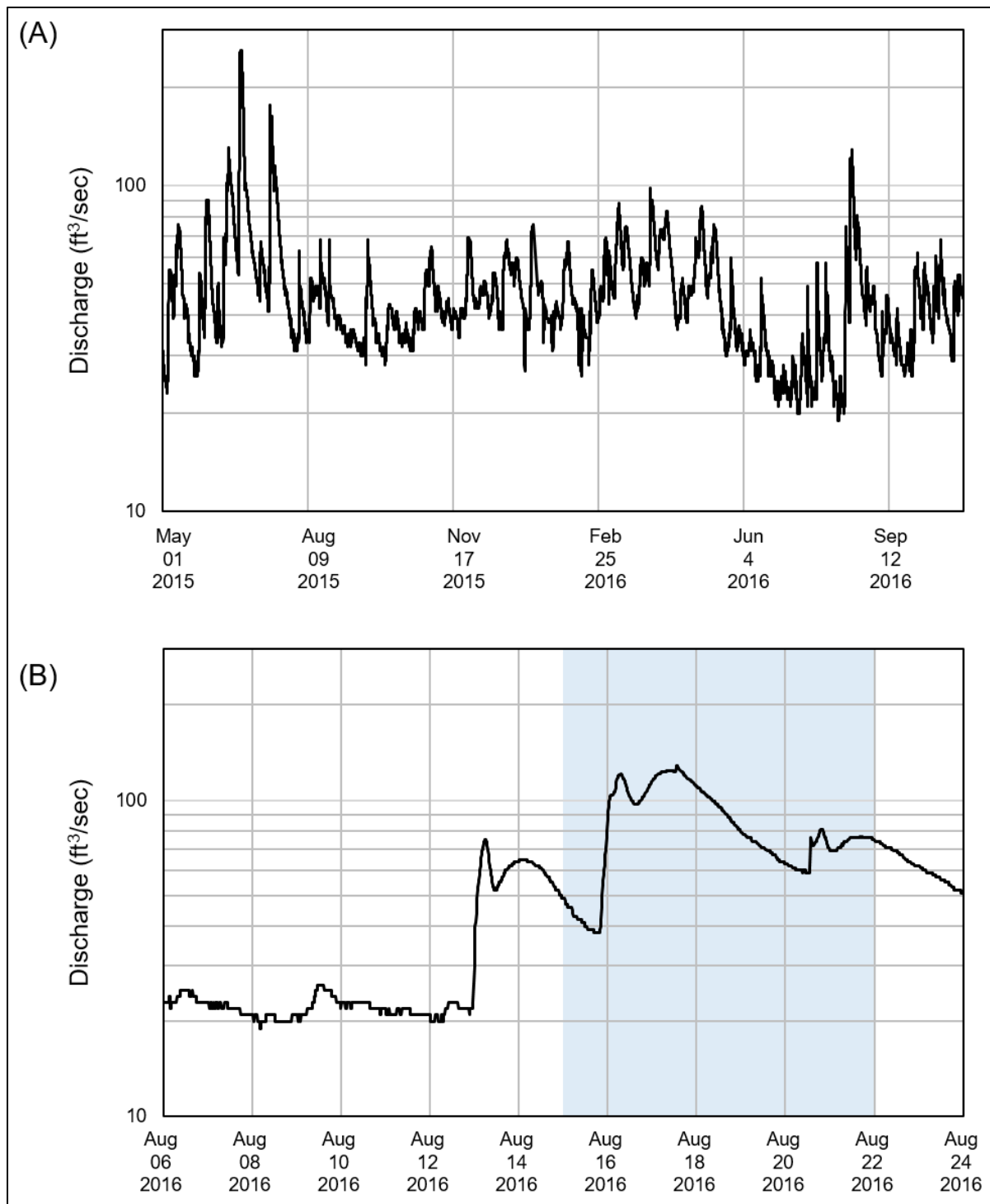


Figure 10: 2016 USGS hydrographs for Augusta Creek. Stream discharge data collected from the Augusta Creek gaging station, #04105700 from A) May 2015 – November 2016 and B) during the synoptic HZ sampling campaign from August 15 – August 22, 2016, highlighted in the blue shaded box. Data from US Geological Survey National Water Information System (nwis.waterdata.usgs.gov, accessed 7 Mar 2017).

3.3 Methods

3.3.1 Sample Collection

Hyporheic Zone porewaters, along with stream water and groundwater, were sampled at 39 sites (Figure 11 and 3.3), varying in land use/cover and stream order (Table B1) across the Augusta Creek watershed. Porewater samples were collected using a MINIPOINT porewater sampler, which is a custom-built system for temporary installation of nested piezometers (Duff et al., 1998; see Chapter 2, Figure 5A). The MINIPOINT consists of six 50-cm long by 0.5 cm-diameter piezometers arranged in a 10 cm-diameter circular array (see Chapter 2, Figure 5A). The piezometers are adjustable allowing for high-resolution, vertical porewater profile sampling that is minimally disruptive to the sediment column as well as the ambient chemical and biological processes occurring in the HZ (Duff et al., 1998). For this study, the 6 piezometers were vertically staggered at sediment depths of 2.5, 5.0, 7.5, 10, 15, and 20 cm. In exchange for increasing the number of sampling sites from the previous year (i.e., 39 sites in 2016 versus 16 sites in 2015), only a single MINIPOINT sampler was deployed at each site. The placement of the MINIPOINT in the stream channel was largely dependent on finding areas where the sediment type was conducive to the piezometer, which means samples were not collected in cobbly or clayey sediments that preclude installation of the sampler. Porewater samples were simultaneously extracted from all 6 HZ depths using a peristaltic pump (i.e., Cole Palmer Masterflex L/S Peristaltic Pump) set at a low flow rate (i.e., 1.5-2.5 mL min⁻¹) to minimize or eliminate the disturbances to the natural groundwater flow field (Harvey and Fuller, 1998). Approximately 60 mL of sample per HZ depth was pumped into a 100-mL BD syringe that was connected with the peristaltic pump and corresponding piezometer using Tygon tubing with a 1.59-mm inner diameter and Masterflex Norprene Food Tubing with a 1.59-mm inner diameter.

In addition, a single stream water sample per site, 60 mL in volume, was collected approximately 25-35 cm below the stream free-surface using a 100-mL BD syringe, and single groundwater sample per site, 60 mL in volume, was collected from a drive-point well installed to a depth of 60 cm below the stream-sediment interface. Prior to groundwater sampling, the drive-point well was purged, allowed to equilibrate and then a vertical head gradient (VHG) was calculated. This was achieved by measuring the difference in head between the drive-point well (H_{GW} , units in cm) and the stream free-surface (H_{SW} , units in cm) and then dividing by the total depth of the well, d (i.e., 60 cm; Equation 3.1). A positive VHG indicates upwelling groundwater, while a negative VHG indicates downwelling stream water (Table 2).

$$\text{VHG} = \frac{H_{GW} - H_{SW}}{d} \quad (3.1)$$

Once the VHG was determined, the groundwater sample was drawn directly into a 100-mL BD syringe. All samples (i.e., stream water, groundwater, and HZ) were filtered in the field, first through a glass microfiber filter (i.e., Whatman GF/F 25 mm-diameter filters, 0.7 μm pore size) and then through a cellulose acetate filter (i.e., Sartorius Stedim, 0.2 μm pore size) directly into two, 30-mL acid-washed HDPE amber bottles (to prevent photodegradation) and kept on ice as required by US EPA method 415.3 (Potter and Wimsatt, 2003). Upon return to the laboratory, the samples were stored in the dark, at 4 °C until analyzed (see Section 3.3.2).

Dissolved oxygen (DO) was measured at each site using a fiber-optic oxygen meter (i.e., Pyro Science FireStingO₂ with Robust Oxygen Probes, Pyro Science, Aachen, Germany). DO readings were taken at all HZ depths using flow-through cells (i.e., Pyro Science Flow-Through Cells, Pyro Science, Aachen Germany) that were connected with each piezometer as well as for stream water and groundwater. In addition, temperature was measured at each HZ depth and in the stream and groundwater samples using, the fiber-optic oxygen meter.

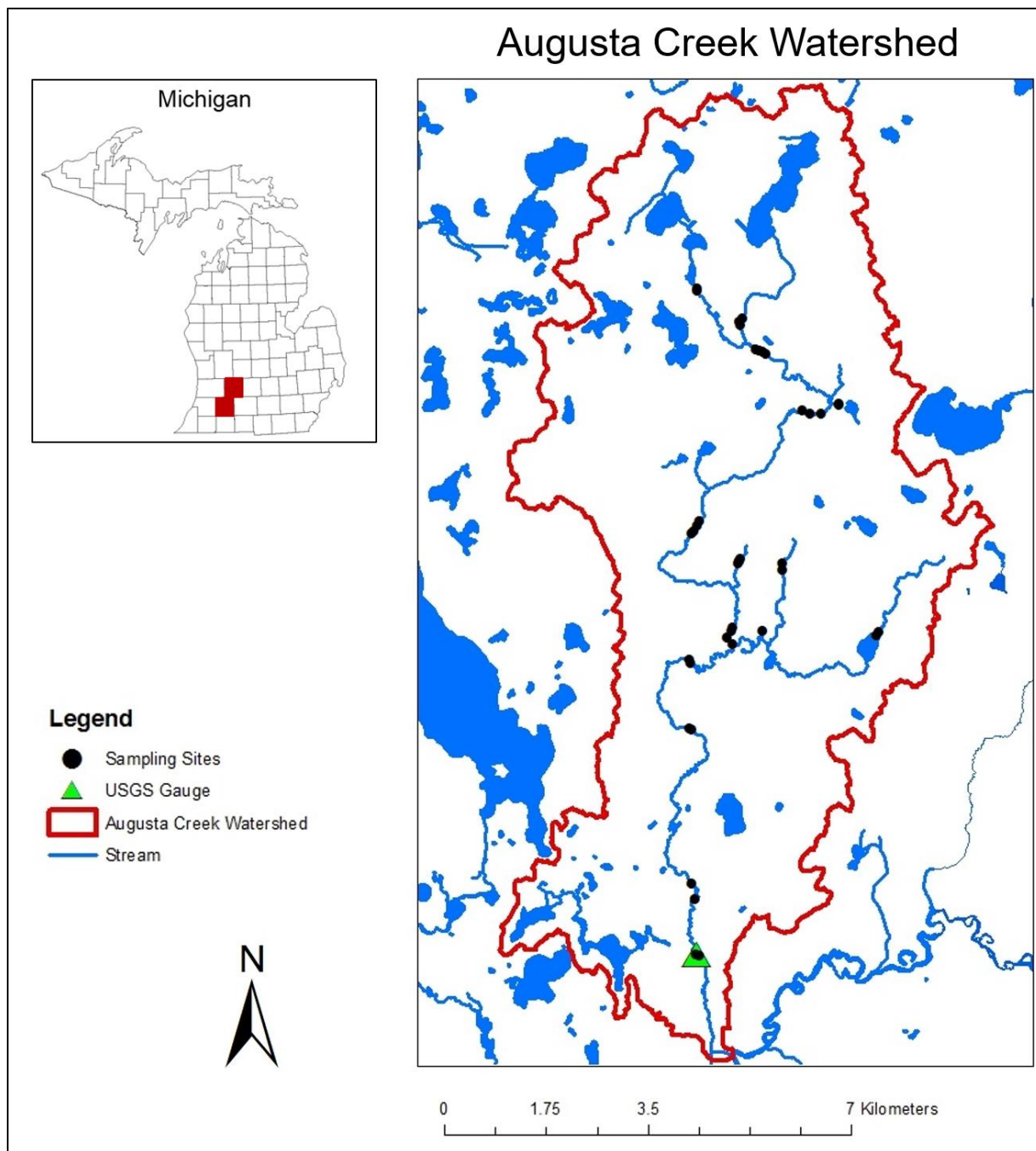


Figure 11: Map of Augusta Creek sampling sites in 2016. A map of the 39 sites sampled during the 2016 synoptic HZ sampling campaign across the third-order, groundwater-fed watershed of Augusta Creek, Michigan, USA.

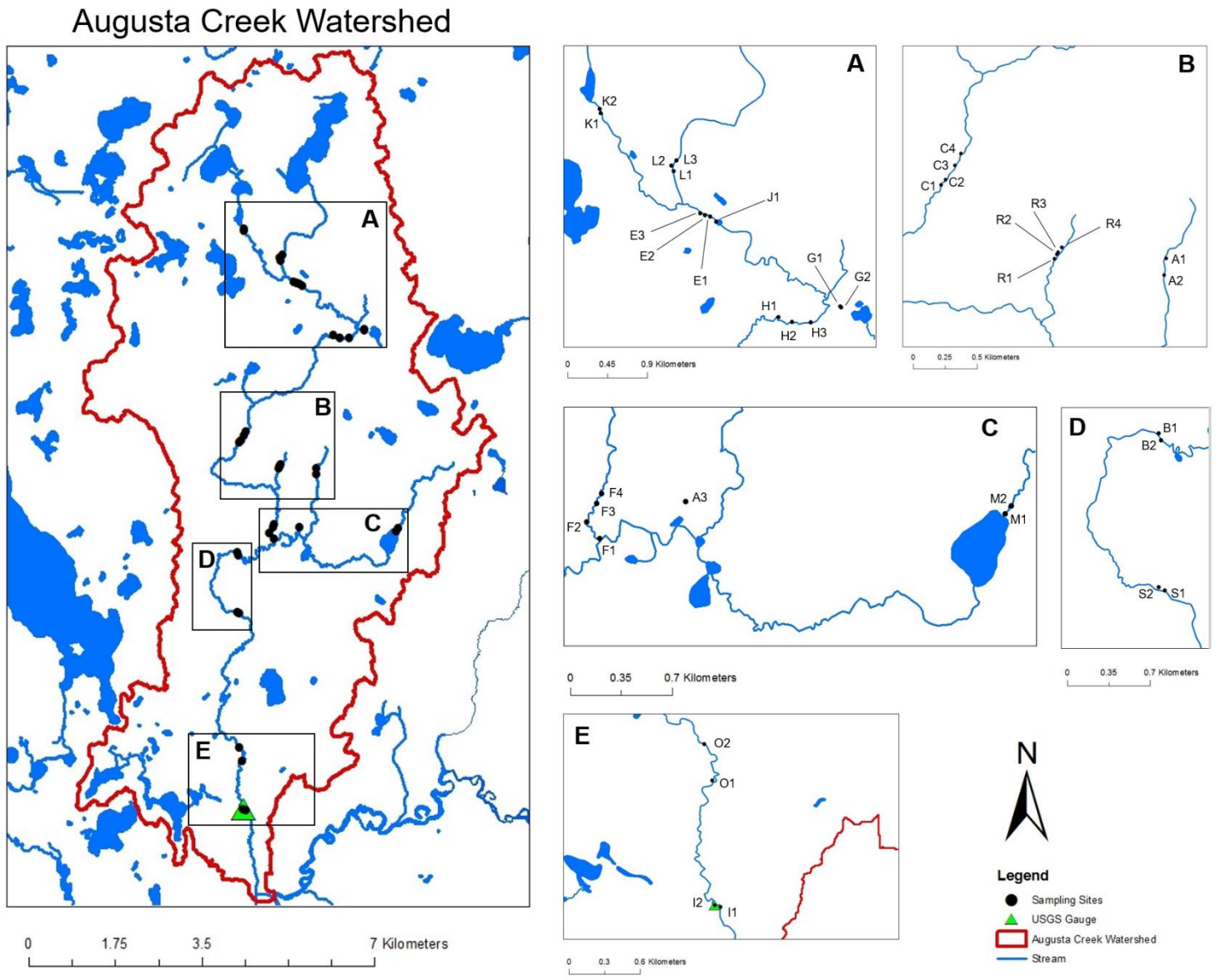


Figure 12: Subplots of labeled sampling sites across Augusta Creek. Map of the 39 labeled sampling sites from the 2016 campaign.

3.3.2 Analytical Methods

All samples were analyzed in the laboratory within 2 months of collection. DOC concentrations (reported as Non-Purgeable Organic Carbon, NPOC) were analyzed via high-temperature combustion using a Shimadzu TOC-L Analyzer (Shimadzu Scientific Instruments, Kyoto, Japan). In addition, a Dionex ICS-2100 ion chromatograph (Thermo Fisher Scientific, Massachusetts, USA) was used to analyze the samples for NO_3^- , Cl^- , and SO_4^{2-} concentrations. Ion analysis was completed using an AS19 Dionex IonPac column (2 x 250 mm) with a potassium hydroxide (KOH) eluent generator and a 0.25 mL min^{-1} flow rate. To infer DOC quality, optically-derived DOC indicators were determined from absorbance data collected on a Shimadzu dual-beam UV 1800 spectrophotometer (Shimadzu Scientific Instruments, Kyoto, Japan). Absorbance readings were taken over the entire UV-VIS range from 220 to 800 nm using semi-micro, BrandTech cuvettes with a 1-cm path length and EPure water (i.e., 18 ohm, Barnstead EPure system) as the blank. Each cuvette was triplicate rinsed with EPure water between samples. For calculations of the optically-derived indicators see Section 3.3.3.

3.3.3 Optical Indices

The structural complexity of DOC makes it difficult to study DOC composition, which is a determining factor of DOC quality and reactivity (Cory et al., 2011). Instead of complex analytical methods (e.g., mass spectrometry), several optical properties of DOC, determined via ultraviolet-visible (UV-VIS) absorbance spectroscopy can be used to assess the chemical structure and thus the quality of DOC (e.g., Weishaar et al., 2003; Cory et al., 2011; Jollymore et al., 2012; Creed et al. 2015). In this study, specific ultraviolet absorbance at a wavelength (λ) of 254 nm (i.e., SUVA_{254}) was used to indicate DOC aromaticity. SUVA_{254} is obtained by

measuring the sample's absorbance at $\lambda=254$ nm and dividing by the DOC concentration of the sample (Equation 3.2; units are L/mg C/m).

$$\text{SUVA}_{254} = \frac{\text{Absorbance}_{254 \text{ nm}}}{\text{DOC concentration}} \quad (3.2)$$

A $\lambda=254$ nm is used because electron structures associated with aromatic C molecules absorb energy at this wavelength, while other structures do not (Weishaar et al., 2003). Therefore the absorbance reading is directly related to the amount of aromatic C within the total DOC sample. Higher SUVA_{254} values are associated with increased aromaticity (Weishaar et al., 2003).

The optical data were also used to calculate a spectral slope ratio (S_R) for each sample. S_R is used as a proxy for molecular weight; S_R increases with decreasing molecular weight (Table 1; Helms et al., 2008). To calculate S_R , absorbance values were measured over 220 to 800 nm and a ratio of the slopes of the 275-295 nm ($S_{275-295}$) absorbance spectra and the 350-400 nm ($S_{350-400}$) absorbance spectra was calculated (Equation 3.3).

$$S_R = \frac{S_{275 \text{ nm} - 295 \text{ nm}}}{S_{350 \text{ nm} - 400 \text{ nm}}} \quad (3.3)$$

3.3.4 Vertical Porewater Profiles

To observe trends in DOC quantity and quality, vertical porewater profiles of the optical properties as well as the sampled chemical species were created for each site. To do so, the HZ data collected from the MINIPOINT along with the stream water and groundwater data for a given site were plotted in order of increasing depth. See Appendix B for the vertical porewater profiles of DOC concentration, DO, SUVA_{254} , S_R , NO_3^- , SO_4^{2-} , Cl^- , and temperature for each site.

3.4 Results

The average DOC concentration in stream water collected from the 39 sampling sites was 8.84 mg/L, which falls within the range for DOC concentration across Augusta Creek of 2-12 mg/L (Hamilton, Unpublished Data). The range of DOC concentration measured in stream water was 5.31 to 13.63 mg/L with a median value of 8.91 mg/L. For groundwater, the average DOC concentration sampled across the watershed was lower than that of stream water at 6.52 mg/L and ranged from 2.42 to 14.15 mg/L with a median value of 5.79 mg/L. The average DOC concentration for groundwater was similar between sampling years (i.e., 6.62 mg/L in 2015 vs. 6.52 mg/L in 2016) even though the sites were different, indicating that groundwater at 60 cm depth has relatively consistent DOC concentrations.

3.4.1 Composite Vertical Porewater Profiles

Individual vertical porewater profiles for all 39 sites were initially averaged to create a composite, watershed vertical porewater profile, representative of the average DOC quantity and quality conditions in the HZ across Augusta Creek (Figure 13, graphs labeled “All Sites”). Vertical profiles were then averaged by stream order for DOC, DO, SUVA₂₅₄, and S_R (Figure 13).

The vertical profiles showed decreasing DOC concentration with depth through the HZ (i.e., 2.5 – 20 cm), in the mean watershed profile and in the mean profiles for each stream order (Figure 13A). However, an increase in DOC concentration was observed between depths 7.5 and 10 cm in the third-order vertical profile (Figure 13A), which may be due to the effect of outliers (e.g., sites with less consistent trends in DOC conditions] such as Site F1 (Figure B13), which exhibited an increase in DOC concentration at intermediate HZ depths. In addition, a slight increase in DOC concentration was observed between depths 2.5 and 5 cm in the first-order

vertical profile (Figure 13A). Again, this is likely due to variations in DOC concentration profiles among the individual sites (see Appendix B).

Stream water across Augusta Creek was oxygenated with DO levels greater than 5 mg/L during the sampling campaign. Dissolved oxygen concentrations decreased with depth through the HZ, in the mean watershed profile and in the mean profile for each stream order, typically becoming depleted (i.e., 2 mg/L DO or less) at deeper HZ depths (Figure 13B). Groundwater measurements taken from 60 cm depth showed lower DO concentrations than stream water, but higher than the DO concentrations observed at the bottom of the HZ.

Regarding the optical properties, $SUVA_{254}$ decreased with depth in the HZ in the mean watershed profile as well as in the mean first-order and third-order profiles (Figure 13C). However, the second-order vertical profile showed an increase in $SUVA_{254}$ at intermediate HZ depths (i.e., ~7.5 – 10 cm), which may also be the result of outliers, including Sites F1 and F2 (Figure B13, B14). Further, S_R increased with depth in the HZ in the mean watershed vertical profile and in the mean profiles for each stream order (Figure 13D).

Increased variance in the optical indices of DOC quality were observed in the HZ when compared to stream water and groundwater (Figure 13C, D), especially for $SUVA_{254}$ (i.e., DOC aromaticity). In addition, increased variance in DOC concentration was observed in the HZ when compared to stream water and groundwater, although the difference is less notable (Figure 13A).

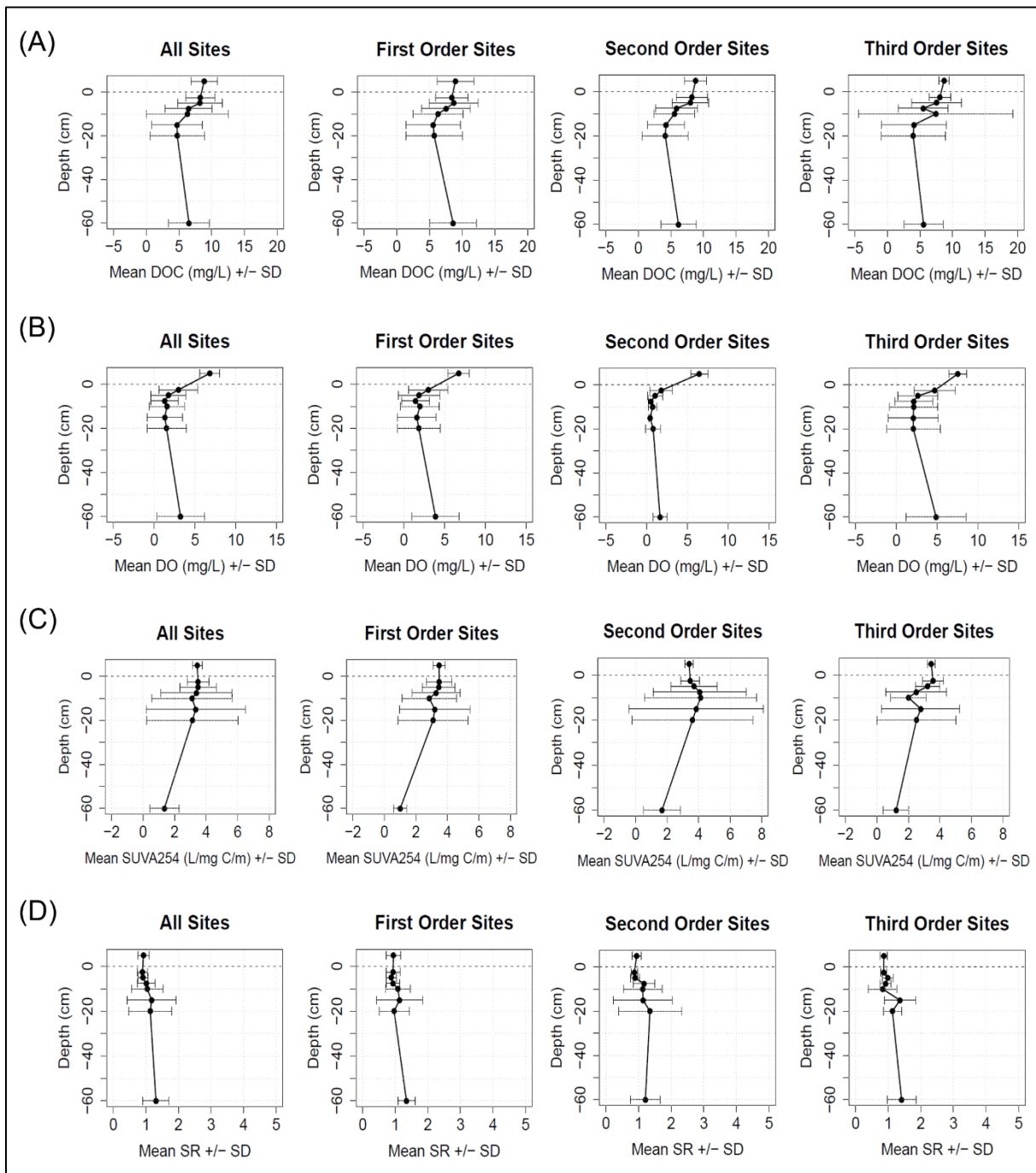


Figure 13: Composite vertical porewater profiles. Vertical profiles of A) mean DOC, B) mean DO, C) mean SUVA₂₅₄, and D) mean S_R of all 39 sites and by stream order. Each plot includes standard deviation bars; n=39 for “all sites”, n=16 for “1st order sites”, n=14 for “2nd order sites” and n=9 for “3rd order sites.”

3.4.2 Rates of Change in DOC Quantity and Quality with Depth

Although the trends in DOC quantity and quality are consistent between the averaged vertical porewater profiles for the watershed and each stream order (see Section 3.4.1, Figure 13), the vertical profiles for individual sites show more variation (see Appendix B). As a result, further analyses were conducted on a site-by-site basis. In order to quantify the changes observed in DOC quantity and quality along the vertical porewater profiles for each site, a rate constant (k , units of cm^{-1}) for DOC concentration (i.e., k_{DOC}) as well as SUVA_{254} (i.e., k_{254}) was calculated over HZ depths (i.e., 2.5 cm to 20 cm), assuming a first-order reaction. The integrated rate law for the first-order reaction is presented in Equation 3.4.

$$[\text{DOC}]_x = [\text{DOC}]_0 e^{-kx} \quad (3.4)$$

To solve for k_{DOC} , the natural log of DOC concentration was plotted against depth (i.e., x) and a linear regression model was applied (Figure 14). The slope of the linear regression represents the negative of k_{DOC} . Similarly, for SUVA_{254} , a k_{254} was calculated for each site.

The rate constants for DOC concentration and SUVA_{254} for all sites are presented in Table 2

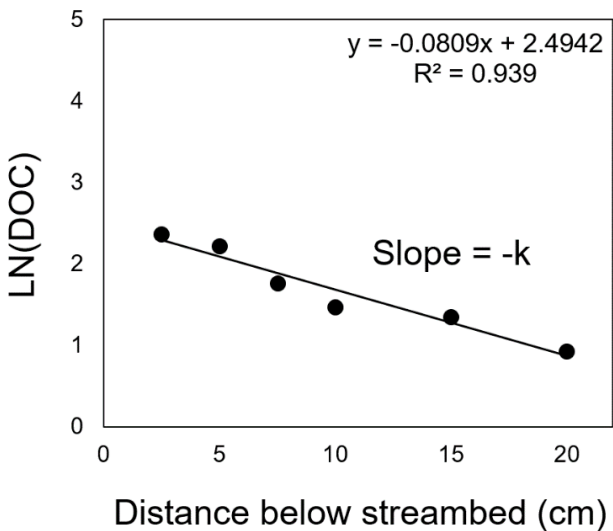


Figure 14: Using a first-order rate law to determine rate constants. An example plot of $\text{LN}(\text{DOC})$ versus distance below the streambed (cm), including a linear regression model. The slope of the linear regression represents the negative of k_{DOC} . In this example, $k_{\text{DOC}} = 0.081 \text{ cm}^{-1}$.

Table 2: Summary of the rate constants for DOC concentration and SUVA₂₅₄

Site	Stream Order	VHG (+, gaining)	k _{DOC} (cm ⁻¹)	k ₂₅₄ (cm ⁻¹)
A1	1	0.145	0.058	0.017
A2	1		-0.008	-0.013
A3	1		-0.006	-0.041
B1	3	0.066	0.086	0.094
B2	3	0.03	0.073	0.018
C1	2		0.097	0.056
C2	2	0.745	0.059	0.026
C3	2		0.107	0.052
C4	2	0.047	0.039	0.015
E1	2	-0.655	0.142	0.039
E2	2	-0.041	0.081	0.016
E3	2	0.381	0.073	0.067
F1	3	-0.447	-0.021	-0.04
F2	2	-0.122	0	-0.054
F3	2		-0.005	-0.032
F4	2	-0.117	0.013	-0.05
G1	1		0.049	0.007
G2	1		0.065	-0.001
H1	2		0.035	-0.015
H2	2		0.053	0.097
H3	2		0.075	0.092
I1	3	0.058	0.101	0.035
I2	3	0.038	0.064	0.146
J1	2		0.066	0.036
K1	1		0.06	0.048
K2	1		0.039	0.039
L1	1		0.077	0.063
L2	1		0.013	-0.018
L3	1		-0.008	0.01
M1	1	-1.885	0.078	-0.046
M2	1		0.016	0.05
O1	3	0.092	0.076	0.027
O2	3	0.051	0.069	0.026
R1	1		0.008	0.002
R2	1	-0.544	0.028	0.057
R3	1	-0.193	0.058	0.057
R4	1	0.152	0.062	0.065
S1	3	0.258	0.025	0.013
S2	3	0.667	0.117	0.033

The majority of sites had positive k_{DOC} values (i.e., 33 out of the 39 sites, see Table 2), indicative of DOC uptake (i.e., consumption or loss). The median k_{DOC} for the watershed was 0.059 cm^{-1} , while the median for first-order sites was 0.044 cm^{-1} , for second-order sites was 0.063 cm^{-1} , and for third-order sites was 0.073 cm^{-1} (Figure 15A). Based on the median values, the magnitude of the rate constant for DOC concentration increased with increasing stream order (i.e., became more positive in higher stream orders, Figure 15A). To test for significance in k_{DOC} between stream orders, an ANOVA was performed using the statistical program, R (version 3.3.2) with an α -value of 0.05. The null hypothesis is that the results are not significantly different between groups. The F-value was 2.215 and $p = 0.124$, thus $p > 0.05$ so the differences in k_{DOC} between stream orders are not statistically significant.

Additionally, the majority of sites had positive k_{254} values (i.e., 29 out of the 39 sites, see Table 2), indicative of decreasing SUVA_{254} with depth in the HZ. The median k_{254} for the watershed was 0.026 cm^{-1} , while the median for first-order sites was 0.014 cm^{-1} , for second-order sites was 0.031 cm^{-1} , and for third-order sites was 0.027 cm^{-1} (Figure 15B). Based on the median values, the magnitude of the rate constant for SUVA_{254} was the largest for second- and third-order sites, with the second-order sites exhibiting a slightly higher median k_{254} (Figure 15B). An ANOVA was again used to test for significance in k_{254} between stream orders, using an α -value of 0.05. The F-value was 0.609 and $p = 0.55$, thus $p > 0.05$, so the differences in k_{254} between stream orders are not statistically significant.

The rate constants for DOC concentration and SUVA_{254} were also compared between upwelling and downwelling sites (Table 2). Figure 15C shows how VHG varies across the stream network. The median VHG for the watershed was 0.047, while the median VHG for first-order sites was -0.193, for second-order sites was -0.041, and for third-order sites was 0.058.

Thus, first-order sites exhibited the largest flux of water moving into the HZ. The median k_{DOC} (rate constant) for upwelling sites across Augusta Creek was 0.069 cm^{-1} and for downwelling sites was 0.043 cm^{-1} . For SUVA_{254} , the median k_{254} for upwelling sites was 0.027 cm^{-1} , and for downwelling sites was -0.012 cm^{-1} . As before, an ANOVA was used to test for significance between rate constants at sites with positive VHG (i.e., upwelling) versus sites with negative VHG (i.e., downwelling). For k_{DOC} the F-value was 1.724 and $p = 0.205$, thus $p > 0.05$, so the differences in k_{DOC} between upwelling and downwelling sites are not statistically significant. While, for k_{254} the F-value was 5.943 and the $p = 0.025$, thus $p < 0.05$, indicating that the differences in k_{254} between upwelling and downwelling sites are statistically significant.

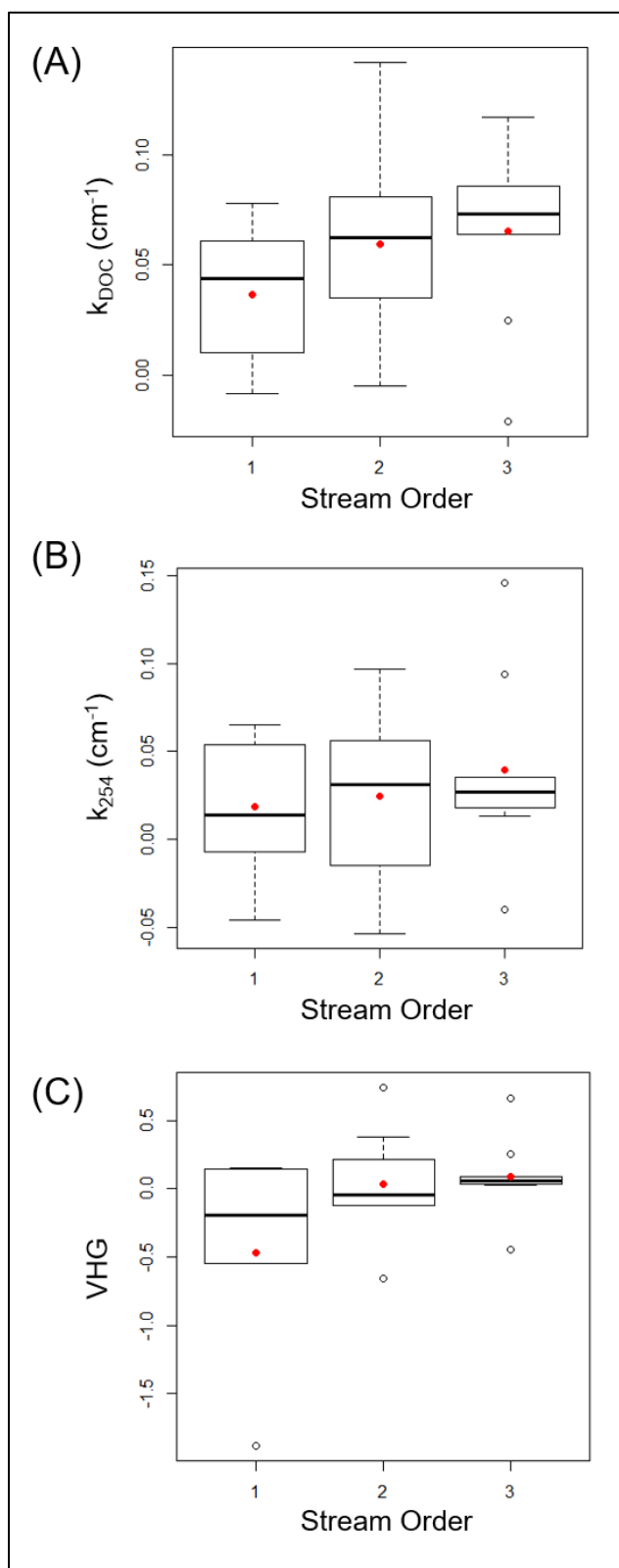


Figure 15: Changes in rate constants and VHG across the stream network. A) Boxplots of k_{DOC} for each stream order, B) boxplots of k_{254} for each stream order, and C) boxplots of VHG for each stream order. The red circle (●) represents the mean.

3.4.3 DOC Metabolism

It was hypothesized in Section 3.1 that the dominant mechanism consuming DOC in the HZ across Augusta Creek is aerobic, microbial respiration. To investigate this hypothesis, “metabolism plots” were used, based on previous methods from Findlay and Sobczak (1996) and Battin (1999). In these metabolism plots, stream DO concentration minus hyporheic DO concentration is plotted against stream DOC concentration minus hyporheic DOC concentration for a given site. If aerobic, microbial respiration is the only transformation mechanism consuming DOC over that range in depth, then the point should fall on the 1:1 molar line (Figure 16), assuming that for every 1 mole of C consumed, 1 mole of O₂ is consumed (Findlay and Sobczak, 1996). This would account for minimal O₂ consumption since the ratio is not corrected for diffusion of O₂ (Findlay and Sobczak, 1996).

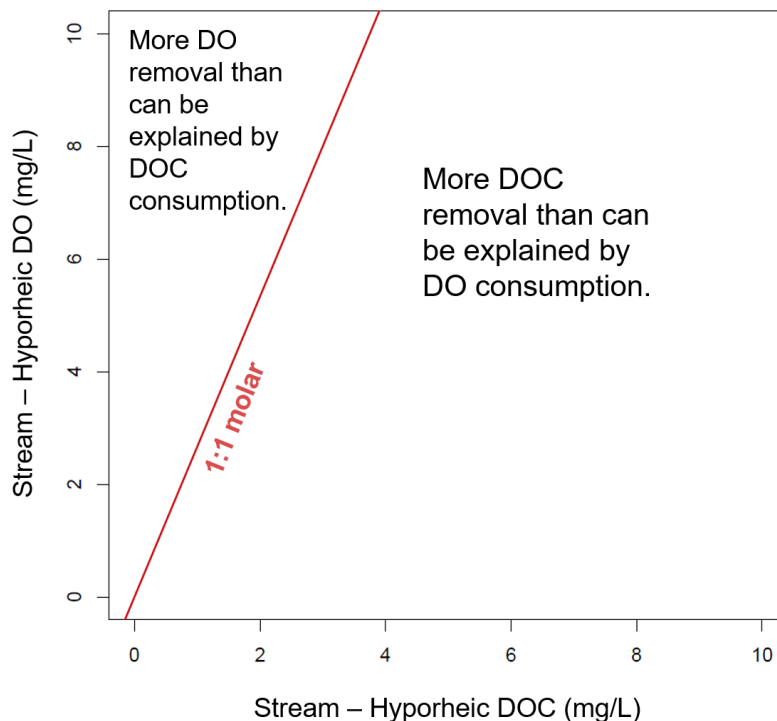


Figure 16: Example of a metabolism plot. Plot of DO consumption versus DOC consumption between two given depths. If aerobic respiration accounts for all DOC loss then points should fall on the 1:1 molar line (–), assuming that 1 mole of O₂ is consumed for every mole of C consumed.

Points that fall to the left of the 1:1 molar line indicate that over the given range of depth, more DO is removed than what can be explained by DOC consumption (via aerobic, microbial respiration) alone, while points that fall to the right of the 1:1 molar line indicate that over the given range of depth, more DOC is removed than what can be explained by DO consumption (via aerobic, microbial respiration) alone (Figure 16). Metabolism plots were created for each range in sampling depth from stream water to 20 cm (e.g., stream – 2.5 cm, 2.5 – 5 cm, and so forth). All 39 sites were plotted on the graphs to allow for assessment of the dominant biogeochemical transformation mechanism in the HZ on a site-by-site basis (Figure 17).

Overall, the hyporheic observations clustered predominantly to the left of the 1:1 molar line in the “stream – 2.5 cm” plot and then shifted towards the right side of the 1:1 molar line as HZ depth increased, indicating that more DOC was removed at intermediate HZ depths than what can be explained by DO consumption alone (Figure 17). Additionally, at these intermediate/deeper HZ depths (i.e., 7.5 to 20 cm) the observations showed little change in DO concentration with depth (i.e., clustered along the horizontal dashed line), but still exhibited changes in DOC, indicating that DOC might be providing electrons to other terminal electron acceptors such as nitrate (NO_3).

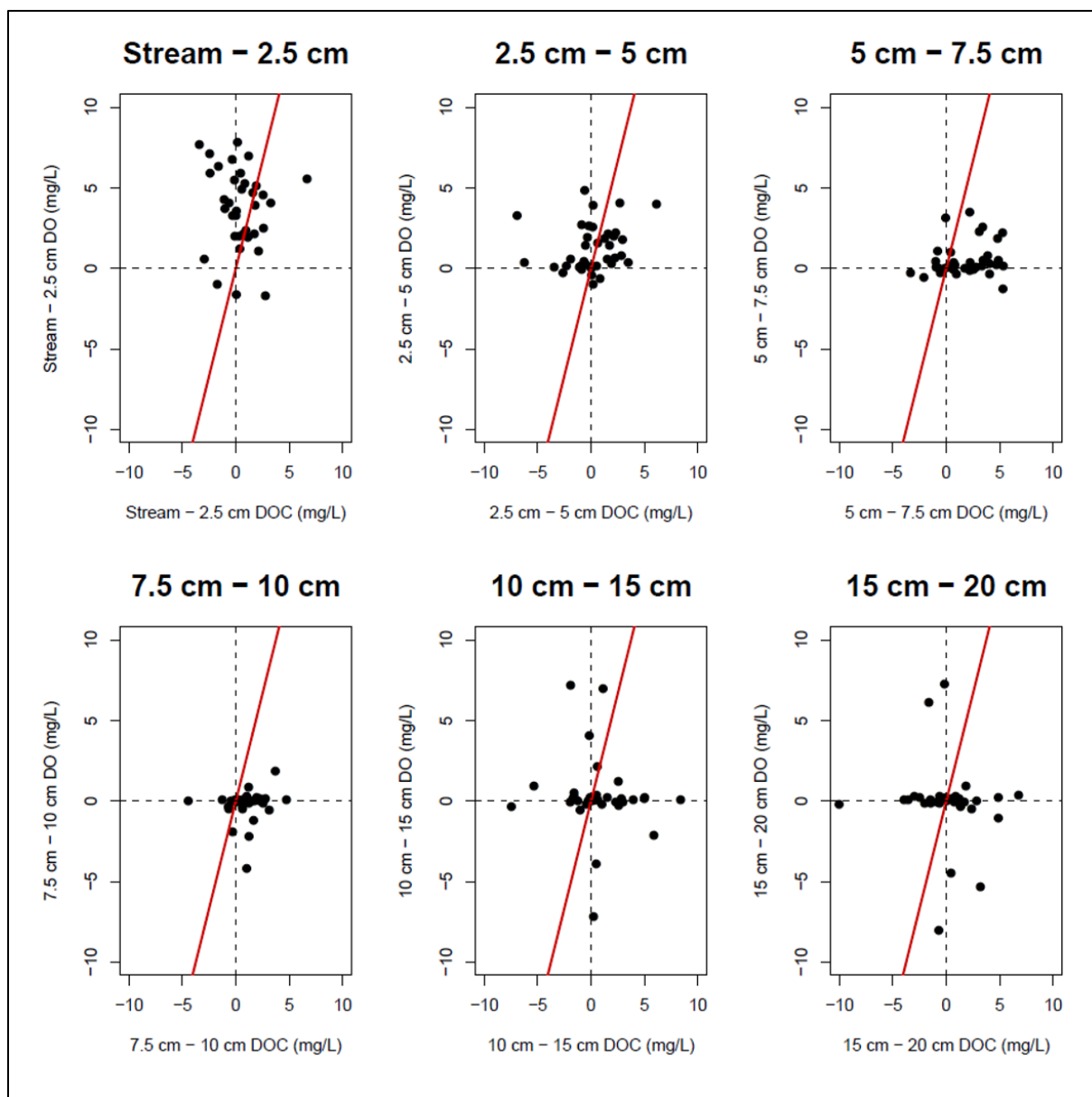


Figure 17: Metabolism plots for Augusta Creek. Metabolism plots including all 39 sampled sites are presented between each measurement depth from stream water to 20 cm. However, site F1 has been removed from the 7.5 cm – 10 cm plot as well as the 10 cm – 15 cm plot as it is an outlier (i.e., shows significant increases in DOC over those depths). If aerobic, microbial respiration accounts for all DOC loss then the points should fall on the 1:1 molar line (–), assuming that 1 mole of O₂ is consumed for every mole of C consumed.

3.5 Discussion

The averaged vertical porewater profiles (see Section 3.4.1, Figure 13) for Augusta Creek in 2016 are consistent with the averaged vertical porewater profiles from 2015 (Chapter 2, Figure 2.6), showing decreasing DOC concentrations with depth through the HZ, and is accompanied by decreasing DO concentrations. Both DOC and DO in the HZ decreased to concentrations lower than that of either the overlying stream water or the underlying groundwater, indicating that mixing of the two end members (i.e., SW and GW) alone cannot account for all of the observed decreases in DOC and DO (e.g., Pinder and Jones, 1969). Thus, some combination of biological (e.g., microbial respiration) and/or physicochemical (e.g., sorption to hyporheic sediments) DOC removal reactions must be occurring in the HZ. The profiles also showed decreasing $SUVA_{254}$ and increasing S_R with depth in the HZ, indicating that DOC aromaticity and molecular weight decreased through the HZ (Weishaar et al., 2003; Helms et al., 2008). These optical trends are suggestive of microbially-driven DOC transformations (e.g., McKnight et al., 2001; Fellman et al., 2010; Cory et al., 2011; Mann et al., 2012; Creed et al., 2015; Helton et al., 2015). Whereas we can conclude from these averaged vertical profiles that DOC was consumed in the HZ at these sites throughout the watershed, we cannot fully determine the dominant biogeochemical transformation mechanisms of DOC in the HZ. To do so, sampling sites from across the entire watershed need to be assessed individually, and a broader suite of biogeochemical measurements may be necessary.

Thus, rate constants (k , units of cm^{-1}) for DOC concentration (i.e., k_{DOC}) as well as $SUVA_{254}$ (i.e., k_{254}) over HZ depths (i.e., 2.5 cm to 20 cm) were calculated for all 39 sites (Table 2, Equation 3.4). The rate constants are informative because, at a minimum, they describe the direction of reaction. For example, a positive rate constant would indicate that DOC

concentration is decreasing (i.e., showing consumption of DOC) with HZ depth, while a negative rate constant would indicate increasing DOC concentration (e.g., production of DOC) with HZ depth (Equation 3.4). In addition, rate constants describe the relative magnitude of change (i.e., processing potential or removal potential). If the rate constant is large and positive for a site, then that site would likely be a strong sink for DOC. Therefore, sites with large (positive or negative) rate constants, in terms of magnitude, indicate the potential for high rates of change (i.e., transformation) in DOC quantity and quality at those locations in the river network. Based on the results presented in Table 2, the majority of sites (see Section 3.4.2) had positive rate constants for DOC concentration and $SUVA_{254}$, indicating that across the watershed, DOC was being removed in the HZ at most sampled locations and that the residual DOC showed decreasing aromaticity with depth through the HZ (e.g., Weishaar et al., 2003). These results are consistent with the averaged vertical profiles and suggest that on a site-by-site basis, aerobic, microbial respiration may be the dominant transformation mechanism for DOC across the watershed (e.g., McKnight et al., 2001; Cory et al., 2011; Mann et al., 2012; Creed et al., 2015; Helton et al., 2015). This would support findings from previous small-scale field and mesocosm studies (Findlay and Sobczak, 1996; Schindler and Krabbenhoft, 1998; Sobczak and Findlay, 2002; Zarnetske et al., 2011).

To determine whether or not aerobic, microbial respiration is controlling the observed trends in DOC quantity, metabolism plots were used (Figure 17; Findlay and Sobczak, 1996; Battin, 1999). The plots showed that at all HZ depths the hyporheic observations clustered around the 1:1 molar line, indicating that 1) aerobic, microbial respiration is predominantly controlling the trends in DOC quantity observed through the HZ and 2) that this dominant transformation mechanism is consistent across the river network. These results support the first

hypothesis that aerobic, microbial respiration is the dominant transformation mechanism of DOC in this river network. However, the deviation from the 1:1 molar line, exhibited by individual observations suggests that additional physicochemical processes (e.g., dilution, sorption to hyporheic sediments, intersecting lateral flowpaths) and/or biological reactions (e.g., anaerobic, microbial respiration using alternative electron acceptors such as NO_3 , SO_4) are occurring in the HZ at some of the sites. For instance, the observations clustered predominantly to the left of the 1:1 molar line in the “stream – 2.5 cm” plot and then shifted towards the right side of the 1:1 molar line as HZ depth increased (Figure 17). It is likely that within the shallow HZ, there is an additional source of organic C in the form of particulate organic carbon (POC) such as leaves and buried logs (e.g., Stelzer et al., 2015). The microbes may also be using the POC for respiration, which would account for the extra, “missing” oxygen (Findlay and Sobczak, 1996). However, the abundance of POC often decreases with depth in a streambed (e.g., Kaplan and Newbold, 2000; Findlay and Sobczak, 2000). Given this for Augusta Creek, it would result in the shift towards the right of the 1:1 molar line at deeper HZ depths.

At a depth of ~7.5 cm and deeper in the HZ, many of the hyporheic observations also began to show little to no change in DO concentrations (i.e., they clustered along the horizontal dashed line) with depth, while still residing predominantly to the right of the 1:1 molar line (Figure 17). This suggests that at deeper HZ depths, DOC is still consumed despite little to no change in DO. Since sorption of DOC to hyporheic sediments tends to be in equilibrium with the DOC concentration of upwelling/downwelling waters in the HZ (e.g., Day et al., 1994; Kaplan and Newbold, 2000), the consumption of DOC at deeper HZ depths is likely due to a shift in electron acceptors used in microbial metabolism. Nitrate (NO_3^-) or sulfate (SO_4^{2-}) may be used for anaerobic, microbial respiration at deeper HZ depths as the system becomes anoxic (e.g.,

Hedin et al, 1998). When using NO_3^- for anaerobic, microbial respiration, 4 moles of NO_3^- are consumed for every 1 mole of C consumed. Likewise, when using SO_4^{2-} for anaerobic, microbial respiration, 2 moles of SO_4^{2-} are consumed for every 1 mole of C consumed.

Furthermore, the rate constants as well as the metabolism plots can also be used to start to address questions about how the role of the HZ as a processor of stream DOC varies across the river network. The results indicate that the HZ acts as a sink for DOC and that aerobic, microbial respiration is one of the dominant transformation mechanisms consuming DOC in the HZ. However, this HZ function (i.e., removal of DOC) may vary based on location in the watershed. Rate constants for DOC concentration and SUVA_{254} were compared between stream orders as well as between sites with varying VHG (i.e., upwelling vs. downwelling, Section 3.4.2) to observe changes in this hyporheic processing potential across the watershed. While the rate constants for both DOC concentration and SUVA_{254} showed increases in magnitude with increasing stream order (i.e., rate constants became more positive at higher stream orders, Figure 15A), the ANOVA results indicate that the observed changes with stream order are not statistically significant (Section 3.4.2). This suggests that the potential for transformation in both DOC quantity and quality in the HZ is relatively similar across stream orders.

Changes in rate constants for DOC concentration between upwelling and downwelling sites were also not significantly different, based on the ANOVA results (Section 3.4.2), further suggesting that the potential for DOC transformation in the HZ is similar across the watershed, despite variation in local VHG among sites. However, the changes in rate constants for SUVA_{254} between upwelling and downwelling sites are statistically significant based on the ANOVA results (Section 3.4.2). This may indicate that local flow patterns (i.e., VHG) impact the potential for transformation in DOC quality in the HZ, across the watershed, considering that

DOC quality can change independently of DOC concentration (Lutz et al., 2012). These ANOVA results may have also been impacted by the lower sampling number since not all 39 sites have VHG measurements (Table 2). In addition, of the eight downwelling sites, four of them have negative SUVA₂₅₄ rate constants, which impacts the average downwelling rate constant (Section 3.4.2, Table 2). However, of those four sites, three of them are for Site F (i.e., F1, F2, and F4). Site F is adjacent to a large wetland complex (Figure 12), which may have complicated the trends in DOC quantity and quality and the associated reactions more so than at other sampling sites less dominated by a large wetland outflow. Finally, it is also important to consider that changes in stream discharge due to small storm events during the August 2016 sampling period did result in small stream stage changes (Figure 10) that may have impacted the VHG at individual sites, causing statistically significant variation in rates between upwelling and downwelling sites.

While the rate constants indicate that the potential for DOC transformation in the HZ is similar (for the most part) across the watershed, rate constants need to be paired with the vertical hydrological flux (i.e., the rate of water upwelling or downwelling through the HZ) as well as stream transport rates to assess the overall role of the HZ in DOC cycling across the river network (i.e., large sink versus small sink). This is because the amount of DOC processing in the HZ is not only dependent on the rate constant, but also the local hydrology controlling the supply of stream water containing DOC to the HZ in relation to the total flux down the stream channel. For example, a site with a large, positive rate constant for DOC concentration (i.e., high potential for DOC removal) and a large, downwelling VHG (i.e., indicative of a constant supply of DOC, DO and nutrients) means that the HZ at that site is likely a large sink for DOC in the river network. On the other hand, a site with a large, positive rate constant for DOC concentration, but

a small, downwelling VHG is likely not as big of a sink for DOC since less water is moving through the HZ, thus hydrologically limiting microbial metabolism. Therefore, we used the product of k_{DOC} and VHG to represent the function of the HZ (i.e., f_{DOC} ; size of sink) for each stream order in terms of DOC concentration. This HZ function was calculated only for sites with positive k_{DOC} and negative VHG values (i.e., $n=6$) since those sites indicate the potential for removal of DOC and stream water flowing into the HZ. This is unlike sites with upwelling groundwater, which should theoretically limit the depth of the HZ and limit the supply of labile DOC to the HZ. Thus, stream orders with a large, negative f_{DOC} indicate that the HZ in those reaches of the river network functions as a large sink for DOC. This process was also repeated for DOC quality, in terms of SUVA_{254} (i.e., $n=4$; Figure 18).

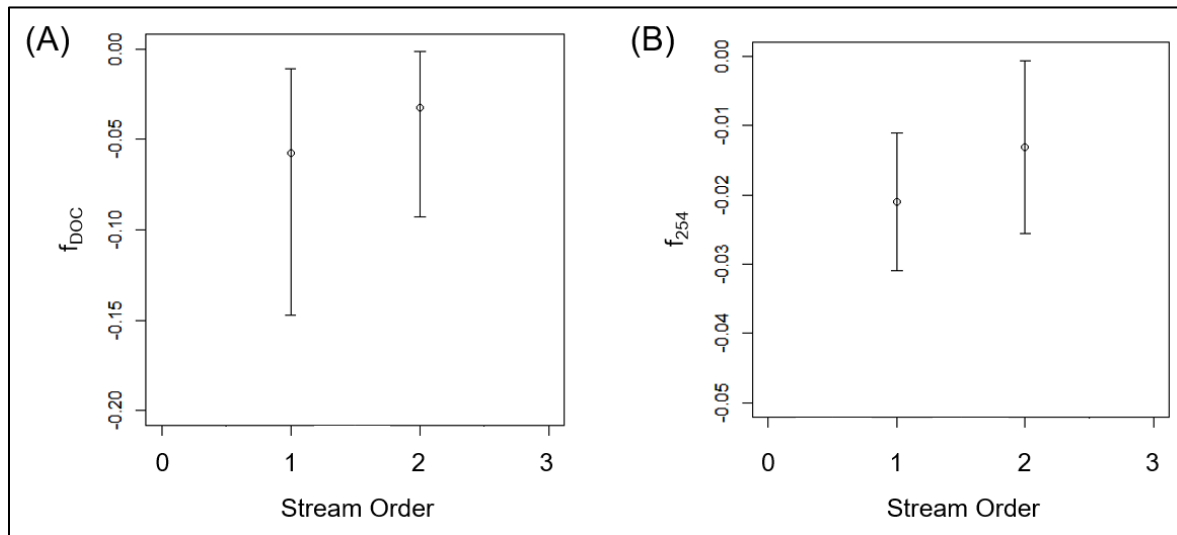


Figure 18: Plots of HZ function. A) f_{DOC} values for first- and second-order streams ($n=3$ for each), and B) f_{254} values for first- and second-order streams ($n=2$ for each). The open-circle represents the mean f_{DOC} value \pm the max/min value. f_{DOC} values for third-order streams are not included, due to insufficient VHG data needed to calculate f_{DOC} .

The first-order streams exhibit more negative f_{DOC} and f_{254} values when compared to the second-order streams. There were no third-order sites with a positive rate constant as well as a negative VHG, which suggests there were no third-order sites observed that have a HZ that is

effective at DOC removal from the stream. Thus, despite the smaller k_{DOC} value, and therefore lower processing potential for first-order streams (Figure 15A), the large, downwelling VHG in those locations likely allows for more removal of DOC in the HZ (Figure 18). This indicates that the HZ may function as a larger sink for DOC in the headwaters of this river network than in higher stream orders, with little to no HZ processing of DOC in larger streams. However, due to the small number of sampling sites that could be used for this analysis, these results should be re-evaluated in the future using additional downwelling sites across the river network.

3.6 Conclusions

We identified the dominant biogeochemical transformation mechanism(s) for DOC in the HZ across Augusta Creek using watershed-wide trends in hyporheic DOC quantity and quality, dissolved oxygen (DO) measurements, and local vertical flow gradients (i.e., upwelling vs. downwelling). The averaged, vertical porewater profiles along with the rate constants for individual sites showed decreasing DOC concentration with depth through the HZ, along with decreasing $SUVA_{254}$. These results, as well as the metabolism plots, demonstrate that the HZ likely acts as a sink for DOC and that aerobic, microbial respiration may be the dominant processing mechanism consuming DOC in the HZ across the watershed. Additionally, the role of the HZ as a processor of stream DOC is likely more significant (i.e., acts as a larger sink) in headwater streams, where strong, downwelling VHGs occur, despite the smaller, observed k_{DOC} and k_{254} values (i.e., lower processing potential). Lastly, the ANOVA results as well as the averaged vertical porewater profiles for $SUVA_{254}$, which showed large variation in $SUVA_{254}$ with depth in the HZ indicate the need for further studies focused on hyporheic DOC quality. It is critical to understand DOC quality, since it can affect the fate of DOC in the HZ as well as the DOC and solutes transported to downstream ecosystems.

CHAPTER 4: USING IN-SITU OPTICAL SENSORS TO STUDY DISSOLVED ORGANIC CARBON DYNAMICS OF STREAMS AND WATERSHEDS: A REVIEW[†]

4.1 Abstract

It is important to understand how dissolved organic carbon (DOC) is processed and transported through stream networks because DOC is a master water quality variable in aquatic ecosystems. High-frequency sampling is necessary to capture important, rapid shifts in DOC source, concentration, and composition (i.e., quality) in streams. Until recently, this high-frequency sampling was logistically difficult or impossible. However, this type of sampling can now be conducted using in-situ optical measurements through long-term, field-deployable fluorimeters and spectrophotometers. The optical data collected from these instruments can quantify both DOC concentration and composition properties (e.g., specific ultra-violet absorbance at 254 nm, spectral slope ratio, and fluorescence index). Previously, the use of these sensors was limited to a small number of specialized users, mainly in Europe and North America, where they were used predominantly in marine DOC studies as well as water treatment and management infrastructure. However, recent field demonstrations across a wide range of river systems reveals a large potential for the use of these instruments in freshwater environments, heightening interest and demand across multiple environmental research and management disciplines. Hence, this review provides an up-to-date synthesis on 1) the use of spectroscopy as a diagnostic tool in stream DOC studies, 2) the instrumentation, its applications, potential limitations and future considerations, and 3) the new watershed DOC research directions made possible via these in-situ optical sensors.

[†] Reprinted from *Science of the Total Environment*, 575, Ruhala, S.S and Zarnetske J.P., Using in-situ optical sensors to study dissolved organic carbon dynamics of streams and watersheds: A review, 713-723, Copyright (2017), with permission from Elsevier. <http://dx.doi.org/10.1016/j.scitotenv.2016.09.113>.

4.2 Introduction

Rivers were traditionally thought to play an insignificant role in the global carbon (C) cycle (Battin et al., 2008). However, recent studies reveal that rivers globally receive 4 petagrams (Pg) of terrestrial organic C and generate 1.8 ± 0.25 Pg C as carbon dioxide (CO₂) each year; a rate 6 times greater than lakes and reservoirs combined (Battin et al., 2008; Raymond et al., 2013). This indicates that rivers are a significant source of CO₂ to the atmosphere and that most of the organic C entering rivers is undergoing significant in-stream biogeochemical processing (Battin et al., 2008). Thus, efforts must be made to better understand C cycling in rivers, so that rivers can be considered in future global C models. Dissolved organic carbon (DOC) is often the dominant form of organic C in streams and plays several critical roles in aquatic ecosystems. DOC fuels stream metabolism, regulates additional biogeochemical cycles (e.g., nitrogen transformations), and impacts trace metal complexation and transport (Cory et al., 2011; Aiken, 2014). As a result, stream DOC dynamics influence C cycling on local to global scales (Battin et al., 2009). Therefore, it is important to measure and identify how DOC is processed (e.g., rates, transformations) and transported (e.g., its sources, pathways, and quantity) in riverine environments.

DOC is composed of a complex grouping of molecules with varying chemical structures (e.g., molecular weight and aromaticity). The chemical structure of DOC is a determining factor of DOC quality and is largely dependent on its source material (i.e., allochthonous versus autochthonous) (Cory et al., 2011). Several optical properties of DOC, determined via absorbance and fluorescence spectroscopy, can be used to assess the chemical structure of DOC, which in turn can be used to infer DOC qualities and bioavailability. Ultraviolet-visible (UV-VIS) absorbance spectroscopy can be used to infer aromaticity and molecular weight (e.g., Cory

et al., 2011; Jollymore et al., 2012), while fluorescence spectroscopy provides insight on redox state, reactivity, and source material (e.g., Fellman et al., 2010; Cory et al., 2011). DOC quality is a critical parameter that must be included in DOC export studies as the quality of DOC impacts its bioavailability and reactivity (i.e., lability), which ultimately affects downstream ecosystems and water quality (Fellman et al., 2010; Cory et al., 2011).

Until recently, optical measurements of DOC were done using field water collections (i.e., grab samples) that were later analyzed in the laboratory (e.g., Hood et al., 2006; Spencer et al., 2009; Inamdar et al., 2011). Utilizing lab measurements of optical properties to assess DOC quality is quick, while still maintaining high analytical precision, and relatively inexpensive when compared to chemical analyses (Fellman et al., 2010). However, there is a lack of temporal resolution in the data from using this method, because grab samples are often collected at low frequencies. Recent studies have revealed that higher temporal resolution of DOC measurements allows for better understanding of DOC flux and C budgets (e.g., Saraceno et al., 2009; Jollymore et al., 2012; Pellerin et al., 2012; Wilson et al., 2013; Jones et al., 2014; Grayson and Holden, 2016), and allows for further exploration of new ecological theories and scales of processes (e.g., Pulse-Shunt Concept, Raymond et al., 2016). Thus, there is a growing demand for high-quality and cost effective, high-frequency measurements of DOC quantity and quality in riverine environments. A potential solution to this demand are the emerging optically-based field sensor technologies (i.e., long-term, field-deployable fluorometers and spectrophotometers such as the WET Labs, WETStar FDOM Fluorometer and spectro::lyser), because they have data collection frequencies of minutes. This high-frequency sampling helps to capture changes in both DOC quantity and quality as the result of shifting pathways and sources (e.g., during storm events when it is difficult to manually collect grab samples) as well as changes due to in-stream

biogeochemical transformations at scales that otherwise would not be seen (e.g., sub-diurnal dynamics, diurnal fluctuations, intra-seasonal trends; Spencer et al., 2007; Pellerin et al., 2012).

These in-situ optically-based field instruments have previously been used by a limited group of specialized users, largely in Europe and North America. The focus of these earlier uses was on DOC dynamics in marine and coastal environments (e.g., Klinkhammer et al., 1997; Chen et al., 1999; Chen and Gardner, 2004; Kowalczyk et al., 2010; Gueguen et al., 2012; Etheridge et al., 2014a; Etheridge et al., 2014b) as well as in water treatment and management infrastructure (e.g., Langergraber et al., 2004; Brinkman and Hozalski, 2011; Boënné et al., 2014; Graham et al., 2015). However, recent riverine field demonstrations reviewed in detail in Section 4 have heightened demand for these optical sensors in many freshwater disciplines, including watershed ecology, biogeochemistry and hydrology (e.g., Spencer et al., 2007; Saraceno et al., 2009; Pellerin et al., 2012).

Despite this growing interest and demand, there is no comprehensive synthesis of the state of the science on using these new technologies (i.e., in-situ optical sensors) in the field. Consequently, potential new users face a daunting task of compiling this information from a wide range of sources (e.g., primary literature to government reports), which inhibits the potential adoption and applications of these new technologies. Consequently, we provide a review on in-situ optical methods used for studying DOC dynamics in riverine environments, specifically via long-term, field-deployable spectrometers and fluorometers. This review will cover 1) what we can learn about DOC from the use of optical properties 2) why in-situ, high-frequency measurements are needed, 3) the instrumentation, its diagnostic uses, limitations, and future considerations, and 4) an illustrative synthesis of future watershed DOC research directions discovered through recent field demonstrations of these instruments.

4.3 Spectroscopy as a Diagnostic Tool for DOC

Below we briefly review how absorbance and fluorescence spectroscopy is used for assessing DOC composition, and in turn DOC quality, across a wide range of natural waters (McKnight et al., 2001; Belzile et al., 2006; Fellman et al., 2010; Cory et al., 2011; Jollymore et al., 2012; Lee et al., 2015). Dissolved organic matter (DOM) is operationally defined as any organic material that is able to pass through a filter of a particularly identified pore size (e.g., typically 0.7 μm , 0.45 μm or smaller; Cory et al., 2011; Jollymore et al., 2012). Since DOM is typically about 50% C by mass (Cory et al., 2011), DOM is measured as DOC. DOC consists of a complex mixture of compounds that vary in size, weight, aromaticity, and reactivity, making it difficult to study DOC composition, and therefore its quality via direct molecular techniques. Hence, spectroscopy methods are a relatively quick and non-invasive means to observe and infer DOC and DOM composition and quality.

4.3.1 Absorbance Spectroscopy

UV-VIS absorbance spectroscopy is used to determine optical properties associated with the light-absorbing or chromophoric fraction of DOM (i.e., CDOM; Fellman et al., 2010; Cory et al., 2011). UV-VIS absorbance (i.e., absorbance from 220 to 720 nm) of CDOM has been shown to be a strong proxy (i.e., $r^2 > 0.95$, based on in-situ data) for DOC concentration (Waterloo et al., 2006; Jollymore et al., 2012; Jeong et al., 2012; Avagyan et al., 2014; Jones et al., 2014) and can also be used to infer aromaticity and molecular weight. It should be noted that UV-VIS absorbance may not be fully representative of all quality properties since CDOM only makes up a fraction of the total DOM pool (Cory et al., 2011).

Algorithms utilizing Beer Lambert's Law are used to determine DOC concentration from a given absorbance (e.g., 350 nm), as seen in Waterloo et al., 2006 (Equation 4.1).

$$\text{DOC} = 0.905 \times \text{Absorbance}_{350 \text{ nm}} \quad (4.1)$$

While specific UV absorbance at 254 nm (i.e., SUVA_{254}) is positively correlated with DOC aromaticity (Cory et al., 2011). Here, the absorbance at 254 nm is divided by the DOC concentration of the sample (units are $\text{L mg}^{-1} \text{ C m}^{-1}$) (Equation 4.2). A wavelength of 254 nm is used because electron structures associated with aromatic C molecules absorb energy at this wavelength, while other structures do not (Weishaar et al., 2003). Therefore the absorbance reading is directly related to the amount of aromatic C within the total DOC sample.

$$\text{SUVA}_{254} = \frac{\text{Absorbance}_{254 \text{ nm}}}{\text{DOC concentration}} \quad (4.2)$$

And lastly spectral slope ratio (S_R) can be used to infer molecular weight. S_R is a dimensionless ratio of the slope of the 275 nm to 295 nm ($S_{275-295}$) absorbance spectra divided by the slope of the 350 nm to 400 nm ($S_{350-400}$) absorbance spectra (Equation 4.3) and exhibits a negative correlation with molecular weight.

$$S_R = \frac{S_{275 \text{ nm} - 295 \text{ nm}}}{S_{350 \text{ nm} - 400 \text{ nm}}} \quad (4.3)$$

4.3.2 Fluorescence Spectroscopy

In addition to chromophores, fluorophores (i.e., molecules that absorb and re-emit light) also make up a fraction of DOM in natural waters (Fellman et al., 2010). When a fluorophore (e.g., fluorescent DOM, FDOM) absorbs light energy, an electron is excited (i.e., transitions) from the original ground state to a higher electronic state (e.g., S_0 to S_2 in Figure 19). Within each electronic state there are numerous vibrational energy levels (e.g., 0, 1, 2 in Figure 19). The electron will often rapidly relax to the lowest vibrational energy level of S_1 prior to emission, via internal conversion (Figure 19; Lakowicz, 2006). Then as the electron returns to ground state, the

energy is emitted as light or fluorescence (Figure 19). The specific excitation and emission wavelengths at which fluorescence occurs is dependent on the concentration, chemical composition, and chemical structure (e.g., bonds between molecules) of the compound (Lakowicz, 2006; Fellman et al., 2010; Cory et al., 2011). Therefore, fluorescence can provide insight on DOC quantity and quality (e.g., redox state, reactivity, and source material; Fellman et al., 2010; Cory et al., 2011). However, it is important to note that FDOM only makes up approximately 1% of the total DOM pool (Cory et al., 2011). Therefore similar to CDOM, a limitation of using fluorescence spectroscopy is that only part of the “DOC pool” (rather than the “whole pool”) is observable.

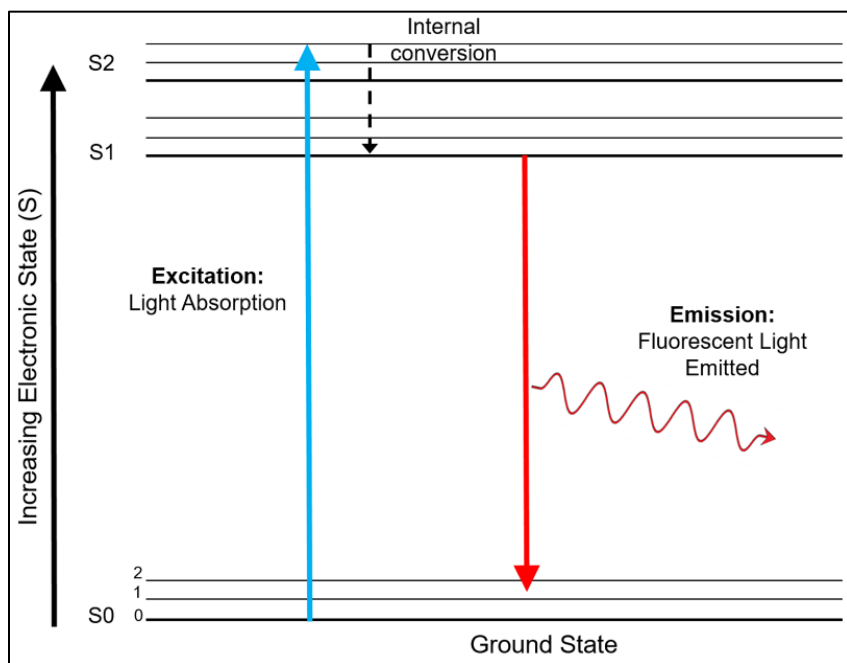


Figure 19: A simplified Jablonski diagram. A simplified Jablonski diagram showing the process of fluorescence. Modified from Lakowicz (2006).

Despite its small fraction, FDOM is used as a proxy for total DOC concentration (Fellman et al., 2010; Cory et al., 2011). To do so, concentration of FDOM is measured in parts per billion (ppb) quinine sulfate equivalents (QSE), using a fluorometer, as seen in Saraceno et

al. (2009), where V_{sig} is the output voltage for the sample, V_{CW} is the output voltage for clean (i.e., blank) water, and SF is an instrument specific scaling factor (Equation 4.4; Saraceno et al., 2009).

$$\text{ppb QSE} = (V_{sig} - V_{CW}) \times SF \quad (4.4)$$

FDOM is also used to infer DOC quality properties. A fluorescence index (FI) value can be calculated to assess potential FDOM source material. The FI uses an excitation wavelength of 370 nm and the resulting emission intensities at 470 nm and 520 nm are then divided (Equation 4.5; McKnight et al., 2001; Fellman et al., 2010).

$$FI = \frac{470\text{nm Emission Intensity}}{520\text{nm Emission Intensity}} \quad (4.5)$$

High FI values (i.e., ~1.8) are indicative of microbial or autochthonous sources, while low FI values (i.e., ~1.2) are indicative of terrestrial or allochthonous sources (McKnight et al., 2001).

In addition to FI, three-dimensional excitation emission matrices (i.e., EEMs) are commonly used to assess DOC composition. EEMs are produced using multiple excitation wavelengths and measuring the resulting emission intensities across a range of wavelengths (Fellman et al., 2010; Cory et al., 2011). This technique is used frequently to study DOC composition in terms of molecular groupings and functions as EEMs contain a large amount of information on the origin and processing of DOC (Fellman et al., 2010; Cory et al., 2011). Additional optical properties including protein-like components (i.e., tyrosine-like and tryptophan-like components), humic-like components, the freshness index, humification index, and redox index can also be determined using fluorescence spectroscopy to better understand DOC composition in natural waters (e.g., see Fellman et al., 2010; Khamis et al., 2015; Bieroza and Heathwaite, 2016).

4.4 Technology and Limitations

4.4.1 *In-Situ Optical Instruments*

Previous work showed that DOC concentration and composition are dynamic and can change over short time scales (i.e., hours to days) (Carstea et al., 2009; Cory et al., 2011; Inamdar et al., 2011; Neal et al., 2012; Grayson and Holden, 2012; Strohmeier et al., 2013; Jones et al., 2014; Mast et al., 2016). Therefore, it is necessary to collect long-term, high-frequency data when studying DOC export as small and/or rapid shifts in DOC quantity and quality are missed with less frequent sampling (Figure 20; Bowes et al., 2009; Inamdar et al., 2011; Jollymore et al., 2012; Jones et al., 2014; Blaen et al., 2016). In-situ optical measurements via long-term, field-deployable spectrophotometers and fluorometers enable researchers to collect this valuable high-resolution temporal data using the spectroscopy methods discussed above. This review focuses on two, representative instruments frequently used in published field studies to date: 1) submersible FDOM fluorometers (e.g., WET Labs, WETStar FDOM fluorometer, Figure 21A) and 2) submersible spectrophotometers (e.g., Seacan, spectro::lyser, Figure 21B). For brevity, this review specifically discusses the WET Labs FDOM sensor and the Seacan spectro::lyser as well-documented examples of these technologies (i.e., these sensors have been and are used in many published studies). However, there are many other manufacturers developing and producing in-situ optical instruments based upon the same fundamental optical methods including, the SeaPoint UV fluorometer (SeaPoint Sensors, Inc.), the Cyclops-7 fluorometer (Turner Designs), the microFLU CDOM fluorometer (TriOS), the UviLux fluorometer (Chelsea Technologies Group), the Satlantic UV spectrophotometer, and the ABB AV400 UV absorbance probe.

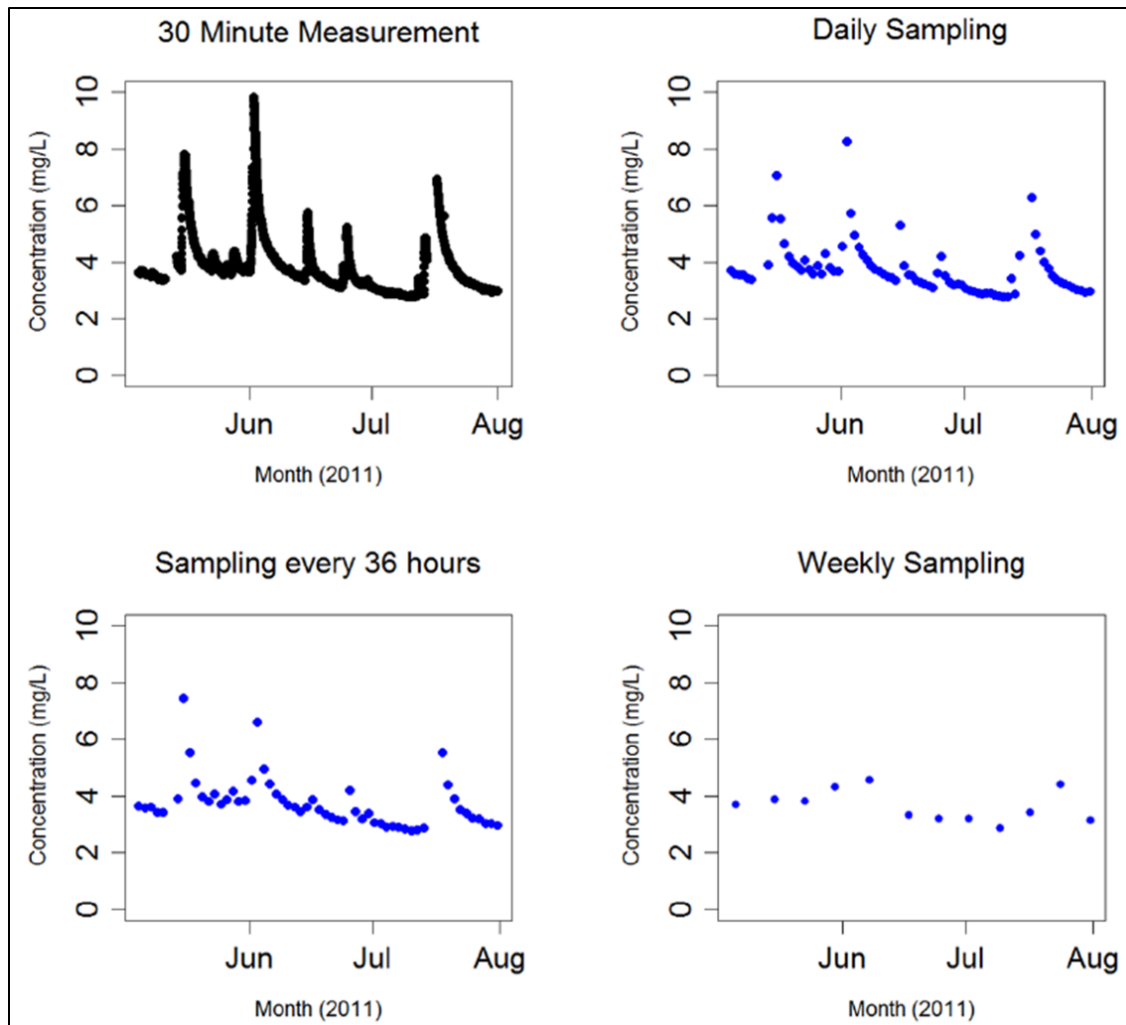


Figure 20: Plots of DOC concentration versus time using a variation of sampling frequencies. Plots of DOC concentration versus time created from data collected at different sampling intervals in order to highlight the importance of high-frequency sampling in DOC dynamics and export studies (Image source: Jollymore et al., 2012).

FDOM fluorometers use a light emitting diode (LED) as a light source and most have a fixed single excitation/emission pair; although there are less well documented and reliable scanning wavelength fluorometers, which measure the emission signal over a range of wavelengths (Saraceno et al., 2009; Lee et al., 2015). The WETStar FDOM fluorometer from WET Labs has a 7 mm optical path length along which light with a fixed wavelength of 370 nm is emitted to excite the FDOM in stream water. The resulting emission at 460 nm is measured to

quantify the amount of FDOM present using Equation 4.4 (Saraceno et al., 2009). This measurement is typically taken at 1 hertz (Hz) for 30 s every 15 min, 30 min, or every hour and stored on a data logger (e.g., CR1000 data logger, Campbell Scientific). Most FDOM fluorimeters can function at depths up to several hundred meters and across a wide temperature range of 0 to 30 degrees Celsius ($^{\circ}\text{C}$; Bergamaschi et al., 2009). However, a temperature correction algorithm may need to be applied in studies with large temperature fluctuations (see Section 4.3.2). Many FDOM sensors also have automated systems to reduce biofouling (e.g., bio-wipers; Bergamaschi et al., 2009). FDOM sensors are relatively inexpensive (e.g., \$3000-6000) compared to CDOM sensors and have low power requirements (due to the use of LEDs), typically consuming 500 milliwatts or less (Bergamaschi et al., 2009; Conmy et al., 2014).



Figure 21: In-situ optical instruments. Images and dimensions of example in-situ optical sensors: A) WETStar FDOM Fluorometer from WET Labs and B) spectro::lyser from s::can. (Image from A) WET Labs and B) s::can).

On the other hand, submersible spectrophotometers measure absorbance across the UV-VIS spectrum. For example, the spectro::lyser from s::can was the first submersible multiparameter probe that could measure absorbance of CDOM in stream water over the UV-VIS range of 220 to 720 nm (Grayson and Holden, 2012). It can also measure NO₃-N, total suspended solids (TSS), and turbidity (Table 3). The spectro::lyser uses a xenon flash lamp and 256 pixel array detector to measure the resulting absorbance of CDOM at a 2.5 nm wavelength interval over an open path length (Jollymore et al., 2012). The path length on the spectro::lyser can be selected by user, providing users with several options to meet different water conditions. For example, an instrument with a path length of 100 mm can accurately measure DOC concentrations from approximately 0 to 15 mg/L (Jollymore et al., 2012; Grayson and Holden, 2016), however higher DOC concentrations (i.e., up to ~70 mg/L) can be measured using smaller path lengths of 35 mm or 5 mm, but with considerable reduced accuracy (Koehler et al., 2009; Grayson and Holden, 2016). Similar to FDOM sensors, these instruments also have systems to reduce biofouling. For example, they use bio-wipers or compressed gas to clean the optical window at a given interval of time (Etheridge et al., 2014a; Grayson and Holden, 2016). However, biweekly to monthly maintenance is still required as biofouling is not completely eliminated when using any antifouling system (Downing et al., 2009; Jollymore et al., 2012). The spectro::lyser can take measurements over the entire wavelength spectrum (i.e., 220 to 720 nm) at a rate as fast as every 2 min, but typical deployments monitor every 15 min, 30 min, or every hour, which are then stored on an internal data logger. External data loggers (e.g., CR1000 data logger, Campbell Scientific) can also be used with most of these in-situ sensors, including the spectro::lyser, for high-frequency sampling over extended deployment periods (e.g., monitoring at a 15 min interval for greater than 2 weeks, which may exceed the internal

memory). When compared to FDOM sensors, the spectro::lyser requires a larger power supply to power the xenon lamp, although there are numerous options for sustained power including battery, solar, and wind, which are helpful for remote field deployment.

4.4.2 Effects of Temperature on Sensors

It is important to note that temperature and turbidity can both interfere with optical measurements when using in-situ FDOM fluorometers and spectrophotometers. Temperature has an insignificant effect on absorbance readings of UV-VIS sensors, however signals received by FDOM sensors can be greatly affected due to thermal quenching (Baker, 2005; Downing et al., 2012; Conmy et al., 2014; Lee et al., 2015). As temperature increases it will cause electrons to return to the original ground state via radiationless decay, therefore reducing the fluorescence signal (i.e., reducing measured (raw) FDOM values by an average of 0.8-1.5% for every 1°C from 1 to 25°C) of FDOM (Watras et al., 2011; Downing et al., 2012; Lee et al., 2015). The extent of thermal quenching depends on the degree of exposure to the heat source, which varies with organic matter composition (Baker, 2005). In environments with large temperature fluctuations (e.g., >10°C), thermal quenching can result in underestimating FDOM concentrations. Thus users of FDOM sensors should: 1) apply temperature compensation equations to field data (e.g., Watras et al., 2014) or 2) use in-situ spectrophotometers as an alternative in studies where temperature variability will be a factor (Lee et al., 2015).

4.4.3 Effects of Turbidity on Sensors

Turbidity is an inherent issue for both FDOM and UV-VIS sensors as it fundamentally interferes with light passage and detection. Suspended particles that make up turbidity can absorb and scatter light thus altering instrument sensor detection (Downing et al., 2012). As a result, UV-VIS sensor outputs increase linearly with increasing turbidity as the suspended particles

absorb more light than the CDOM would alone. If not accounted for, this turbidity effect results in over estimating CDOM concentration. On the other hand for the FDOM sensor, the scattering of light due to suspended particles will reduce both the excitation signal from the FDOM light emitter and the resulting emission signal to the FDOM detector. If not accounted for, this turbidity effect results in underestimating FDOM concentration (Downing et al., 2012). In fact, FDOM sensors are more sensitive to turbidity than UV-VIS sensors, as FDOM signals decrease exponentially with increasing turbidity (Lee et al., 2015). Saraceno et al. (2009) demonstrated the effect of turbidity on FDOM measurements by including two FDOM sensors, one of which filtered the water prior to measurement and the other that left the water unfiltered. The study showed that at peak discharge during a storm flow event in a stream, when turbidity was highest, the unfiltered FDOM sensors received a dampened signal, thus underestimating the amount of FDOM in the stream by >10% during that point in time (Figure 22; Saraceno et al., 2009). Thus, FDOM field data should be calibrated using turbidity correction equations. To do so, an in-situ turbidimeter must be deployed to simultaneously measure turbidity (Downing et al., 2012). Once turbidity is known, correction equations can be developed based on the specific fluorometer and turbidimeter used as well as the matrix waters, since the extent of reduction of the FDOM signal due to light attenuation is dependent on both the instrument and nature (composition and size) of suspended particles (Downing et al., 2012; Khamis et al., 2015). For example equations see Saraceno et al. (2009), Downing et al. (2012), and Lee et al. (2015). To account for the turbidity effect on CDOM measurements, some UV-VIS instruments, including the scan spectrolyser, estimate turbidity directly from its UV-VIS measurements (Jollymore et al., 2012).

Due to the potential interference of temperature and turbidity, it is recommended that studies using in-situ optical instruments 1) use closed path FDOM sensors with a filtering system

(e.g., see Saraceno et al., 2009) to reduce turbidity effects, and 2) deploy probes for temperature and turbidity in order to correct the FDOM signals received by the sensors with instrument dependent correction functions (Downing et al., 2012; Khamis et al., 2015; Lee et al., 2015). Similarly, turbidity measurements and corrections must be made for UV-VIS instruments, if turbidity correction equations are not already built into the sensor system.

In addition to specific temperature and turbidity interferences, there are a number of other more general logistical strengths and limitations to using FDOM and UV-VIS sensor systems in the field that have been discussed in other studies (e.g., Bergamaschi et al., 2009; Downing et al., 2012; Jollymore et al., 2012). We briefly summarize these strengths and limitations of the technology in Table 3.

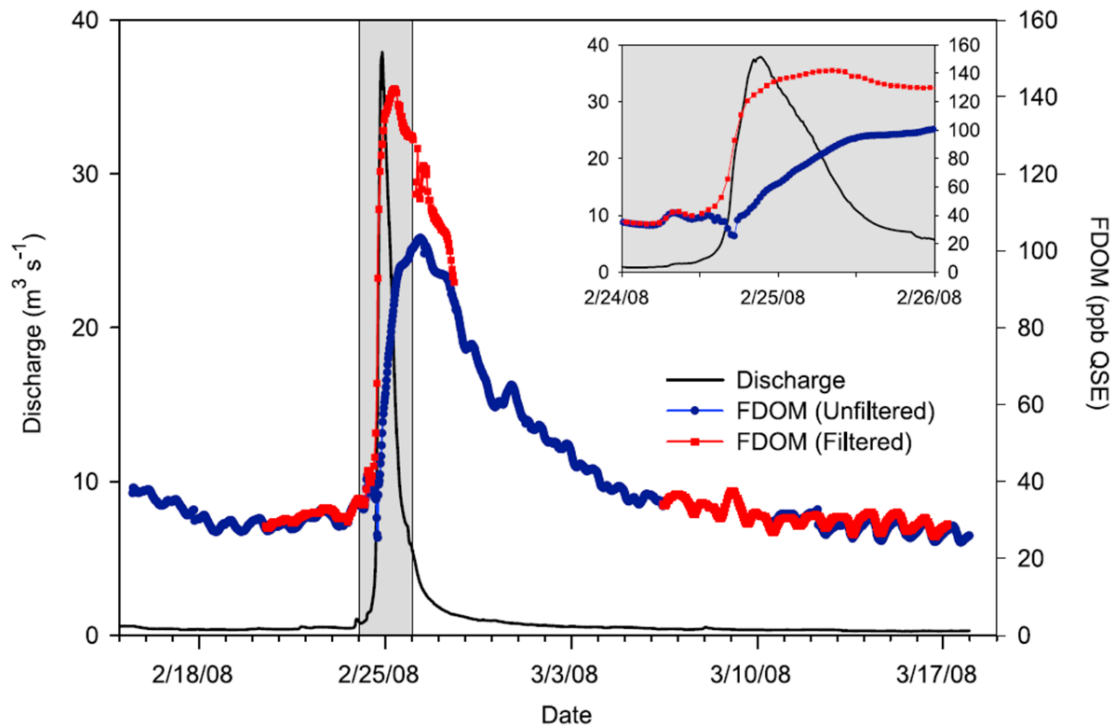


Figure 22: Plot of discharge and FDOM concentration versus time. Both unfiltered and filtered FDOM is plotted showing the importance of using a filter on in-situ FDOM sensors as turbidity can interfere with the sensor, reducing the FDOM signal (Image from Saraceno et al., 2009).

Table 3: Summary of the known strengths and limitations of in-situ optical instruments.

Instrument Type	Strengths	Limitations
<p style="text-align: center;">In-situ FDOM sensors</p>	<ul style="list-style-type: none"> • Use in multiparameter probes • Functions at a range of depths; depth rating of 600 m • Relatively low power requirements; minimal need for sustained power supply • Communicates easily with most data loggers • Data collection frequency of minutes • Anti-biofouling devices available • Use in wide range of water types • Relatively inexpensive • No reagents needed, no waste products 	<ul style="list-style-type: none"> • Sensitive to only small fluorescent fraction of DOM • Temperature interference • Turbidity interference • Biofouling still occurs and requires regular maintenance (biweekly to monthly) • General lack of user-support for system set-up and maintenance (e.g., interfacing between power supply and data logger) • Occasional data loss (e.g., due to power interruptions or exceeding internal memory)
<p style="text-align: center;">In-situ UV-VIS sensors</p>	<ul style="list-style-type: none"> • Use in multiparameter probes • Covers large range in DOC (typically 0-15 mg/L, but larger depending on path length) • Can also measure NO₃-N, TSS, Turbidity • Use in remote field areas • Compressed air and wipers to reduce biofouling • Little to no temperature interference • Data collection frequency of minutes • Numerous sustained power supply options (e.g., battery, wind, solar) • Use in wide range of water types • No reagents needed, no waste products 	<ul style="list-style-type: none"> • Sensitive to only small chromophoric fraction of DOM • Turbidity interference • Biofouling still occurs and requires regular maintenance (biweekly to monthly) • General lack of user-support for system set-up and maintenance (e.g., interfacing between power supply and data logger) • Relatively large power demand and power supply infrastructure needed • Occasional data loss (e.g., due to concentrations outside of measurement range, power interruptions, or exceeding internal memory) • Expensive

4.5 Examples of Utility in Riverine DOC Studies

High-frequency, in-situ optical monitoring is emerging as a critical tool for understanding C transport and processing from hillslopes to streams and from streams to downgradient ecosystems (Waterloo et al, 2006; Saraceno et al., 2009; Jones et al., 2014; Blaen et al., 2016; Grayson and Holden, 2016; Raymond et al., 2016). In order to use in-situ optical methods (e.g., FDOM fluorometers and spectrophotometers) most effectively, they should be coupled with discrete DOC sampling (Downing et al., 2009; Saraceno et al., 2009; Pellerin et al., 2012; Sobczak and Raymond, 2015). The discrete samples allow for direct calibration of DOC concentrations measured from CDOM and FDOM proxies against laboratory measurements as well as allow for quantification of optical properties that require different measurements outside of the range of in-situ optical instruments (e.g., FI values). Automatic pump samplers (e.g., Teledyne ISCO automatic water sampler) are an option for remotely collecting these discrete DOC samples. Some recent studies focused on DOC cycling in stream catchments have leveraged these high-frequency, in-situ optical monitoring technologies to provide new insight on 1) seasonal, event, and diurnal variations in DOC quantity and quality, 2) sources and pathways of DOC to the stream channel and 3) annual DOC flux. These studies and insights are summarized below to illustrate potential future uses of these in-situ optical DOC sampling technologies.

4.5.1 *Revealing Seasonal, Event, and Diurnal Variations in DOC Quantity and Quality*

High-frequency sampling over extended time periods (e.g., multiple months to years) allows for analysis of changes in DOC across numerous time scales. Several studies with sampling periods of months to years have been able to observe seasonal variations in DOC quantity and quality consistent with other long-term DOC studies. For example, Wilson et al.

(2013) examined DOC processes in the steep, humid, forested catchment of Bigelow Brook in Massachusetts, USA. Using a Turner Designs Cyclops-7 CDOM fluorometer, Wilson et al. (2013) sampled at intervals of 15 min for approximately 300 days from October 2009 to November 2010. They observed that DOC concentrations were highest during the summer (July-August) and fall (September-October) seasons. A summer peak in DOC concentrations is also seen in many other regions. For example, Grayson and Holden (2012) saw the highest DOC concentrations during summer months in the upland peat catchment of Cottage Hill Sike in northern England and Jeong et al. (2012) observed large summer DOC concentrations in the mountainous catchment of Haean Basin in northern South Korea. Both Grayson and Holden (2012) and Jeong et al. (2012) were able to observe these seasonal trends using submersible spectrophotometers from s::can (Messtechnik GmbH, Austria). The consistency between results from DOC studies using in-situ optical methods (after site-specific calibration) and those from studies using low-frequency grab samples, supports their ability to provide comparable measures of DOC in riverine systems and confirms our previous understanding of DOC dynamics across seasons. However, beyond just confirming these long-term seasonal patterns, they are revealing new shorter timescale patterns and processes (Figure 20).

Given the high sampling frequency of studies that incorporated in-situ optical instruments, these studies were also able to observe intra-seasonal and multiple individual event flow DOC dynamics, which was previously difficult to near impossible (Figure 20). For instance, Wilson et al. (2013) observed that the DOC response to storm events changed between seasons. DOC concentration increased rapidly with the onset of a storm flow during the summer and fall. DOC then quickly reached a peak concentration and remained elevated throughout the storm event, followed by a rapid decrease in concentration, tracking the decrease in discharge as the storm

ceased. On the other hand, during the spring and winter seasons, DOC concentration showed slower rates of increase at the onset of an event, and DOC also reached a lower maximum concentration and declined more gradually after the event when compared to summer and fall events (Wilson et al., 2013). These seasonally consistent patterns were possible because the sensors captured all the storm events across all the seasons (Figure 20).

As another example of new insight, Saraceno et al. (2009) used in-situ optical methods (i.e., WETStar FDOM fluorometer coupled with discrete grab sampling) to examine DOC variations during individual storm events in the disturbed agricultural watershed of Willow Slough in Sacramento, California, USA. The fluorometer took measurements at 1 h intervals for 4 weeks, during which there was one large precipitation induced storm flow event. Saraceno et al. (2009) observed that in-stream DOC concentration increased with discharge, in this case to 4 times the concentration observed during baseflow (Figure 22). By coupling the in-situ FDOM sensors with discrete sampling, Saraceno et al. (2009) was also able to measure DOC quality parameters such as $SUVA_{254}$, S_R , and FI (although $SUVA_{254}$ and S_R could also be measured had they used an in-situ UV-VIS sensor). These discrete samples paired with the FDOM data, indicated that the DOC in the stream channel during the event was largely of terrestrial origin illustrating that the storm DOC was primarily allochthonous and rapidly mobilized from hillslopes to the stream.

Additionally, in-situ optical instruments have been used to study DOC dynamics during snowmelt events. Pellerin et al. (2012) studied variations in DOC quantity and quality associated with a snowmelt event in the Sleeper's River watershed in Vermont, USA. Using a WETStar FDOM fluorometer, measurements were taken at 30 min intervals for 2 months. Here, they also observed increasing DOC concentrations with increasing snowmelt. It should be noted that there

are studies, which show clear decreasing or decoupled DOC concentration with discharge. Grayson and Holden (2012) examined DOC processes in an upland peat catchment using an in-situ spectrophotometer, which took measurements every 15 to 20 min from July to December 2009. They observed decreasing CDOM absorbance (i.e., CDOM concentration) along the rising limb of numerous storm hydrographs and overall found discharge and CDOM absorbance to be poorly correlated. Similarly, Koehler et al. (2009) used an in-situ spectrophotometer to study DOC dynamics in an Atlantic blanket bog in southwest Ireland. Sampling was conducted every 30 min over the course of 2007. DOC concentration was shown to have a weak, negative correlation with discharge, and instead a strong correlation with temperature, indicating that temperature dynamics rather than flow dynamics are the primary control on DOC in these bog systems. These studies, where discharge and DOC concentration were inversely related, hypothesized that the decrease in DOC during the rising limb of the hydrograph is likely due to 1) dilution as the hydrological response in peatland catchments is different from steeper hillslope catchments and 2) that DOC production in the peatlands may be limited by the time in between storms (as microbes break down organic matter at times when the water table is low), and therefore the pool of DOC available for export is depleted over the wet season (Koehler et al., 2009; Grayson and Holden, 2012).

Being able to consistently monitor DOC responses across storm events and seasons will allow for new ways to compare watersheds and their responses to flow events. This is crucial to understand the annual DOC flux out of watersheds and delivered to downstream ecosystems and water resources, a large portion of which occurs during these intermittent flow events (Jones et al., 2014; Raymond et al., 2016). These in-situ optical sensors enable researchers to more safely

and consistently sample during both low and high magnitude storm events, the timing of which is not always predictable (Figure 20).

At an even finer temporal resolution, in-situ optical sensors are revealing short-lived, diurnal changes in DOC quantity and quality (e.g., Spencer et al., 2007; Worrall et al., 2015) as a result of ecosystem processes (e.g., autochthonous DOC production). Spencer et al. (2007) used a WETStar FDOM fluorometer along with two in-situ spectrophotometers (AC-9 photometer for the visible range and a Satlantic UV spectrophotometer for the UV range) in order to assess diurnal variations in DOC in the San Joaquin River in California, USA. Spencer et al. (2007) observed that DOC does exhibit measurable diurnal variations. CDOM absorbance values peaked in the early evening and bottomed out at dawn, while CDOM fluorescence and S_R were highest in the early morning (Figure 23). In addition to the CDOM peak in the early morning, CDOM fluorescence exhibited a second peak at dusk. Through these unprecedented measurements, Spencer et al. (2007) were able to conclude that the decreasing daytime CDOM fluorescence is likely suggestive of photobleaching, while the imposed second CDOM peak on the overall diurnal trend is hypothesized to be the result of zooplankton grazing. When the S_R trends were compared to CDOM absorbance and fluorescence trends, the decreasing S_R values throughout the daytime help support the hypothesis that DOC quantity and quality is controlled on a diurnal scale by photochemical processing and in-situ biological production (possibly from zooplankton grazing). However, Spencer et al. (2007) acknowledges that the diurnal variations in DOC are complex and the controlling processes need to be further studied as these short-term DOC variations may complicate DOC source studies. These new hypotheses along with intra-seasonal, event, and diurnal DOC variations can now be more regularly evaluated across systems where these high-frequency measurements can be made. This will allow for cross-site,

transferable understanding of how short-term processes may impact longer timescale observations and ecosystem processes.

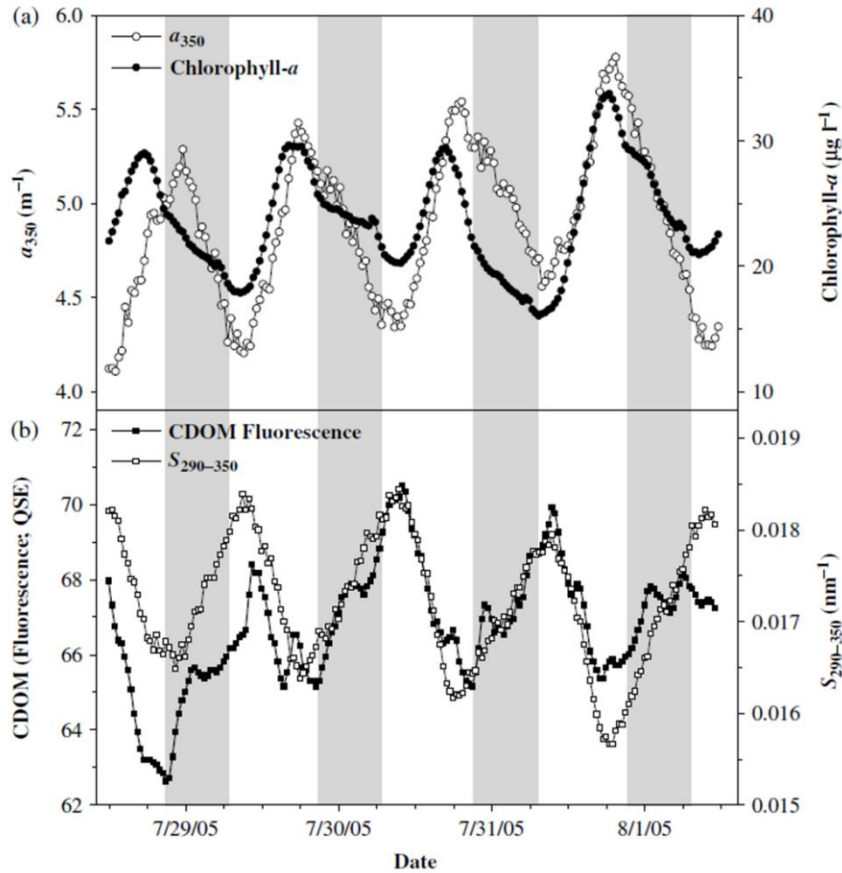


Figure 23: Diurnal trends for CDOM and absorbance. Absorbance peaks in the early evening, while CDOM peaks in the early morning (Image from Spencer et al., 2007).

4.5.2 Revealing Sources and Pathways of DOC to the Stream Channel

In-situ optical methods also provide insight on shifts in sources and pathways of DOC through time (e.g., during storm events, between seasons, etc.) by utilizing temporal data of DOC quantity and molecular characteristics. As mentioned earlier, Saraceno et al. (2009) observed that terrestrially-derived DOC increased in the stream channel during the storm event, by measuring SUVA_{254} , S_R , and FI (again SUVA_{254} and S_R could be measured using an in-situ UV-VIS sensor to achieve a higher sampling frequency). However, the FI values observed (i.e., 1.5-1.7) were

higher than predicted for a disturbed agricultural watershed. Therefore, Saraceno et al. (2009) concluded that the terrestrially-derived DOC was likely “fresh” or less degraded, specifically coming from plant leachates in surface runoff over organic-rich agricultural soils. In addition, by conducting high-frequency sampling of FDOM using an in-situ optical sensor, Saraceno et al. (2009) observed a time lag between peak FDOM, discharge, and turbidity, where the FDOM lagged ~11 to 15 h behind peak discharge and turbidity. This suggests that in their disturbed agricultural watershed, shallow soil flowpaths remain important for several days after the precipitation event and that the suspended sediment (i.e., turbidity) and FDOM may have different watershed sources, because they peak at different times. Without the continuous high sampling frequency of in-situ optical sensors this lag in variables would likely have gone unnoticed.

A time lag between peak discharge and peak FDOM was also observed in other optically-based studies. Wilson et al. (2013) saw a similar length time lag between the FDOM and discharge during storm events in their forested headwater catchment as Saraceno et al. (2009), while Pellerin et al. (2012) observed a much shorter (~60 min) time lag during snowmelt events in Vermont, USA. The tight coupling of peak discharge and peak FDOM seen by Pellerin et al. (2012), along with their observed increasing $SUVA_{254}$ and decreasing FI values, indicated that surficial flowpaths along organic-rich soils were dominant during the snowmelt events (similar to Saraceno et al., 2009). Other studies also found that increasing DOC concentrations during storm events are likely derived from surface and shallow subsurface flowpaths. For example, Waterloo et al. (2006) used an *in-situ* spectrolyser to examine DOC variations in blackwater streams of the Amazon rainforest. Measurements were made at 30-min intervals from February to September 2002. By additionally estimating shallow and deep groundwater flow using

Darcy's Equation, Waterloo et al. (2006) was able to use the spectro:lyser data to determine that solute paths shifted from deeper groundwater regions to shallow subsurface layers in the valley soils that are rich in organic material during the many observed storm events.

Finally, high-frequency data can also be used to observe and characterize detailed hysteresis relationships between discharge and FDOM concentration to infer DOC sources and processing. Pellerin et al. (2012) observed a counter-clockwise hysteresis relationship (Figure 24), which is hypothesized to be the result of a delayed contribution from surface and shallow subsurface flowpaths and suggests that DOC export in the Sleeper's River watershed is transport limited rather than source limited. While many studies have also seen counter-clockwise hysteresis relationships for discharge and FDOM concentration (e.g., Strohmeier et al. 2013), some have observed clockwise hysteresis relationships. Jeong et al. (2012) saw a clockwise hysteresis relationship when studying DOC dynamics in the mountainous watershed in South Korea suggesting that DOC export in this watershed is source limited (i.e., DOC rich soil pools are depleted along the falling limb of the hydrograph). The discrepancy between hysteresis relationships for discharge and FDOM concentration is an important area of future research and may be dependent on watershed characteristics (e.g., slope, land cover, antecedent conditions, etc.). Having the ability to observe many hysteretic responses (via in-situ optical sensors) across a gradient of storm types in one watershed or across many watersheds will provide greater insight to what spatial and temporal watershed conditions are the primary controls on DOC concentrations and molecular characteristics. Overall, the ability to generate more transferable ideas and theories about DOC dynamics in watersheds and riverine systems is growing due to the ability of optical sensors to more consistently document DOC storm event dynamics across a huge range of watersheds (Figure 20).

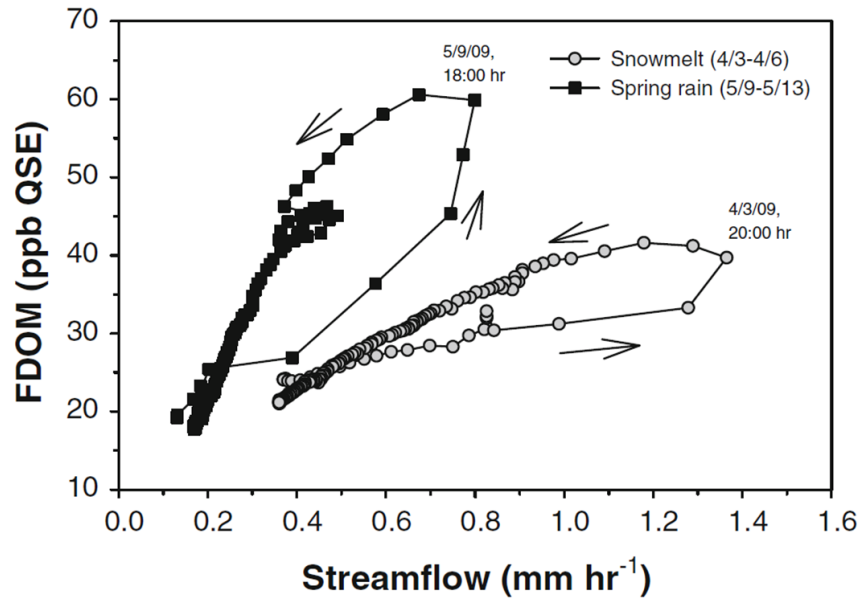


Figure 24: Hysteresis trends. Counter-clockwise hysteresis observed during both snowmelt and precipitation events for FDOM (Image from Pellerin et al., 2012).

4.5.3 Annual DOC Flux

Previous work on sampling frequency, especially across dynamic stream flow conditions, found that infrequent sampling of DOC results in large underestimations of DOC fluxes (i.e., -10 to -88%), especially during moderate to low flow periods (Saraceno et al., 2009; Jollymore et al., 2012; Pellerin et al., 2012; Wilson et al., 2013; Jones et al., 2014; Grayson and Holden, 2016). As a result high-frequency, in-situ sampling of FDOM concentration should be used to improved DOC flux quantification. Thus far, studies that have incorporated in-situ optical sensor methods were able to better calculate short-term and annual DOC fluxes from watersheds (e.g., Koehler et al., 2009; Jones et al., 2014).

Most studies using in-situ optical sensors found that a significant amount of the annual DOC flux is exported during isolated brief storm events or, if in a more Mediterranean climate, during the wet season. Wilson et al. (2013) found that 63% of the annual DOC flux was exported during these brief, reoccurring hydrologic storm events, while Koehler et al. (2009) and Jeong et

al. (2012) found that 45% and 48% respectively, was exported during storm events. Additionally, Waterloo et al. (2006) observed that 69 to 72% of annual export occurred during the wet season, all of which corroborates the need to sample on intra-seasonal and diurnal time scales. Waterloo et al. (2006) also quantified a relationship between DOC flux and stream discharge. The largest fluxes of DOC were typically seen in the top 10% of high flows (Koehler et al., 2009), thus as stream discharge increases, DOC flux will typically increase and in a predictable manner. For example, given the high temporal characterization of DOC across a large range of flow conditions (Figure 25), Waterloo et al. (2006) was able to generate two empirical models for DOC flux as there appears to be a threshold behavior in the specific DOC flux response to a given discharge (Figure 25). Specifically Waterloo et al. (2006) showed that DOC flux, F_{DOC} , when stream flow (Q_{stream}) is less than 2.8 mm d^{-1} (Equation 4.6; $r^2 = 0.79$) is,

$$F_{\text{DOC}} = 0.0075 \times Q_{\text{stream}}^{1.5630} \quad (4.6)$$

and when Q_{stream} is greater than 2.8 mm d^{-1} (Equation 4.7; $r^2 = 0.99$).

$$F_{\text{DOC}} = 0.0278 \times Q_{\text{stream}} - 0.0432 \quad (4.7)$$

Overall, more accurate estimates of flux dynamics were possible using the high resolution in-situ optical sensors in both cases of flux budgets and flux response to changes in flow.

Understanding these consistently observed “pulses” of DOC in response to variable flow conditions is important to future research of ecosystem processes at the watershed scale. Specifically, C gains and losses are important for understanding and accurately quantifying net ecosystem productivity and net ecosystem C balance (Wilson et al., 2013). Thus, missing or misappropriating the key portion of C in the form of DOC will result in erroneous net ecosystem C balance models. In addition, understanding changes in sources and pathways of DOC to the

stream channel is key to determining DOC quality moving through riverine environments, because DOC quality is largely dependent on C source material (Cory et al., 2011). The timing of both DOC quantity and molecular characteristics impacts DOC bioavailability and, therefore, timing of DOC flux can have a large effect on organisms, downstream ecosystems, and water quality. These in-situ sensors seem to be capable of greatly improving our ability to “take the pulse” of key ecosystem parameters, specifically, DOC moving through watersheds and ecosystems (Roley et al., 2014). In taking the pulse of DOC in streams, we are also able to use that information to guide the study design and monitoring of other watershed attributes that control ecosystems and water quality, such as limiting nutrients (Blaen et al., 2016).

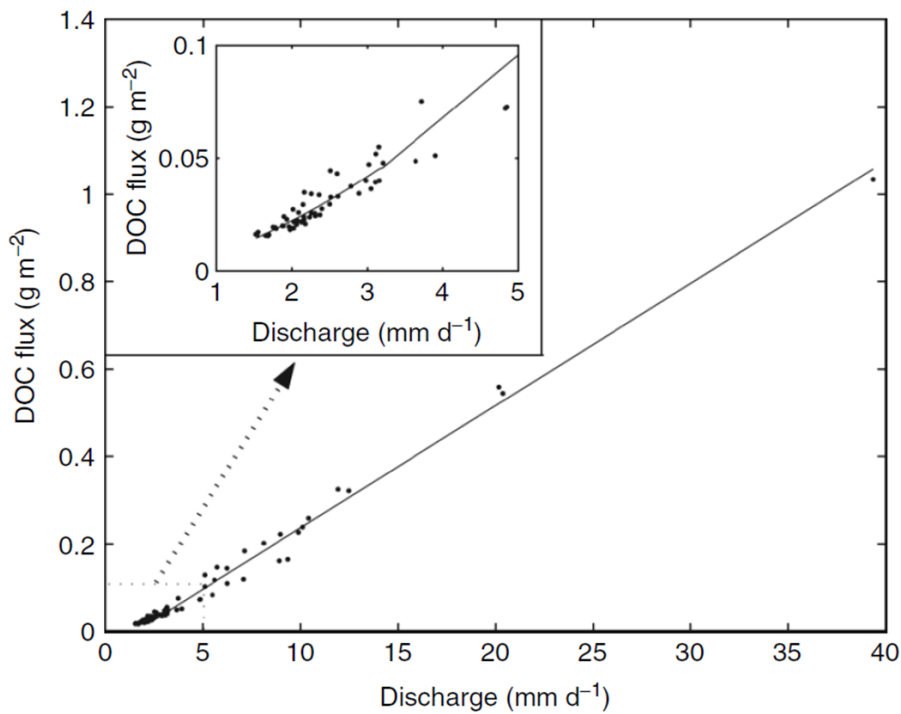


Figure 25: DOC flux versus discharge. DOC flux increases linearly with discharge, although the relationship shifts slightly from low to high discharge (Image from Waterloo et al., 2006).

4.6 Conclusions & Future Considerations

High-frequency, in-situ optical monitoring allows for much higher resolution temporal observations of DOC processes in riverine environments than ever previously thought possible (i.e., dynamics operating on temporal scales of seconds to minutes, Figure 20 and 4.5). Thus, new processes and understanding of DOC in watershed and riverine systems are being revealed. In particular, these sensors are facilitating novel observations, conceptual understanding, and models that address fundamental questions about watershed DOC quantity and quality through time, the sources and pathways of DOC to the river network, and DOC mass flux. Future research on these important DOC dynamics will benefit from the use of these technologies. These early adopters of these in-situ optical sensor technologies have already made great advances as discussed above.

The in-situ optical methods are quick, precise, and relatively inexpensive when compared to collecting discrete water samples in the field and later completing chemical C analyses. However, they still have limitations that must be addressed by users. In particular, in-situ FDOM fluorometers and spectrophotometers should still be coupled with some discrete sampling to include the full range of DOC optical properties as well as cross check DOC concentrations against CDOM and FDOM proxies. In addition, temperature and turbidity correction equations should be applied (if not already built-in within the sensor system), especially in watersheds with large temperature fluctuations and/or high suspended sediment loads. There are emerging methods to make these temperature and turbidity corrections as this is an active area of research. It is worth noting again, as discussed in Section 4.2.1 and 4.2.2, FDOM and CDOM sensors only measure a fraction of the total DOM pool so all interpretation of bulk DOM processes and dynamics must be done in light of this limitation. Nonetheless, these in-situ optical methods can

provide valuable information on DOC processes in streams and watersheds that is otherwise logistically prohibitive and therefore unavailable. As more users adopt this technology, user-support will also increase, eliminating numerous potential concerns (e.g., interfacing with power supplies and data loggers). In addition, these sensors could be used to standardize protocol between research groups and environmental regulators, creating opportunity for better networking and data sharing plans. As the climate and anthropogenic uses of land and water continues to change, in-situ optical instruments are likely to become crucial to measuring the pulse of riverine and watershed responses to these changes. Having this information will help to diagnose and understand both associated short- and long-term changes in DOC quantity and quality, C cycling in watersheds, as well as help guide the development of future watershed-scale management strategies.

4.7 Acknowledgements

The authors would like to thank the editor and three anonymous reviewers for their helpful suggestions. Support for this research was also provided by the NSF Long-term Ecological Research Program (DEB 1027253) at the Kellogg Biological Station and by Michigan State University AgBioResearch.

CHAPTER 5: SYNTHESIS & IMPLICATIONS

This thesis focused on understanding the role of the stream water-groundwater interface in dissolved organic carbon (DOC) cycling in river networks. The central research questions addressed in Chapters 2 and 3 were 1) is the hyporheic zone (HZ) a significant processor of stream DOC at the watershed scale in a lowland river, and if so, 2) how is DOC being processed? To assess these questions, two synoptic HZ sampling campaigns were conducted in August 2015 and 2016 across the Augusta Creek watershed in southwestern, Michigan. The results presented in Chapter 2 indicate that the HZ is a (potentially important) location for DOC processing in stream networks and that the processing signal can be observed across stream orders throughout the watershed. However, it was concluded that even at the watershed-scale, analyses needed to be conducted on a site-by-site basis, and that improved chemical and hydrological data (e.g., dissolved oxygen, vertical head gradient) were necessary to more accurately interpret the trends in hyporheic DOC quantity and quality. With the improved chemical and hydrological data in 2016, we were able to assess how DOC is processed in the HZ (i.e., the dominant transformation mechanisms). The results presented in Chapter 3 indicate that the HZ acts as a sink for DOC and that aerobic, microbial respiration may be the dominant processing mechanism removing DOC in the HZ.

By studying the HZ at the watershed scale, we can ask questions about the larger ecosystem function (i.e., sink) of the HZ. Specifically, does the role of the HZ as a processor of stream DOC change based on location in the watershed (e.g., across stream orders). The results presented in Chapter 3 suggest that, the HZ may function as a larger sink for DOC in headwater streams than in higher stream orders across the watershed, despite the observed, lower processing potentials. However, the results were inconclusive in terms of the fate of DOC

quality, which appeared to be influenced by changes in local VHG. Thus, further studies focused on DOC quality need to be conducted since changes in DOC quality due to hyporheic processes may alter the fate of DOC transported downstream.

Chapter 4 provided a review of in-situ, optical instruments that can be used in stream networks to better understand the short-term dynamics of DOC quality in a cost-effective way. These new technologies offer the potential to dramatically improve our understanding of stream DOC fluxes, including the variation in sources and transformations in space and time.

In conclusion, previous HZ studies of DOC processing have predominantly been small-scale field and mesocosm studies (e.g., Findlay et al., 1993; Findlay and Sobczak, 1996; Schindler and Krabbenhoft, 1998; Sobczak and Findlay, 2002; Zarnetske et al., 2011), yet hyporheic processes are also expected to impact stream DOC cycling on larger scales (e.g., watershed scale; Boano et al., 2014). To the best of our knowledge, the present work represents one of the first watershed-scale HZ sampling efforts and in doing so, we were able to more accurately assess the role of the HZ on DOC cycling throughout the stream network, concluding that the HZ acts as a sink for DOC within the larger carbon (C) cycle of Augusta Creek, Michigan, USA.

If these results are transferrable to other watersheds, hyporheic processing of stream DOC may be a potential mechanistic explanation for the recently observed, large carbon dioxide (CO₂) efflux from streams (Butman and Raymond 2011; Raymond et al., 2013). Nonetheless, this research indicates the need to include streams and the associated HZ processes in global C budgets, since accurately modeling the global carbon (C) cycle is necessary for mitigating future climate change. In addition, this thesis highlights several gaps in our understanding of how to study HZ processes at the watershed scale that need to be addressed going forward:

- 1) When sampling at the watershed-scale, how important is local variation in hyporheic DOC conditions (i.e., within a single site), versus the variation observed across a stream reach or an entire stream order? This will control how we sample the HZ over an entire watershed (e.g., choosing between triplicate, duplicate, or single porewater sampling schemes).
- 2) The use of distributed, in-situ sensor technologies across watersheds is improving our understanding of DOC quality dynamics in the open stream channel. However, advancements in using similar distributed, in-situ sensor networks to study the coupling of the stream and HZ are needed.
- 3) Lastly, to better identify the dominant transformation mechanisms of DOC in the HZ, studies are needed that incorporate dissolved inorganic carbon (DIC) measurements such as CO₂ since it is often a product of biotic processes which remove DOC as well as direct measurements of microbial respiration rates across entire stream networks.

APPENDICES

APPENDIX A

2015 Synoptic Hyporheic Zone Sampling Data

Table A1: Supplemental information for the 2015 sampling sites.

Sampling Site	Longitude	Latitude	Stream Order	Drainage Area (km ²)	Depths with Mixing Zone Signal	D ₅₀ (mm)	Land Use % Agriculture	Land Use % Forest	Land Use % Wetland
A	-85.332	42.4197	1	1.92	NA	0.41	41	29	18
B	-85.3547	42.4037	3	69.69	2.5-15 cm	0.81	48	21	22
C	-85.3534	42.427	2	41.66	2.5-10 cm	0.69	48	21	21
D	-85.3517	42.4176	2	47.69	2.5-7.5 cm	0.47	53	19	19
F	-85.3449	42.407	3	68.17	NA	0.29	48	21	22
G	-85.319	42.4479	1	1.77	2.5-20cm	0.46	60	13	13
H	-85.3233	42.4468	2	32.47	2.5-7.5 cm	0.47	44	24	22
I	-85.3539	42.3534	3	95.39	2.5-5.0 cm	0.43	43	28	19
J	-85.3366	42.4573	2	26.30	2.5-5.0 cm	0.53	41	22	23
K	-85.3525	42.4688	1	7.78	NA	2.71	30	23	28
L	-85.3425	42.4628	1	9.56	NA	0.38	35	25	18
M	-85.3107	42.4089	1	7.38	2.5-5.0 cm	0.71	39	27	19
O	-85.343	42.4213	1	0.80	2.5-5.0 cm	0.52	77	5	9
P	-85.3441	42.4113	2	50.02	2.5-10 cm	2.56	53	19	19
Q	-85.3516	42.3906	3	73.18	2.5-5.0 cm	1.93	47	22	21
R	-85.3599	42.3688	3	86.15	NA	1.01	46	25	19

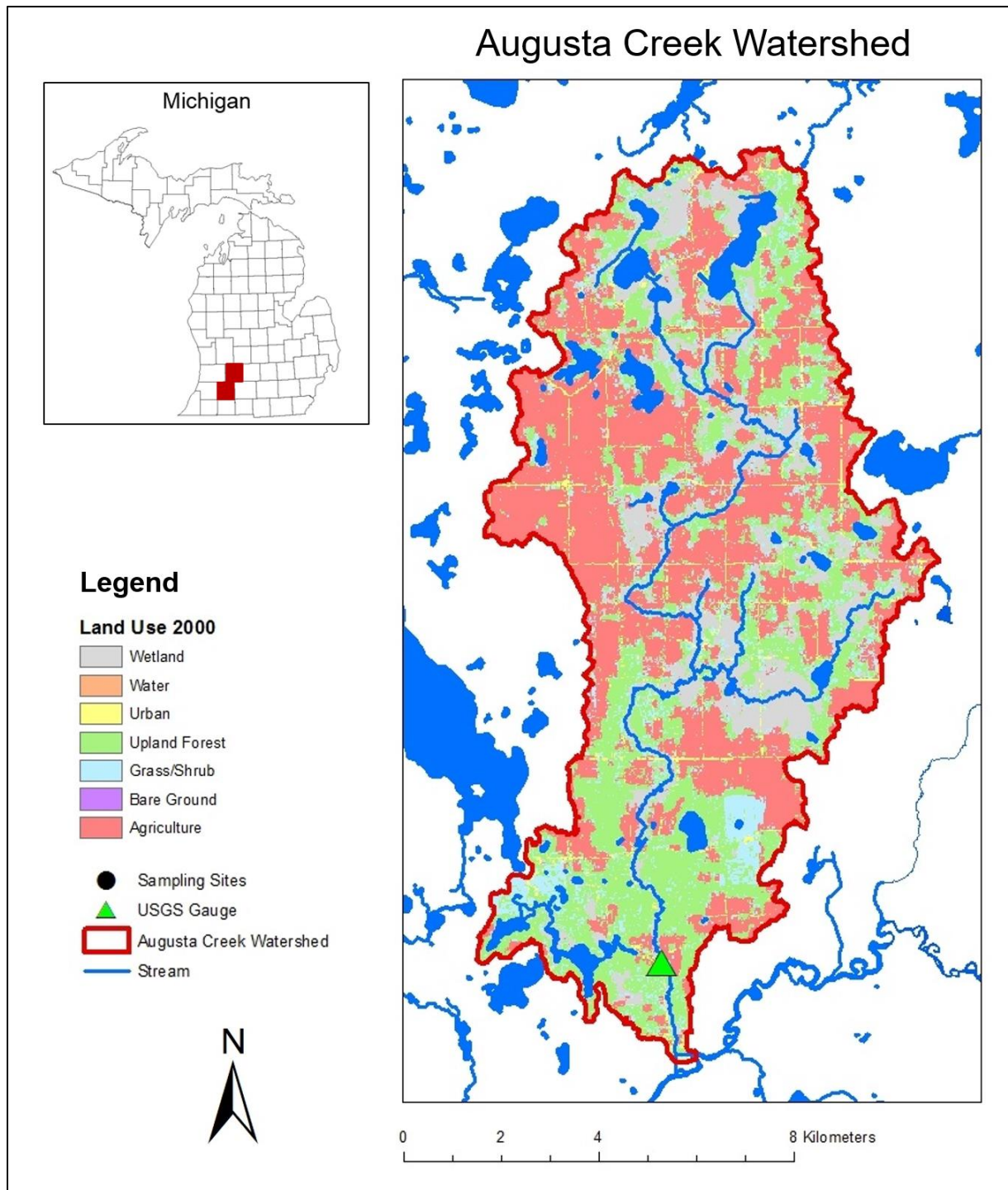


Figure A1: Map of Augusta Creek watershed with land use. Map of the Augusta Creek watershed in Barry and Kalamazoo counties, MI, USA. The map shows the dominant land use types across the watershed including upland forest, wetland, and agriculture.

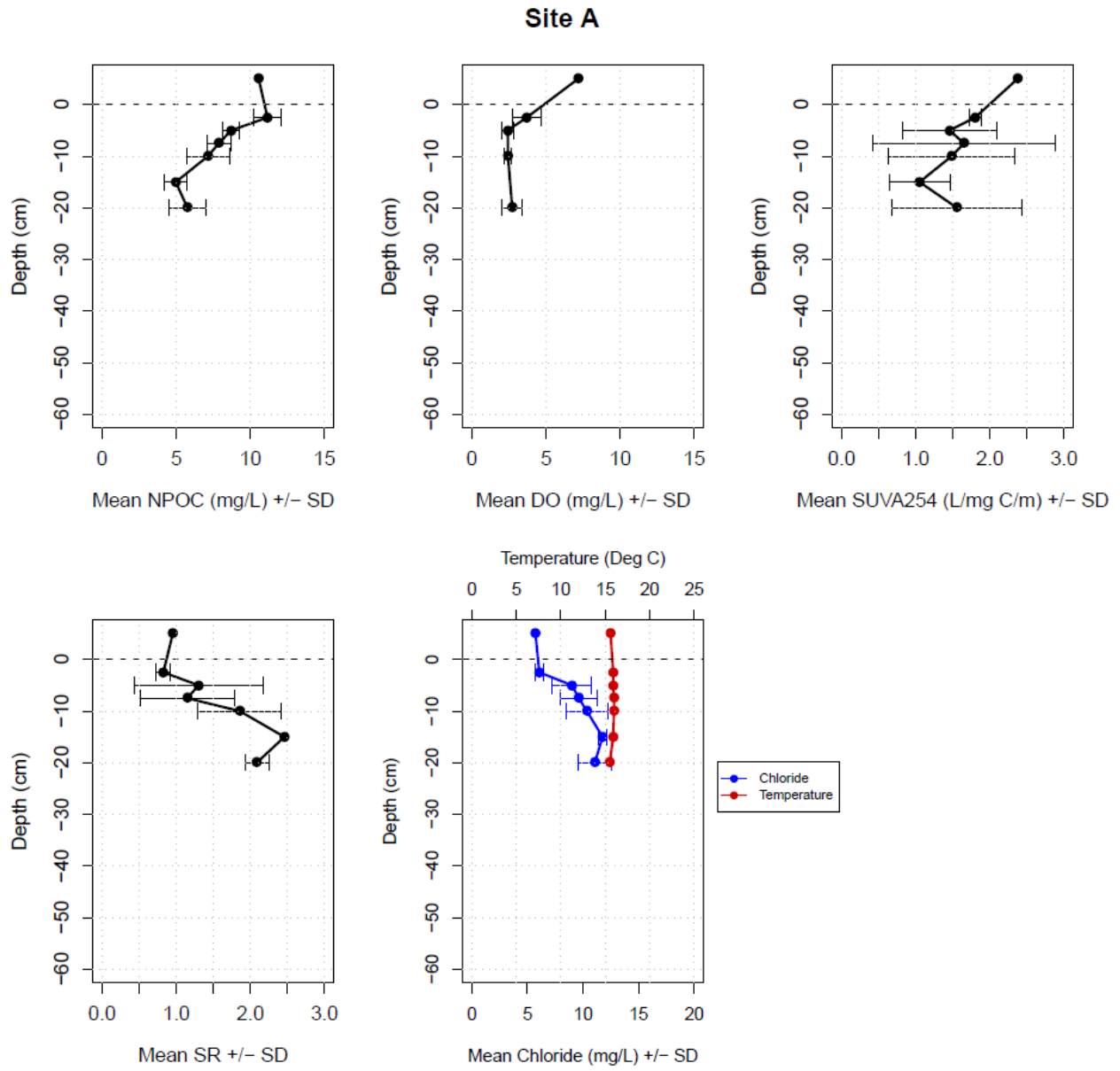


Figure A2: Site A Vertical Porewater Profiles

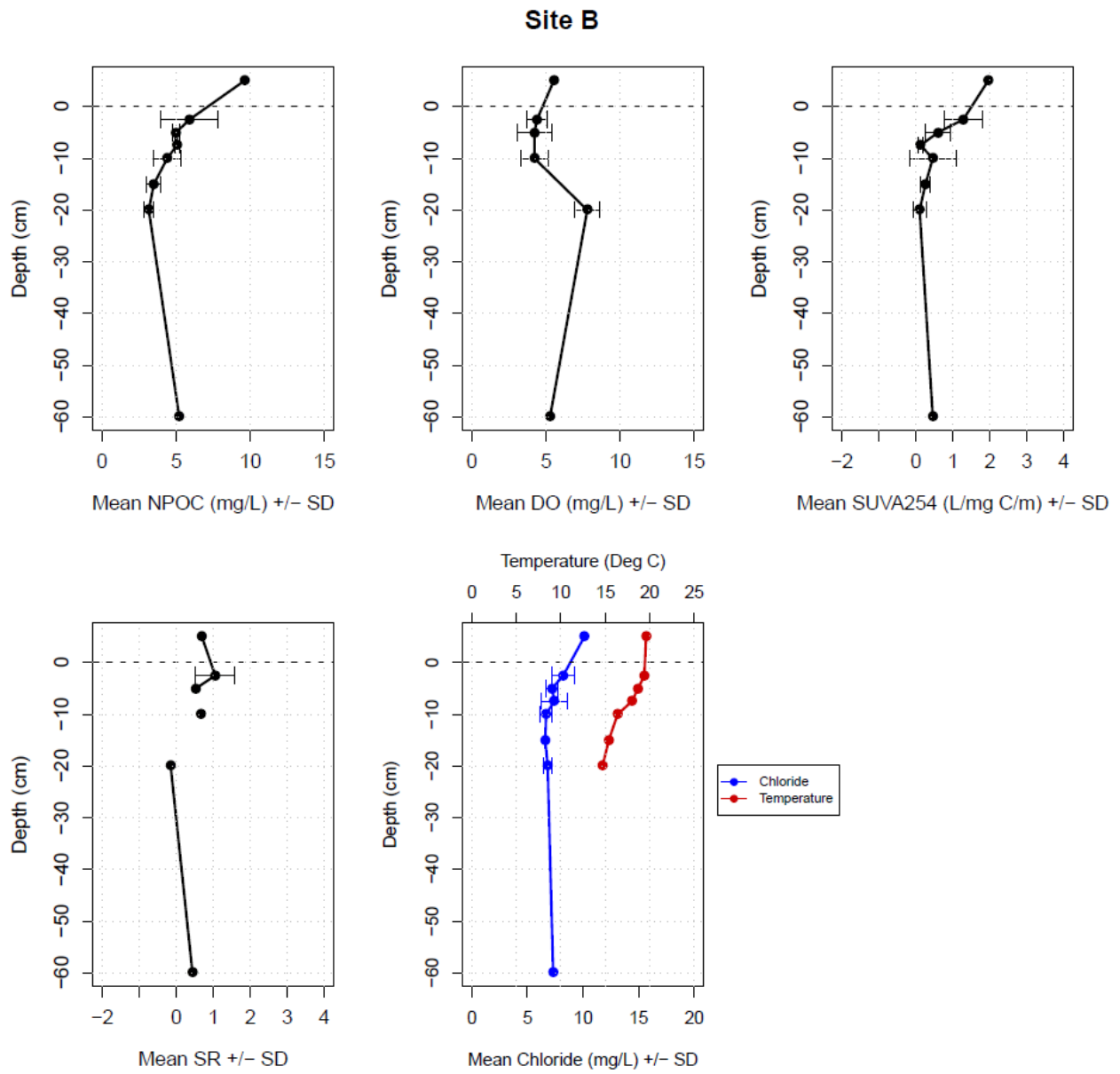


Figure A3: Site B Vertical Porewater Profiles

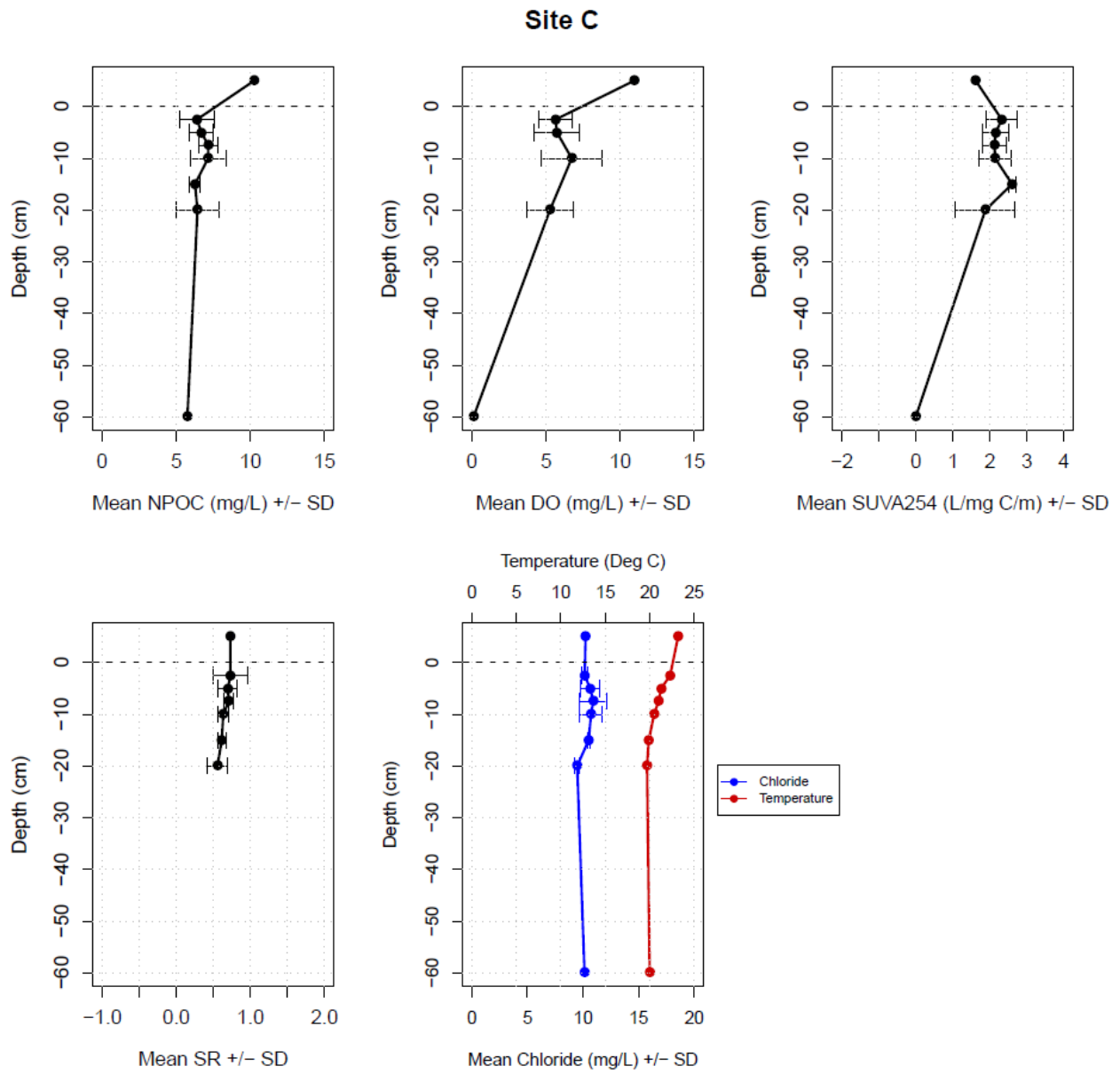


Figure A4: Site C Vertical Porewater Profiles

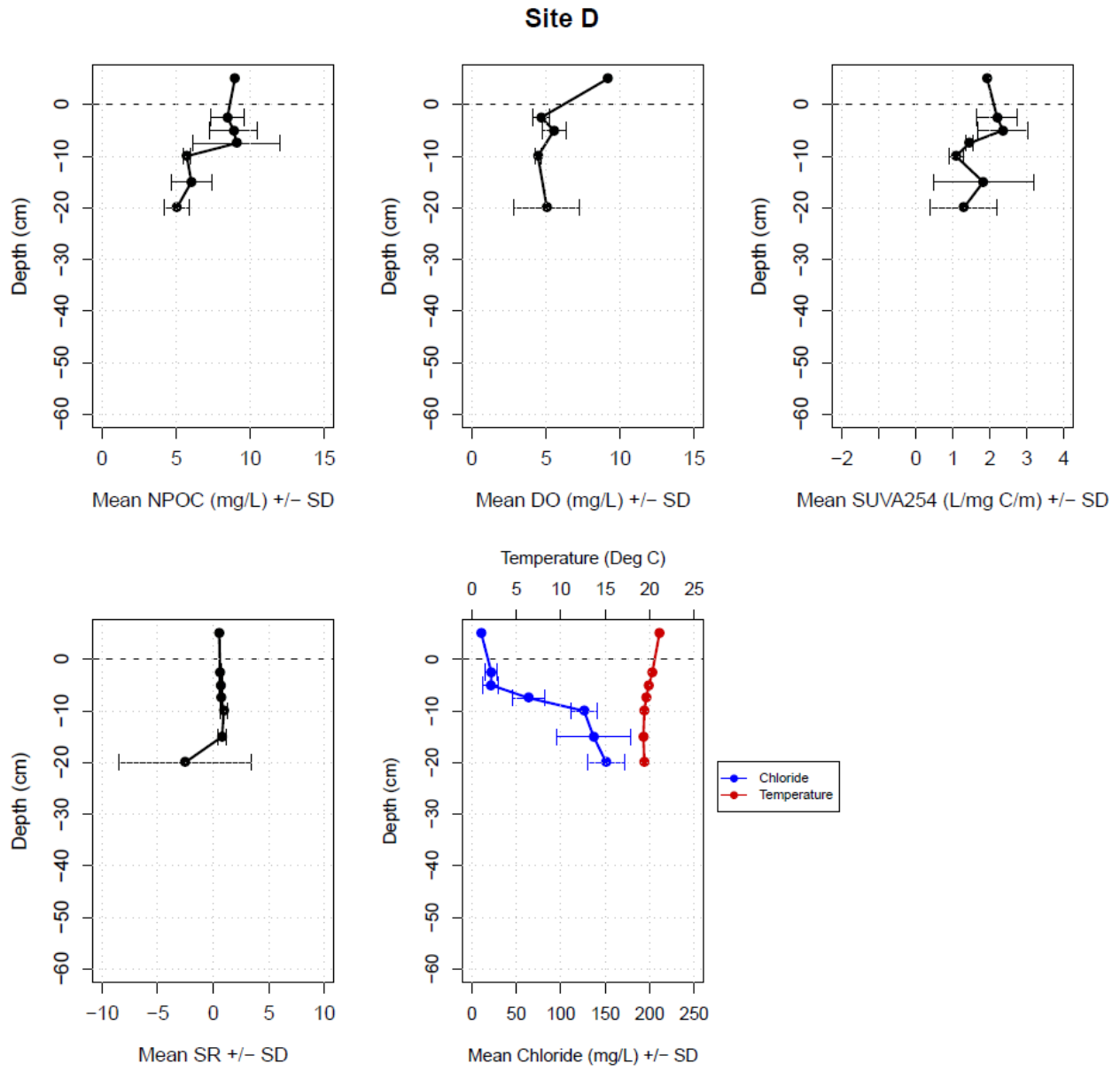


Figure A5: Site D Vertical Porewater Profiles

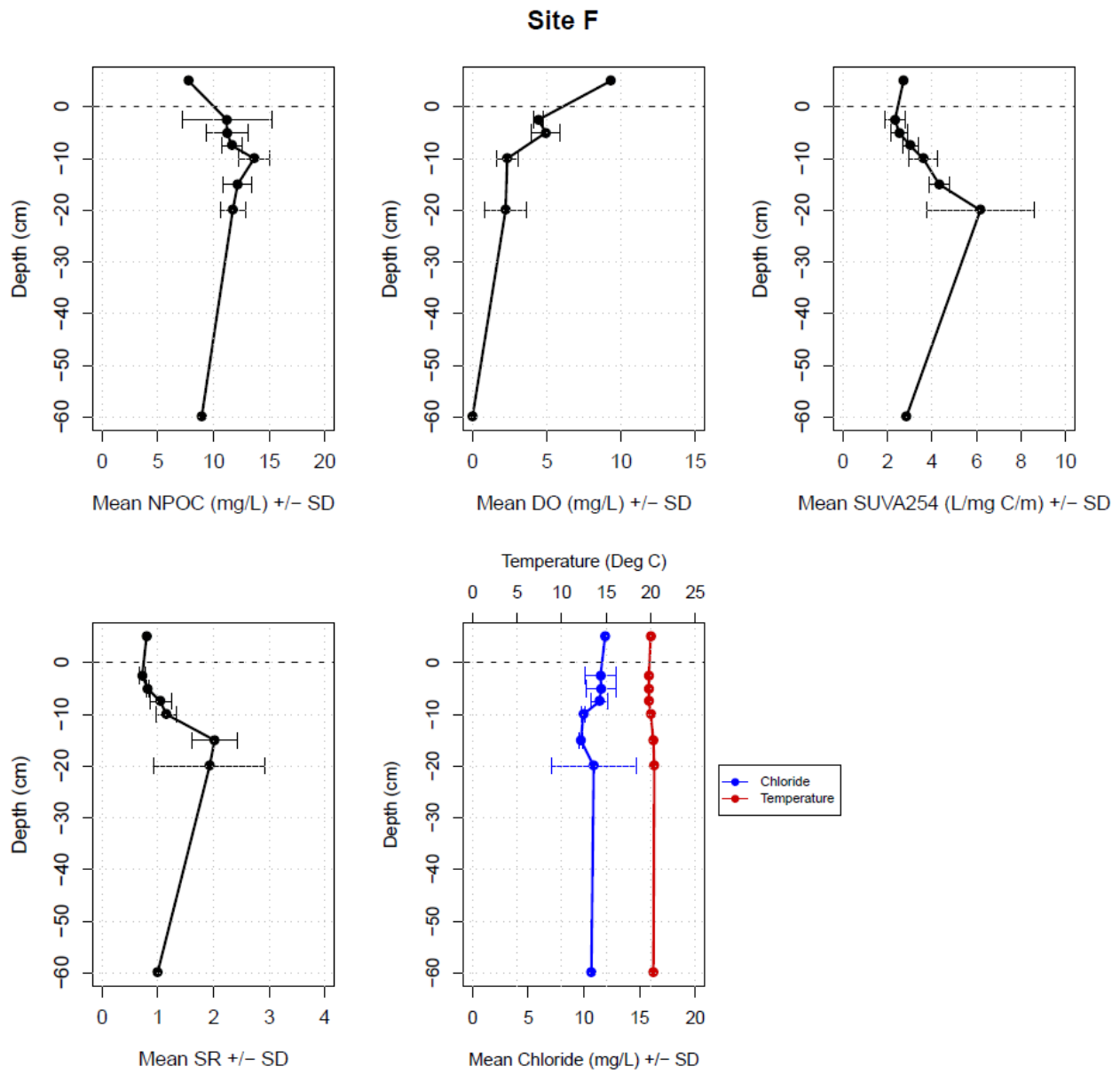


Figure A6: Site F Vertical Porewater Profiles

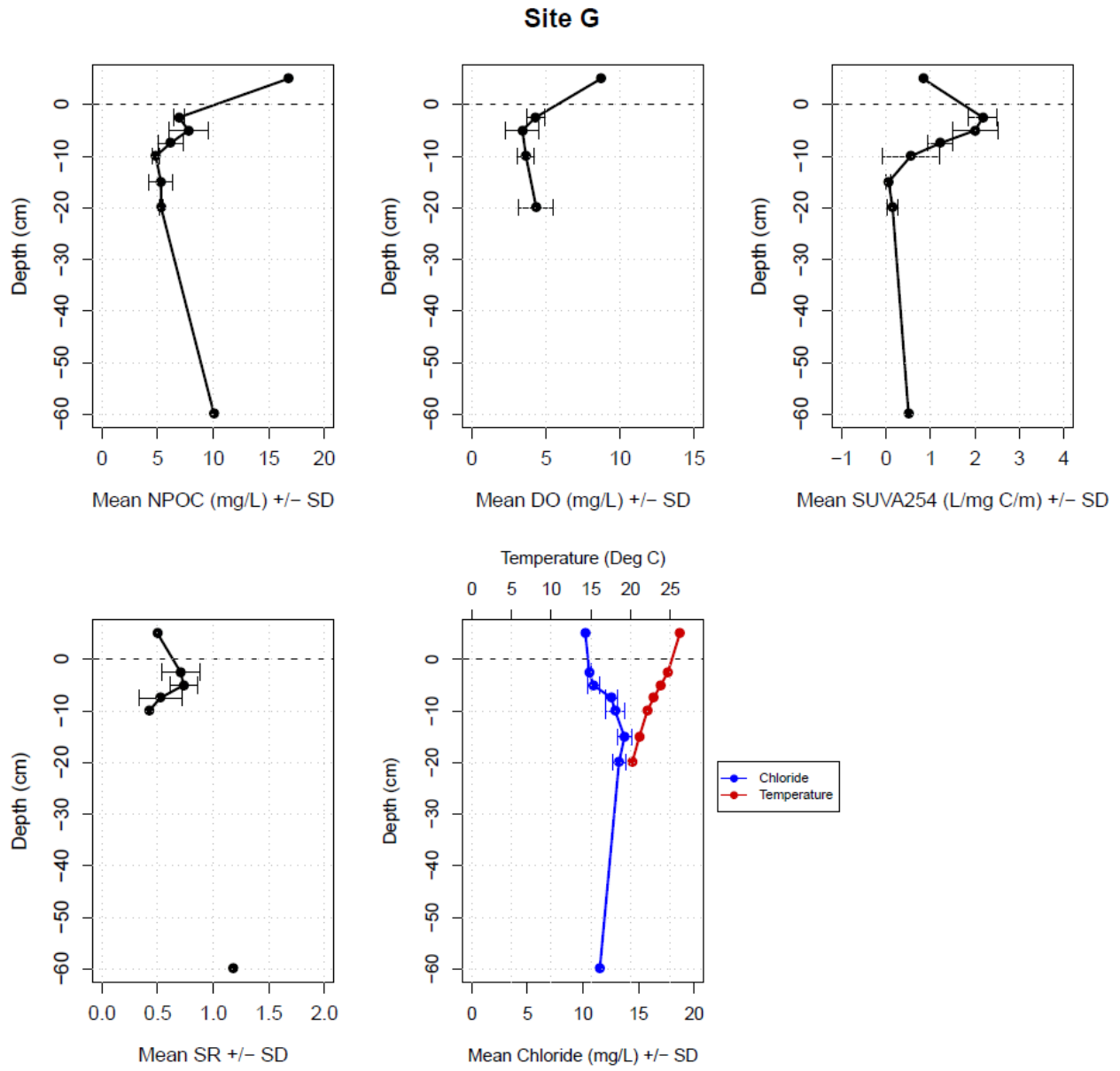


Figure A7: Site G Vertical Porewater Profiles

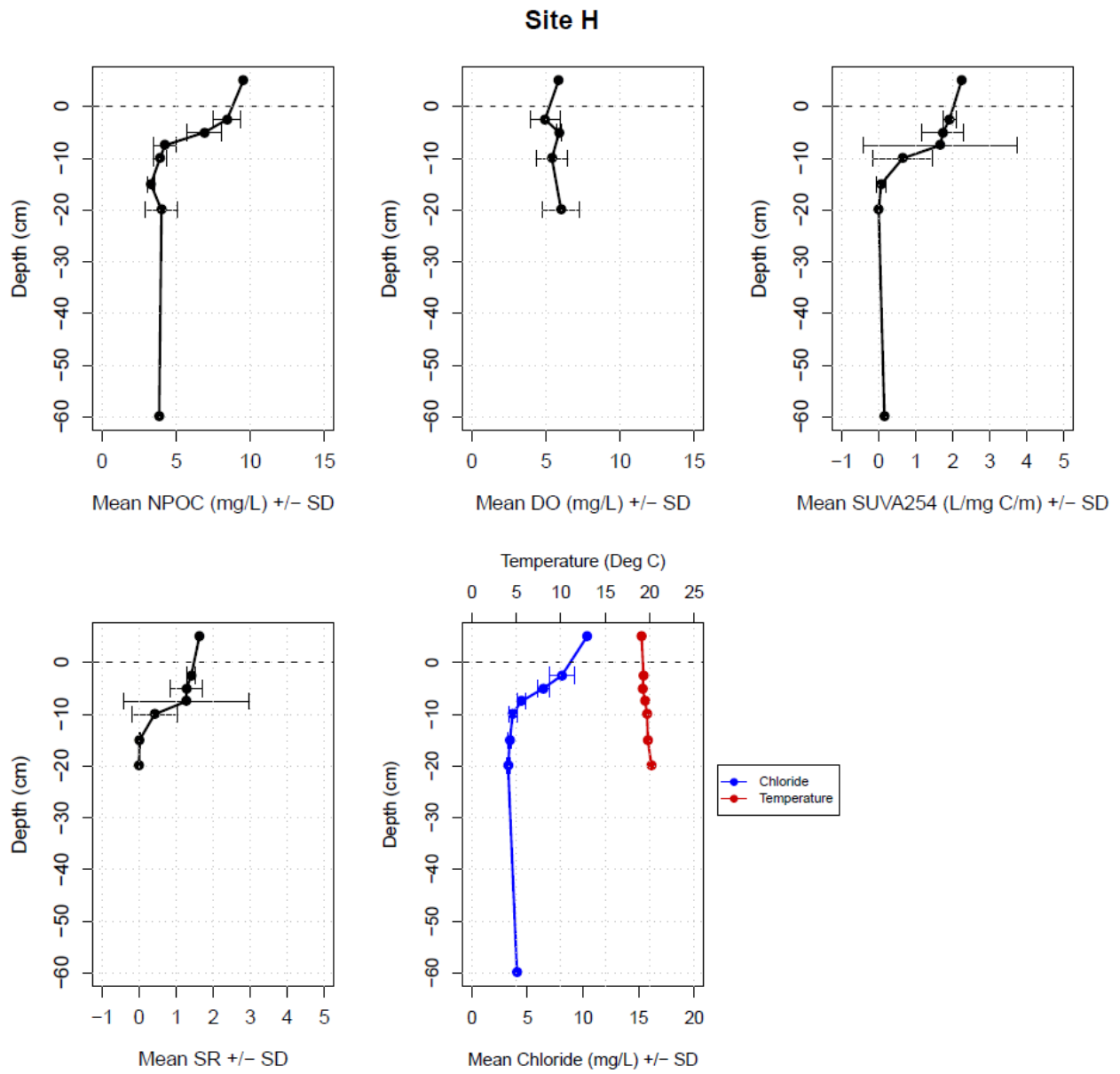


Figure A8: Site H Vertical Porewater Profiles

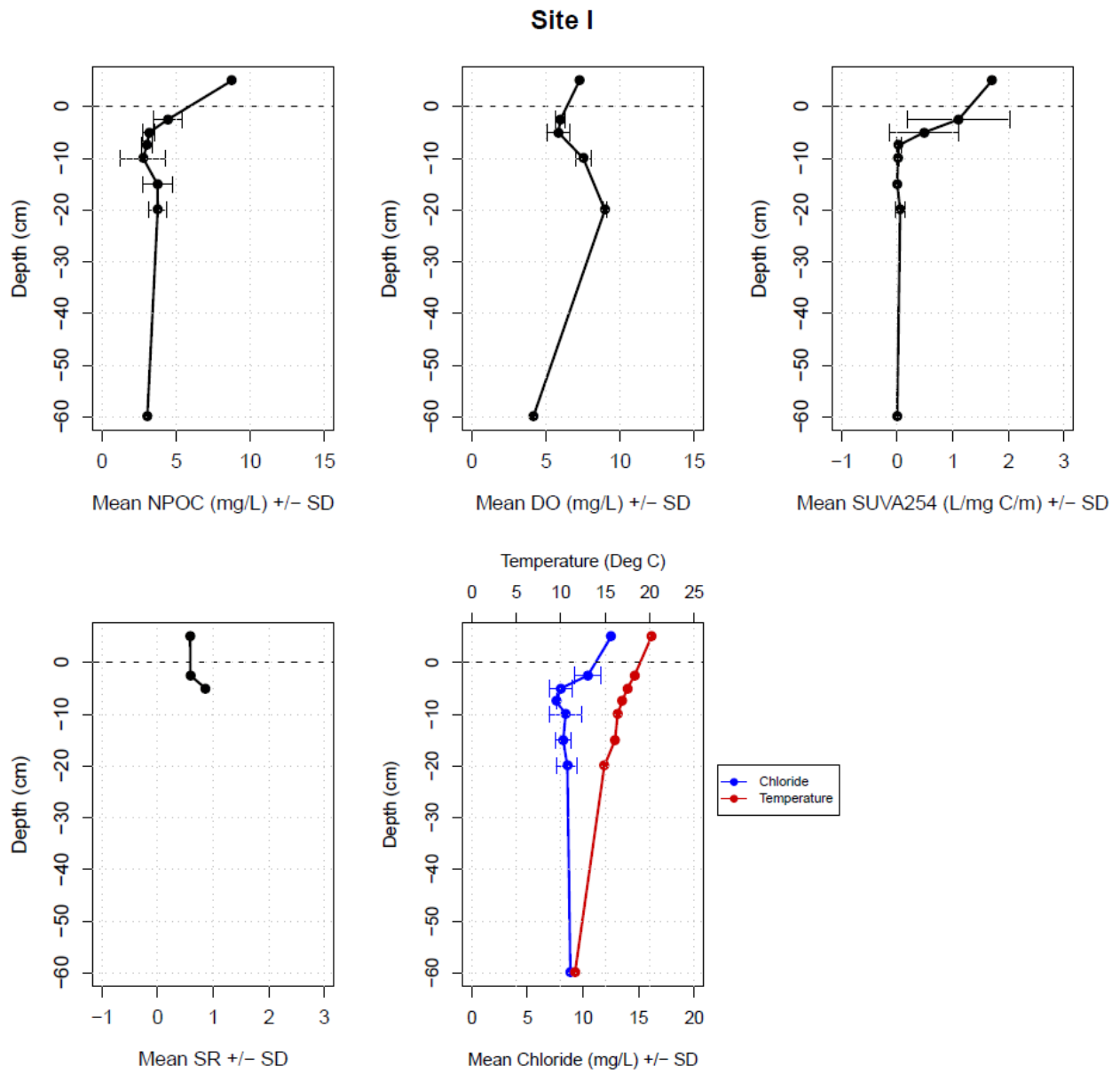


Figure A9: Site I Vertical Porewater Profiles

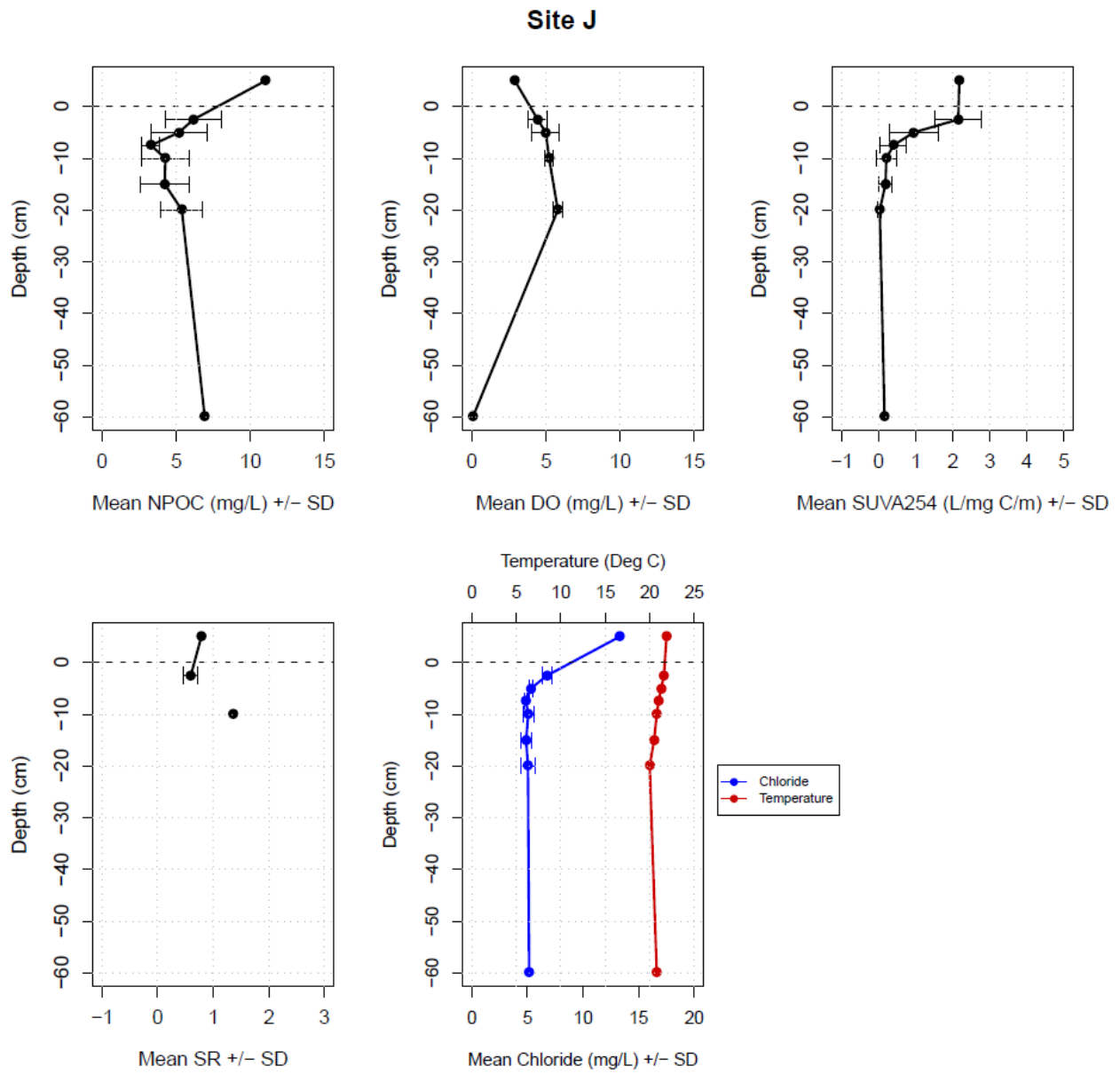


Figure A10: Site J Vertical Porewater Profiles

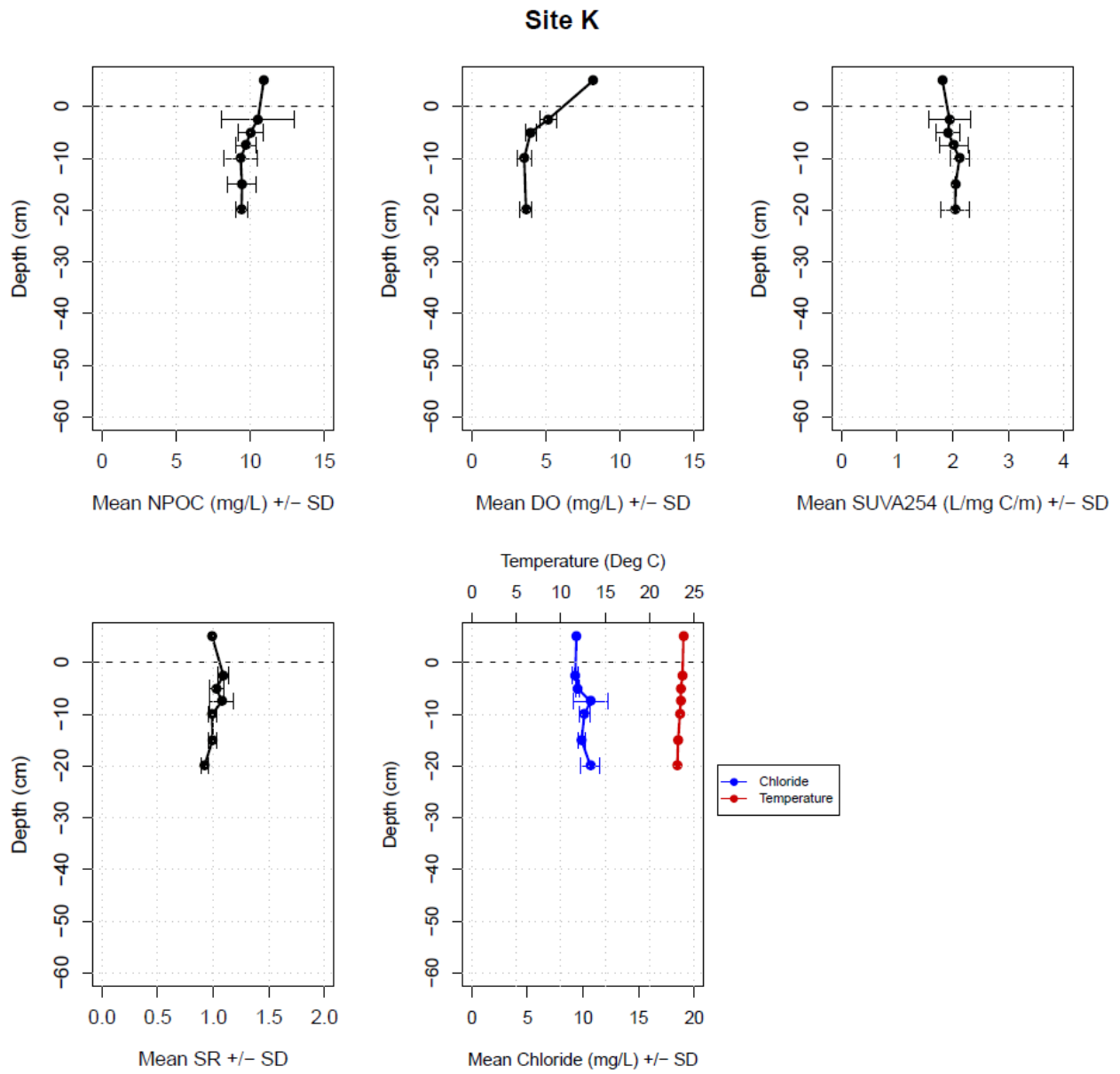


Figure A11: Site K Vertical Porewater Profiles

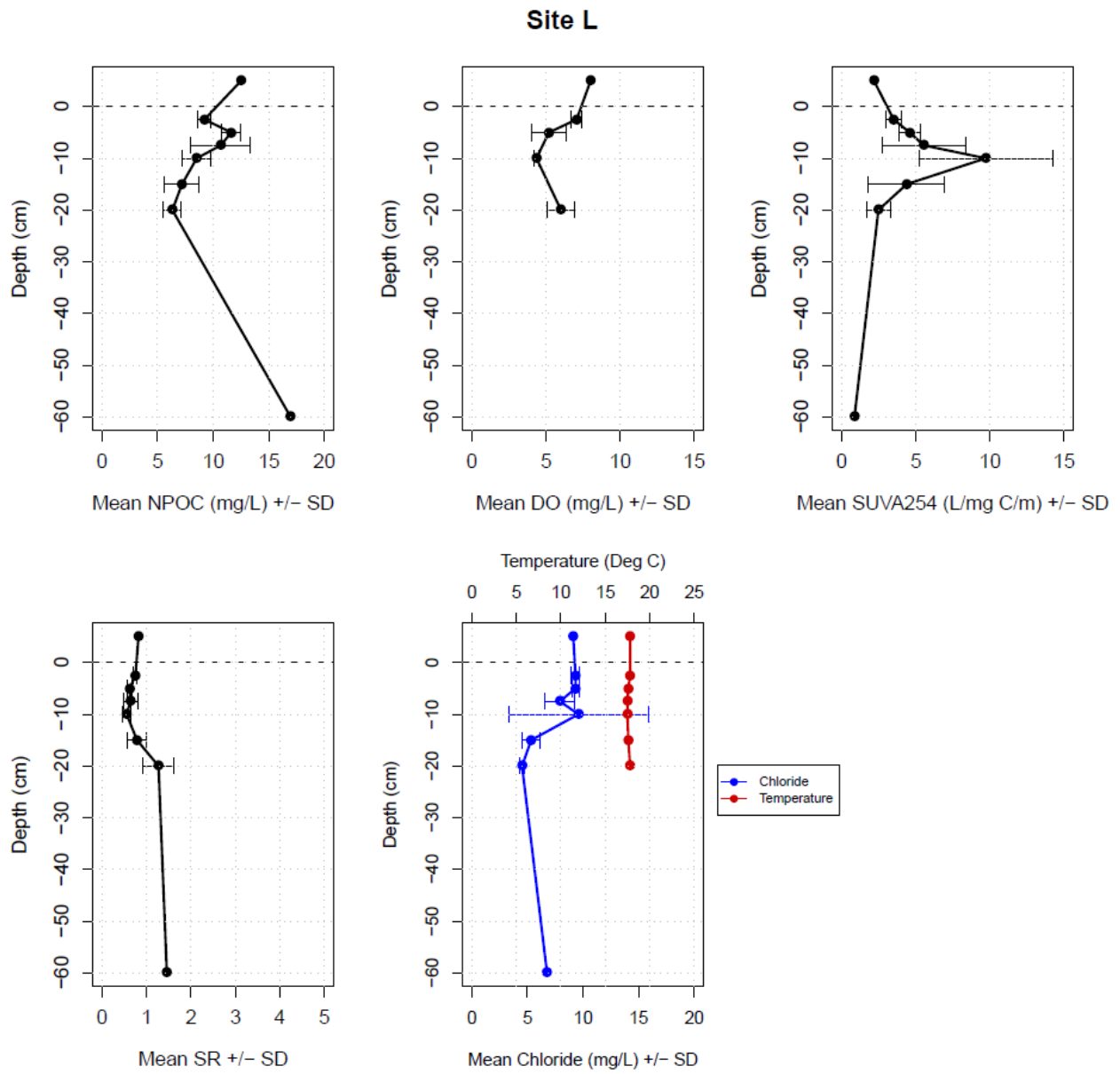


Figure A12: Site L Vertical Porewater Profiles

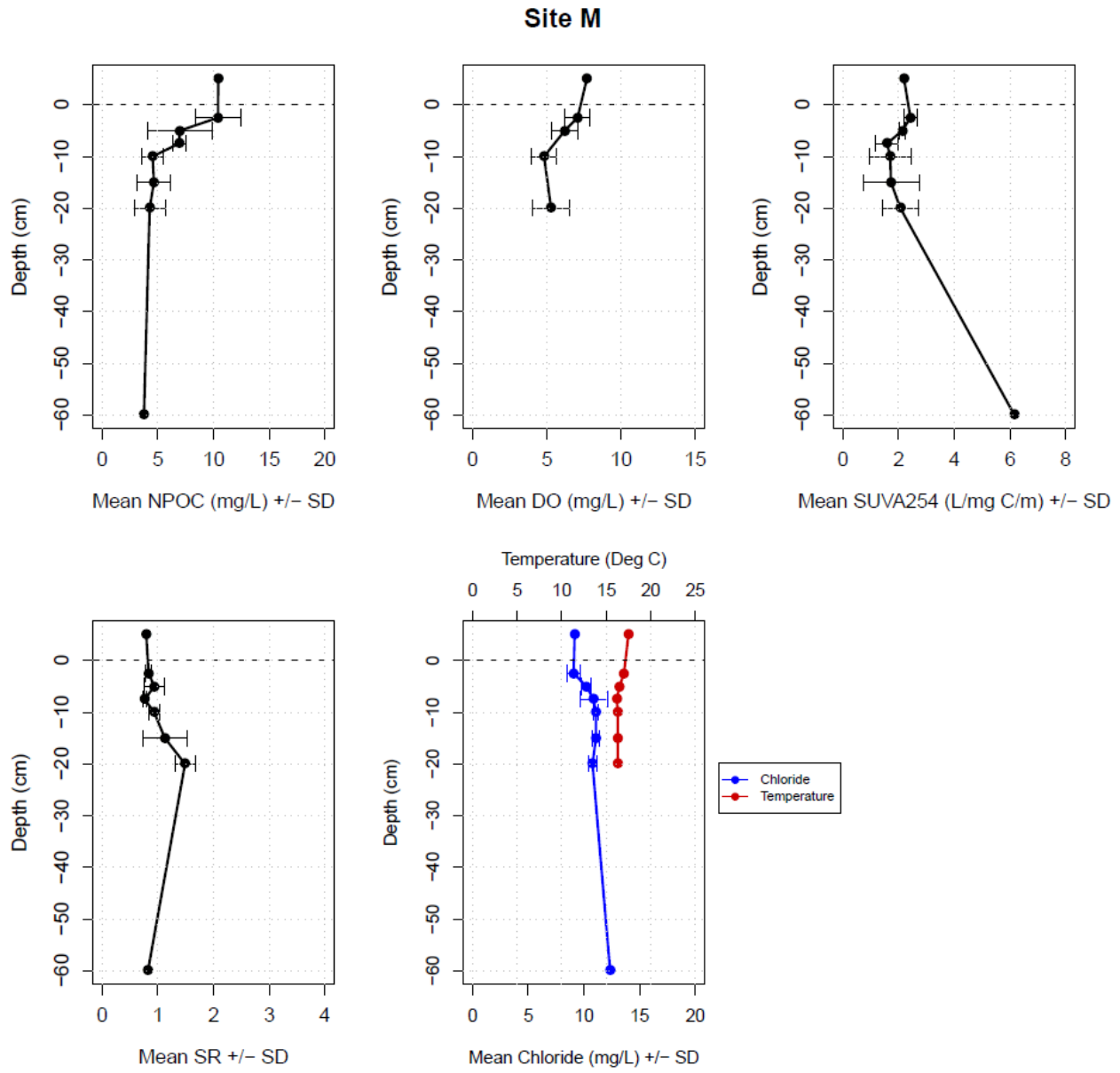


Figure A13: Site M Vertical Porewater Profiles

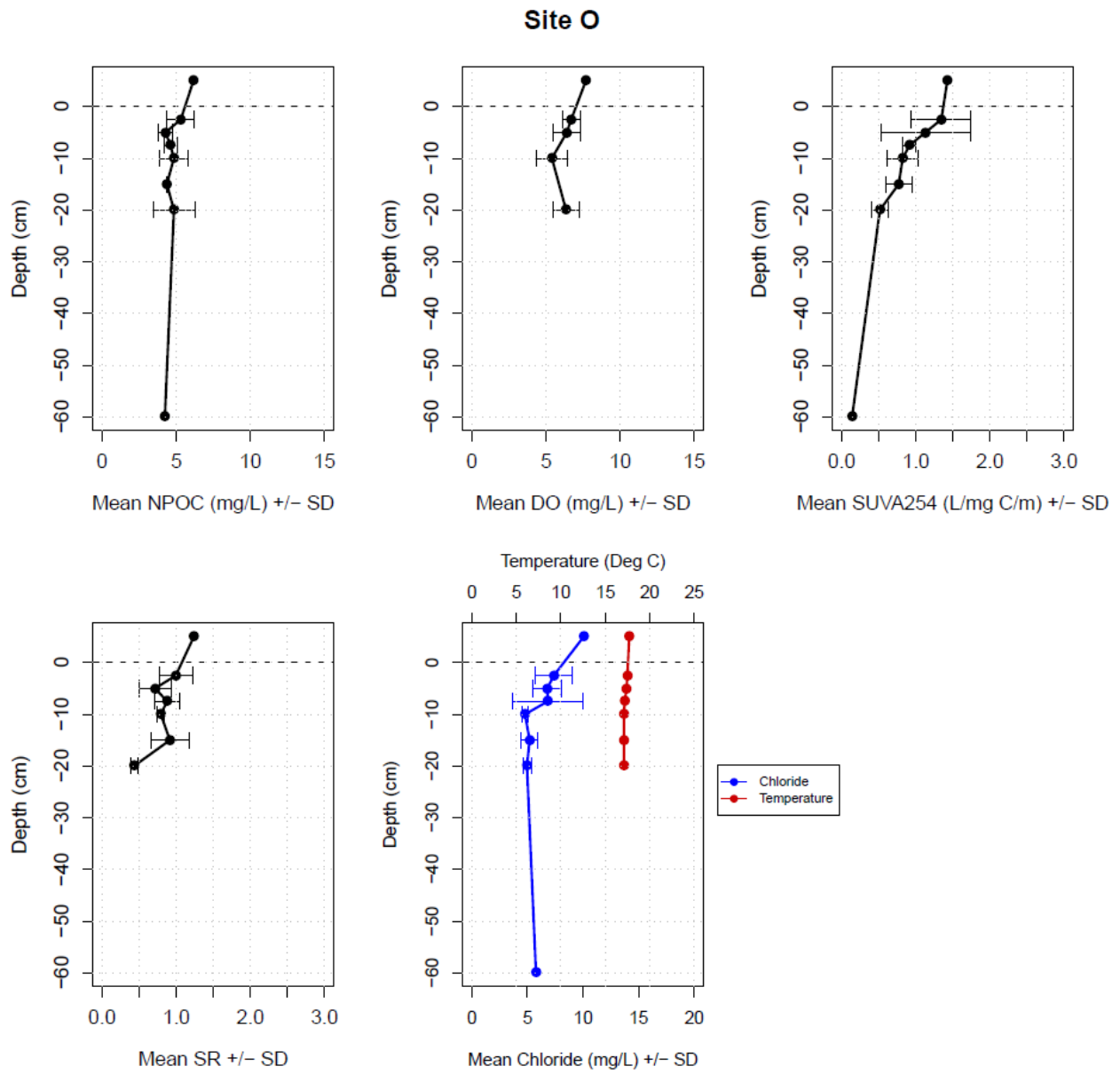


Figure A14: Site O Vertical Porewater Profiles

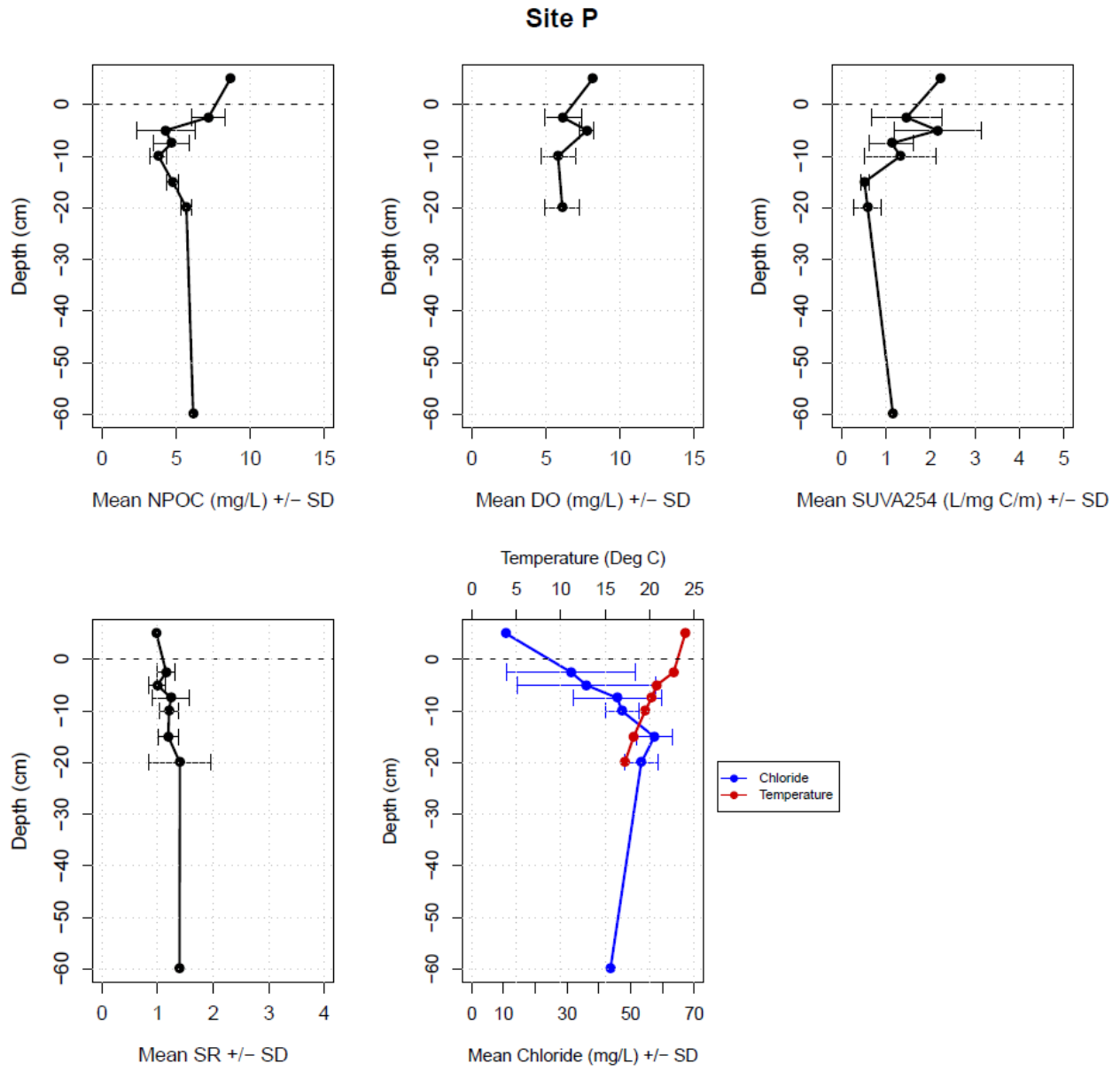


Figure A15: Site P Vertical Porewater Profiles

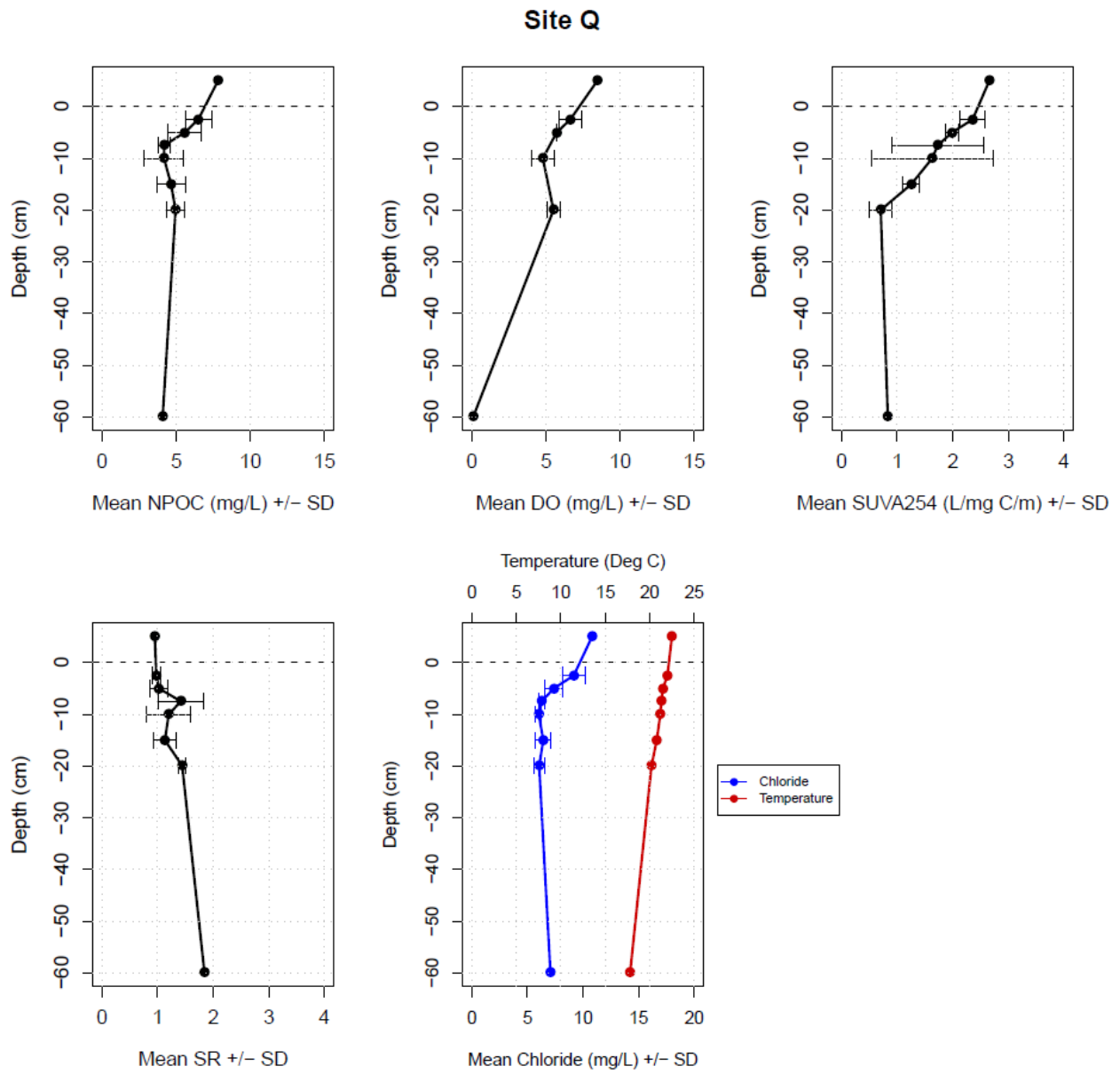


Figure A16: Site Q Vertical Porewater Profiles

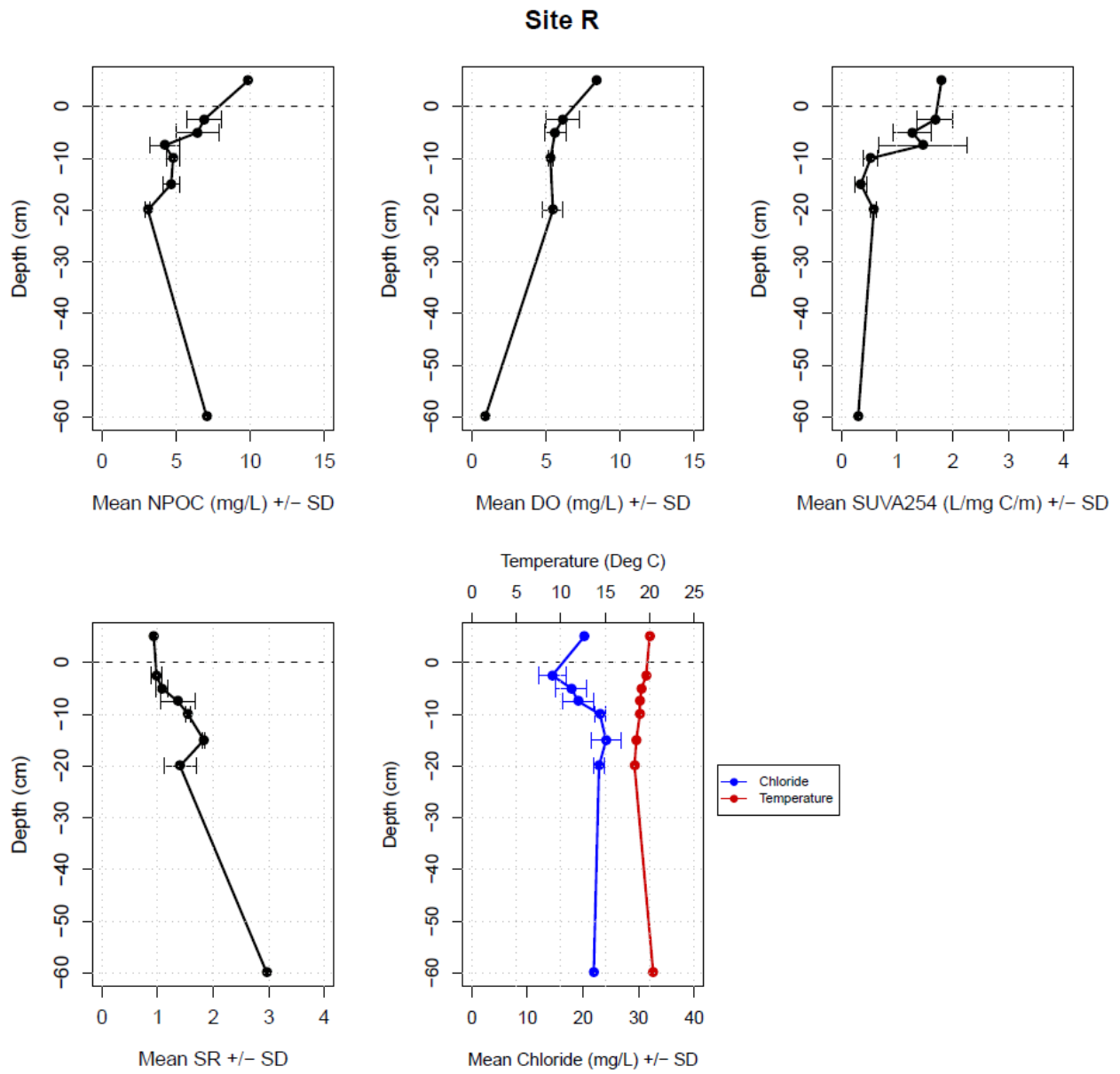


Figure A17: Site R Vertical Porewater Profiles

Table A2: Synoptic sampling data for 2015

Site	Minipoint	Depth (cm)	DO (mg/L)	DOC (mg/L)	SUVA ₂₅₄ (L/mg C/m)	S _R	Cl ⁻ (mg/L)	NO ₃ -N (mg/L)	SO ₄ (mg/L)
A	1	-2.5	4.786	11.53	1.87	0.72	5.98	2.44	4.58
A	1	-5	2.801	8.78	0.90	1.20	10.96	3.30	0.07
A	1	-7.5		8.11	1.13	0.99	8.48	2.62	3.43
A	1	-10	2.178	5.52	1.30	1.46	9.71	3.40	0.03
A	1	-15		4.21	0.83		12.03	2.65	2.59
A	1	-20	3.442	5.43	2.54	2.25	11.61	2.66	2.68
A	2	-2.5	3.054	11.84	1.71	0.85	5.74	2.34	4.69
A	2	-5	1.971	9.27	2.15	2.22	7.48	2.57	3.17
A	2	-7.5		8.53	3.05	1.85	8.85	2.62	2.46
A	2	-10	2.511	8.27	2.42	2.26	8.91	3.24	0.01
A	2	-15		5.70	1.53	2.46	11.35	2.65	3.17
A	2	-20	2.616	7.18	1.25	2.08	9.33	2.61	2.70
A	3	-2.5	3.276	10.13	1.82	0.91	6.51	2.32	4.26
A	3	-5	2.506	8.10	1.32	0.48	8.58	2.62	2.65
A	3	-7.5		7.01	0.77	0.61	11.56	2.64	2.74
A	3	-10	2.635	7.64	0.73		12.43	2.72	2.91
A	3	-15		5.03	0.80		11.91	2.67	2.64
A	3	-20	2.115	4.68	0.88	1.93	12.25	2.56	9.07
A		SW	7.175	10.57	2.37	0.95	5.72	2.36	4.90
B	1	-2.5	5.0791	5.91	1.49	1.43	7.85	3.64	17.23
B	1	-5	5.2787	4.92	0.37		6.75	2.42	21.84
B	1	-7.5		5.15	0.14		6.70	4.46	19.49
B	1	-10	4.9858	5.25	0.00		6.47	5.15	19.60
B	1	-15		3.45	0.14		6.55	4.82	19.21
B	1	-20	8.784	3.49	0.00		6.37	6.30	18.96
B	2	-2.5	3.744	7.83	1.66	0.68	9.37	2.21	12.48
B	2	-5	2.9913	4.79	0.98	0.53	7.13	2.46	17.19
B	2	-7.5		4.87	0.18		8.82	2.58	21.63
B	2	-10	3.2275	3.46	1.18	0.67	7.31	0.02	23.58
B	2	-15		3.02	0.40		6.62	5.87	19.24
B	2	-20	7.4165	2.82	0.00		6.97	6.39	19.15
B	3	-2.5	4.3689	3.98	0.70		7.46	3.72	19.36
B	3	-5	4.4027	5.27	0.46		7.80	4.12	20.10
B	3	-7.5		5.13	0.06		6.72	4.55	20.97
B	3	-10	4.4532	4.50	0.20		6.29	4.78	19.01
B	3	-15		4.01	0.25		6.64	6.10	19.34
B	3	-20	7.1647	3.16	0.32	-0.15	7.14	6.46	19.32
B		SW	5.5331	9.61	1.96	0.69	10.12	2.03	10.56
B		-60	5.2764	5.21	0.46	0.44	7.32	6.34	19.22

Table A2 (cont'd)

Site	Minipoint	Depth (cm)	DO (mg/L)	DOC (mg/L)	SUVA ₂₅₄ (L/mg C/m)	S _R	Cl ⁻ (mg/L)	NO ₃ -N (mg/L)	SO ₄ (mg/L)
C	1	-2.5	4.6084	7.52	1.86	0.63	9.90	2.09	11.99
C	1	-5	4.1218	6.39	2.19	0.60	10.34	2.09	12.43
C	1	-7.5		7.41	1.97	0.69	12.34	1.15	13.81
C	1	-10	4.3592	6.37	2.51	0.68	9.96	2.14	11.09
C	1	-15		6.43	2.71	0.65	10.56	2.30	9.50
C	1	-20	3.6418	5.25	1.07	0.41	9.70	1.69	4.49
C	2	-2.5	6.838	5.17	2.67	0.56	10.39	1.96	12.33
C	2	-5	5.9089	7.62	1.79	0.65	11.63	1.93	12.20
C	2	-7.5		6.45	2.50	0.78	10.28	1.92	12.31
C	2	-10	7.8844	8.53	1.66	0.56	10.32	1.97	12.23
C	2	-15		6.55	2.60	0.65	10.40	2.18	9.35
C	2	-20	5.3488	8.03	1.89	0.59	9.24	2.47	11.97
C	3	-2.5	5.5127	6.53	2.44	1.00	10.19	2.00	11.90
C	3	-5	7.1918	6.11	2.50	0.84	9.96	1.99	11.76
C	3	-7.5		7.65	1.91	0.67	10.16	1.96	11.99
C	3	-10	7.9835	6.57	2.25	0.67	11.89	1.96	11.93
C	3	-15		5.84	2.50	0.55	10.57	2.07	12.10
C	3	-20	6.822	6.04	2.68	0.67	9.51	2.47	12.39
C		SW	10.9533	10.26	1.62	0.73	10.23	2.01	11.73
C		-60	0.114	5.76	0.00		10.14	2.30	32.56
D	1	-2.5	4.197	7.59	1.79	0.68	19.89	2.05	11.94
D	1	-5	4.602	8.03	1.93	0.84	30.92	2.26	9.36
D	1	-7.5		7.66	1.36	0.81	84.72	2.61	6.45
D	1	-10	4.543	5.90	1.31	1.21	137.45	2.95	1.81
D	1	-15		4.75	2.00	0.54	161.76	2.82	11.77
D	1	-20	3.64	4.60	2.15	1.65	167.58	2.76	19.61
D	2	-2.5	4.51	9.69	2.82	0.67	16.04	2.05	10.94
D	2	-5	5.961	10.76	3.12	0.73	20.08	2.63	4.08
D	2	-7.5		12.44	1.44	0.69	52.29	2.89	3.22
D	2	-10	4.613	5.80	1.02	0.72	131.16	3.08	0.95
D	2	-15		7.44	3.08	1.05	88.26	3.00	2.89
D	2	-20	3.944	6.01	1.38	-6.72	127.94	2.66	20.04
D	3	-2.5	5.338	8.09	1.99	0.50	29.82	2.20	9.66
D	3	-5	6.091	7.87	2.01	0.54	13.70	1.95	11.52
D	3	-7.5		7.13	1.54	0.64	54.54	0.71	9.27
D	3	-10	4.23	5.45	0.94		110.13	2.74	6.19
D	3	-15		5.91	0.39		160.87	1.78	3.73
D	3	-20	7.622	4.53	0.35		157.84	1.60	22.15
D		SW	9.171	8.96	1.93	0.54	10.69	1.88	12.15

Table A2 (cont'd)

Site	Minipoint	Depth (cm)	DO (mg/L)	DOC (mg/L)	SUVA ₂₅₄ (L/mg C/m)	S _R	Cl ⁻ (mg/L)	NO ₃ -N (mg/L)	SO ₄ (mg/L)
F	1	-2.5	4.036	9.94	1.93	0.65	10.66	2.18	9.49
F	1	-5	5.0278	10.66	2.21	0.80	10.95	2.34	6.11
F	1	-7.5		11.13	2.63	0.88	10.55	2.67	3.34
F	1	-10	2.548	15.25	3.63	1.15	9.78	3.40	0.07
F	1	-15		12.74	4.47	2.09	9.80	4.30	0.01
F	1	-20	1.3197	12.50	5.35	3.02	15.26	3.45	0.02
F	2	-2.5	4.5746	7.93	2.84	0.76	10.74	2.26	8.07
F	2	-5	3.9368	9.67	2.92	0.82	10.60	2.53	3.92
F	2	-7.5		11.07	3.32	0.99	11.51	2.83	2.88
F	2	-10	1.5163	12.81	2.97	0.98	10.16	4.07	0.01
F	2	-15		13.05	3.79	1.57	9.58	1.87	0.07
F	2	-20	1.5378	12.24	4.27	1.73	8.33	4.14	0.02
F	3	-2.5	4.7068	15.69	2.24	0.75	13.08	2.83	4.73
F	3	-5	5.8287	13.30	2.45	0.83	13.11	3.10	1.38
F	3	-7.5		12.74	3.09	1.26	12.12	4.33	0.06
F	3	-10	2.9567	12.88	4.21	1.33	9.94	3.34	
F	3	-15		10.72	4.70	2.40	9.78	1.37	3.11
F	3	-20	3.8107	10.45	8.89	1.05	9.05	3.28	0.64
F		SW	9.3037	7.77	2.72	0.80	11.90	1.78	12.97
F		-60	-0.0085	8.94	2.84	0.99	10.67	1.43	1.67
G	1	-2.5	3.6075	6.58	1.82	0.63	10.72	0.97	19.72
G	1	-5	2.149	6.21	2.51	0.78	10.77	2.10	12.73
G	1	-7.5		6.18	1.44	0.66	11.92	2.37	14.13
G	1	-10	3.1354	4.75	0.29		12.45	2.49	36.93
G	1	-15		5.41	0.07		14.28	2.47	37.98
G	1	-20	3.2389	5.13	0.21		12.83	2.46	39.17
G	2	-2.5	4.677	7.46	2.47	0.91	10.53	1.99	9.22
G	2	-5	4.342	9.71	2.02	0.83	10.50	2.09	9.97
G	2	-7.5		5.01	1.32		12.84	2.72	8.25
G	2	-10	3.5645	4.56	1.29	0.42	12.30	2.75	8.57
G	2	-15		4.19	0.10		13.95	2.56	41.36
G	2	-20	4.2422	5.33	0.23		13.91	2.43	50.19
G	3	-2.5	4.5921	6.74	2.24	0.59	10.47	1.92	12.00
G	3	-5	3.7545	7.42	1.48	0.60	11.52	2.26	11.63
G	3	-7.5		7.26	0.90	0.39	12.93	1.67	29.29
G	3	-10	4.2596	5.19	0.08		13.91	2.50	45.35
G	3	-15		6.30	0.00		12.98	2.47	28.51
G	3	-20	5.5695	5.50	0.00		12.98	2.49	55.45
G		SW	8.7079	16.75	0.84	0.50	10.21	1.94	12.36
G		-60		10.08	0.51	1.18	11.51	2.42	45.36

Table A2 (cont'd)

Site	Minipoint	Depth (cm)	DO (mg/L)	DOC (mg/L)	SUVA ₂₅₄ (L/mg C/m)	S _R	Cl ⁻ (mg/L)	NO ₃ -N (mg/L)	SO ₄ (mg/L)
H	1	-2.5	4.368	9.37	2.02	1.48	8.97	2.15	6.69
H	1	-5	5.799	5.79	2.21	1.62	6.49	2.32	8.00
H	1	-7.5		3.38	4.05	3.22	4.42	1.64	23.46
H	1	-10	4.911	4.45	0.13	0.00	3.45	1.57	35.55
H	1	-15		3.42	0.00	0.00	3.60	2.27	45.27
H	1	-20	4.651	3.46	0.00	0.00	3.13	2.18	44.55
H	2	-2.5	4.364	7.52	1.70	1.29	6.82	2.26	10.41
H	2	-5	5.777	8.11	1.89	1.41	6.94	2.17	9.12
H	2	-7.5		4.92	0.51	0.32	4.82	1.58	26.97
H	2	-10	4.69	3.55	1.58	1.13	4.12	1.61	23.02
H	2	-15		2.99	0.20	0.03	3.24	2.37	34.59
H	2	-20	7.052	5.26	0.00	0.00	3.42	2.30	44.01
H	3	-2.5	6.089	8.41	2.01	1.45	8.51	2.17	10.05
H	3	-5	6.098	6.83	1.11	0.81	5.88	1.53	22.82
H	3	-7.5		4.41	0.43	0.27	4.12	2.38	34.77
H	3	-10	6.605	3.73	0.24	0.13	3.47	2.33	41.95
H	3	-15		3.46	0.00	0.00	3.41	2.27	44.66
H	3	-20	6.384	3.31	0.00	0.00	3.24	1.61	42.05
H		SW	5.847	9.53	2.24	1.63	10.36	1.94	8.19
H		-60		3.86	0.16		4.06	2.34	48.38
I	1	-2.5	5.7679	4.38	1.48		10.57	3.59	13.24
I	1	-5	6.3187	3.65	1.18	0.86	9.13	4.86	14.45
I	1	-7.5		2.78	0.07		7.61	2.86	14.51
I	1	-10	7.8805	4.47	0.00		10.11	8.79	13.88
I	1	-15		4.88	0.00		7.76	1.04	14.43
I	1	-20	9.0974	4.35	0.16		9.08	1.04	13.82
I	2	-2.5	5.8565	5.42	1.77	0.59	11.56	0.02	12.58
I	2	-5	4.9757	2.94	0.00		7.47	1.10	13.58
I	2	-7.5		2.81	0.00		7.61	1.06	13.53
I	2	-10	7.7452	2.37	0.04		7.53	1.10	13.66
I	2	-15		3.26	0.00		7.93	1.08	13.28
I	2	-20	8.9049	3.09	0.00		7.54	1.06	12.86
I	3	-2.5	6.3363	3.54	0.06		9.18	1.08	15.54
I	3	-5	6.1942	2.95	0.27		7.40	1.56	12.55
I	3	-7.5		3.48	0.00		7.59	1.05	12.59
I	3	-10	6.9396	1.50	0.00		7.67	1.09	13.00
I	3	-15		3.08	0.00		8.98	1.05	13.04
I	3	-20	8.924	3.83	0.00		9.17	1.51	13.81
I		SW	7.2594	8.75	1.70	0.59	12.53	1.97	13.85
I		-60	4.1425	3.06	0.00		8.86	2.67	14.70

Table A2 (cont'd)

Site	Minipoint	Depth (cm)	DO (mg/L)	DOC (mg/L)	SUVA ₂₅₄ (L/mg C/m)	S _R	Cl ⁻ (mg/L)	NO ₃ -N (mg/L)	SO ₄ (mg/L)
J	1	-2.5	4.5898	5.69	2.49	0.69	6.40	2.43	5.39
J	1	-5	5.0039	4.09	1.32		5.24	2.45	6.15
J	1	-7.5		3.99	0.18		4.78	2.32	13.66
J	1	-10	5.4169	2.86	0.11		4.82	1.51	21.44
J	1	-15		3.08	0.03		5.37	1.50	21.15
J	1	-20	6.167	5.21	0.00		5.27	1.49	23.13
J	2	-2.5	3.735	8.28	1.42	0.45	7.16	2.22	3.96
J	2	-5	4.054	7.35	0.18		5.24	2.28	15.09
J	2	-7.5		2.84	0.21		5.02	2.32	13.45
J	2	-10	4.898	3.96	0.00		4.80	1.50	21.24
J	2	-15		3.50	0.37		4.78	1.49	22.56
J	2	-20	5.776	4.05	0.00		5.53	1.50	23.15
J	3	-2.5	5.0065	4.52	2.52	0.65	6.78	2.26	4.86
J	3	-5	5.9112	4.13	1.33		5.47	2.41	4.16
J	3	-7.5		3.08	0.81		4.82	2.39	6.09
J	3	-10	5.3322	6.00	0.52	1.36	5.62	2.43	6.71
J	3	-15		6.12	0.15		4.50	1.51	21.70
J	3	-20	5.4617	6.89	0.09		4.34	1.46	21.08
J		SW	2.9024	11.03	2.18	0.79	13.30	2.10	9.45
J		-60	0.0708	6.93	0.16		5.16	1.52	22.91
K	1	-2.5	4.89	13.29	1.51	1.12	9.01	1.83	4.36
K	1	-5	4.376	10.97	1.67	1.00	9.41	1.88	4.21
K	1	-7.5		10.12	1.73	1.03	12.42	1.87	4.29
K	1	-10	4.016	8.80	2.00	1.02	9.61	1.87	4.21
K	1	-15		8.88	2.05	0.99	9.47	1.86	4.16
K	1	-20	4.043	9.65	2.20	0.89	9.86	1.93	3.27
K	2	-2.5	5.796	9.70	2.09	1.04	9.38	1.84	4.26
K	2	-5	3.677	9.46	2.07	1.10	9.70	1.87	4.33
K	2	-7.5		10.05	2.07	1.20	9.57	1.87	4.14
K	2	-10	3.53	8.59	2.32	0.95	10.27	1.90	4.35
K	2	-15		8.88	2.04	1.04	10.09	1.99	1.34
K	2	-20	3.709	9.68	2.18	0.92	10.61	1.93	4.06
K	3	-2.5	4.763	8.58	2.22	1.11	9.53	1.94	4.69
K	3	-5	3.841	9.62	2.01	0.99	9.40	1.85	4.81
K	3	-7.5		8.92	2.24	1.00	10.08	1.98	2.47
K	3	-10	3.054	10.66	2.05	1.01	10.51	1.98	2.03
K	3	-15		10.57	2.06	0.96	10.06	1.99	2.65
K	3	-20	3.224	8.92	1.75	0.95	11.54	2.69	0.03
K		SW	8.177	10.91	1.81	0.99	9.41	1.84	4.24

Table A2 (cont'd)

Site	Minipoint	Depth (cm)	DO (mg/L)	DOC (mg/L)	SUVA ₂₅₄ (L/mg C/m)	S _R	Cl ⁻ (mg/L)	NO ₃ -N (mg/L)	SO ₄ (mg/L)
L	1	-2.5	6.7621	8.59	3.63	0.76	8.97	1.66	4.18
L	1	-5	5.7043	12.57	4.79	0.64	9.01	1.67	4.30
L	1	-7.5		13.67	7.70	0.51	8.81	1.75	3.13
L	1	-10	4.3215	9.55	10.82	0.53	5.45	2.51	2.62
L	1	-15		8.98	5.88	0.66	5.94	3.23	0.07
L	1	-20	5.2336	7.20	2.04	1.33	4.66	2.41	2.00
L	2	-2.5	6.9817	9.79	3.98	0.70	9.71	1.69	4.50
L	2	-5	3.877	10.97	5.20	0.57	9.31	1.64	3.95
L	2	-7.5		9.93	6.55	0.60	6.38	3.13	0.04
L	2	-10	4.213	7.07	13.60	0.47	6.53	2.41	2.50
L	2	-15		6.18	5.88	0.66	4.44	3.26	0.03
L	2	-20	5.8218	6.22	2.01	1.58	4.30	3.12	0.01
L	3	-2.5	7.4587	9.26	2.92	0.78	9.31	1.72	4.74
L	3	-5	6.0244	11.35	3.81	0.67	9.69	1.62	3.76
L	3	-7.5		8.44	2.37	0.81	8.55	1.91	3.67
L	3	-10	4.5548	8.95	4.77	0.66	16.80	2.14	2.54
L	3	-15		6.43	1.41	1.04	5.64	2.50	2.72
L	3	-20	6.9916	5.57	3.40	0.90	4.59	3.23	0.02
L		SW	8.0165	12.52	2.18	0.82	9.12	1.69	4.20
L		-60		16.96	0.87	1.46	6.77	2.48	2.10
M	1	-2.5	7.796	8.58	2.60	0.85	8.83	2.20	7.04
M	1	-5	5.2039	8.39	2.04	1.15	10.48	2.52	4.64
M	1	-7.5		6.96	1.34	0.78	12.24	2.92	3.88
M	1	-10	3.917	3.75	1.49	1.01	11.30	3.04	2.89
M	1	-15		5.01	1.78	0.90	11.22	2.90	4.46
M	1	-20	3.97	5.86	1.33	1.60	11.02	2.88	5.19
M	2	-2.5	7.2669	10.00	2.14	0.78	8.61	2.23	7.16
M	2	-5	6.6305	3.62	2.27	0.85	10.49	1.04	4.32
M	2	-7.5		6.31	1.36	0.72	9.89	2.76	4.01
M	2	-10	4.9617	4.26	2.51	0.96	10.97	2.93	4.36
M	2	-15		5.91	0.69	1.58	11.32	2.83	4.67
M	2	-20	6.3889	3.26	2.58	1.59	10.95	2.79	10.42
M	3	-2.5	6.1701	12.64	2.53	0.87	9.80	2.60	6.53
M	3	-5	6.812	8.94	2.10	0.81	9.70	2.68	5.76
M	3	-7.5		7.48	2.05	0.80	10.49	2.90	6.05
M	3	-10	5.57	5.58	1.09	0.83	10.99	3.03	4.56
M	3	-15		3.03	2.71	0.90	10.70	2.97	4.49
M	3	-20	5.5045	3.69	2.28	1.28	10.36	2.81	6.31
M		SW	7.6948	10.43	2.20	0.79	9.17	2.17	6.61
M		-60		3.75	6.16	0.82	12.36	2.77	5.91

Table A2 (cont'd)

Site	Minipoint	Depth (cm)	DO (mg/L)	DOC (mg/L)	SUVA ₂₅₄ (L/mg C/m)	S _R	Cl ⁻ (mg/L)	NO ₃ -N (mg/L)	SO ₄ (mg/L)
O	1	-2.5	7.2353	4.37	1.79	1.26	5.63	1.04	25.09
O	1	-5	7.307	4.70	0.64	0.48	5.47	0.95	28.39
O	1	-7.5		4.14	0.92	0.70	4.76	0.99	29.15
O	1	-10	6.3216	5.56	1.06	0.80	5.02	0.94	28.44
O	1	-15		4.39	0.77	0.86	4.95	0.94	29.03
O	1	-20	6.087	3.85	0.60	0.43	4.80	0.96	26.45
O	2	-2.5	6.0437	6.23	1.00	0.85	7.55	1.13	19.69
O	2	-5	6.4516	3.72	1.80	0.93	7.98	0.64	18.10
O	2	-7.5		4.70	0.83	0.92	5.26	1.00	27.21
O	2	-10	5.5656	5.21	0.75	0.84	4.78	0.99	27.98
O	2	-15		4.39	0.59	0.69	4.60	1.00	26.34
O	2	-20	5.6459	6.46	0.39	0.38	5.38	0.99	27.06
O	3	-2.5	6.8293	5.34	1.25	0.88	8.97	0.01	15.64
O	3	-5	5.465	4.43	0.95	0.74	6.90	1.07	19.83
O	3	-7.5		5.01	1.00	1.02	10.50	1.09	15.44
O	3	-10	4.3251	3.76	0.66	0.74	4.56	0.98	25.93
O	3	-15		4.35	0.94	1.20	6.05	1.05	25.02
O	3	-20	7.3476	4.25	0.56	0.48	4.69	0.93	25.38
O		SW	7.7004	6.17	1.43	1.24	10.06	2.96	12.44
O		-60		4.24	0.14		5.77	1.02	49.80
P	1	-2.5	4.7057	6.06	0.56	1.33	52.33	4.09	24.15
P	1	-5	8.3209	2.08	1.34	0.83	58.44	0.01	23.63
P	1	-7.5		3.36	1.01	1.61	60.16	4.61	24.24
P	1	-10	7.159	4.47	0.67	1.36	52.74	3.96	24.75
P	1	-15		5.05	0.46	1.35	61.69	0.95	23.92
P	1	-20	5.3128	5.43	0.92	1.73	55.35	0.01	21.83
P	2	-2.5	6.6728	7.16	1.73	1.12	29.35	0.01	18.68
P	2	-5	7.5781	5.94	1.89	1.11	34.64	2.73	22.71
P	2	-7.5		5.70	0.70	0.95	44.92	0.01	24.43
P	2	-10	5.1153	3.47	1.07	1.04	46.80	1.05	27.86
P	2	-15		4.95	0.46	1.00	51.00	3.41	30.98
P	2	-20	7.4234	6.12	0.31	0.76	47.44	3.82	29.50
P	3	-2.5	7.0445	8.31	2.08	1.02	12.00	1.67	12.42
P	3	-5	7.409	4.86	3.25	1.05	15.05	0.02	13.98
P	3	-7.5		5.02	1.67	1.16	32.41	0.01	22.34
P	3	-10	5.1853	3.51	2.22	1.22	42.21	0.01	23.54
P	3	-15		4.33	0.62	1.23	59.71	0.86	32.51
P	3	-20	5.5822	5.53	0.52	1.71	57.27	1.09	33.18
P		SW	8.1596	8.66	2.23	0.98	10.75	1.47	11.76
P		-60		6.15	1.15	1.39	43.65	1.03	28.98

Table A2 (cont'd)

Site	Minipoint	Depth (cm)	DO (mg/L)	DOC (mg/L)	SUVA ₂₅₄ (L/mg C/m)	S _R	Cl ⁻ (mg/L)	NO ₃ -N (mg/L)	SO ₄ (mg/L)
Q	1	-2.5	7.4736	7.30	2.55	0.92	9.83	1.64	12.05
Q	1	-5	5.704	5.83	1.89	0.90	8.22	2.40	6.68
Q	1	-7.5		4.45	1.17	1.04	6.05	2.56	3.49
Q	1	-10	3.9802	3.39	2.89	0.79	6.32	1.95	1.88
Q	1	-15		3.54	1.16	0.91	5.86	2.58	4.92
Q	1	-20	5.338	4.43	0.61	1.49	6.60	2.47	7.82
Q	2	-2.5	5.9583	6.64	2.41	1.06	9.65	0.52	9.75
Q	2	-5	5.7141	6.56	2.10	1.22	7.33	2.53	4.35
Q	2	-7.5		4.37	1.35	1.37	6.34	2.59	4.07
Q	2	-10	4.8569	5.71	0.98	1.24	5.95	2.69	2.92
Q	2	-15		5.27	1.42	1.33	7.19	2.66	3.09
Q	2	-20	5.1982	5.61	0.94	1.47	5.88	2.47	3.53
Q	3	-2.5	6.4908	5.55	2.11	0.95	8.02	2.06	12.38
Q	3	-5	5.7649	4.36	1.97	0.95	6.58	2.21	13.31
Q	3	-7.5		3.78	2.67	1.85	6.48	2.28	14.36
Q	3	-10	5.5324	3.44	1.02	1.57	5.79	2.31	17.16
Q	3	-15		5.17	1.18	1.15	6.24	2.31	16.72
Q	3	-20	5.9948	4.84	0.56	1.37	5.69	1.50	4.97
Q		SW	8.4709	7.83	2.66	0.95	10.82	0.01	12.82
Q		-60	0.0924	4.09	0.83	1.84	7.07	1.47	27.73
R	1	-2.5	5.0548	6.11	1.34	0.89	17.26	2.06	17.27
R	1	-5	5.0424	4.85	1.52	1.19	20.06	2.13	16.21
R	1	-7.5		3.18	2.36	1.23	17.20	2.06	17.26
R	1	-10	5.1888	5.08	0.41	1.50	23.66	2.26	18.89
R	1	-15		4.03	0.47	1.82	27.21	2.22	20.39
R	1	-20	4.7927	3.26	0.64	1.61	23.65	1.39	23.05
R	2	-2.5	6.0829	6.35	1.99	0.98	13.07	1.97	15.46
R	2	-5	5.38	6.76	0.89	1.06	18.91	2.18	15.52
R	2	-7.5		4.40	0.86	1.73	22.38	2.23	18.54
R	2	-10	5.501	5.03	0.50	1.59	23.49	2.25	17.74
R	2	-15		4.88	0.27	1.82	23.23	1.46	22.49
R	2	-20	6.145	2.93	0.55	1.07	23.33	1.40	24.51
R	3	-2.5	7.2601	8.21	1.73	1.07	13.08	1.90	15.13
R	3	-5	6.4179	7.72	1.41	0.98	14.79	2.01	15.60
R	3	-7.5		5.11	1.17	1.14	17.87	2.09	13.25
R	3	-10	5.2351	4.28	0.65	1.55	22.02	1.37	22.08
R	3	-15		5.07	0.30	1.86	22.02	2.14	21.04
R	3	-20	5.475	3.09	0.55	1.53	21.67	1.38	21.60
R		SW	8.4221	9.85	1.80	0.93	20.22	1.34	13.24
R		-60	0.9091	7.07	0.30	2.96	21.93	1.33	27.52

APPENDIX B

2016 Synoptic Hyporheic Zone Sampling Data

Table B1: Supplemental information for the 2016 sampling sites

Sampling Site	Longitude	Latitude	Stream Order	Drainage Area (km ²)
A1	42.42095	-85.33289	1	1.88
A2	42.41977	-85.33311	1	1.91
A3	42.40931	-85.33774	1	3.00
B1	42.4043	-85.35506	3	69.80
B2	42.40375	-85.35481	3	69.70
C1	42.42623	-85.35413	2	41.72
C2	42.42658	-85.3537	2	41.71
C3	42.4276	-85.35283	2	41.60
C4	42.42841	-85.35222	2	41.48
E1	42.45768	-85.33739	2	25.65
E2	42.45783	-85.33812	2	25.63
E3	42.45801	-85.33878	2	25.61
F1	42.40707	-85.34488	3	68.17
F2	42.40812	-85.34597	2	50.19
F3	42.40926	-85.34513	2	50.09
F4	42.40984	-85.34469	2	50.05
G1	42.44843	-85.31959	1	1.78
G2	42.4483	-85.31949	1	1.77
H1	42.44739	-85.32814	2	32.58
H2	42.4469	-85.32623	2	32.57
H3	42.44679	-85.32371	2	32.48
I1	42.35322	-85.35327	3	95.69
I2	42.35336	-85.35385	3	95.39
J1	42.45716	-85.33657	2	25.66
K1	42.4683	-85.35236	1	7.78
K2	42.46873	-85.3525	1	7.78
L1	42.46234	-85.34238	1	9.72
L2	42.46291	-85.34268	1	9.57
L3	42.46341	-85.34198	1	9.55
M1	42.40838	-85.31111	1	7.39
M2	42.40889	-85.31058	1	7.38
O1	42.36286	-85.35401	3	87.22
O2	42.36563	-85.3548	3	86.81
R1	42.42099	-85.34346	1	0.80
R2	42.4213	-85.34322	1	0.80
R3	42.42145	-85.34313	1	0.80
R4	42.42178	-85.34277	1	0.76
S1	42.39225	-85.35455	3	72.80
S2	42.39254	-85.35516	3	72.75

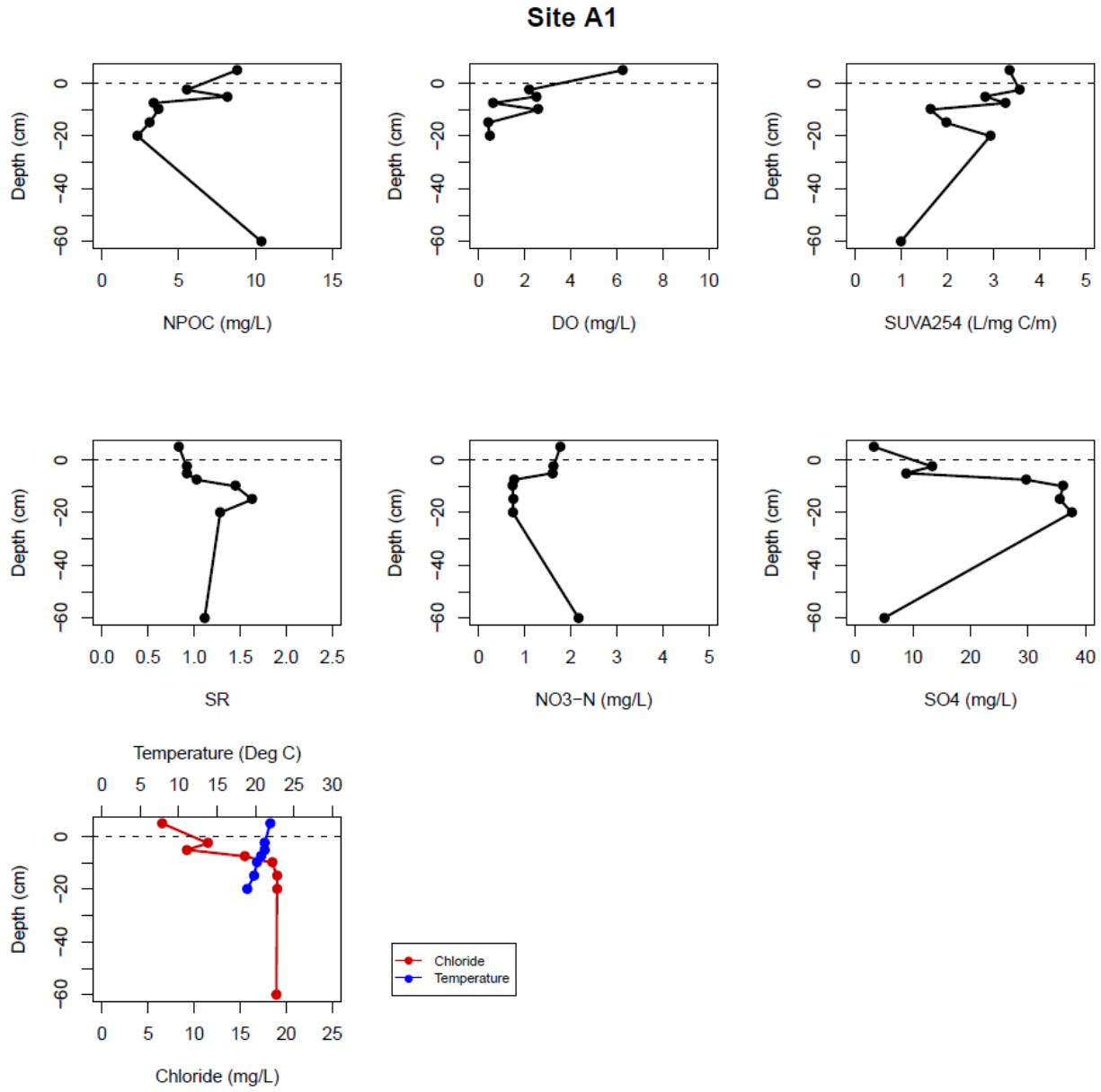


Figure B1: Site A1 Vertical Porewater Profiles

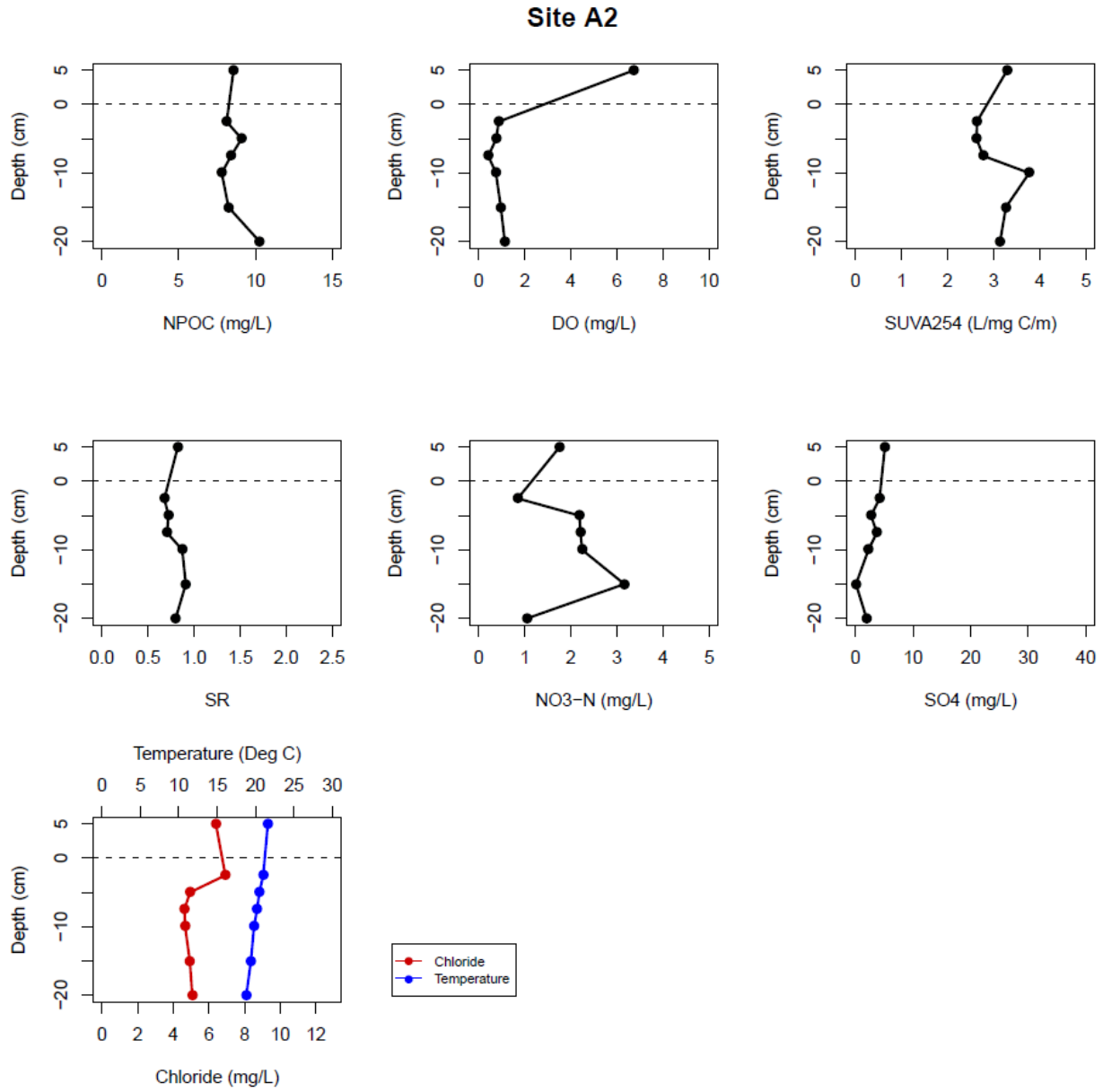


Figure B2: Site A2 Vertical Porewater Profiles

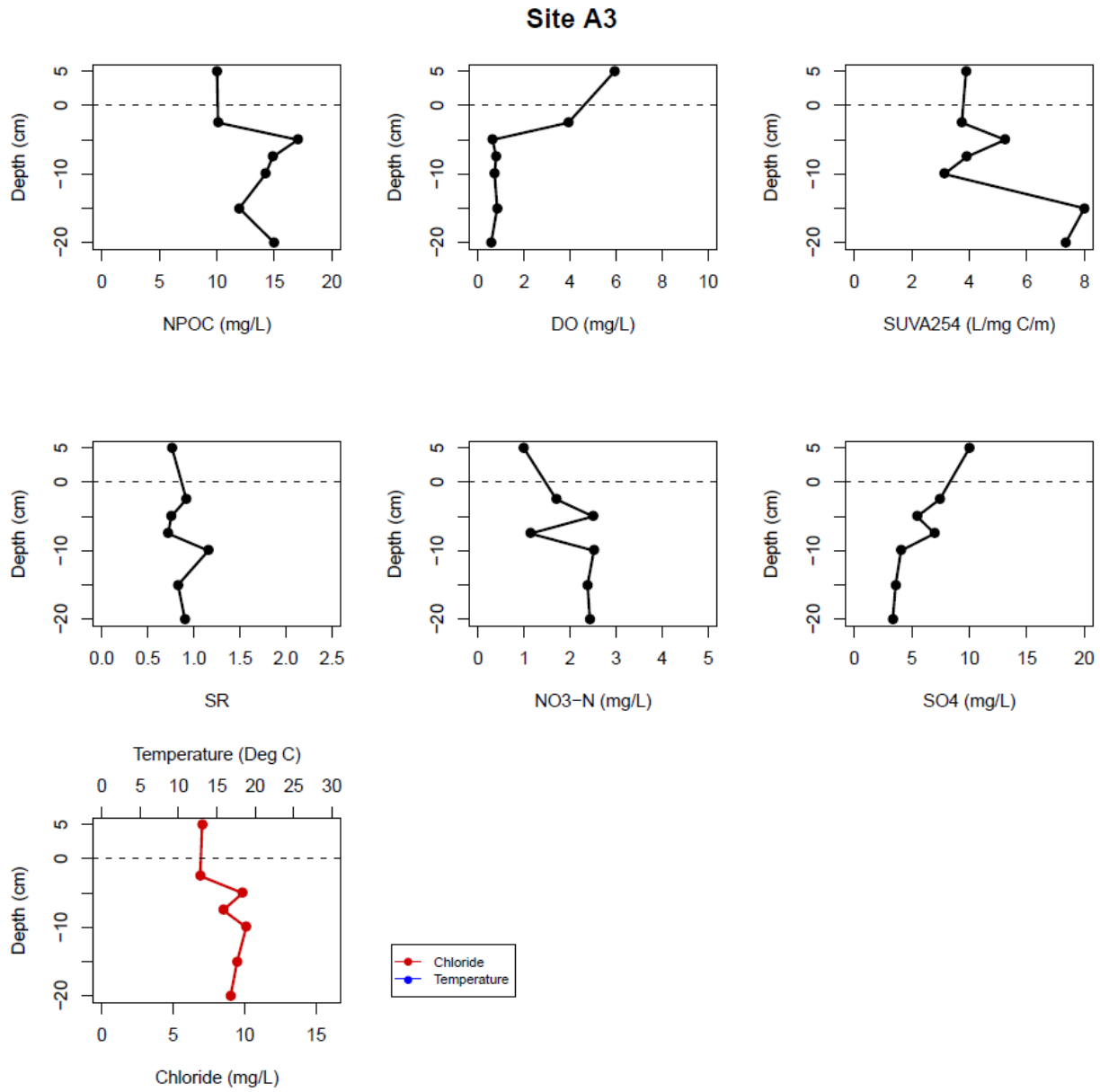


Figure B3: Site A3 Vertical Porewater Profiles

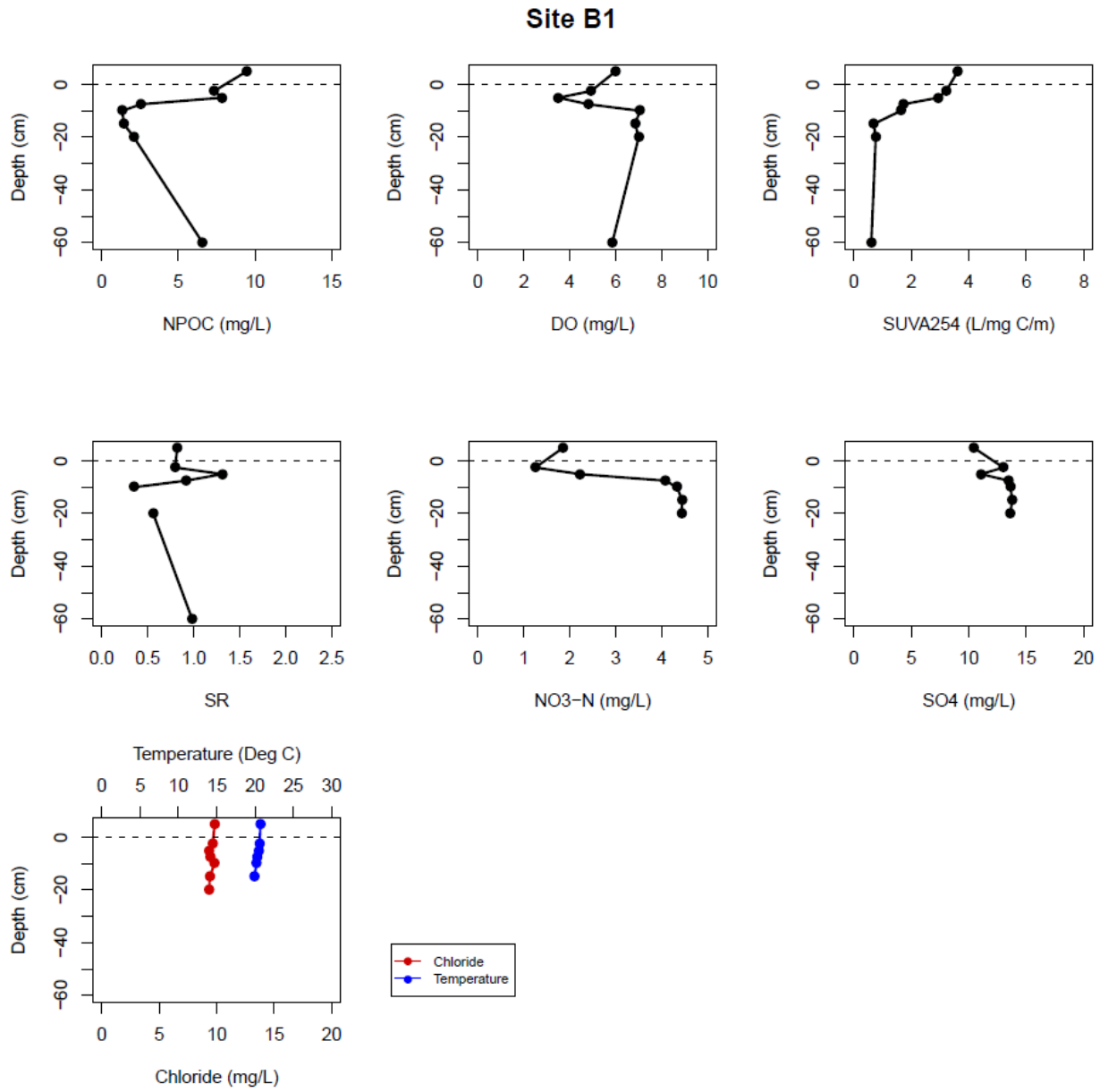


Figure B4: Site B1 Vertical Porewater Profiles

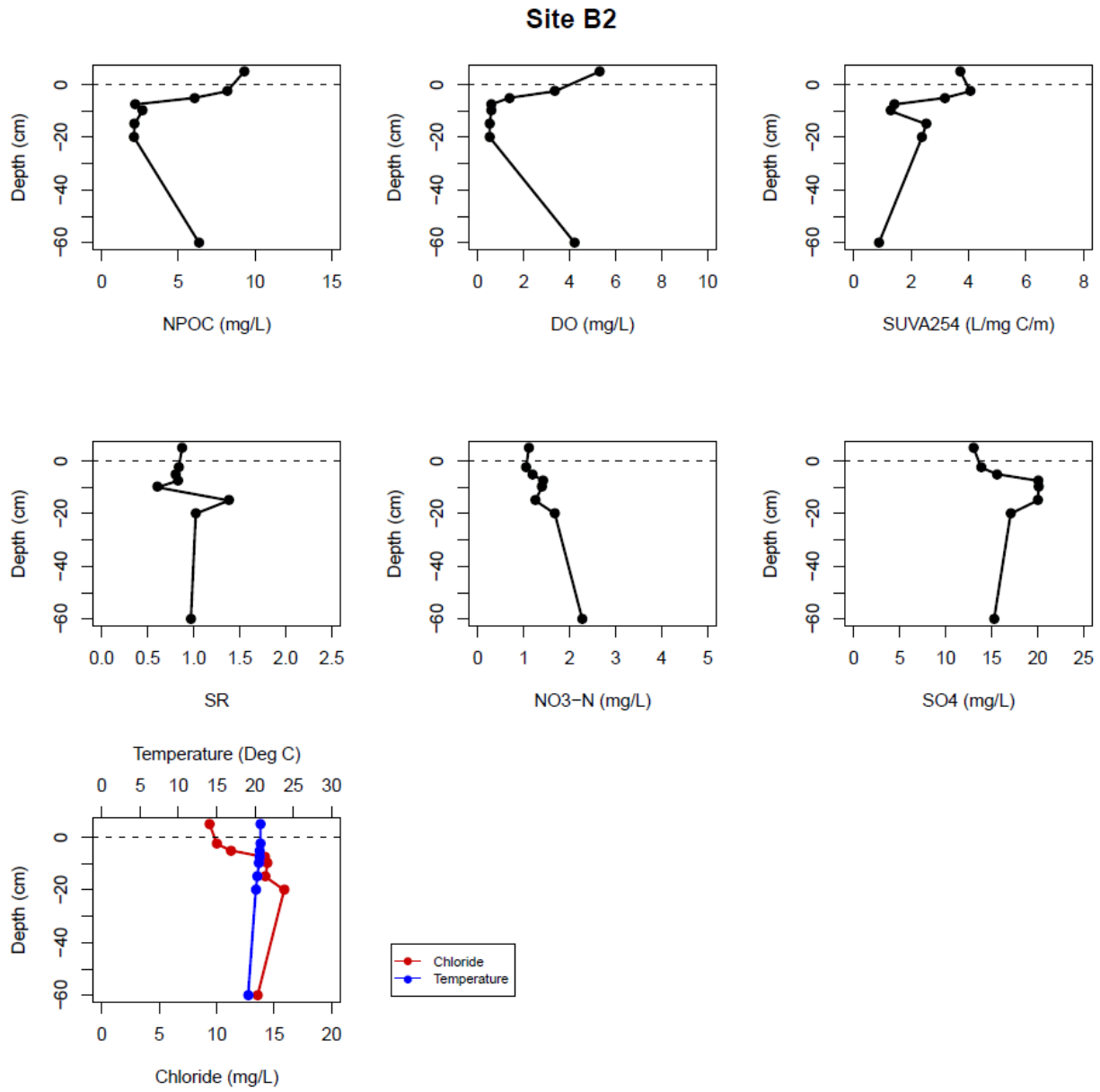


Figure B5: Site B2 Vertical Porewater Profiles

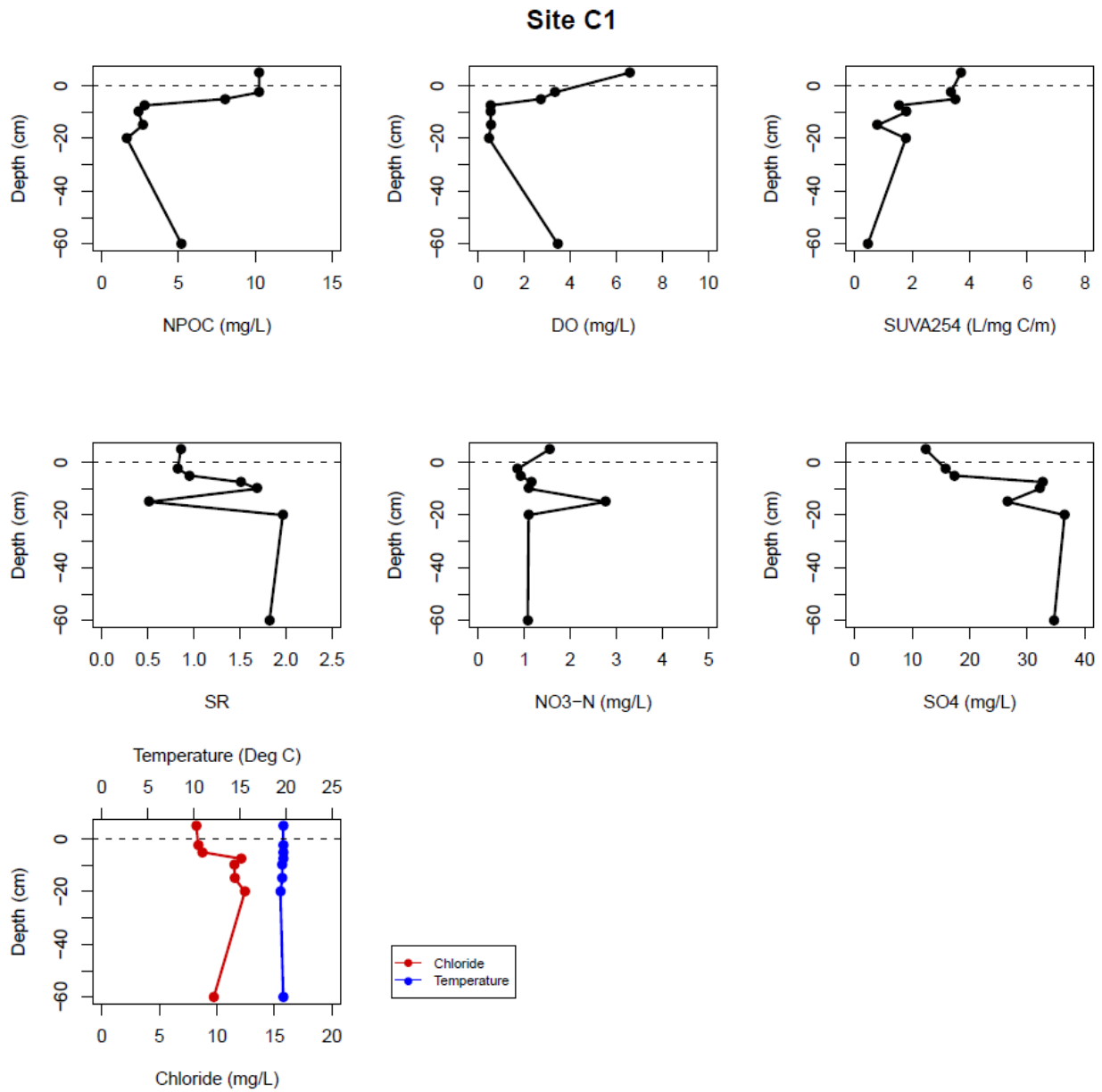


Figure B6: Site C1 Vertical Porewater Profiles

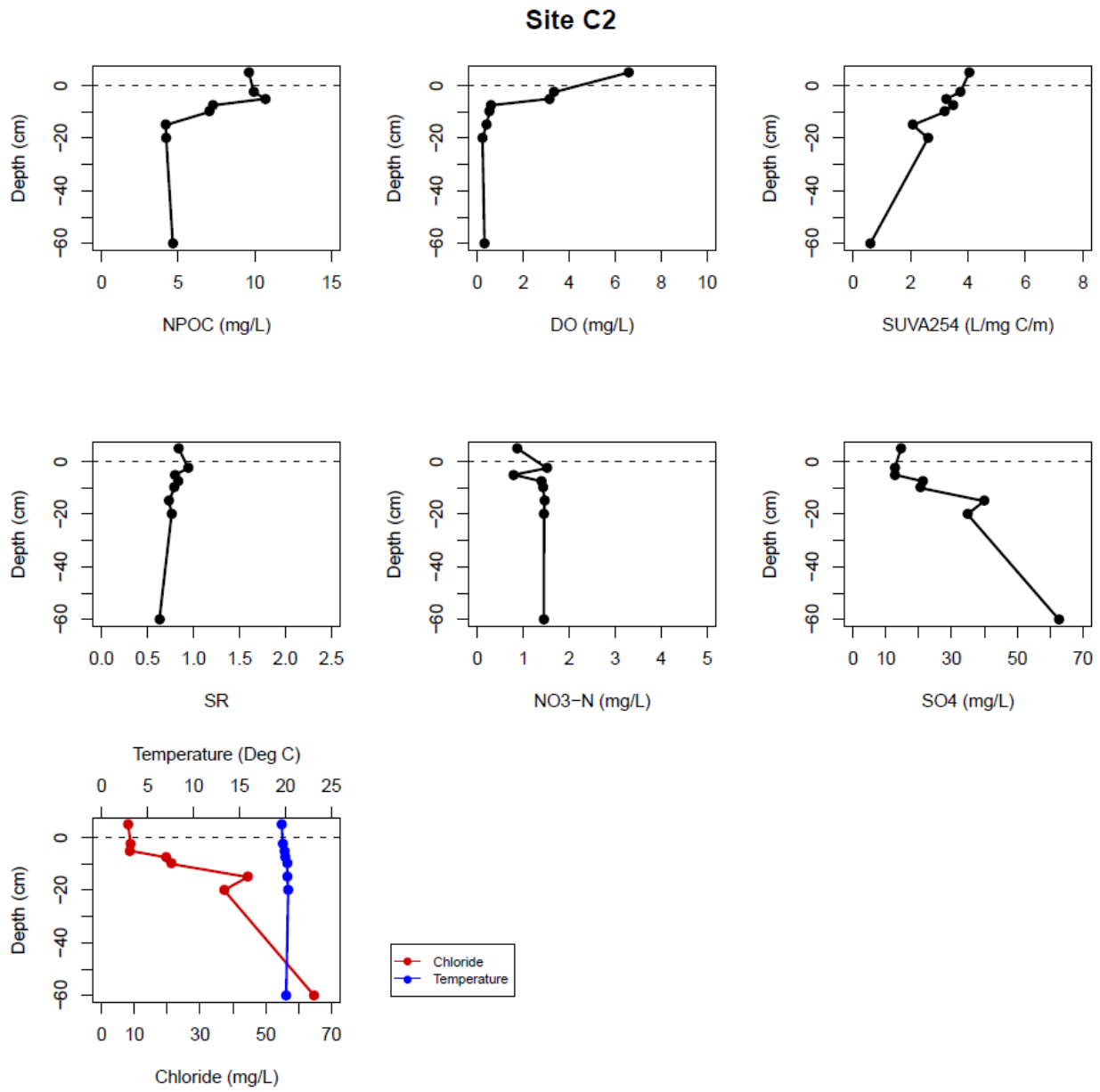


Figure B7: Site C2 Vertical Porewater Profiles

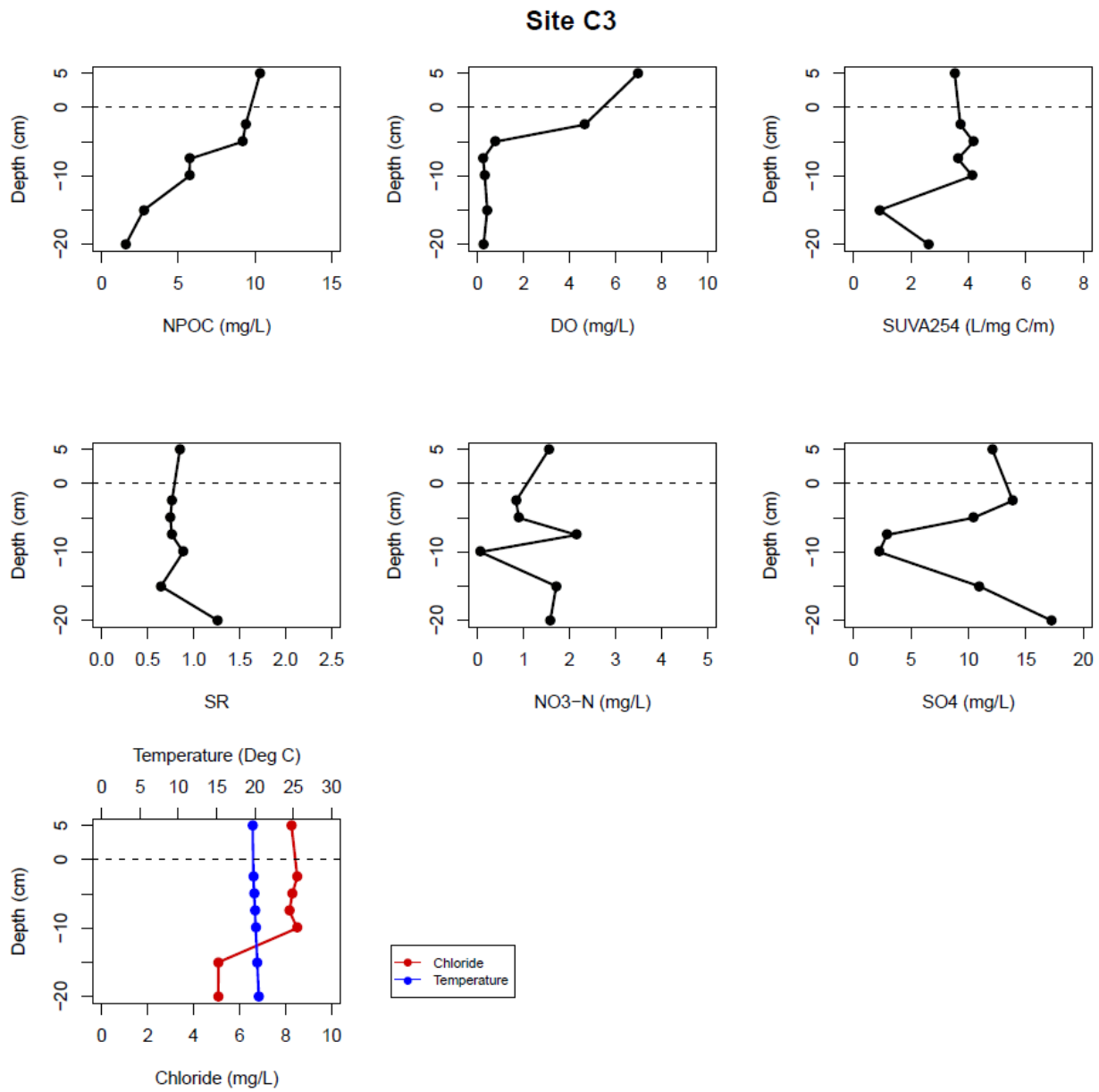


Figure B8: Site C3 Vertical Porewater Profiles

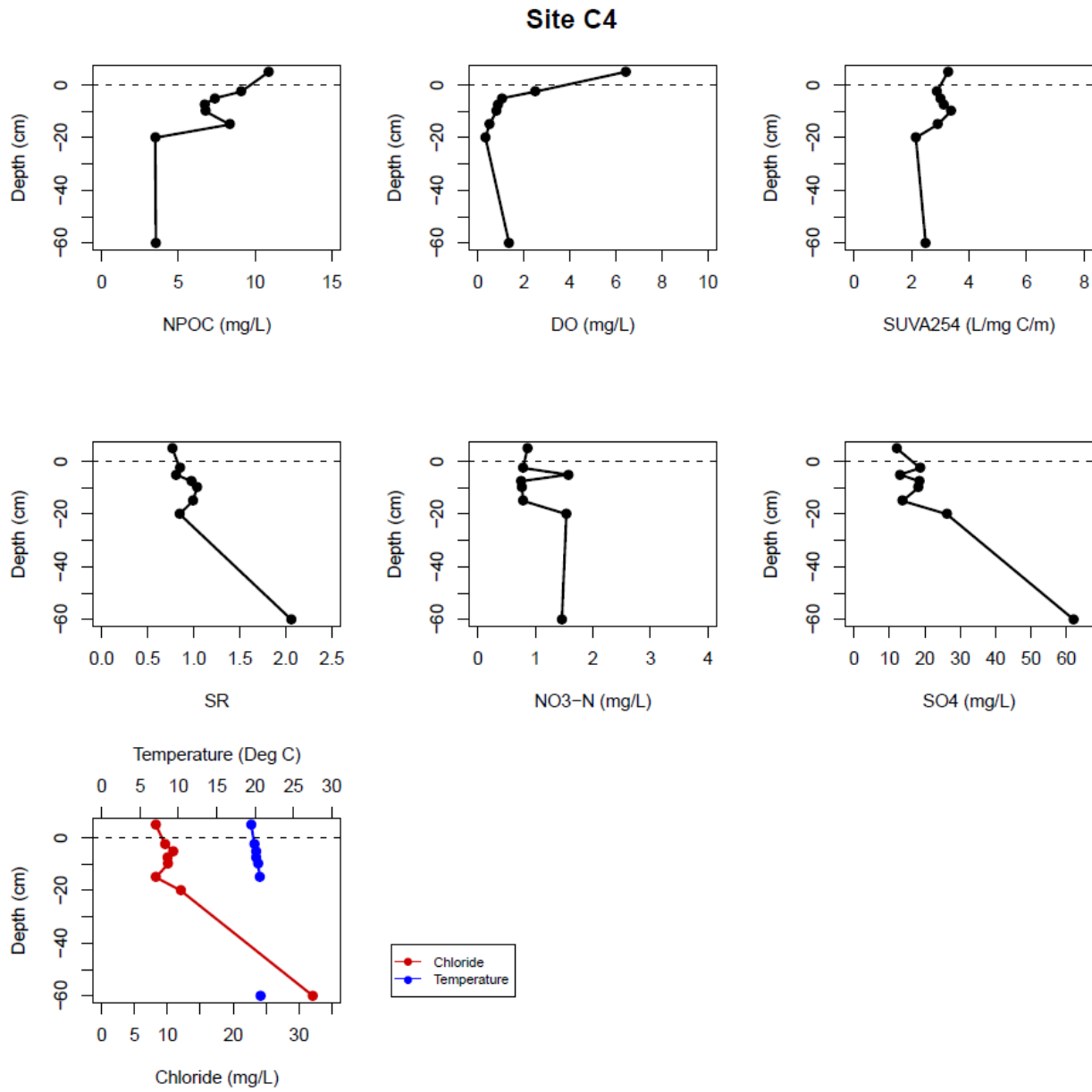


Figure B9: Site C4 Vertical Porewater Profiles

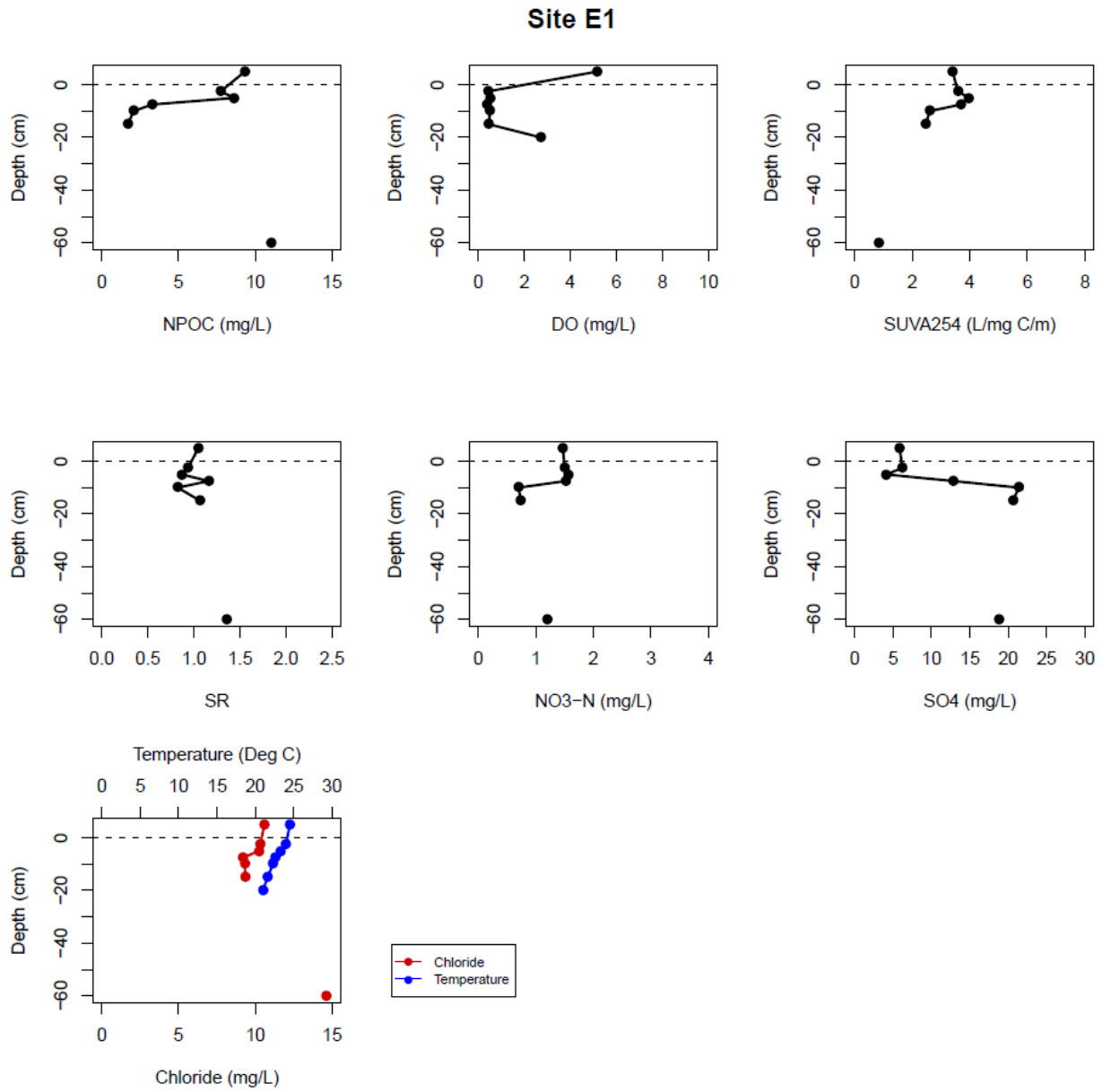


Figure B10: Site E1 Vertical Porewater Profiles

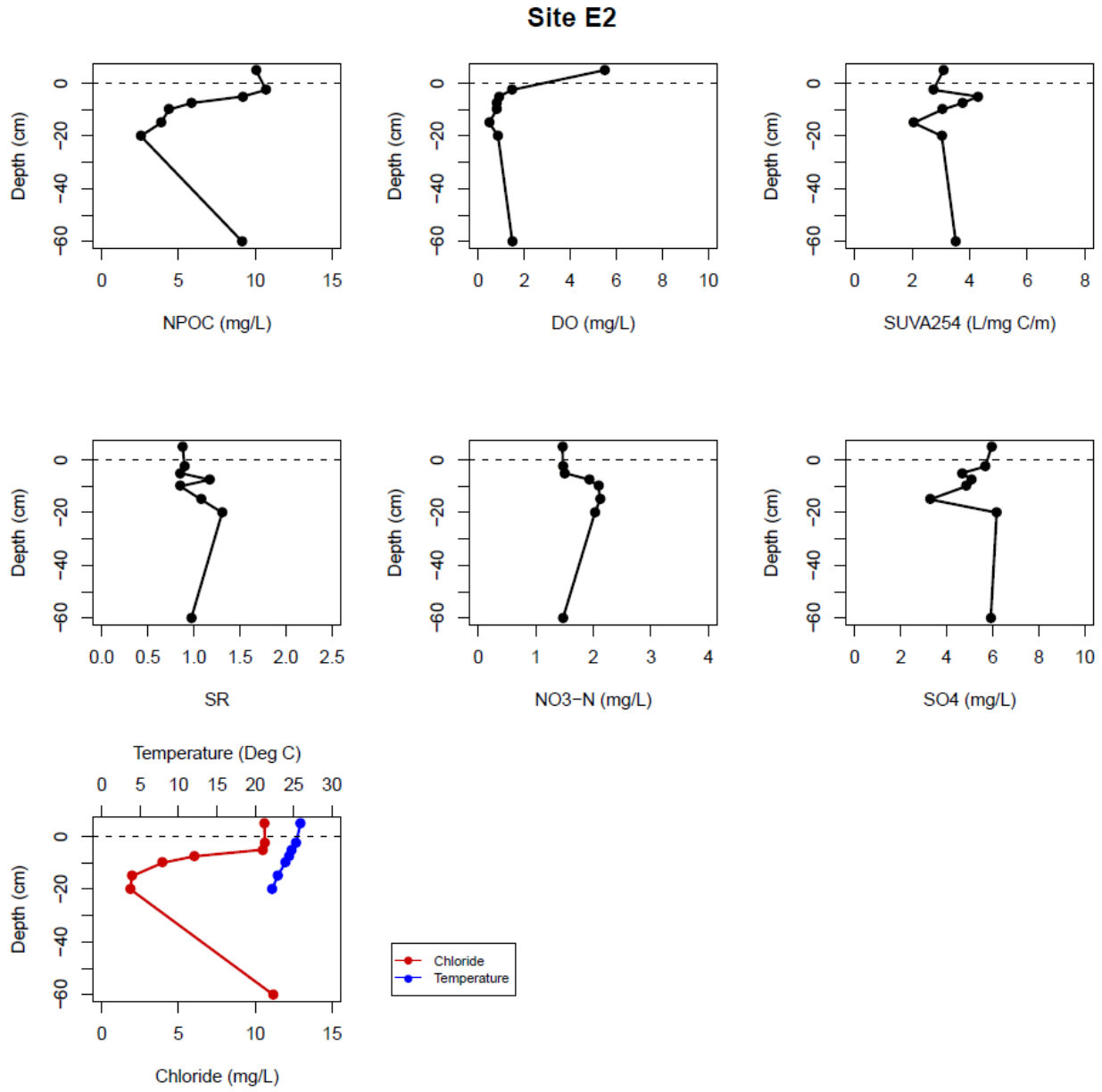


Figure B11: Site E2 Vertical Porewater Profiles

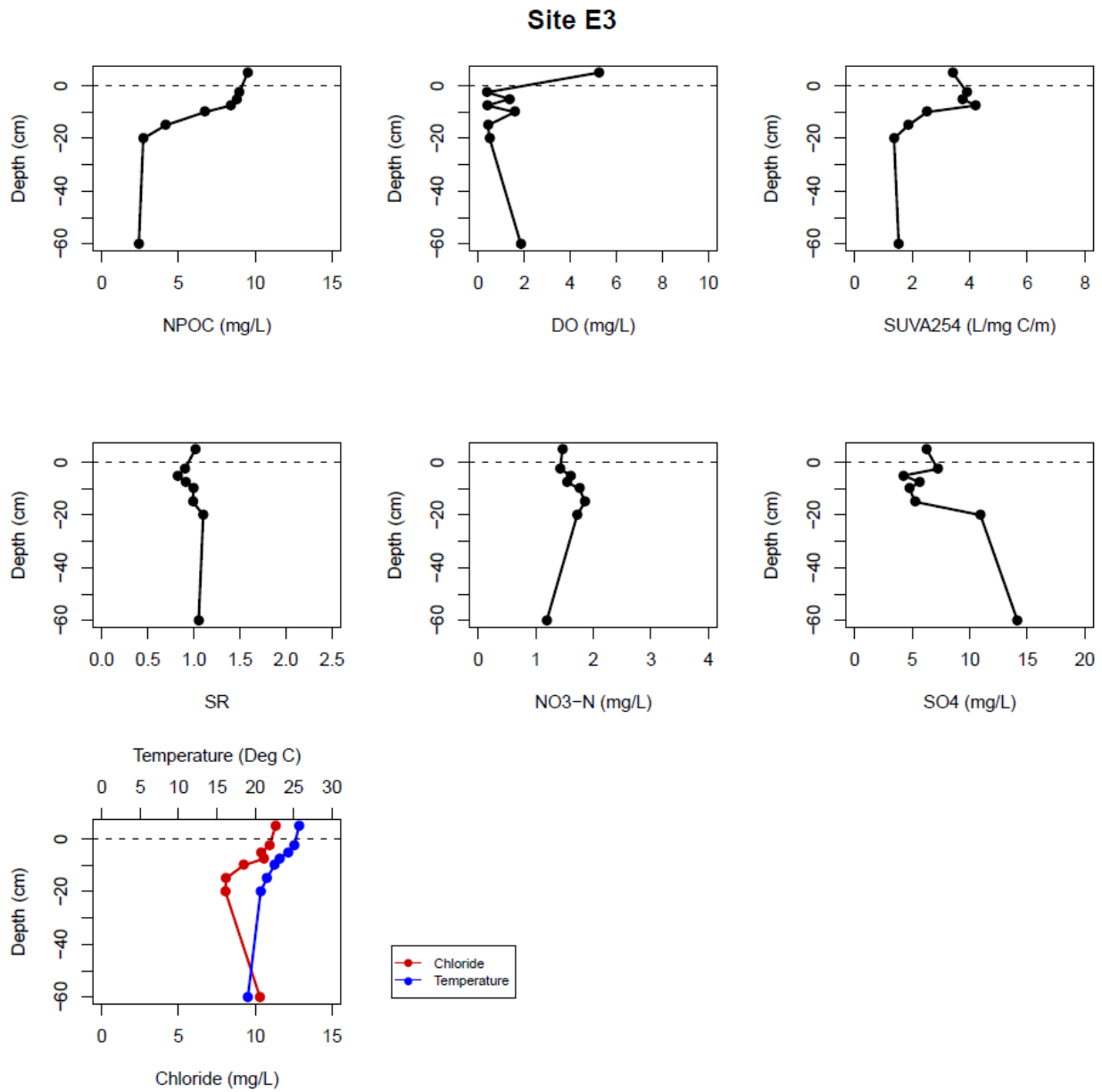


Figure B12: Site E3 Vertical Porewater Profiles

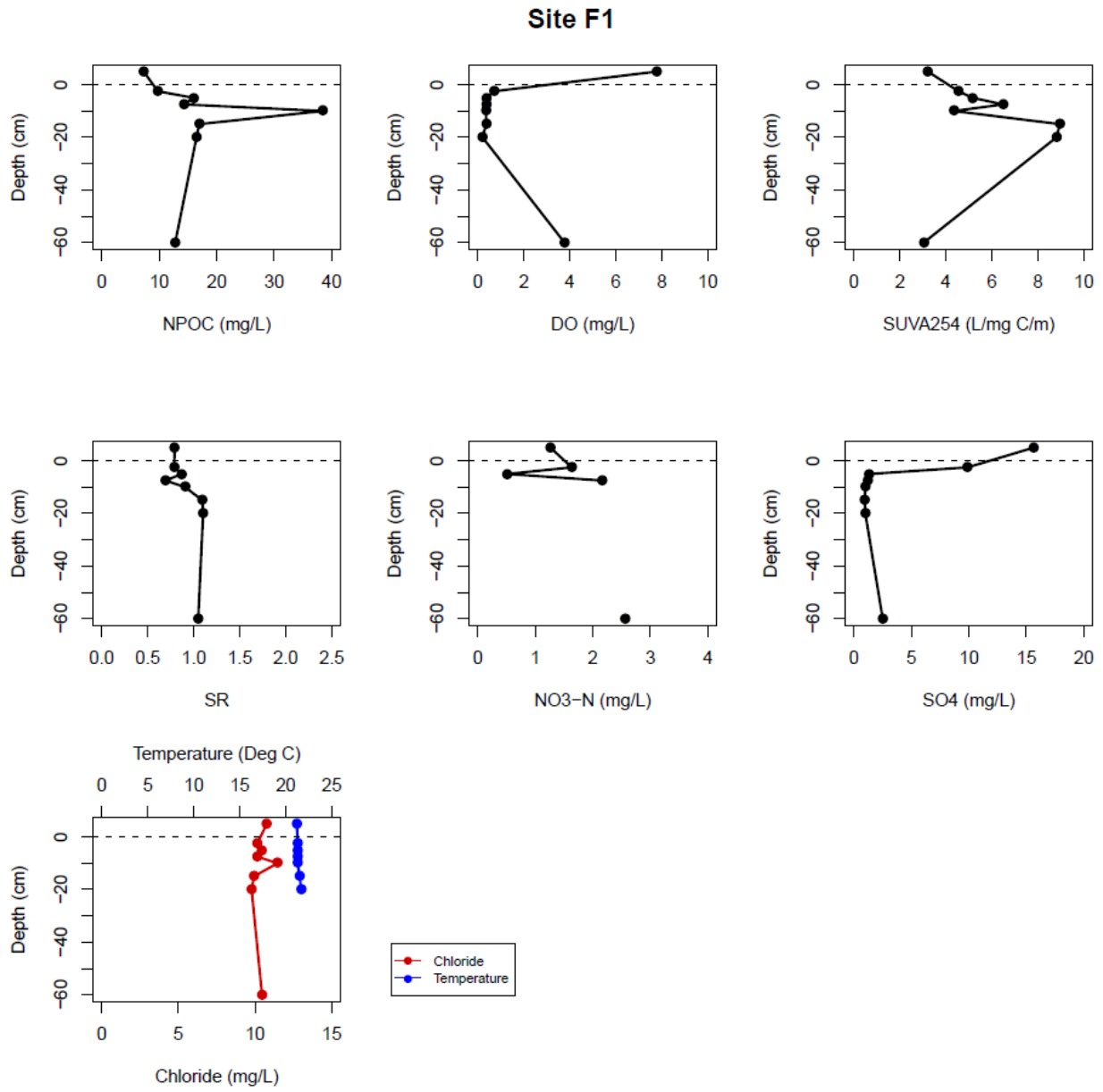


Figure B13: Site F1 Vertical Porewater Profiles

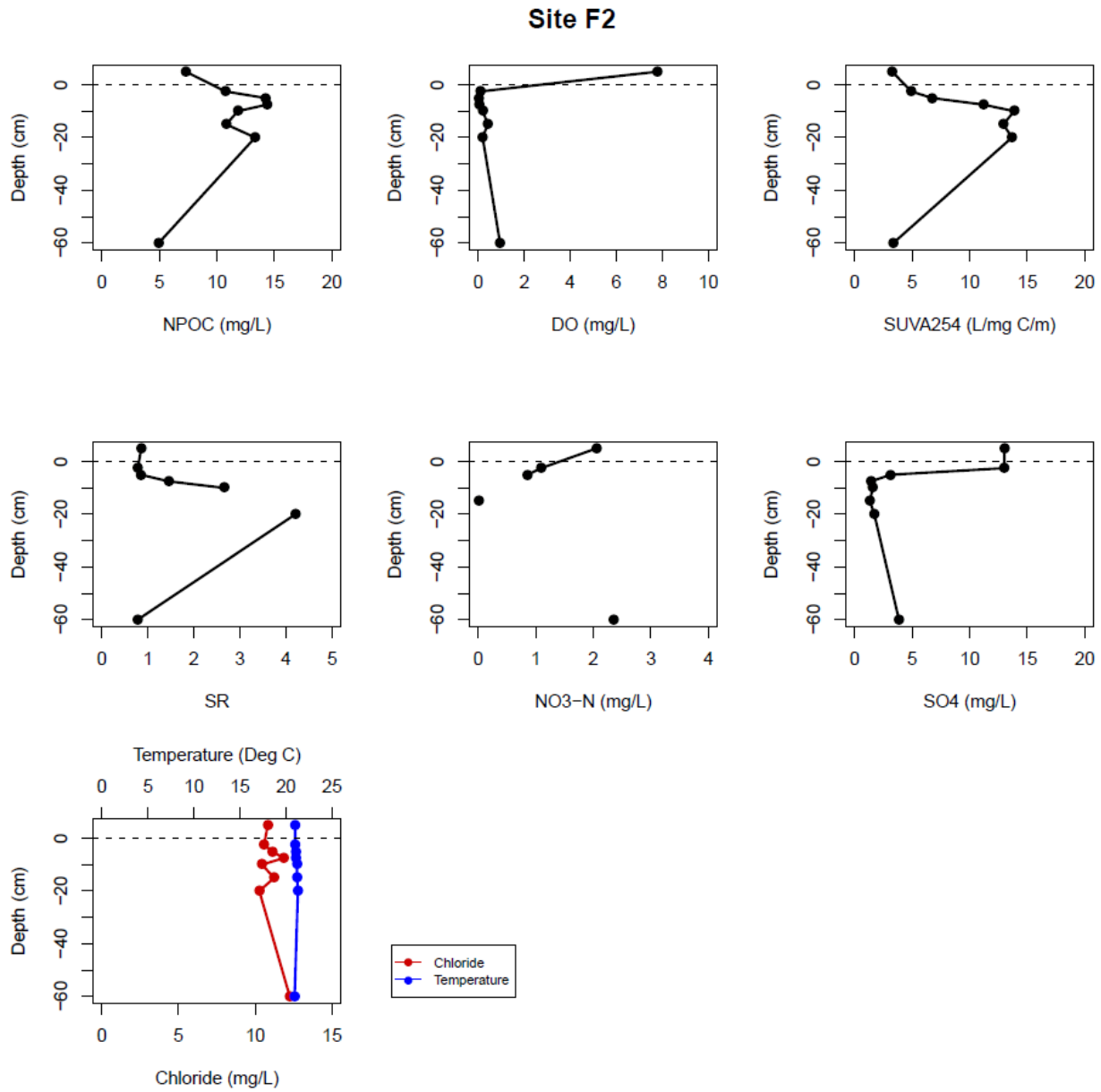


Figure B14: Site F2 Vertical Porewater Profiles

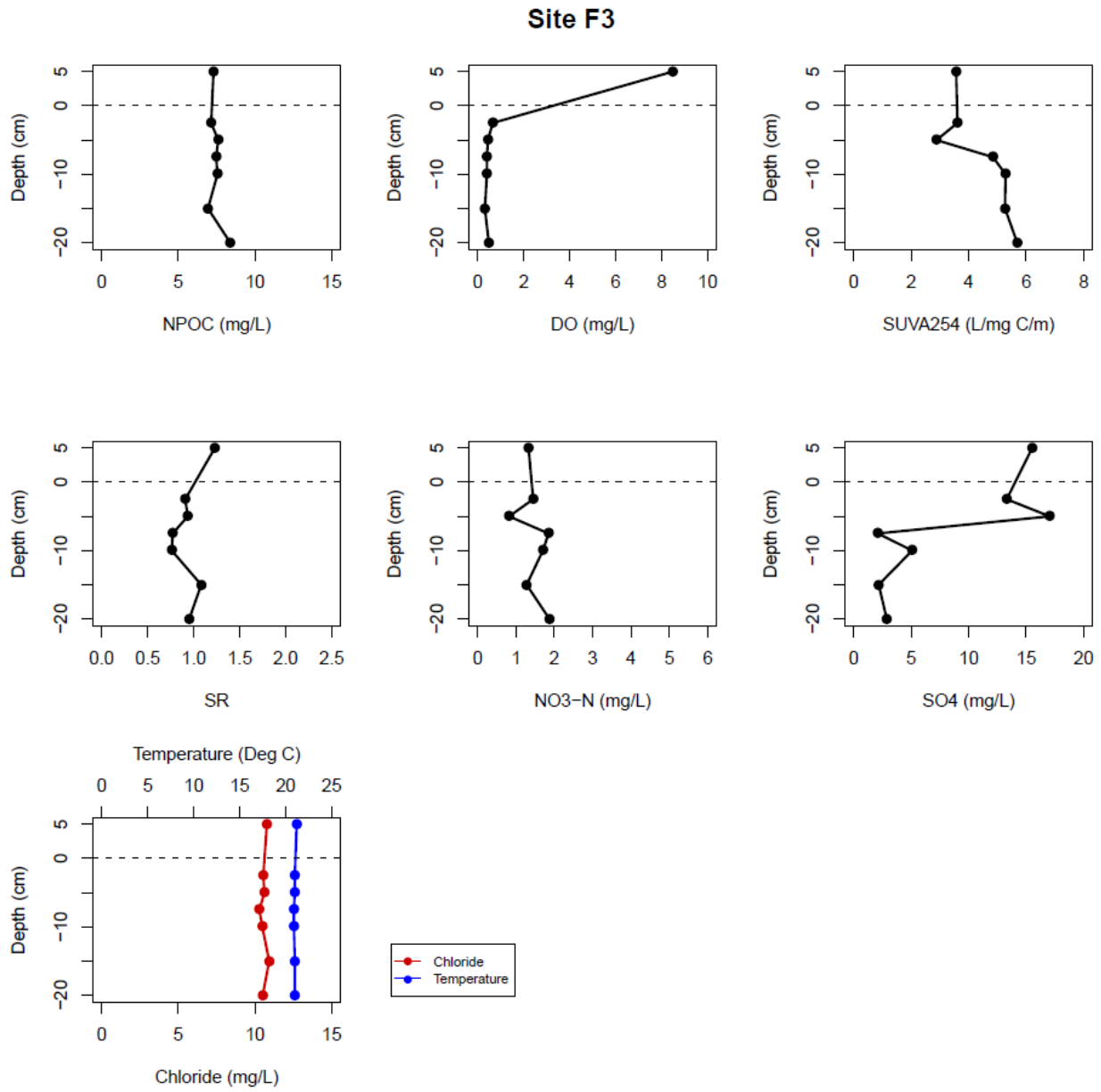


Figure B15: Site F3 Vertical Porewater Profiles

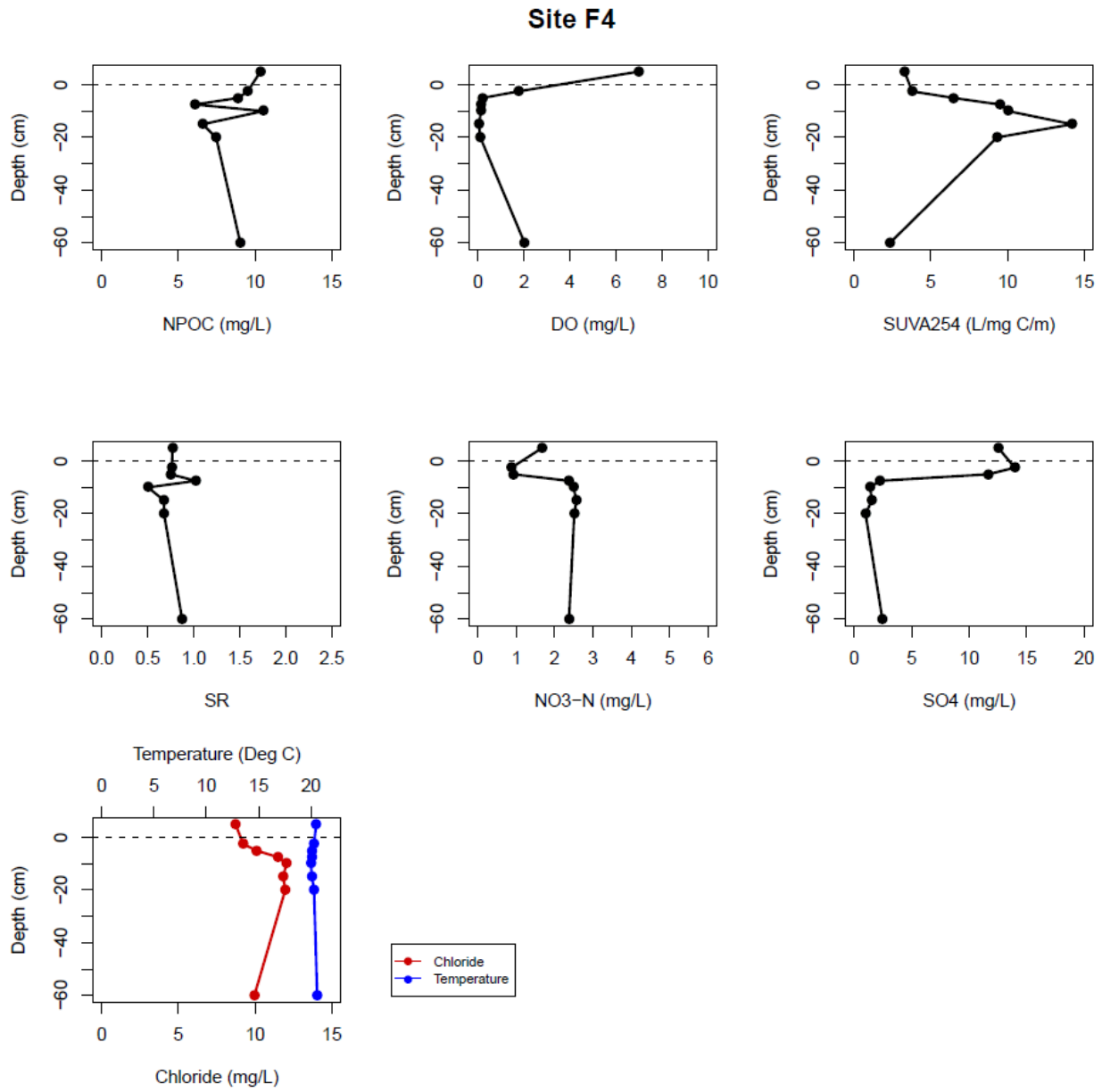


Figure B16: Site F4 Vertical Porewater Profiles

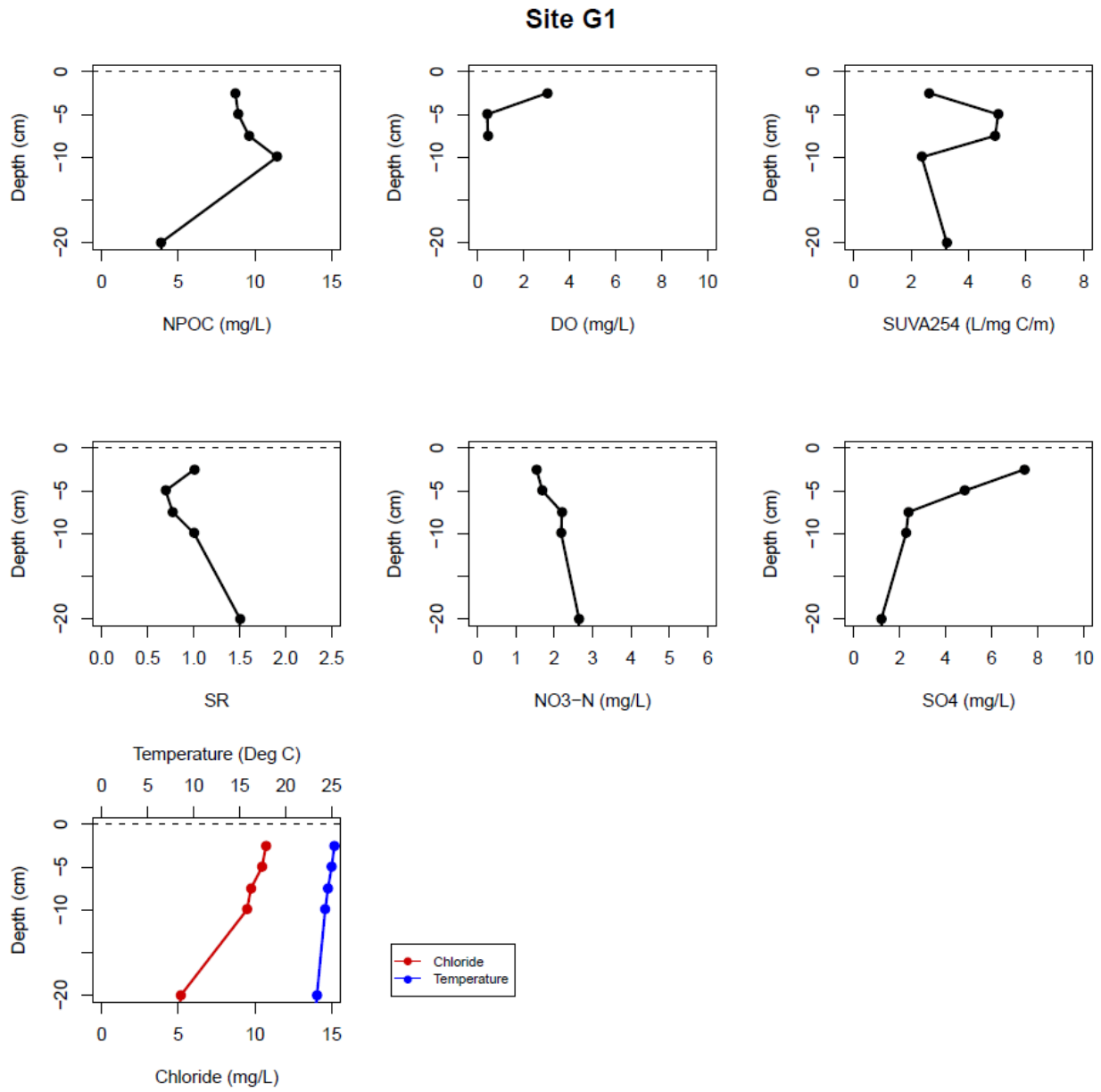


Figure B17: Site G1 Vertical Porewater Profiles

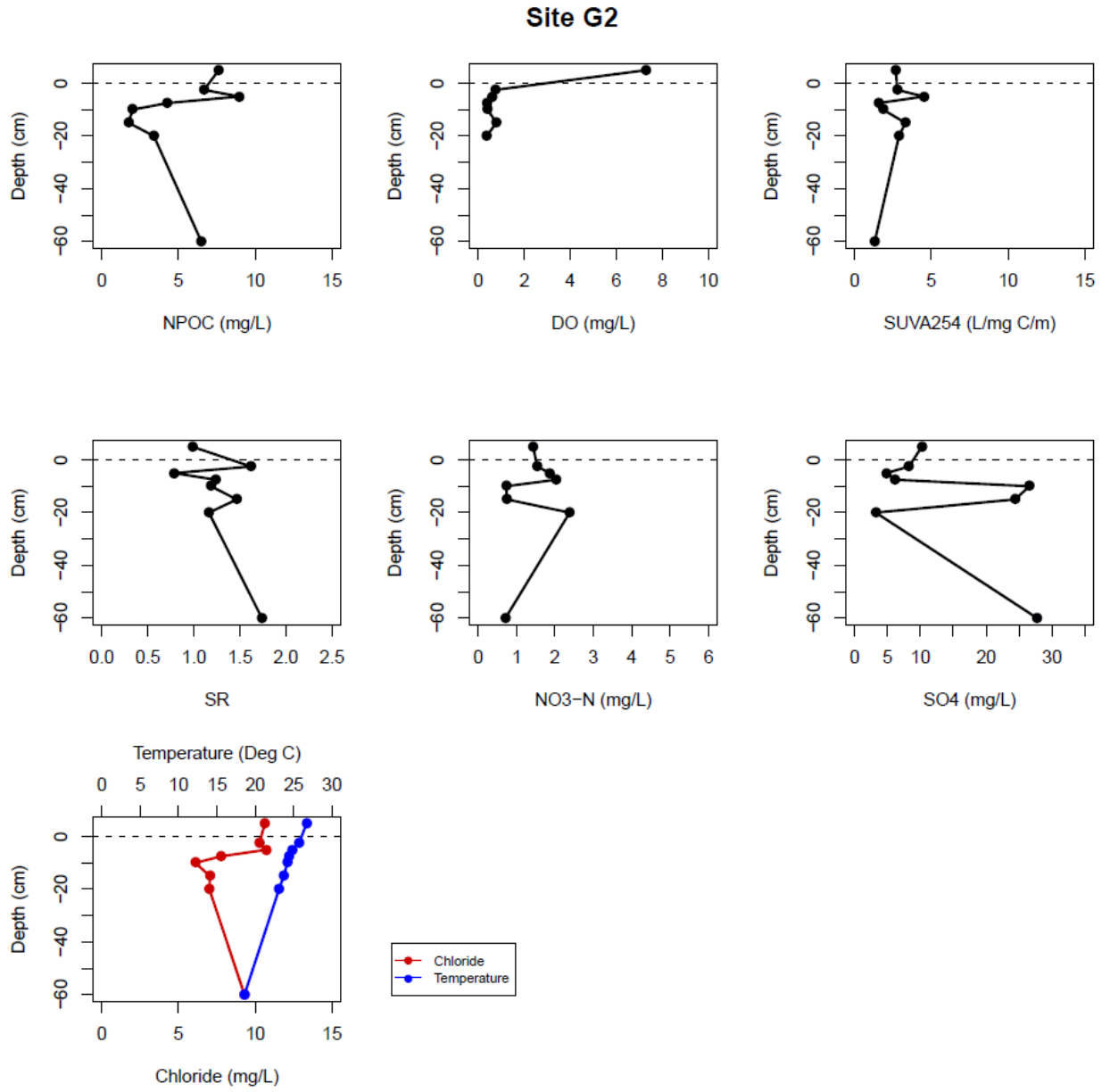


Figure B18: Site G2 Vertical Porewater Profiles

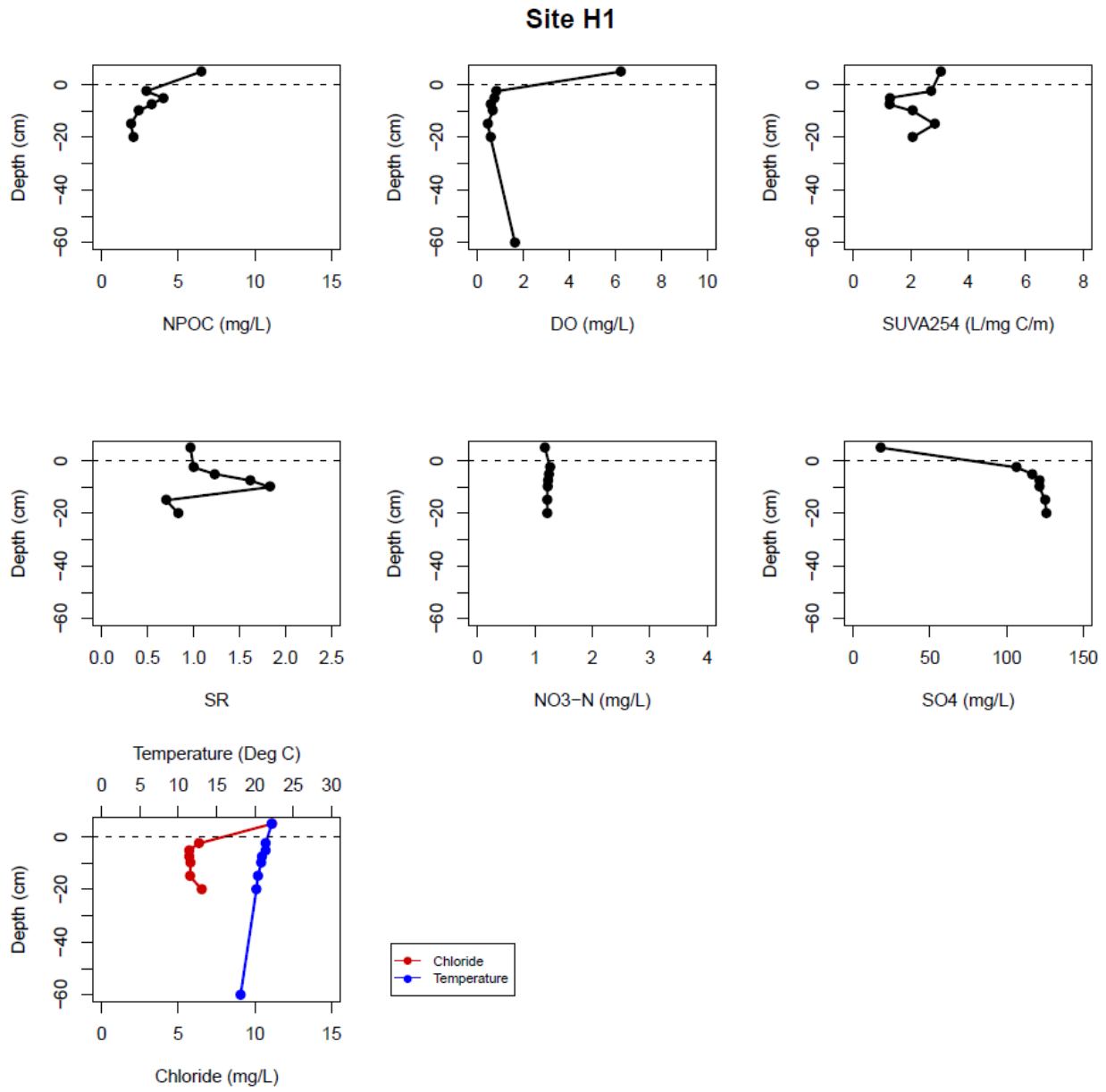


Figure B19: Site H1 Vertical Porewater Profiles

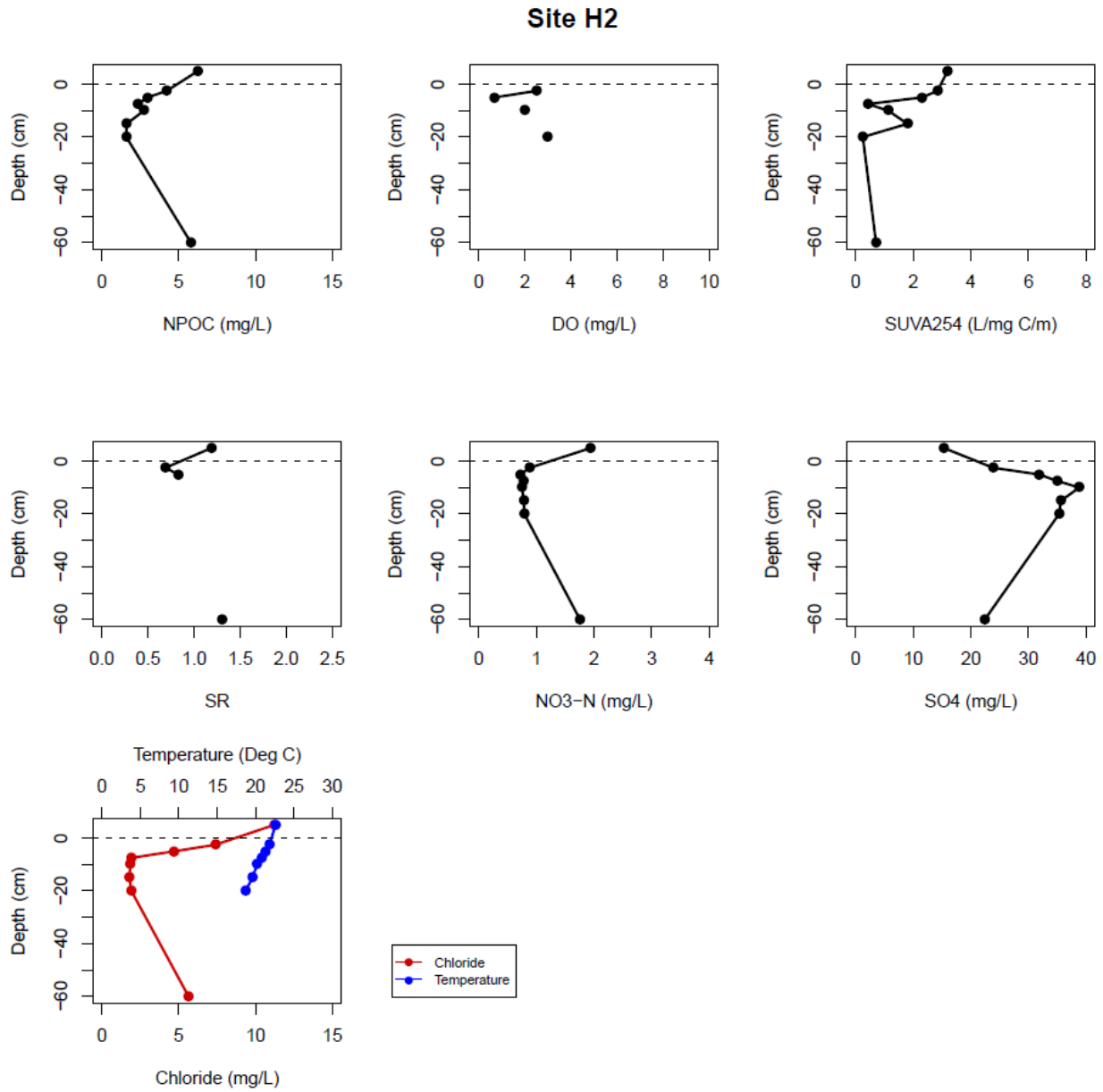


Figure B20: Site H2 Vertical Porewater Profiles

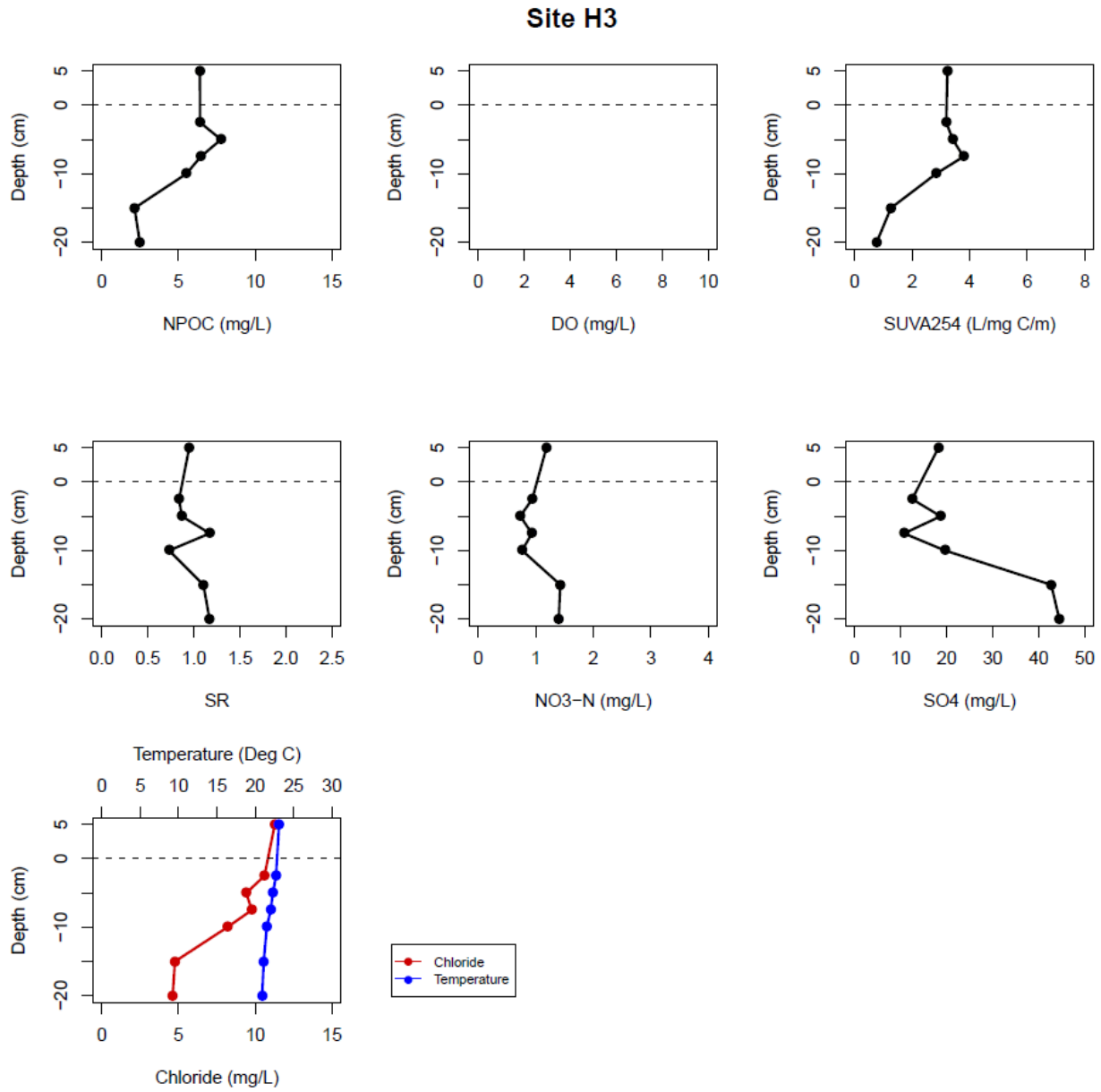


Figure B21: Site H3 Vertical Porewater Profiles

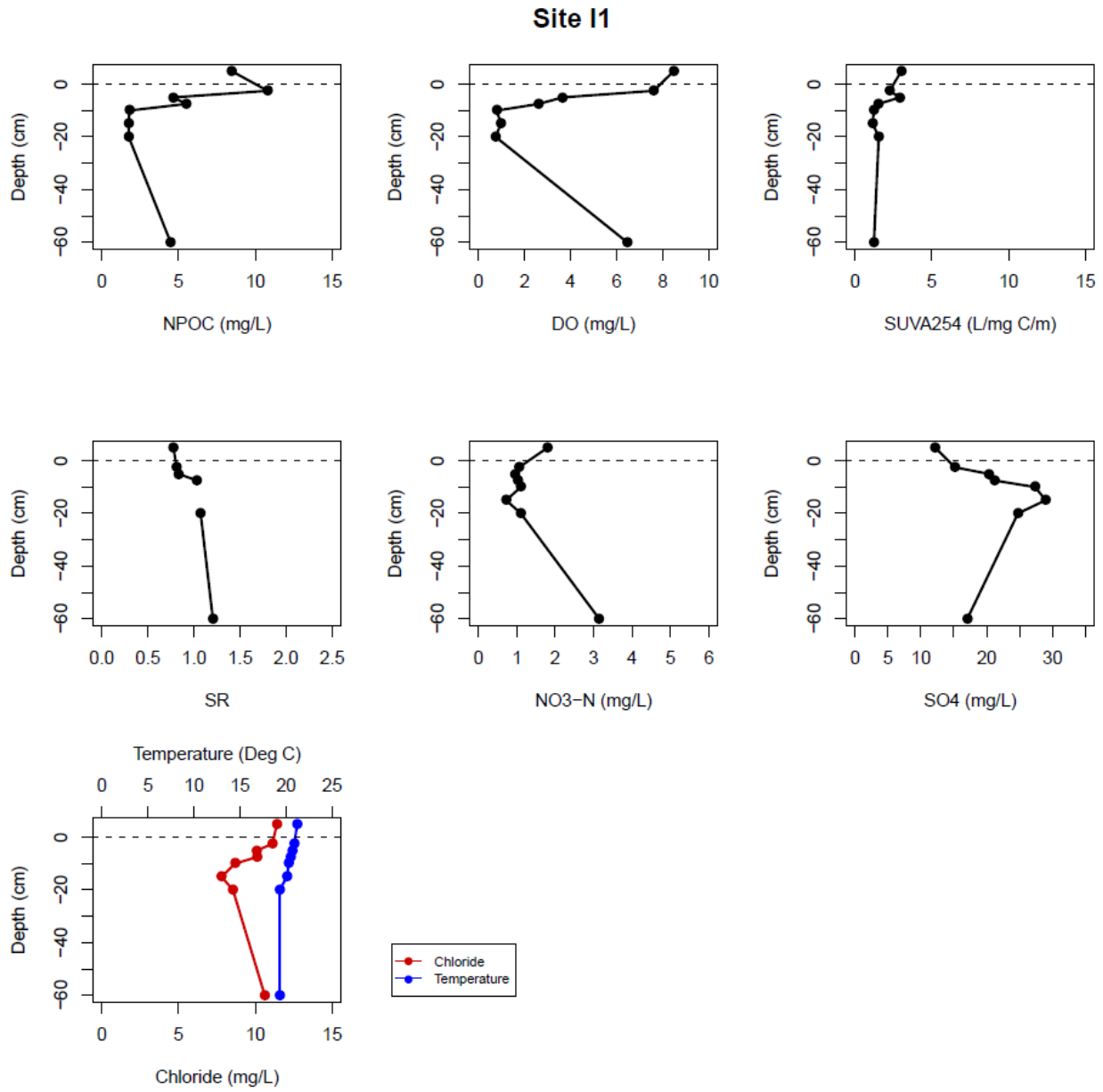


Figure B22: Site I1 Vertical Porewater Profiles

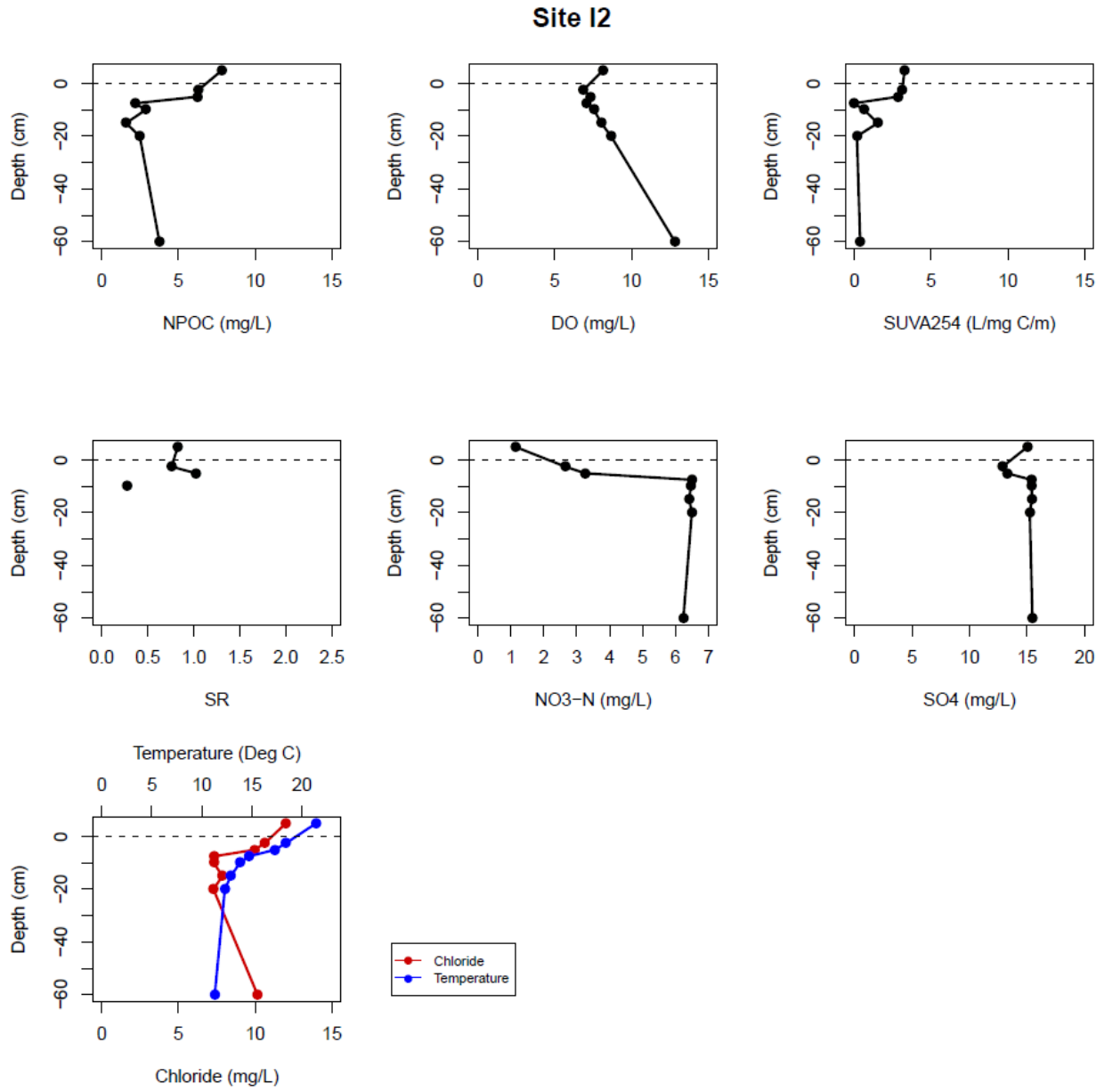


Figure B23: Site I2 Vertical Porewater Profiles

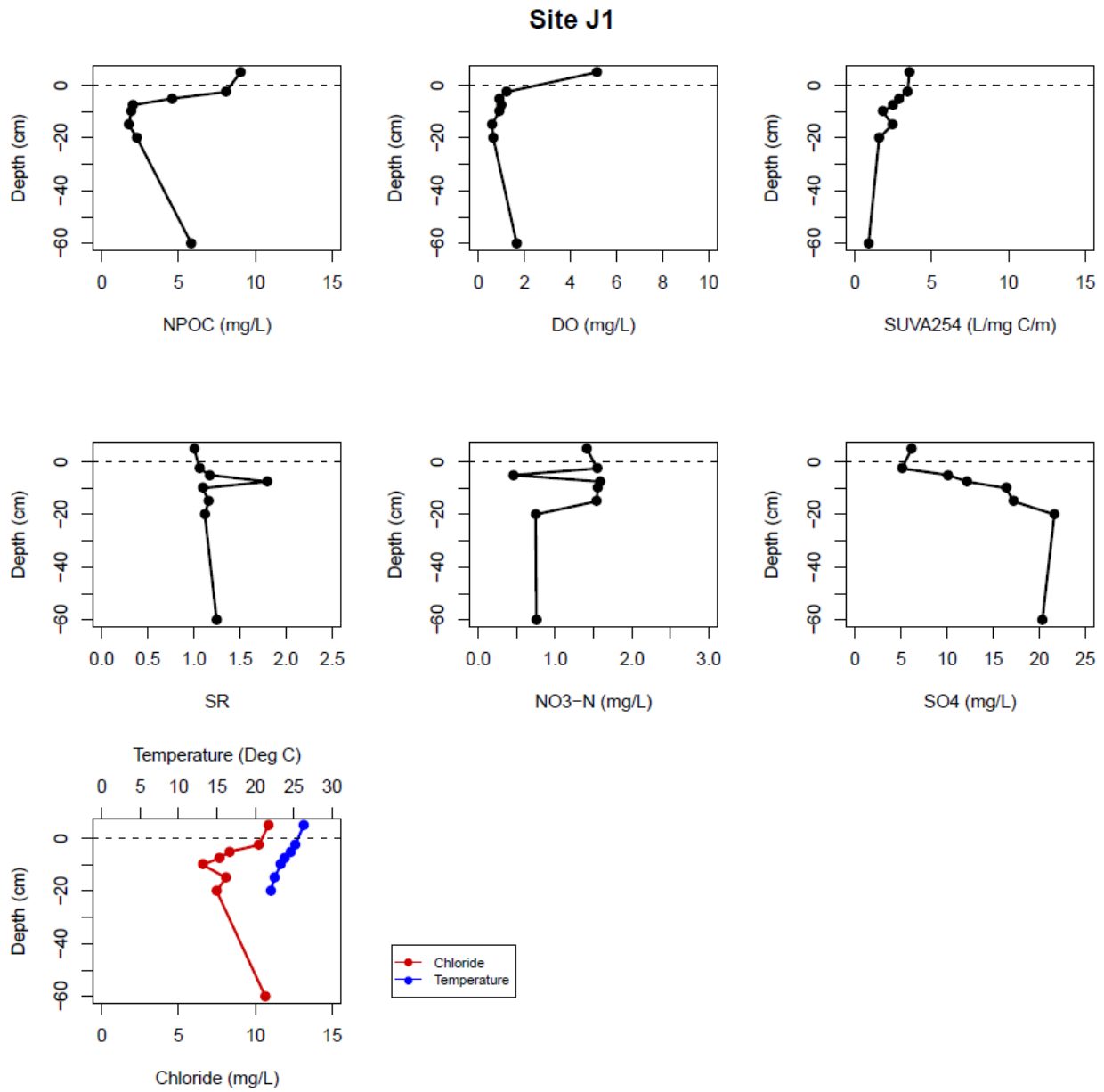


Figure B24: Site J1 Vertical Porewater Profiles

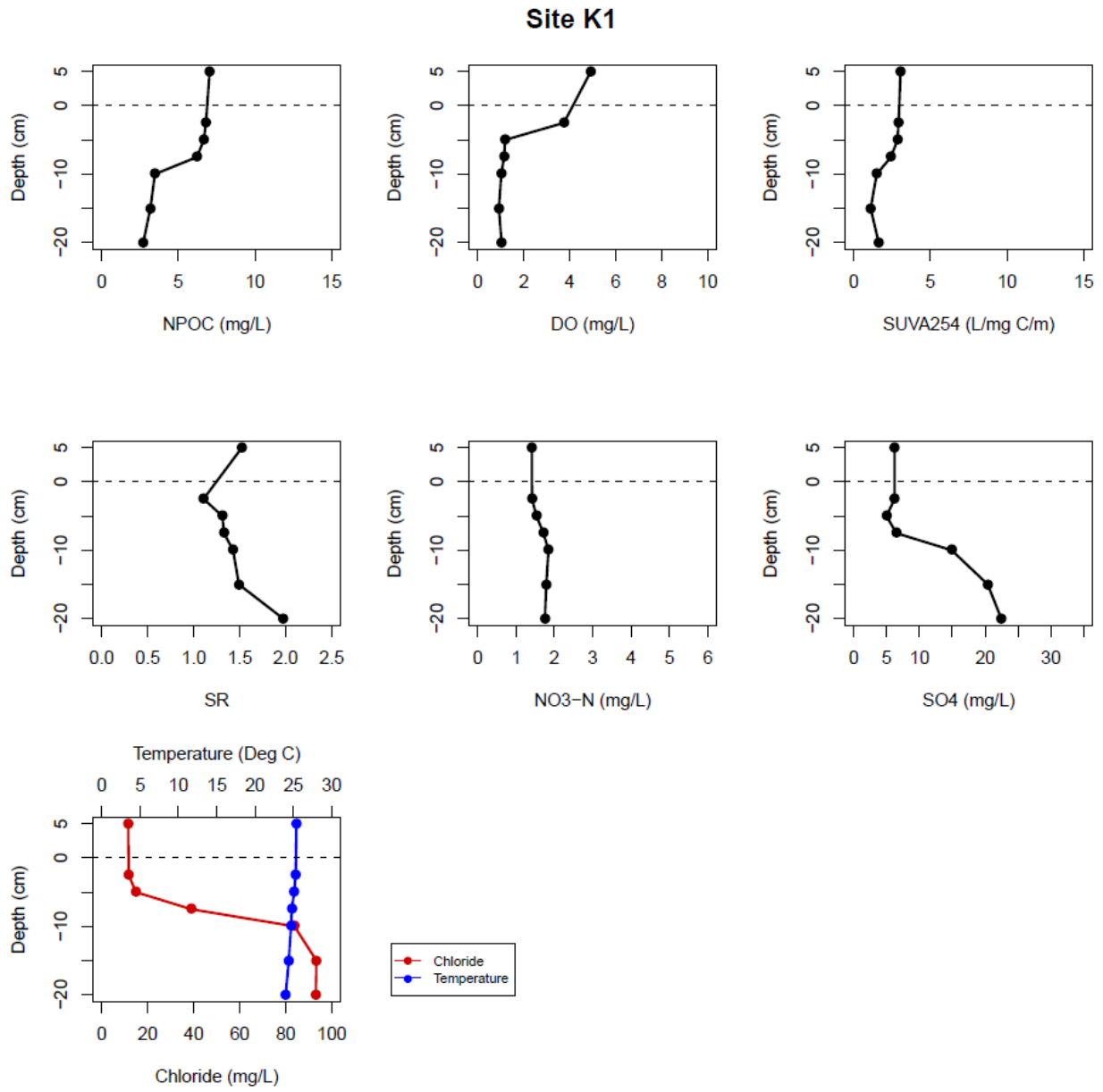


Figure B25: Site K1 Vertical Porewater Profiles

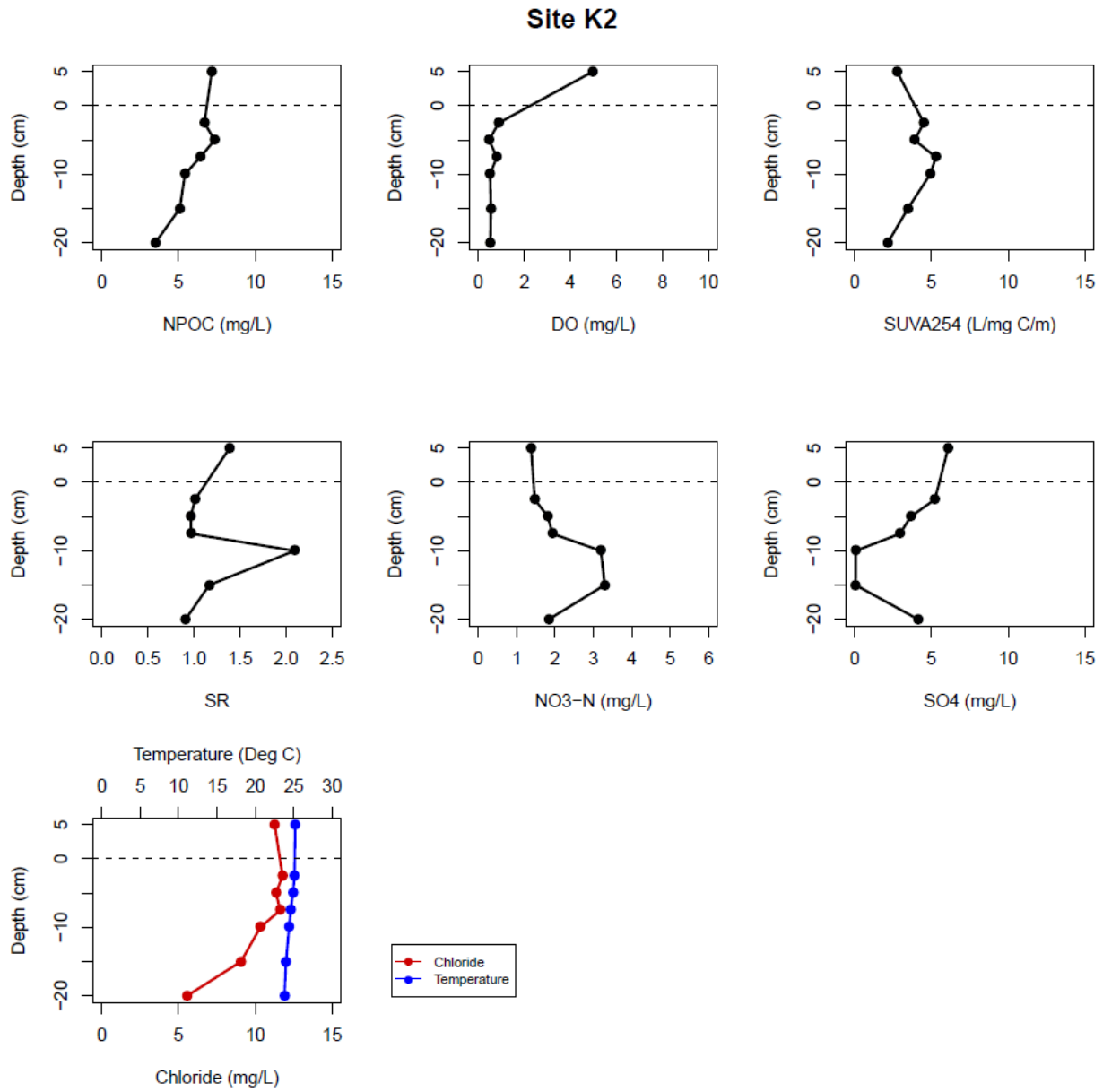


Figure B26: Site K2 Vertical Porewater Profiles

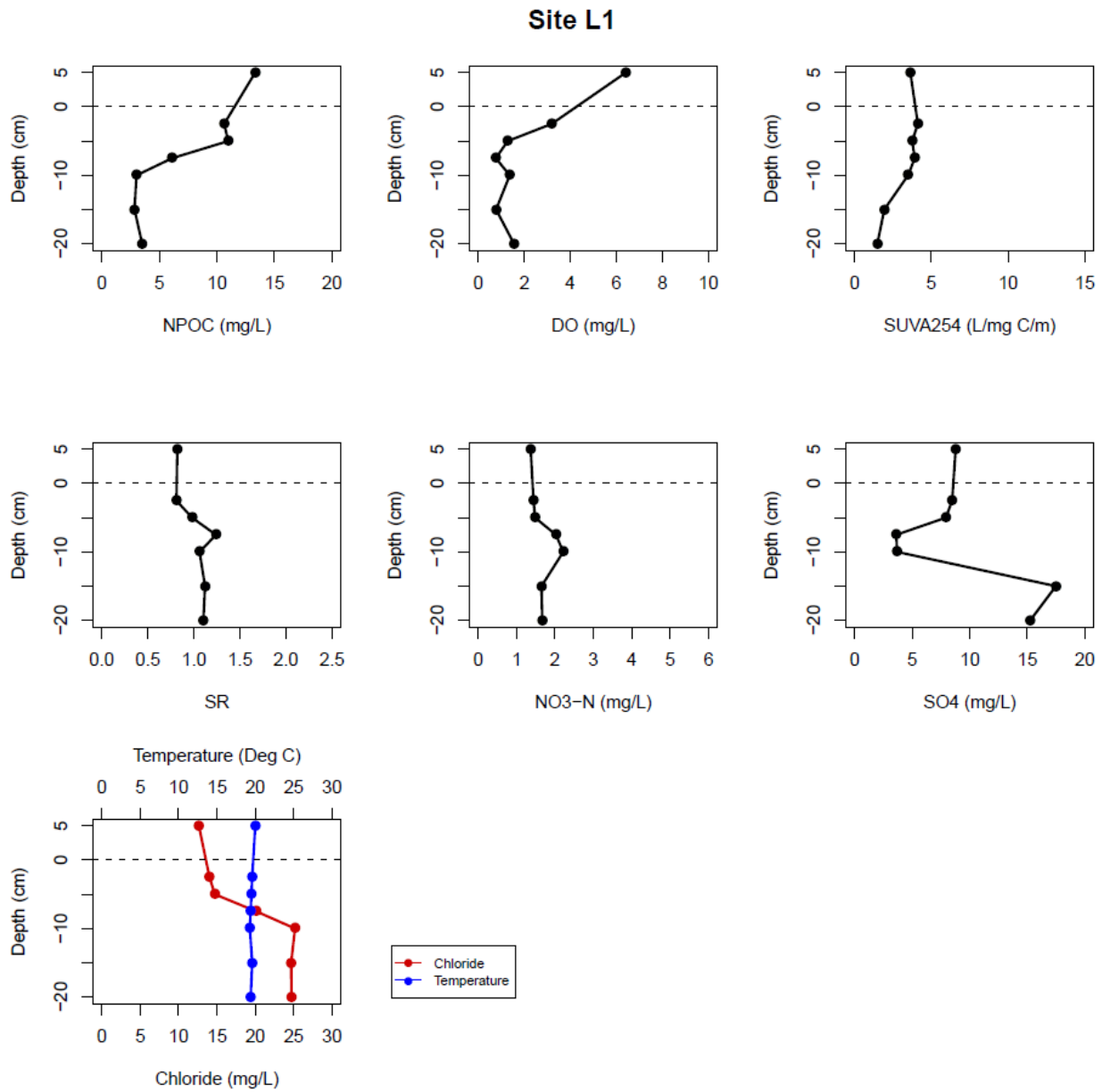


Figure B27: Site L1 Vertical Porewater Profiles

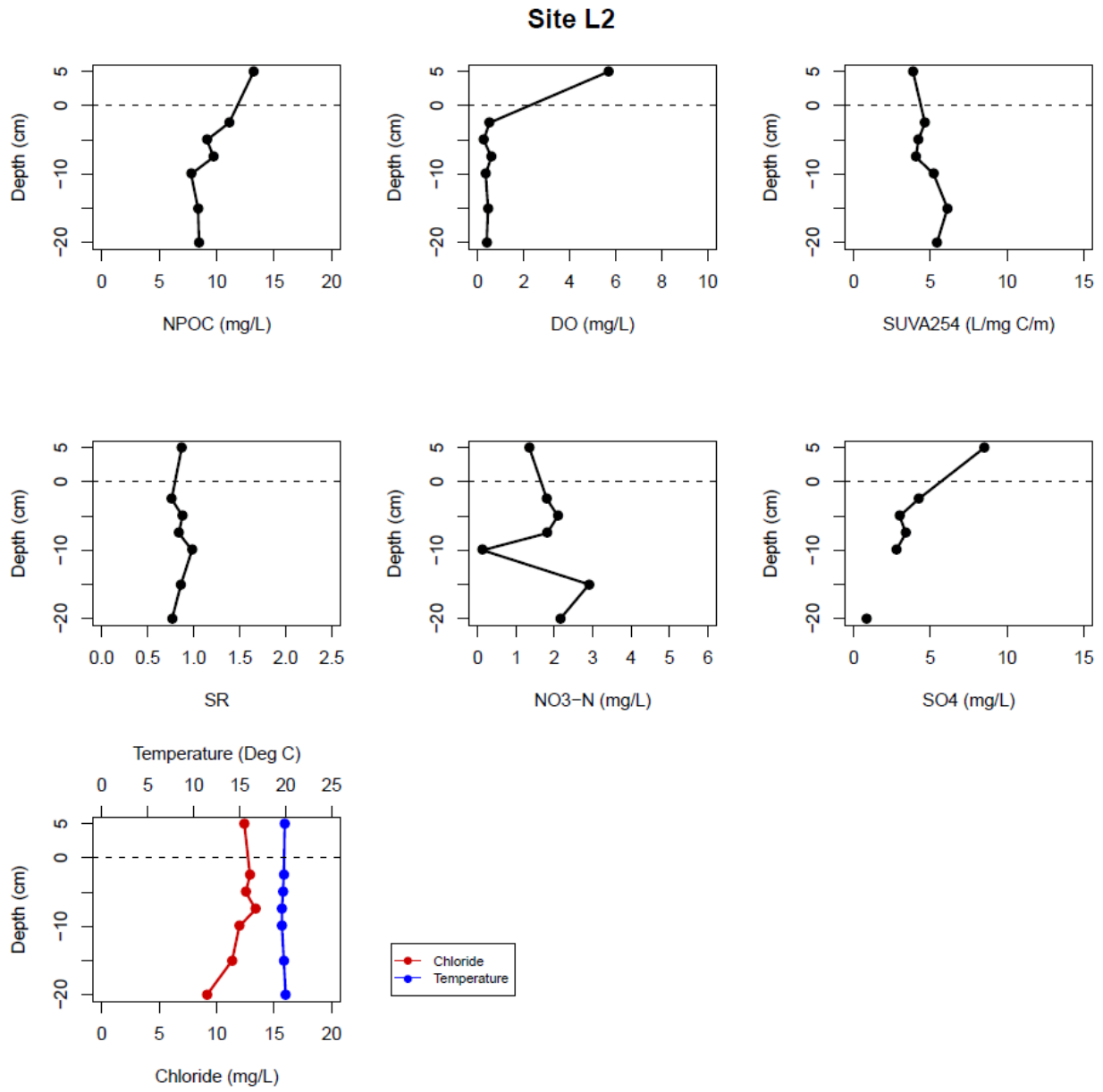


Figure B28: Site L2 Vertical Porewater Profiles

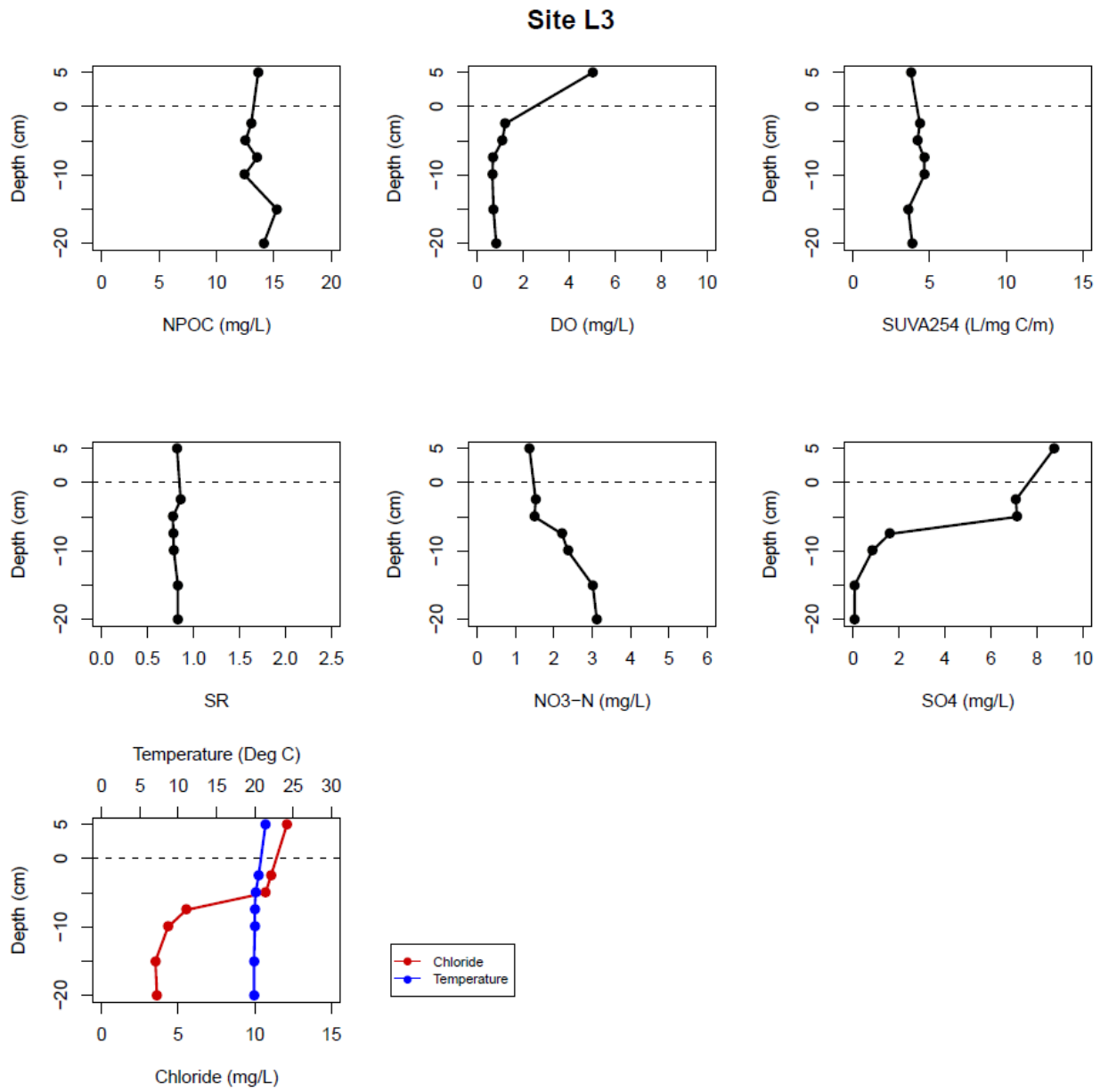


Figure B29: Site L3 Vertical Porewater Profiles

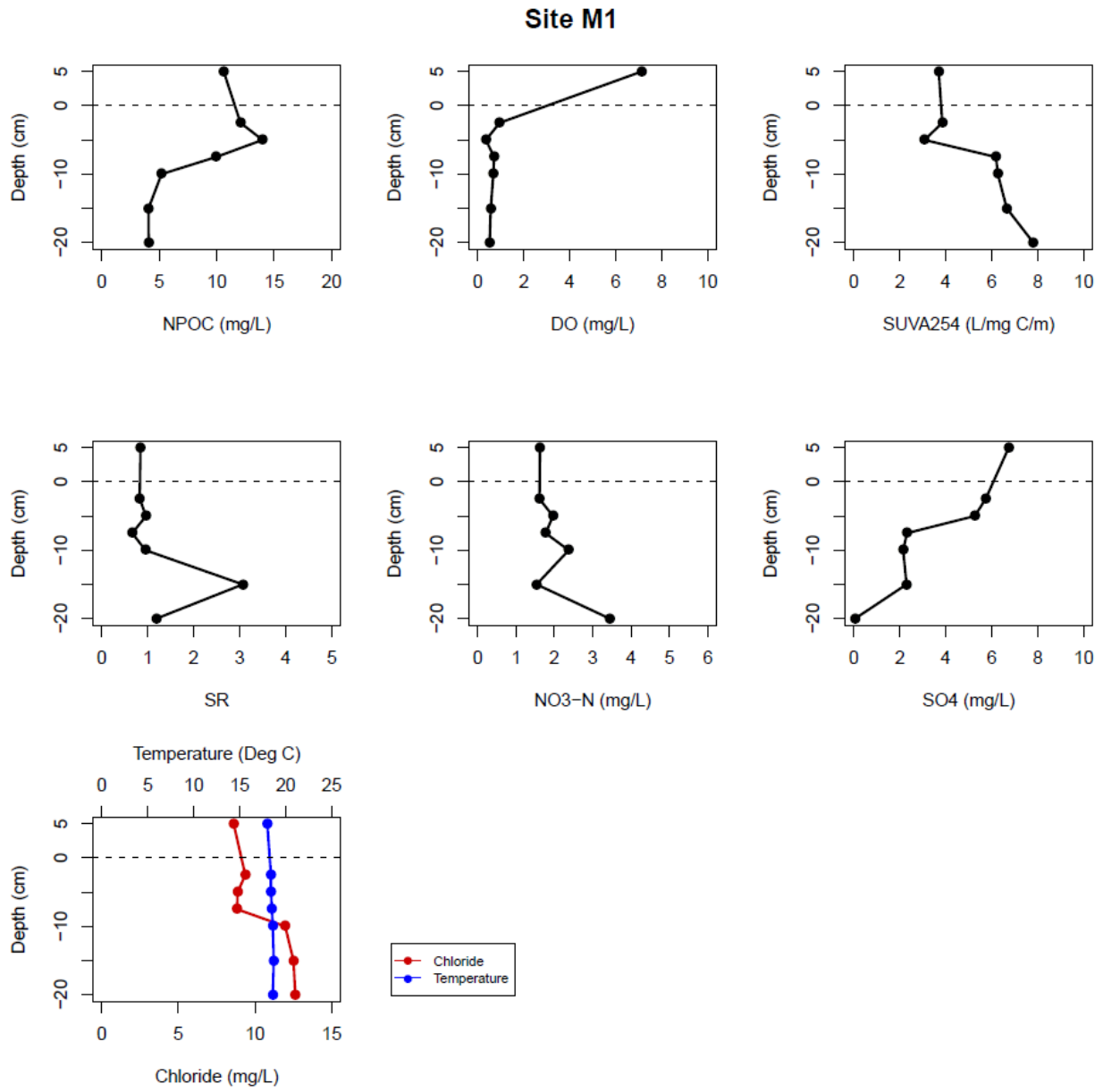


Figure B30: Site M1 Vertical Porewater Profiles

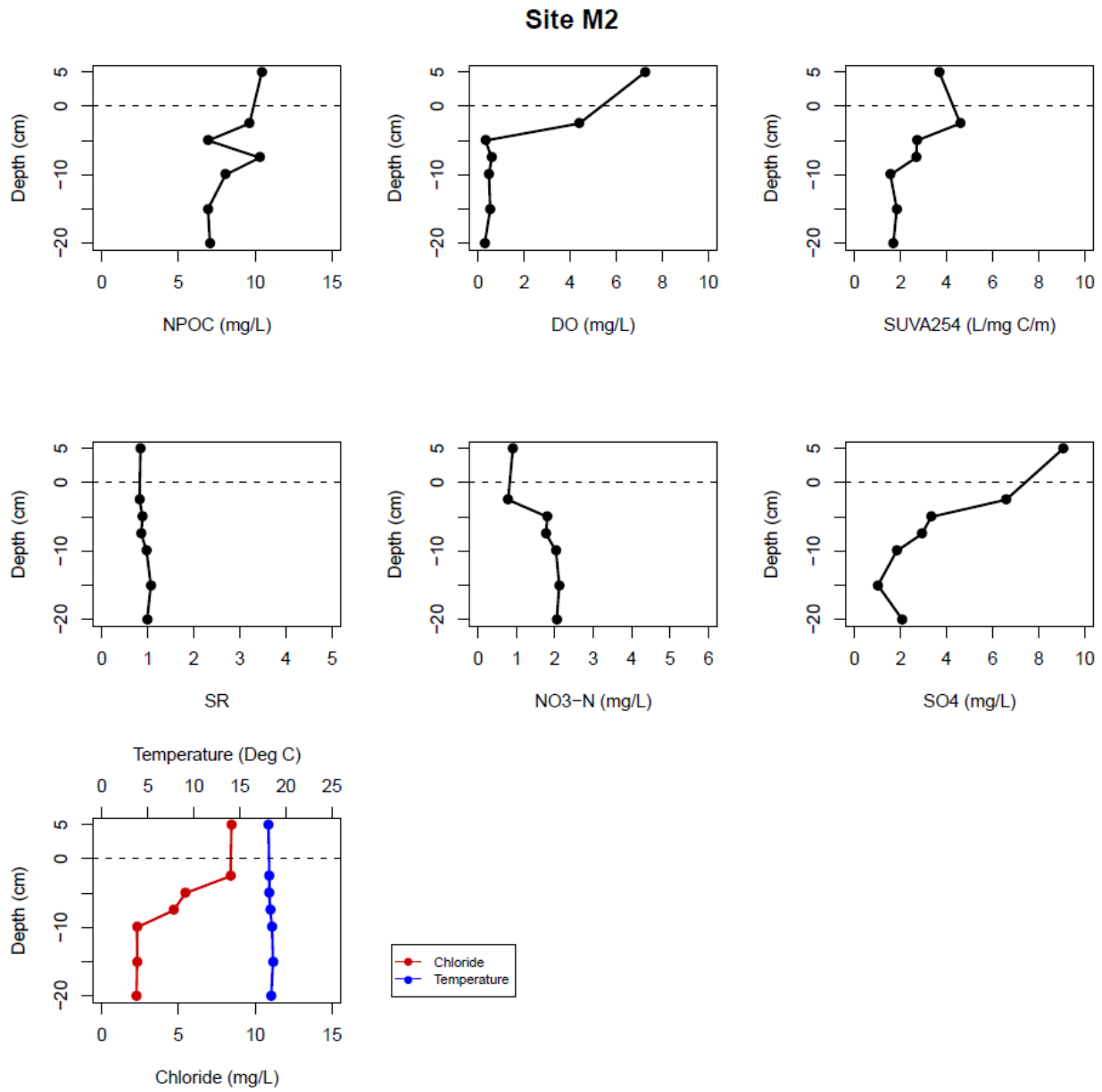


Figure B31: Site M2 Vertical Porewater Profiles

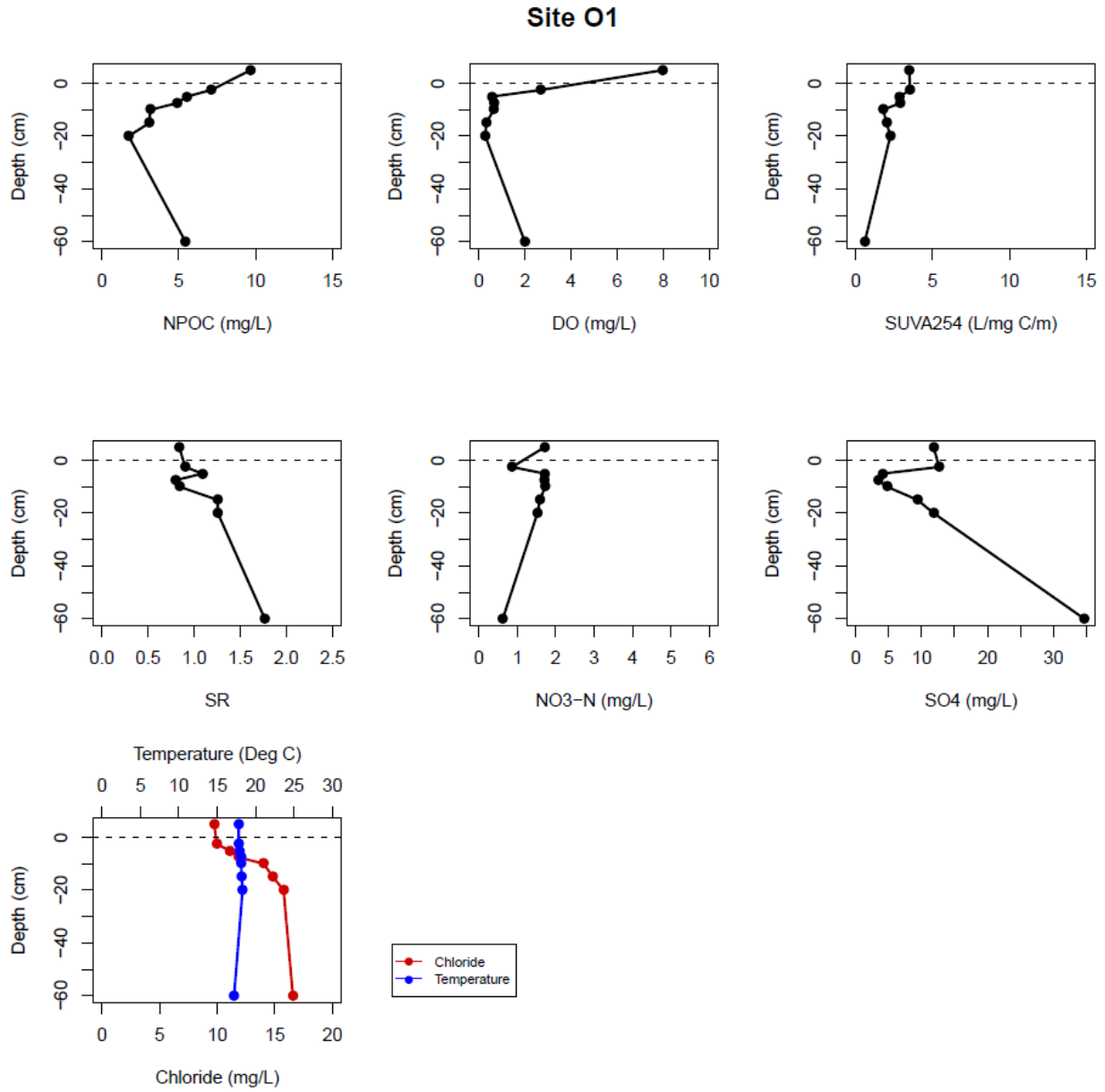


Figure B32: Site O1 Vertical Porewater Profiles

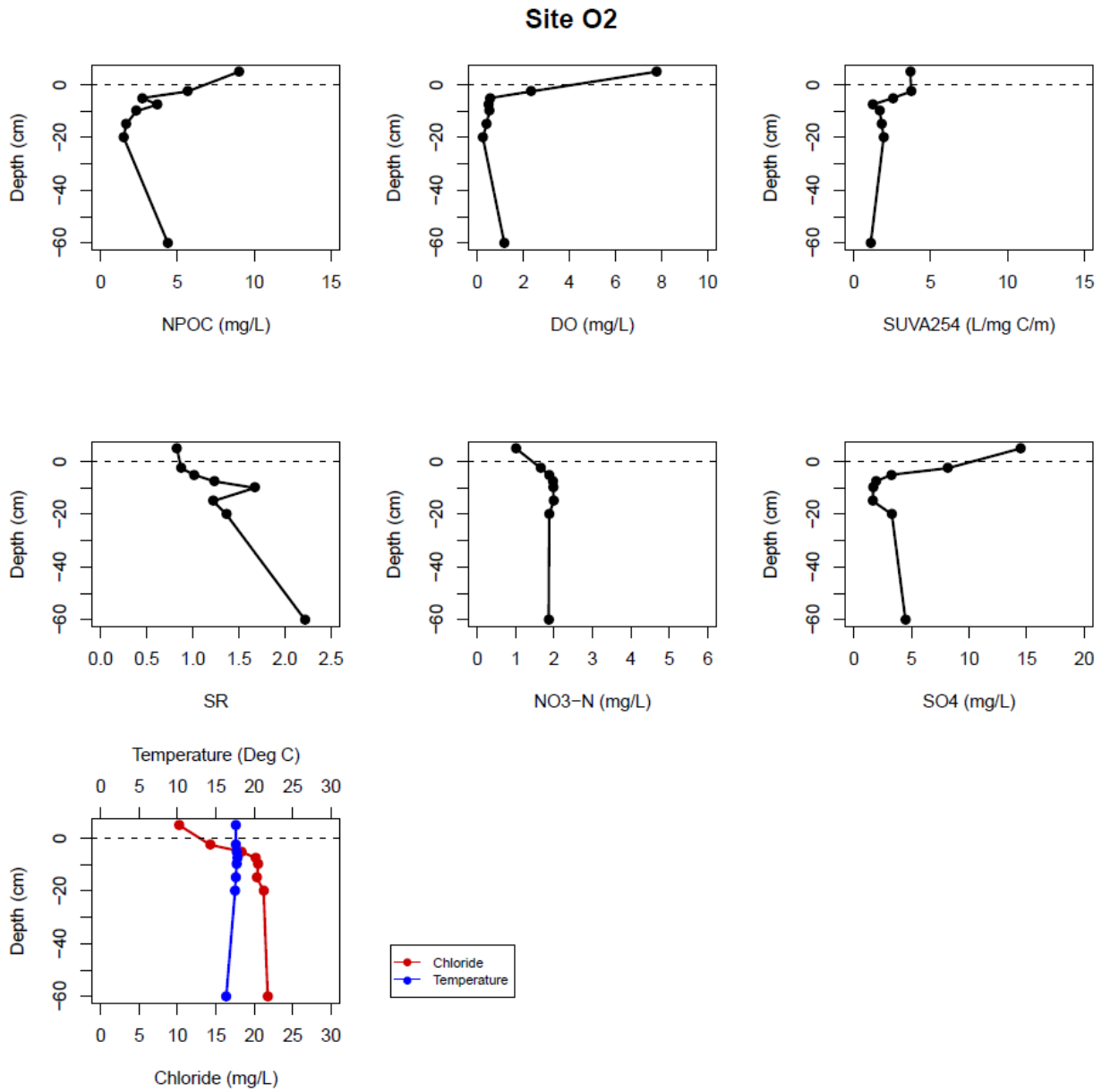


Figure B33: Site O2 Vertical Porewater Profiles

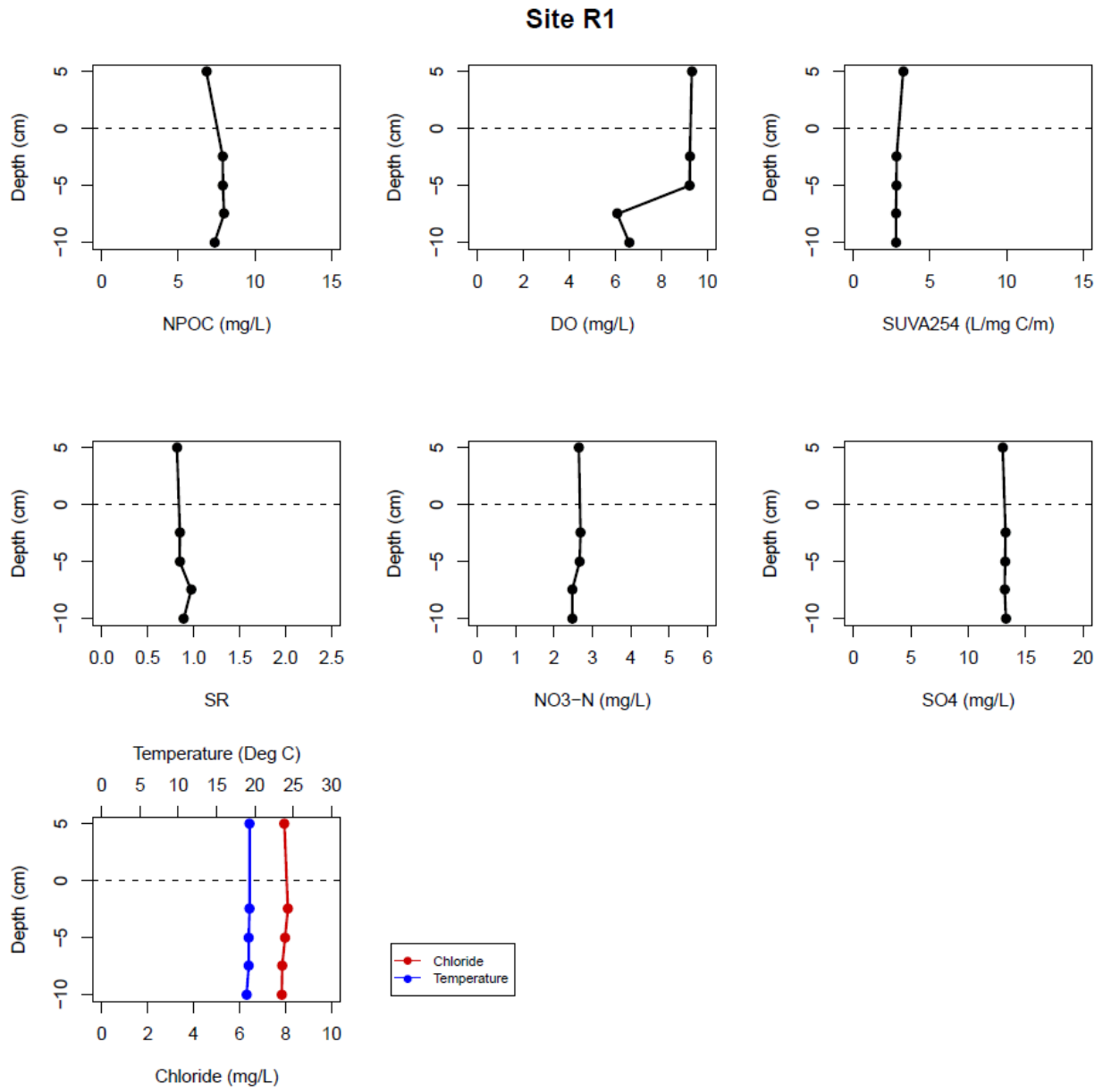


Figure B34: Site R1 Vertical Porewater Profiles

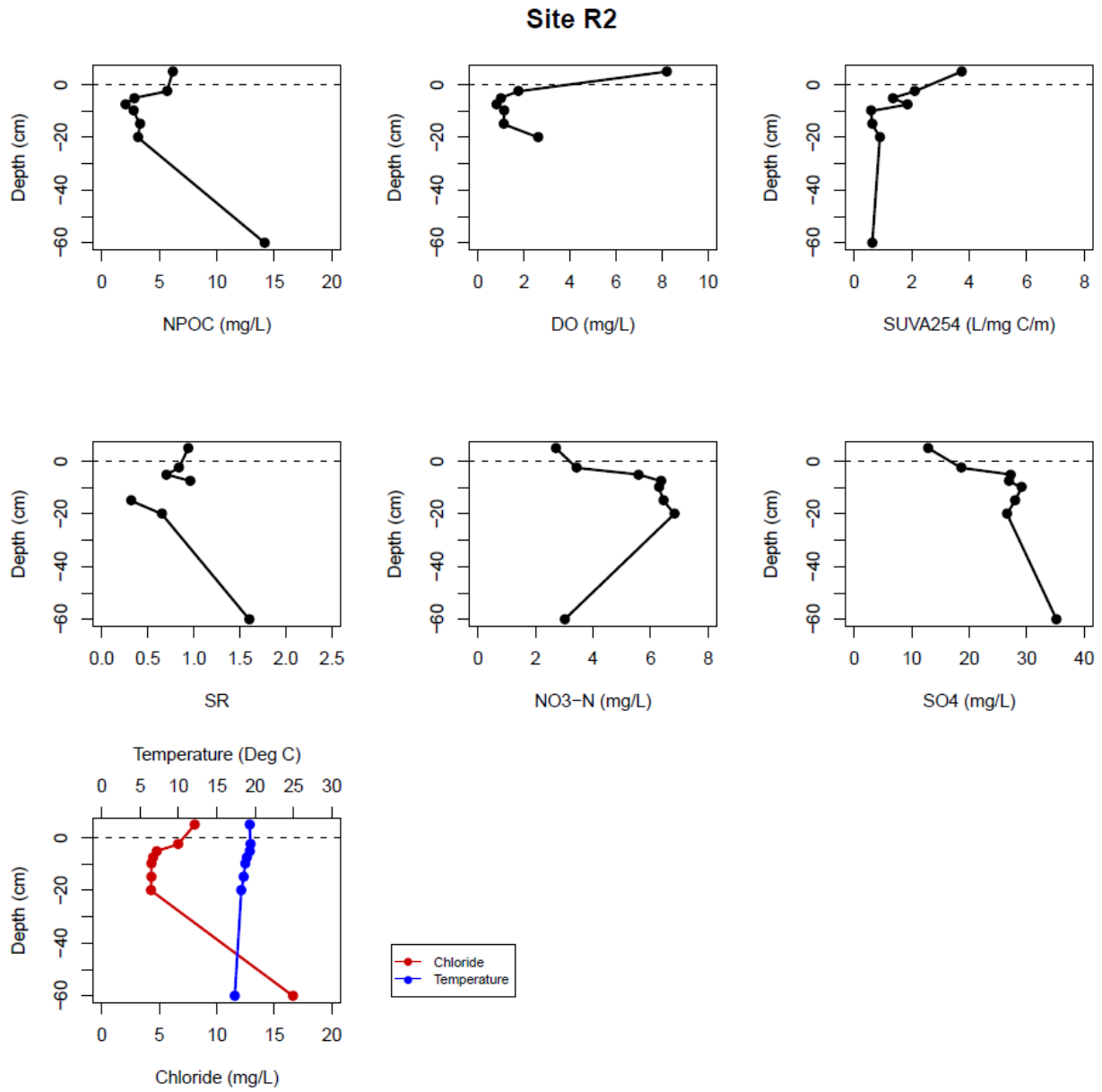


Figure B35: Site R2 Vertical Porewater Profiles

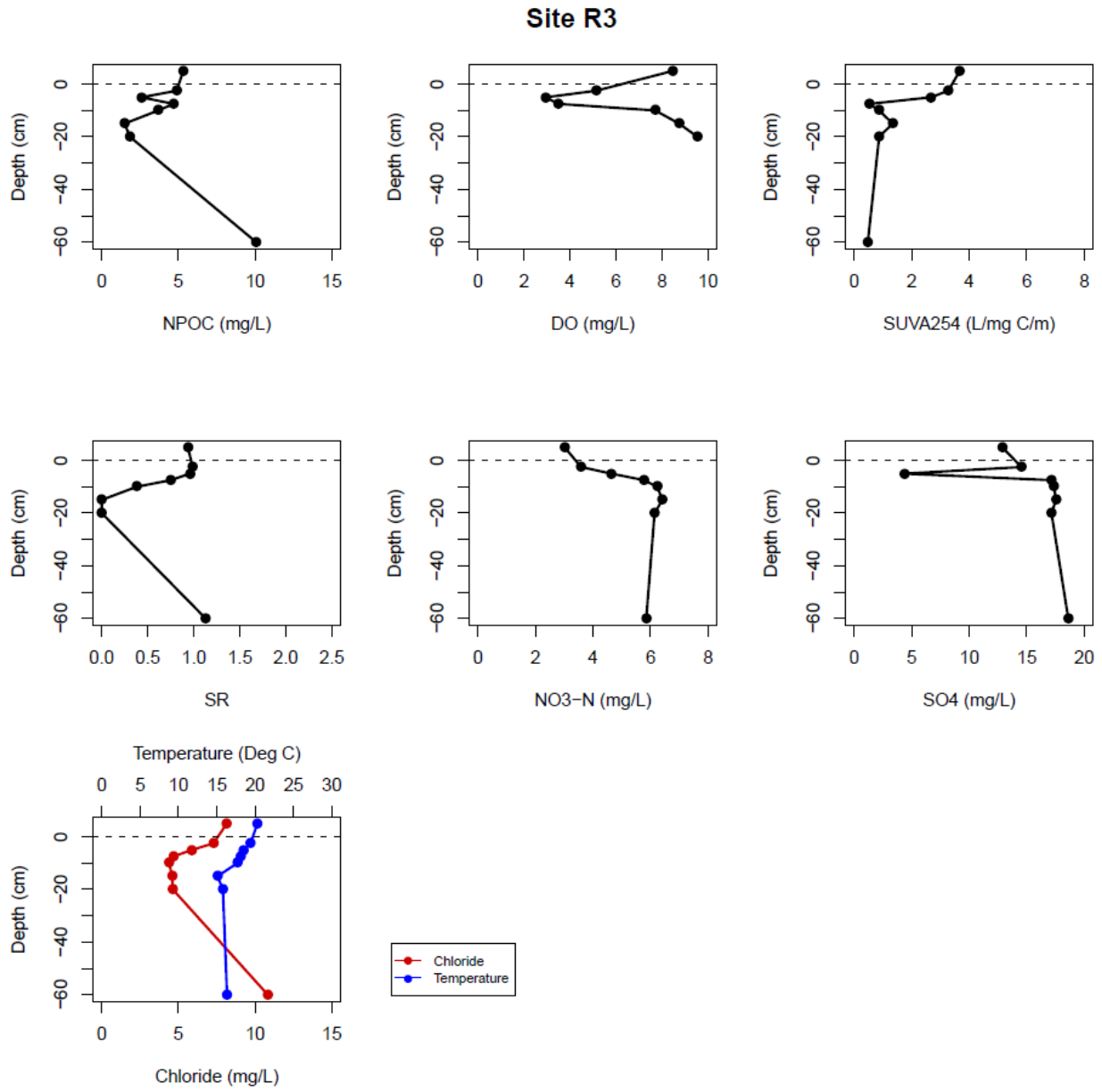


Figure B36: Site R3 Vertical Porewater Profiles

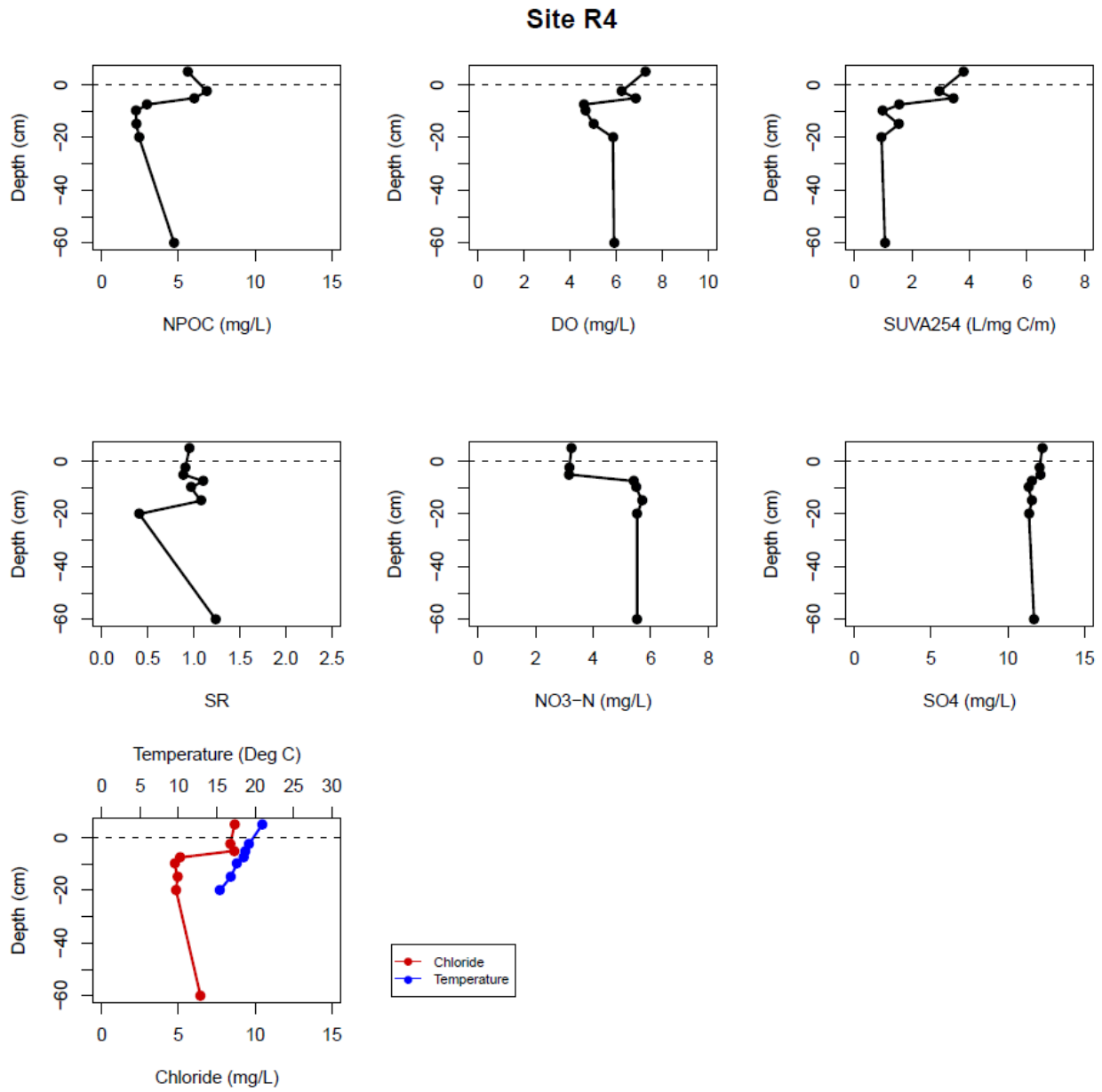


Figure B37: Site R4 Vertical Porewater Profiles

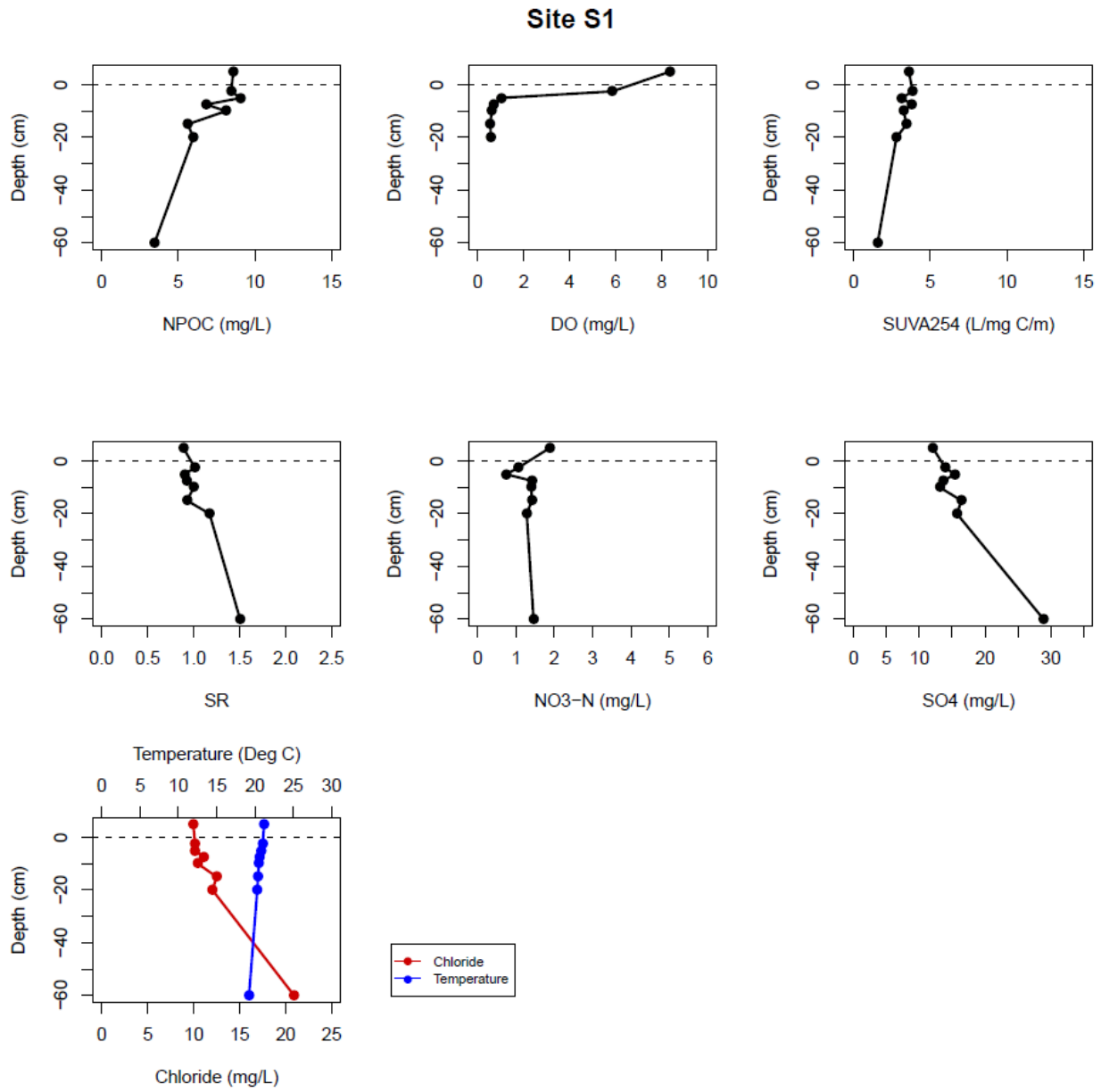


Figure B38: Site S1 Vertical Porewater Profiles

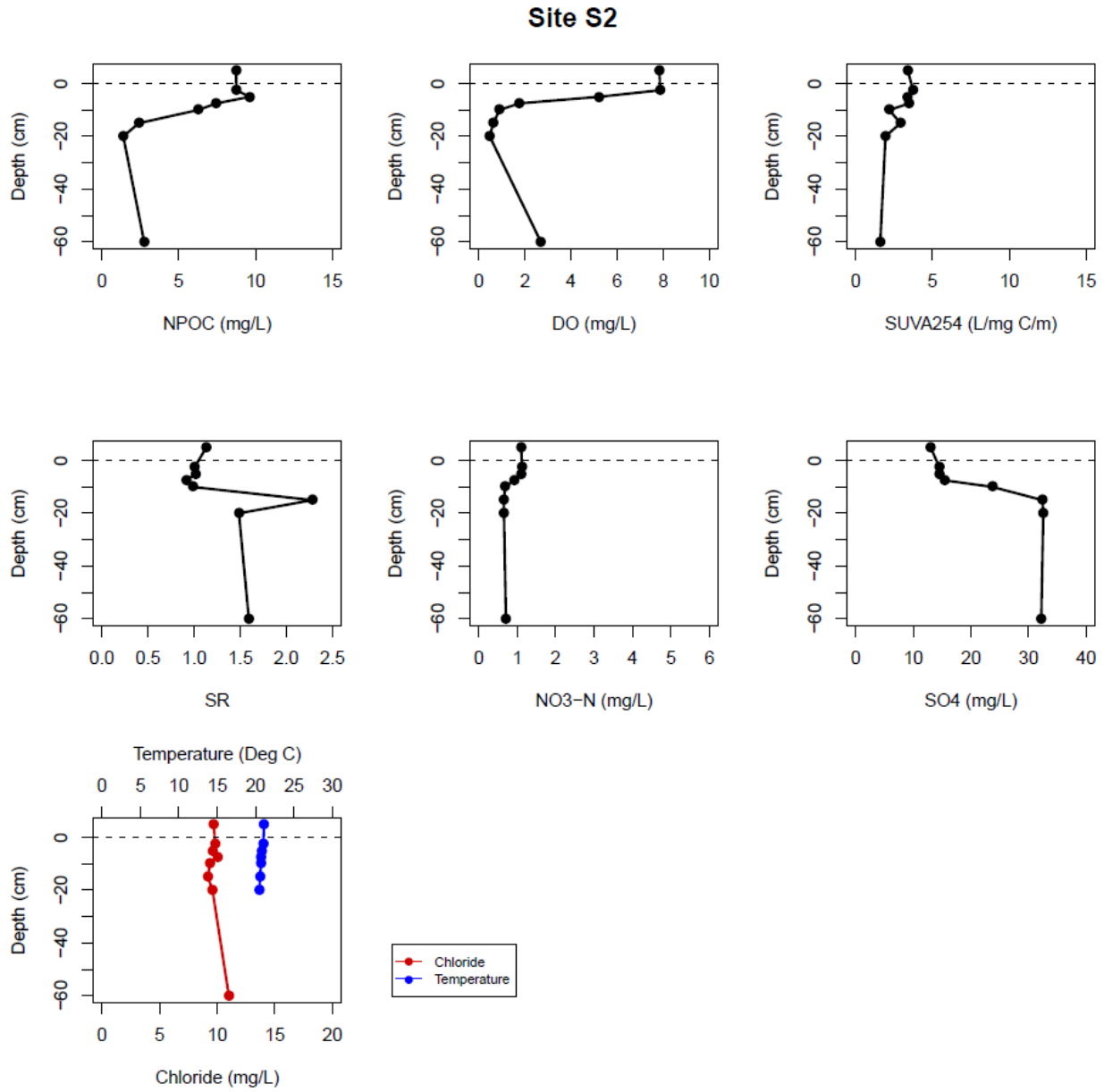


Figure B39: Site S2 Vertical Porewater Profiles

REFERENCES

REFERENCES

- Aiken, G.R., 2014. Dissolved organic matter in aquatic systems. *Comp. Water Quality and Purification*. 1, pp. 205–220, <http://dx.doi.org/10.1016/B978-0-12-382182-9.00014-1>.
- Avagyan, A., Runkle, B.R.K., Kutzbach, L., 2014. Application of high-resolution spectral absorbance measurements to determine dissolved organic carbon concentration in remote areas, *J. Hydrol.* 517, 435–446, <http://dx.doi.org/10.1016/j.jhydrol.2014.05.060>.
- Baker, M.A., Dahm, C.N., Valett, H.M., 1999. Acetate retention and metabolism in the hyporheic zone of a mountain stream. *Limnol. Oceanogr.* 44, 1530-1539, <http://dx.doi.org/10.4319/lo.1999.44.6.1530>.
- Baker, A., 2005. Thermal fluorescence quenching properties of dissolved organic matter, *Water Research* 39, 4405-4412, <http://dx.doi.org/10.1016/j.watres.2005.08.023>.
- Battin, T.J., 1999. Hydrologic flow paths control dissolved organic carbon fluxes and metabolism in an alpine stream hyporheic zone. *Water Resour. Res.* 35(10), 3159-3169, <http://dx.doi.org/10.1029/1999WR900144>.
- Battin, T.J., Kaplan, L.A., Findlay, S., Hopkinson, C.S., Marti, E., Packman, A.I., Newbold, J.D., Sabater, F., 2008. Biophysical controls on organic carbon fluxes in fluvial networks. *Nat. Geosci.* 1(2), 95–100, <http://dx.doi.org/10.1038/ngeo101>.
- Battin, T.J., Luysaert, S., Kaplan, L.A., Aufdenkampe, A.K., Richter, A., Tranvik, L.J., 2009. The boundless carbon cycle. *Nat. Geosci.* 2(9), 598–600, <http://dx.doi.org/10.1038/ngeo618>.
- Belzile, C., Roesler, C.S., Christensen, J.P., Shakhova, N., Semiletov, I., 2006. Fluorescence measured using the WETStar DOM fluorometer as a proxy for dissolved matter absorption, *Estuar. Coast. Shelf Sci.* 67, 441–449, <http://dx.doi.org/10.1016/j.ecss.2005.11.032>.
- Bergamaschi, B., Downing, B., Pellerin B., Saraceno J.F., 2009. In situ sensors for dissolved organic matter fluorescence: bringing the lab to the field, *Instrument News, Water Resources Discipline*, USGS, 125.
- Bieroza, M.Z., Heathwaite, A.L., 2016. Unravelling organic matter and nutrient biogeochemistry in groundwater-fed rivers under baseflow conditions: Uncertainty in in situ high-frequency analysis, *Sci. Total Environ.* 572, 1520-1533, <http://dx.doi.org/10.1016/j.scitotenv.2016.02.046>.
- Blaen, P.J., Khamis, K., Lloyd, C.E.M., Bradley, C., Hannah, D., Krause, S., 2016. Real-time monitoring of nutrients and dissolved organic matter in rivers: Capturing event dynamics,

- technological opportunities and future directions, *Sci. Total Environ.* 569-570, 647–660, <http://dx.doi.org/10.1016/j.scitotenv.2016.06.116>.
- Boano, F., Revelli, R., Ridolfi, L., 2009. Quantifying the impact of groundwater discharge on the surface-subsurface exchange. *Hydrol. Process.* 23, 2108-2116, <http://dx.doi.org/10.1002/hyp.7278>.
- Boano, F., Harvey, J.W., Marion, A., Packman, A.I., Revelli, R., Ridolfi, L., Wörman, A., 2014. Hyporheic flow and transport processes: Mechanisms, models, and biogeochemical implications. *Reviews of Geophysics* 52(4), 603-679, <http://dx.doi.org/10.1002/2012RG000417>.
- Boëne, W., Desmet, N., Van Looy, S., Seuntjens, P., 2014. Use of online water quality monitoring for assessing the effects of WWTP over flows in rivers, *Environ. Sci. Process. Impacts* 16, 1510–1518, <http://dx.doi.org/10.1039/c3em00449j>.
- Boulton, A.J., Findlay, S., Marmonier, P., Stanley, E.H., Valett, H.M., 1998. The functional significance of the hyporheic zone in streams and rivers. *Annu. Rev. Ecol. Syst.* 29, 59–81, <http://dx.doi.org/10.1146/annurev.ecolsys.29.1.59>.
- Bowes, M.J., Smith, J.T., Neal, C., 2009. The value of high-resolution nutrient monitoring: A case study of the River Frome, Dorset, UK, *J. Hydrol.* 378, 82–96, <http://dx.doi.org/10.1016/j.jhydrol.2009.09.015>.
- Brinkman, B.M., Hozalski, R.M., 2011. Temporal variation of NOM and its effects on membrane treatment, *Am. Water Work. Assoc.* 103(2), 98–106.
- Butman, D., Raymond, P.A., 2011. Significant efflux of carbon dioxide from streams and rivers in the United States. *Nat. Geosci.* 4(12), 839–842, <http://dx.doi.org/10.1038/ngeo1294>.
- Cardenas, M.B., Wilson, J.L., 2007. Dunes, turbulent eddies, and interfacial exchange with permeable sediments. *Water Resour. Res.* 43, <http://dx.doi.org/10.1029/2006WR005787>.
- Carstea, E.M., Baker, A., Pavelescu, G., Boomer, I., 2009. Continuous fluorescence assessment of organic matter variability on the Bournbrook River, Birmingham, UK, *Hydrol. Process.* 23(13), 1937–1946, <http://dx.doi.org/10.1002/hyp.7335>.
- Chen, R.F., 1999. In situ fluorescence measurements in coastal waters, *Org. Geochem.* 30, 397–409, [http://dx.doi.org/10.1016/S0146-6380\(99\)00025-X](http://dx.doi.org/10.1016/S0146-6380(99)00025-X).
- Chen, R.F., Gardner, G.B., 2004. High-resolution measurements of chromophoric dissolved organic matter in the Mississippi and Atchafalaya River plume regions, *Mar. Chem.* 89, 103–125, <http://dx.doi.org/10.1016/j.marchem.2004.02.026>.

- Conmy, R.N., Del Castillo, C.E., Downing, B.D., Chen R.F., 2014. Experimental design and quality assurance: In situ fluorescence instrumentation, *Aquat. Org. Matter Fluoresc.* 190-230.
- Cory, R.M., Boyer, E.W., McKnight, D.M., 2011. Spectral methods to advance understanding of dissolved organic carbon dynamics in forested catchments. *Forest Hydrology and Biogeochemistry: Synthesis of past Research and Future Directions.* 117–135, <http://dx.doi.org/10.1007/978-94-007-1363-5>.
- Creed, I.F. et al., 2015. The river as a chemostat: fresh perspectives on dissolved organic matter flowing down the river continuum. *J. Fish. Aquat. Sci.* 72(8), 1272–1285, <http://dx.doi.org/10.1139/cjfas-2014-0400>.
- Dahm, C.N., 1981. Pathways and mechanism for removal of dissolved organic carbon from leaf and leachate in streams. *Can. J. Fish. Aquat. Sci.* 38, 68-76, <http://dx.doi.org/10.1139/f81-009>.
- Day, G.M., Hart, B.T., McKelvie, I.D., Beckett, R., 1994. Adsorption of natural organic matter onto goethite. *Colloid Surface A*, 89, 1-13, [http://dx.doi.org/10.1016/0927-7757\(94\)02855-9](http://dx.doi.org/10.1016/0927-7757(94)02855-9).
- Downing, B.D., Pellerin, B.A., Bergamaschi, B.A., Saraceno, J.F., Kraus, T.E.C., 2012. Seeing the light: The effects of particles, dissolved materials, and temperature on in situ measurements of DOM fluorescence in rivers and streams, *Limnol. Oceanogr. Methods* 10, 767–775, <http://dx.doi.org/10.4319/lom.2012.10.767>.
- Downing, B.D., Boss, E., Bergamaschi, B.A., Fleck, J.A., Lionberger, M.A., Ganju, N.K., Schoellhamer, D.H., Fujii, R., 2009. Quantifying fluxes and characterizing compositional changes of dissolved organic matter in aquatic systems in situ using combined acoustic and optical measurements, *Limnol. Oceanogr. Methods* 7, 119–131, <http://dx.doi.org/10.4319/lom.2009.7.119>.
- Dunbar, C.O., 1962. Historical Geology. *John Wiley and Sons, Inc., New York.* 2nd Ed, 500.
- Duff, J.H., Murphy, F., Fuller, C.C., Triska, F.J., Harvey, J.W., Jackman, A.P., 1998. A mini drivepoint sampler for measuring pore-water solute concentrations in the hyporheic zone of sand-bottom streams. *Limnol. Oceanogr.* 43(6), 1378–1383, <http://dx.doi.org/10.4319/lo.1998.43.6.1378>.
- Etheridge, J.R., Birgand, F., Ii, M.R.B., Smith, B.T., 2014a. Addressing the Fouling of In Situ Ultraviolet-Visual Spectrometers Used to Continuously Monitor Water Quality in Brackish Tidal Marsh Waters, *J. Environ. Qual.* 42, 1896–1901, <http://dx.doi.org/10.2134/jeq2013.02.0049>.
- Etheridge, J.R., Birgand, F., Osborne, J.A., Osburn, C.L., Ii, M.R.B., Irving, J., Handsel, L., Dixon, J., Mackenzie, L., James, J., 2014b. Using in situ ultraviolet-visual spectroscopy

- to measure nitrogen, carbon, phosphorus, and suspended solids concentrations at a high frequency in a brackish tidal marsh, *Limnol. Oceanogr. Methods* 12, 10–22, <http://dx.doi.org/10.4319/lom.2014.12.10>.
- Fellman, J.B., Hood, E., Spencer, R.G.M., 2010. Fluorescence spectroscopy opens new windows into dissolved organic matter dynamics in freshwater ecosystems: a review. *Limnol. Oceanogr.* 55(6), 2452–2462, <http://dx.doi.org/10.4319/lo.2010.55.6.2452>.
- Fiebig, D.M., Lock M.A., 1991. Immobilization of dissolved organic matter from groundwater discharging through stream bed. *Freshwater Biol.* 26, 45-55, <http://dx.doi.org/10.1111/j.1365-2427.1991.tb00507.x>.
- Fiebig D.M., 1995. Groundwater discharge and its contribution of dissolved organic carbon to an upland stream. *Archiv Für Hydrobiologie*, 134, 129-155.
- Figure 22, Reprinted from Journal of Geophysical Research, 114, Saraceno, J.F., Pellerin, B.A., Downing, B.D., Boss, E., Bachand, P.A.M., Bergamaschi, B.A., High-Frequency in situ optical measurements during a storm event : assessing relationships between dissolved organic matter, sediment concentrations, and hydrologic processes, G00F09, Copyright 2009 by the American Geophysical Union with permission from John Wiley and Sons. <http://dx.doi.org/10.1029/2009JG000989>
- Figure 23, Reprinted from Hydrological Processes, 21, Spencer, R.G.M., Pellerin, B.A., Bergamaschi, B.A., Downing, B.D., Kraus, T.E.C., Smart, D.R., Dahlgren, R.A., Hernes, P.J., Diurnal variability in riverine dissolved organic matter composition determined by in situ optical measurement in the San Joaquin River (California, USA), 3181-3189, Copyright 2007 with permission from John Wiley and Sons. <http://dx.doi.org/10.1002/hyp.6887>.
- Figure 24, Reprinted from Biogeochemistry, 108, Pellerin, B.A., Saraceno, J.F., Shanley, J.B., Sebestyen, S.D., Aiken, G.R., Wollheim, W.M., Bergamaschi, B.A., Taking the pulse of snowmelt : in situ sensors reveal seasonal, event and diurnal patterns of nitrate and dissolved organic matter variability in an upland forest stream, 183-198, Copyright US Government 2011 with permission from Springer. <http://dx.doi.org/10.1007/s10533-011-9589-8>.
- Figure 25, Reprinted from Hydrological Processes, 20, Waterloo, M.J., Oliveira, S.M., Drucker, D.P., Nobre, A.D., Cuartas, L.A., Hodnett, M.G., Langedijk, I., Jans, W.W.P., Tomasella, J., Araujo, A.C., Pimentel, T.P., Munera Estrada, J.C., Export of organic carbon in runoff from an Amazonian rainforest blackwater catchment, 2581-2597, Copyright 2006 with permission from John Wiley and Sons. <http://dx.doi.org/10.1002/hyp.6217>.
- Findlay, S., Strayer, D., Goumbala, C., Gould, K., 1993. Metabolism of streamwater dissolved organic carbon in the shallow hyporheic zone. *Limnol. Oceanogr.* (38)7, 1493-1499, <http://dx.doi.org/10.4319/lo.1993.38.7.1493>.

- Findlay, S., Sobczak, W.V., 1996. Variability in removal of dissolved organic carbon in hyporheic sediments. *J. North Am. Benthol. Soc.* 15(1), 35–41, <http://dx.doi.org/10.2307/1467431>.
- Findlay, S., Sobczak, W.V., 2000. Microbial communities in hyporheic sediments, in *Streams and Ground Waters*, edited by J.A. Jones and P.J. Mulholland, 287-306, Academic Press, San Diego, Calif.
- Fischer, H., Kloep, F., Wilzcek, S., Pusch, M.T., 2005. A river's liver – microbial processes within the hyporheic zone of a large lowland river. *Biogeochem.* 76, 349-371, <http://dx.doi.org/10.1007/s10533-005-6896-y>.
- Four Townships Water Resources Council (FTWRC), 2011. Gull and Augusta Creeks Watershed Management Plan: the Four Township Watershed Area. Accessed from http://www.ftwrc.org/publications/FTWA_WMP_final.pdf.
- Gomez-Velez, J.D., Harvey, J.W., 2014. A hydrogeomorphic river network model predicts where and why hyporheic exchange is important in large basins. *Geophysical Research Letters* 41(18), 6403-6412, <http://dx.doi.org/10.1002/2014GL061099>.
- Graham, P.W., Baker, A., Andersen, M.S., 2015. Field measurement of fluorescent dissolved organic material as a means of early detection of leachate plumes, *Water Air Soil Pollut.* 226(211), <http://dx.doi.org/10.1007/s11270-015-2475-6>.
- Grayson, R., Holden, J., 2012. Continuous measurement of spectrophotometric absorbance in peatland streamwater in northern England : implications for understanding fluvial carbon fluxes, *Hydrol. Process.* 39, 27–39, <http://dx.doi.org/10.1002/hyp.8106>.
- Grayson, R.P., Holden, J., 2016. Improved automation of dissolved organic carbon sampling for organic-rich surface waters, *Sci. Total Environ.* 543, 44–51, <http://dx.doi.org/10.1016/j.scitotenv.2015.10.149>.
- Gueguen, C., McLaughlin, F.A., Carmack, E.C., Itoh, M., Narita, H., Nishino, S., 2012. The nature of colored dissolved organic matter in the southern Canada Basin and East Siberian Sea, *Deep Sea Res. II* 81-84, 102–113, <http://dx.doi.org/10.1016/j.dsr2.2011.05.004>.
- Hamilton, S.K., Augusta Creek DOC concentrations from 1997-2015. Unpublished Laboratory Data. Accessed 2015.
- Harvey, J.W., Fuller, C.C., 1998. Effect of enhanced manganese oxidation in the hyporheic zone on basin-scale geochemical mass balance. *Water Resour. Res.* 34(4), 623-636, <http://dx.doi.org/10.1029/97WR03606>.
- Harvey J.W., Böhlke, J.K., Voytek, M.A., Scott, D., Tobias, C.R., 2013. Hyporheic zone denitrification: Controls on effective reaction depth and contribution to whole-stream

- mass balance. *Water Resour. Res.* 49(10), 6298-6316, <http://dx.doi.org/10.1002/wrcr.20492>.
- Hedin, L.O., von Fischer, J.C., Ostrom, N.E., Kennedy, B.P., Brown, M.G., Robertson, G.P., 1998. Thermodynamic constraints on nitrogen transformations and other biogeochemical processes at soil-stream interfaces. *Ecology* 79(2), 684-703, <http://dx.doi.org/10.2307/176963>.
- Helms, J.R., Stubbins, A., Ritchie, J.D., Minor, E.C., 2008. Absorption spectral slopes and slope ratios as indicators of molecular weight, source, and photobleaching of chromophoric dissolved organic matter. *Limnol. Oceanogr.* 53(3), 955-969. <http://dx.doi.org/10.4319/lo.2008.53.3.0955>.
- Helton, A.M., Wright, M.S., Bernhardt, E.S., Poole, G.C., Cory, R., Stanford, J.A., 2015. Dissolved organic carbon lability increases with water residence time in the alluvial aquifer of a river-floodplain ecosystem. *J. Geophys. Res. Biogeosciences*, 120(4), 693-706, <http://dx.doi.org/10.1002/2014JG002832>.
- Hood, E., Gooseff, M.N., Johnson, S.L., 2006. Changes in the character of stream water dissolved organic carbon during flushing in three small watersheds, Oregon, *J. Geophys. Res. Biogeosciences* 111(1), 1-8, <http://dx.doi.org/10.1029/2005JG000082>.
- Inamdar, S., Singh, S., Dutta, S., Levia, D., Mitchell, M., Scott, D., Bais, H., McHale, P., 2011. Fluorescence characteristics and sources of dissolved organic matter for stream water during storm events in a forested mid-Atlantic watershed, *J. Geophys. Res.* 116, <http://dx.doi.org/10.1029/2011JG001735>.
- Jeong, J.J., Bartsch, S., Fleckenstein, J.H., Matzner, E., Tenhunen, J.D., Lee, S.D., Park, S.K., Park, J.H., 2012. Differential storm responses of dissolved and particulate organic carbon in a mountainous headwater stream, investigated by high-frequency, in situ optical measurements, *J. Geophys. Res. Biogeosciences* 117(3), 1-13, <http://dx.doi.org/10.1029/2012JG001999>.
- Jollymore, A., Johnson, M.S., Hawthorne, I., 2012. Submersible UV-Vis spectroscopy for quantifying streamwater organic carbon dynamics: implementation and challenges before and after forest harvest in a headwater stream. *Sensors* 12, 3798-3813, <http://dx.doi.org/10.3390/s120403798>.
- Jones, T.D., Chappell, N.A., Tych, W., 2014. First dynamic model of dissolved organic carbon derived directly from high-frequency observations through contiguous storms, *Environ. Sci. Technol.* 48(22), 13289-13297, <http://dx.doi.org/10.1021/es503506m>.
- Kaplan, L.A., Newbold, J.D., 2000. Surface and subsurface dissolved organic carbon, in *Streams and Ground Waters*, edited by J. A. Jones, and P. J. Mulholland, 237-258, Academic, San Diego, Calif..

- KBS-LTER, Dataset KBS002. Annual Temperature and Precipitation, Data Table KBS002-008.61. Accessed on 7 Mar 2017. Permission to use data granted from lead investigator, Phil Robertson.
- Khamis, K., Sorensen, J.P.R., Bradley, C., Hannah, D.M., Lapworth, D.J., Stevens, R., 2015. In-situ tryptophan-like fluorometers: assessing turbidity and temperature effects for freshwater applications, *Environ. Sci. Process. Impacts* 17, 740–752, <http://dx.doi.org/10.1039/C5EM00030K>.
- Kiel, B.A., Cardenas, M.B., 2014. Lateral hyporheic exchange throughout the Mississippi River network. *Nat. Geo.* 7, 413–417, <http://dx.doi.org/10.1038/ngeo2157>.
- King, R.H., 1978. Natural history and ecology of the stictochironomous annulicrus (townes) (diptera:chrionomidae), Augusta Creek, Kalamazoo County, Michigan. A Dissertation. Proquest Web. 5 Nov. 2016.
- Klinkhammer, G.P., Chin, C.S., Wilson, C., Rudnicki, M.D., German, C.R., 1997. Distributions of dissolved manganese and fluorescent dissolved organic matter in the Columbia River estuary and plume as determined by in situ measurement, *Mar. Chem.* 56, 1–14, [http://dx.doi.org/10.1016/S0304-4203\(96\)00079-5](http://dx.doi.org/10.1016/S0304-4203(96)00079-5).
- Koehler, A.K., Murphy, K., Kiely, G., Sottocornola, M., 2009. Seasonal variation of DOC concentration and annual loss of DOC from an Atlantic blanket bog in South Western Ireland, *Biogeochemistry* 95(2), 231–242, <http://dx.doi.org/10.1007/s10533-009-9333-9>.
- Kowalczyk, P., Zablocka, M., Sagan, S., Kulinski, K., 2010. Fluorescence measured in situ as a proxy of CDOM absorption and DOC concentration in the Baltic Sea, *Oceanologia* 52(3), 431–471, <http://dx.doi.org/10.5697/oc.52-3.431>.
- Lakowicz, J.R., 2006. Principles of fluorescence spectroscopy, 3rd ed., Springer Science and Business Media.
- Langergraber, G., Gupta, J.K., Pressl, A., Hofstaedter, F., Lettl, W., Weingartner, A., Fleischmann, N., 2004. On-line monitoring for control of a pilot-scale sequencing batch reactor using a submersible UV/VIS spectrometer, *Water Sci. Technol.* 50(10), 73–80.
- Laudon, H., Berggren, M., Ågren, A., Buffam, I., Bishop, K., Grabs, T., Jansson, M., Köhler, S., 2011. Patterns and dynamics of dissolved organic carbon (DOC) in boreal streams: The role of processes, connectivity, and scaling. *Ecosystems*, 14(6), 880–893, <http://dx.doi.org/10.1007/s10021-011-9452-8>.
- Lee, E.J., Yoo, G.Y., Jeong, Y., Kim, K.U., Park, J.H., Oh, N.H., 2015. Comparison of UV-VIS and FDOM sensors for in situ monitoring of stream DOC concentrations, *Biogeosciences* 12(10), 3109–3118, <http://dx.doi.org/10.5194/bg-12-3109-2015>.

- Lutz, B.D., Bernhardt, E.S., Roberts, B.J., Cory, R.M., Mulholland, P.J., 2012. Distinguishing dynamics of dissolved organic matter components in a forested stream using kinetic enrichments. *Limnol. Oceanogr.* 57, 76-89, <http://dx.doi.org/10.4319/lo.2012.57.1.0076>.
- Mann, P.J., Davydova, A., Zimov, N., Spencer, R.G.M, Davydov, S., Bulygina, E., Zimov, S., Holmes, R.M., 2012. Controls on the composition and lability of dissolved organic matter in Siberia's Kolyma River basin. *J. Geophys. Res. Biogeosciences* 117(1), 1–15, <http://dx.doi.org/10.1029/2011JG001798>
- Manny, B.A., Wetzel, R.G., 1973. Diurnal changes in dissolved organic and inorganic carbon and nitrogen in a hardwater stream. *Freshw. Biol.* 3(1), 31–43, <http://dx.doi.org/10.1111/j.1365-2427.1973.tb00060.x>.
- Mahan, D.C., Cummins, K.W., 1974. A profile of Augusta Creek in Kalamazoo and Barry Counties, Michigan. Tech. Rep. No. 3. W.K. Kellogg Biological Station, Michigan State University.
- Mast, M.A., Murphy, S.F., Clow, D.W., Penn, C.A., Sexstone, G.A., 2016. Water-quality response to a high-elevation wild fire in the Colorado Front Range, *Hydrol. Process.* 30, 1811–1823, <http://dx.doi.org/10.1002/hyp.10755>.
- McDonald, S., Bishop, A.G., Prenzler, P.D., Robards, K., 2004. Analytical chemistry of freshwater humic substances. *Analytica Chimica Acta* 527(2), 105-124, <http://dx.doi.org/10.1016/j.aca.2004.10.011>.
- McDowell, W.H., 1985. Kinetics and mechanisms of dissolved organic carbon retention in a headwater stream. *Biogeochemistry* 4, 329-352, <http://dx.doi.org/10.1007/BF02187376>.
- McKnight, D.M., Boyer, E.W., Westerhoff, P.K., Doran, P.T., Kulbe, T., Andersen, D.T., 2001. Spectrofluorometric characterization of dissolved organic matter for indication of precursor organic material and aromaticity. *Limnol. Oceanogr.* 46(1), 38–48, <http://dx.doi.org/10.4319/lo.2001.46.1.0038>.
- Monteith, D.T., et al., 2007. Dissolved organic carbon trends resulting from changes in atmospheric deposition chemistry. *Nature* 450(7169), 537–540, <http://dx.doi.org/10.1038/nature06316>.
- Neal, C. et al., 2012. High-frequency water quality time series in precipitation and stream flow: From fragmentary signals to scientific challenge, *Sci. Total Environ.* 434, 3–12, <http://dx.doi.org/10.1016/j.scitotenv.2011.10.072>.
- Nogaro, G., Datry, T., Mermillod-Blondin, F., Foulquier, A., Montuelle, B., 2013. Influence of hyporheic zone characteristics on the structure and activity of microbial assemblages. *Freshw. Biol.* 58(12), 2567-2583, <http://dx.doi.org/10.1111/fwb.12233>.

- Pellerin, B.A., Saraceno, J.F., Shanley, J.B., Sebestyen, S.D., Aiken, G.R., Wollheim, W.M., Bergamaschi, B.A., 2012. Taking the pulse of snowmelt : in situ sensors reveal seasonal, event and diurnal patterns of nitrate and dissolved organic matter variability in an upland forest stream, *Biogeochemistry* 108, 183–198, <http://dx.doi.org/10.1007/s10533-011-9589-8>.
- Peters, N.E., Ratcliffe, E.B., 1998. Tracing Hydrologic Pathways Using Chloride at the Panola Mountain Research Watershed, Georgia, USA. *Water, Air, and Soil Pollution* 105, 263-275, <http://dx.doi.org/10.1023/A:1005082332332>.
- Pinder, G.F., Jones, J.F., 1969. Determination of the ground-water component of peak discharge from the chemistry of total runoff. *Water Resour. Res.* 5(2), 438-445, <http://dx.doi.org/10.1029/WR005i002p00438>.
- Poff, N.L., Allan, J.D., Bain, M.B., Karr, J.R., Prestegard, K.L., Richter, B.D., Sparks, R.E., Stromberg, J.C., 1997. The Natural Flow Regime: A paradigm for river conservation and restoration. *Bioscience* 47(11), 769–784, <http://dx.doi.org/10.2307/1313099>.
- Potter, B., Wimsatt J., 2003. USEPA Method 415.3 –Determination of TOC and SUVA at 254nm in Source Water and Drinking Water. National Exposure Research Laboratory, Office of Research and Development, USEPA, Cincinnati, OH.
- Raymond, P.A., et al., 2013. Global carbon dioxide emissions from inland waters. *Nature* 503(7476), 355–359, <http://dx.doi.org/10.1038/nature12760>.
- Raymond, P.A., Saiers, J.E., Sobczak, W.V., 2016. Hydrological and biogeochemical controls on watershed dissolved organic matter transport: pulse-shunt concept. *Ecology* 97(1), 5-16, <http://dx.doi.org/10.1890/14-1684.1>.
- Roley, S.S., Griffiths, J.R., Levi, P.S., Patrick, C.J., Sadro, S., Zarnetske, J.P., 2014. Taking the pulse of the ecosystem: progress in quantifying aquatic ecosystem health, In P.F. Kemp [ed.], *Eco-DAS X Symposium Proceedings*, ASLO, <http://dx.doi.org/10.4319/ecodas.2014.978-0-9845591-4-5-88>.
- Ruhala, S.S., Zarnetske, J.P., 2017. Using in-situ optical sensors to study dissolved organic carbon dynamics of streams and watersheds: A review. *Sci. Total Environ.* 575, 713-723, <http://dx.doi.org/10.1016/j.scitotenv.2016.09.113>.
- Saraceno, J.F., Pellerin, B.A., Downing, B.D., Boss, E., Bachand, P.A.M., Bergamaschi, B.A., 2009. High-Frequency in situ optical measurements during a storm event : assessing relationships between dissolved organic matter, sediment concentrations, and hydrologic processes, *J. Geophys. Res.* 114, <http://dx.doi.org/10.1029/2009JG000989>.
- Schindler, J.E., Krabbenhoft, D.P., 1998. The hyporheic zone as a source of dissolved organic carbon and carbon gases to a temperate forested stream. *Biogeochem.* 43(2), 157-174, <http://dx.doi.org/10.1023/A:1006005311257>.

- Sobczak, W.V., Findlay, S., 2002. Variation in bioavailability of dissolved organic carbon among stream hyporheic flowpaths. *Ecology* 83(11), 3194–3209, <http://dx.doi.org/10.2307/3071853>.
- Sobczak W.V., Raymond, P.A., 2015. Watershed hydrology and dissolved organic matter export across time scales: minutes to millennium, *Freshwater Science* 34, 392-398, <http://dx.doi.org/10.1086/679747>.
- Spencer, R.G.M., Aiken, G.R., Butler, K.D., Dornblaser, M.M., Striegl, R.G., Hernes, P.J., 2009. Utilizing chromophoric dissolved organic matter measurements to derive export and reactivity of dissolved organic carbon exported to the Arctic Ocean: A case study of the Yukon River, Alaska, *Geophys. Res. Lett.* 36(6), 1–6, <http://dx.doi.org/10.1029/2008GL036831>.
- Spencer, R.G.M., Pellerin, B.A., Bergamaschi, B.A., Downing, B.D., Kraus, T.E.C., Smart, D.R., Dahlgren, R.A., Hernes, P.J., 2007. Diurnal variability in riverine dissolved organic matter composition determined by in situ optical measurement in the San Joaquin River (California, USA). *Hydrol. Process.* 21, 3181–3189, <http://dx.doi.org/10.1002/hyp.6887>.
- Stelzer, R.S., Scott, J.T., Bartsch, L.A., 2015. Buried particulate organic carbon stimulates denitrification and nitrate retention in stream sediments at the groundwater-surface water interface. *Freshwater Science* 34, 161-171, <http://dx.doi.org/10.1086/678249>.
- Storey, R.G., Fulthorpe, R.R., Williams, D.D., 1999. Perspectives and predictions on the microbial ecology of the hyporheic zone. *Freshwater Biology* 41(1), 119-130, <http://dx.doi.org/10.1046/j.1365-2427.1999.00377.x>.
- Strahler, A.N., 1957. Quantitative analysis of watershed geomorphology. *Trans. Amer. Geophys. Un.* 38, 913-920.
- Strohmeier, S., Knorr, K., Reichert, M., Frei, S., Fleckenstein, J.H., Peiffer, S. Matzner, E., 2013. Concentrations and fluxes of dissolved organic carbon in runoff from a forested catchment: insights from high frequency measurements, *Biogeosciences* 10, 905–916, <http://dx.doi.org/10.5194/bg-10-905-2013>.
- Thurman, E. M., 1985. Amount of organic carbon in natural waters. *Organic geochemistry of natural waters*. Vol. II in *Developments in Biogeochemistry*, 7-65.
- United States Geological Survey (USGS), 2016. National Water Information System data available on the World Wide Web (USGS Water Data for the Nation). Accessed November 4, 2016 at https://waterdata.usgs.gov/mi/nwis/uv?site_no=04105700.
- United States Geological Survey (USGS), 2017. National Water Information System data available on the World Wide Web (USGS Water Data for the Nation). Accessed March 7, 2017 at https://waterdata.usgs.gov/mi/nwis/uv?site_no=04105700.

- Url, S., Hart, D.D., 2012. International Association for Ecology Community Organization in Streams: The Importance of Species Interactions. 91(2), 220–228, <http://dx.doi.org/10.1007/BF00317787>.
- Valett, H.M., Morrice, J.A., Dahm, C.N., 1996. Parent lithology, surface-groundwater exchange, and nitrate retention in headwater streams. *Limnol. Oceanogr.* 41(2), 333–345, <http://dx.doi.org/10.4319/lo.1996.41.2.0333>.
- Vannote, R.L., Minshall, W.G., Cummins, K.W., Sedell, J.R., Cushing, C.E., 1980. The River Continuum Concept. *Can. J. Fish. Aquat. Sci.* 37(1), 130–137, <http://dx.doi.org/10.1139/f80-017>.
- Waterloo, M.J., Oliveira, S.M., Drucker, D.P., Nobre, A.D., Cuartas, L.A., Hodnett, M.G., Langedijk, I., Jans, W.W.P., Tomasella, J., Araujo, A.C., Pimentel, T.P., Munera Estrada, J.C., 2006. Export of organic carbon in run-off from an Amazonian rainforest blackwater catchment, *Hydrol. Process.* 20, 2581–2597, <http://dx.doi.org/10.1002/hyp.6217>.
- Watras, C.J., Hanson, P.C., Stacy, T.L., Morrison, K.M., Mather, J., Hu, Y., Milewski, P., 2011. A temperature compensation method for CDOM fluorescence sensors in freshwater, *Limnol. Oceanogr. Methods* 9, 296–301, <http://dx.doi.org/10.4319/lom.2011.9.296>.
- Watras, C.J., Morrison, K.A., Mather, J., Milewski, P., Hanson, P.C., 2014. Correcting CDOM fluorescence measurements for temperature effects under field conditions in freshwaters. *Limnol. Oceanogr. Methods* 12(1), 23–24, <http://dx.doi.org/10.4319/lom.2014.12.23>.
- Weishaar, J.L., Aiken, G.R., Bergamaschi, B.A., Fram, M.S., Fujii, R., Mopper, K., 2003. Evaluation of specific ultra-violet absorbance as an indicator of the chemical composition and reactivity of dissolved organic carbon. *Environ. Sci. Technol.* 37, 4702–4708, <http://dx.doi.org/10.1021/es030360x>.
- Wilson, H.F., Saiers, J.E., Raymond, P.A., Sobczak, W.V., 2013. Hydrologic drivers and seasonality of dissolved organic carbon concentration, nitrogen content, bioavailability, and export in a forested New England stream, *Ecosystems* 16(4), 604–616, <http://dx.doi.org/10.1007/s10021-013-9635-6>.
- Wondzell, S.M., 2011. The role of the hyporheic zone across stream networks. *Hydrol. Process.* 25, 3525–3532, <http://dx.doi.org/10.1002/jhyp.8119>.
- Worrall, F., Howden, N.J.K., Burt, T.P., 2015. Understanding the diurnal cycle in fluvial dissolved organic carbon – The interplay of in-stream residence time, day length and organic matter turnover, *J. Hydrol.* 523, 830–838, <http://dx.doi.org/10.1016/j.jhydrol.2015.01.075>.
- Zarnetske, J.P., Haggerty, R., Wondzell, S.M., Baker, M.A., 2011. Labile dissolved organic carbon supply limits hyporheic denitrification. *J. Geophys. Res. Biogeosciences* 116(4), <http://dx.doi.org/10.1029/2011JG001730>.